

Electronic Structure and Reactivity of Metal Complexes

Thesis by
Alexandra Teresa Barth

In Partial Fulfillment of the Requirements for
the degree of
Doctor of Philosophy

The logo for the California Institute of Technology (Caltech), featuring the word "Caltech" in a bold, orange, sans-serif font.

CALIFORNIA INSTITUTE OF TECHNOLOGY
Pasadena, California

2023
(Defended December 5, 2022)

© 2023

Alexandra Teresa Barth
ORCID: 0000-0002-1813-4029

To my family, for their love and support.

ACKNOWLEDGEMENTS

I am immensely grateful to the community of support I have received as I pursued this work over the past five years at Caltech. The work reflected in this thesis was only possible because of this community of family, friends, mentors, mentees, coworkers, and advisors.

Foremost, I have undying gratitude to my thesis advisor Prof. Harry B. Gray. Working under Harry's advisorship has allowed me to realize my full potential as a scientist. I work every day to model your leadership as a pioneering scientist, impassioned educator, empathetic mentor, and community builder. Further, the support I have received from Dr. Jay Winkler has been instrumental in mentoring my spectroscopy work and critical eye. I could not be more grateful for the opportunity to work with both of you.

Alongside these experiences, the relationships I have developed with other Caltech faculty have been influential in shaping my doctoral studies. I am grateful for the relationships I have developed with the members of my committee, Prof. Kim See, Prof. Scott Cushing, and Prof. Mitchio Okamura. I'm grateful for your support as I look forward.

The final six months of my graduate studies were conducted at the SLAC National Accelerator Laboratory under the advisorship of Dr. Amy Cordones-Hahn and Dr. Kelly Gaffney. I am grateful for their advisement of this experience and the community provided by members of the SLAC PULSE Solution Phase Chemistry group.

Members of the Gray group have immeasurably supportive and inspiring to completing my own work. Working alongside Ethan Simonoff, Maryann Morales, Jill Clinton, Rahaleh Ravanfar, and Yuling Li has been consistently uplifting. I'm always inspired by Javier Fajardo's high research integrity and have frequently collaborated and mused with Brendon McNicholas about many of these projects. Finally, I appreciate the support of my roommate Jieun Shin, whose perspective was invaluable as I entered the final stages of my degree.

A finite list of my peers would be incomplete. I am invaluablely grateful for the kindness and support from my friendship with Molly McFadden. Charlie Arnett served as my most significant mentor, and I remain grateful for his dedication and encouragement. Community members across the division have always extended their warmth and encouragement, significantly members of the Agapie, Peters, Hadt, See, Cushing, Wei, Resiman, and Robb groups.

I am grateful for the teaching and mentoring experiences that helped me put my love of science into practice. Meeting Dr. Jennifer Weaver significantly changed my approach to teaching, and I am grateful for her leadership alongside staff and volunteers of the Caltech Center for Teaching, Learning, and Outreach for the pedagogical experiences and opportunities. I am appreciative of the time I shared with my mentees Grace Chen and Elisabeth Gallmeier, and I remain enthusiastic for the scientific journeys ahead for each of you.

My involvement on campus has opened doors. I'm grateful to Sarah Reisman's advisement of our Women in Chemistry chapter, and Margot Clifford's advisement of the Caltech Alumni student engagement initiatives.

Finally, a significant nod to an incomplete list of Caltech community members that made this thesis possible: Alison Ross, Mike Takase, Larry Henling, Dave Vander Velde, Paul Oyala, Mona Shahgholi, Nathan Hart, Nate Siladke, Rebecca Fox, Victor Rivera, Joe Drew, Margarita Davis, Elisha Jung Okawa, and Pat Anderson.

ABSTRACT

Transition metals are at the core of addressing global energy needs. Functioning as catalysts, these systems have long demonstrated competency to promote thermodynamically challenging reactions, lowering energetic barriers and facilitating desired transformations with applied light or potential. Employing infrared, visible, ultraviolet, and x-ray spectroscopy, chemists are afforded insight into the electronic structures of transition metal complexes, investigating ligand field strengths and metal-ligand interactions. Addition of time-resolved techniques affords resolution of dynamic processes in molecular species, such as electron transfer pathways.

Chapter 1 reviews the electronic structure and reactivity of homoleptic tungsten(0) arylisocyanides $W(CNAr)_6$ to provide the foundation for much of this work.

In Chapter 2, application of $W(CNAr)_6$ species for one- and two-photon photoredox catalysis are explored. The two-photon absorption cross-sections of $W(CNAr)_6$ are remarkably large ($\delta_{810} = 180\text{-}1900\text{ GM}$) and enable these photocatalysts to operate under excitation from visible or near infrared light. Photoredox activity is evaluated *via* base-promoted homolytic aromatic substitution (BHAS) reaction of thermodynamically challenging substrates. In Chapter 3, solvent perturbations enhance visible light-activated BHAS catalysis from $W(CNAr)_6$. Increased solvent dielectric (benzene to 1,2-difluorobenzene) and solvated electrolyte combine to increase $^*W(CNAr)_6$ quenching rates up to one order of magnitude with greater cage-escape yields.

In Chapter 4, the electronic structure of linear gold(I) arylisocyanide complexes ($[Au(CNDipp-R)_2]^+$; $CNDipp = 2,6\text{-diisopropylphenylisocyanide}$) are assigned using insights from UV-visible spectroscopy and time-dependent density functional theory (TD-DFT) calculations. In Chapter 5, the electronic structure of Fe(II) and Co(II) quaterpyridine photo-/electro-catalysts for CO_2 reduction are evaluated using UV-visible-NIR, 1H NMR, Mössbauer, and infrared spectra. Assignment of the absorption transitions are supported by TD-DFT calculations.

PUBLISHED CONTENT AND CONTRIBUTIONS

Parts of this thesis have been adapted from both published articles and those that are currently in preparation.

Chapter 1. Spectroscopy and Reactivity of Tungsten(0) Arylisocyanides

A.T.B. wrote the manuscript alongside the other authors (J.F.J., J.R.W., and H.B.G.).

Chapter 2: Photoredox Catalysis Mediated by Tungsten(0) Arylisocyanides

Adapted with permission from the American Chemical Society.

DOI: <https://doi.org/10.1021/jacs.1c07617>

A.T.B. acquired ^1H NMR spectra and performed data analysis alongside the other authors (J.F.J., M.M., M.K.T., J.R.W., and H.B.G.).

Chapter 3: Photoredox Catalysis Mediated by Tungsten(0) Arylisocyanides in 1,2-Difluorobenzene

Adapted with permission from the American Chemical Society.

DOI: <https://doi.org/10.1021/acs.inorgchem.1c03767>

A.T.B. acquired all compound characterization data, UV-visible spectra, luminescence spectra, transient luminescence spectra, and NMR spectra, performed all data analysis, and wrote the manuscript alongside the other authors (M.M., J.R.W., and H.B.G.).

Chapter 4: Syntheses and Spectra of Gold(I) Arylisocyanides

A.T.B. performed all theoretical calculations, data analysis, and wrote the manuscript alongside the other authors (E.D.S., B.J.M., J.F.J., M.K.T., J.R.W., and H.B.G.).

Chapter 5: Spectroscopic and Magnetic Properties of Fe(II) and Co(II) Quaterpyridine Photo/electrocatalysts

A.T.B. conceived the idea for this project, synthesized all materials, acquired room and variable temperature UV Visible-NIR spectra, ^1H NMR spectra, Mössbauer spectra, and DFT/TD-DFT data, performed all data analysis, and wrote the manuscript.

TABLE OF CONTENTS

| | |
|---|-------------|
| Acknowledgements | iv |
| Abstract | vi |
| Published Content and Contributions | vii |
| Table of Contents | viii |
| List of Figures | x |
| List of Tables | xiv |
| | |
| Chapter 1 | 1 |
| Spectroscopy and Reactivity of Tungsten(0) Arylisocyanides | |
| 1.1. Conspectus | 1 |
| 1.2. Introduction | 2 |
| 1.3. Fundamentals | 3 |
| 1.4. First Generation: Monoarylisocyanides | 6 |
| 1.5. Second Generation: Oligioarylisocyanides | 10 |
| 1.6. Third Generation: Fused-Ring and Alkenyl-Bridged Arylisocyanides | 17 |
| 1.7. Summary and Outlook | 21 |
| 1.8. References | 24 |
| | |
| Chapter 2 | 30 |
| Photoredox Catalysis Mediated by Tungsten(0) Arylisocyanides | |
| 2.1. Abstract | 30 |
| 2.2. Introduction | 30 |
| 2.3. Results and Discussion | 33 |
| 2.4. Conclusion | 50 |
| 2.5. References | 51 |
| | |
| Chapter 3 | 58 |
| Photoredox Catalysis Mediated by Tungsten(0) Arylisocyanides in 1,2-Difluorobenzene | |
| 3.1. Abstract | 58 |
| 3.2. Introduction | 58 |
| 3.3. Results and Discussion | 60 |
| 3.4. Conclusion | 67 |
| 3.5. Experimental Section | 67 |
| 3.6. References | 90 |
| | |
| Chapter 4 | 94 |
| Syntheses and Spectra of Gold(I) Arylisocyanides | |
| 4.1. Abstract | 94 |

| | |
|---|------------|
| | ix |
| 4.2 Introduction | 94 |
| 4.3. Results and Discussion | 95 |
| 4.4. Experimental Section | 101 |
| 4.5. References | 145 |
| Chapter 5 | 150 |
| Spectroscopic and Magnetic Properties of Fe(II) and Co(II) Quaterpyridine Photo/electrocatalysts | |
| 5.1. Abstract | 150 |
| 5.2. Introduction | 150 |
| 5.3. Results and Discussion | 151 |
| 5.4. Conclusion | 158 |
| 5.5. Experimental Section | 159 |
| 5.6. References | 170 |
| Curriculum Vitae | 173 |

LIST OF FIGURES

- Figure 1.1.** Scope of homoleptic tungsten(0) arylisocyanide $W(CNAr)_6$ complexes.
- Figure 1.2.** Qualitative Jablonski diagram for $W(CNDipp)_6$.
- Figure 2.1.** $[M(CN^R Ar_3 NC)_3]^n$ and $W(CNAr)_6$ homoleptic arylisocyanide photocatalysts.
- Figure 2.2.** Time profiles of the BHAS photoredox reaction catalyzed by $W(CNAr)_6$ employing one-photon 445-nm excitation.
- Figure 2.3.** Proposed mechanism of BHAS photoredox catalysis in benzene solution mediated by $W(CNAr)_6$ complexes.
- Figure 2.4.** Stacked luminescence spectra collected upon one-photon (top) and two-photon (810 nm; bottom) excitation of $W(CNDipp)_6$.
- Figure 2.5.** Structure of crystalline $WI_2(CNDipp)_5$ with thermal ellipsoids set at 50% probability.
- Figure 2.6.** Cyclic voltammograms of $WI_2(CNDipp)_5$ at a scan rate of 100 mV s^{-1} in THF with 0.1 M $[^nBu_4N][PF_6]$ supporting electrolyte (vs $Fe^{+/0}$).
- Figure 3.1.** Mechanism for BHAS photoredox catalysis mediated by $W(CNAr)_6$ in benzene solution.
- Figure 3.2.** Luminescence spectra of 5 mol% $W(CNDipp)_6$ catalyst, 2 equivalents TMP, and 50 mM IBP in DFB.
- Figure 3.3.** Catalyst loading dependence of substrate conversion to cyclized product: $W(CNDipp)_6$ photocatalyst with, 100 mM TMP, and 50 mM IBP in DFB solution.
- Figure 3.4.** Luminescence spectra acquired during irradiation of $W(CNDipp)_6$, TMP, and 1-(2-bromobenzyl)-pyrrole substrate in DFB.
- Figure 3.5.** Luminescence spectra acquired during irradiation of $W(CNDipp)_6$, TMP, and 1-(2-bromobenzyl)-pyrrole substrate in DFB with 0.2 M TBAPF₆.
- Figure 3.6.** ¹H NMR spectra (methine resonances) of $WI_2(CNDipp)_5$ and $[WI(CNDipp)_6]I$ after irradiation with 1-(2-iodobenzyl)-pyrrole in DFB solution.
- Figure 3.7.** ¹H NMR spectrum of $[WI(CNDipp)_6]I$.
- Figure 3.8.** ¹³C{¹H} NMR spectrum (101 MHz, d₈-THF) of $[WI(CNDipp)_6]I$.
- Figure 3.9.** ATR-IR spectrum of $[WI(CNDipp)_6]I$, deposited as a thin film from THF.
- Figure 3.10.** Beer's law test of $W(CNDipp)_6$ absorbance in 1,2-difluorobenzene.
- Figure 3.11.** Molar absorption spectrum of $W(CNDipp)_6$ in 1,2-difluorobenzene.
- Figure 3.12.** Beer's law test of $WI_2(CNDipp)_5$ absorbance in 1,2-difluorobenzene.
- Figure 3.13.** Molar absorption spectrum of $WI_2(CNDipp)_5$ in 1,2-difluorobenzene.
- Figure 3.14.** Beer's law test of $[WI(CNDipp)_6]I$ absorbance in 1,2-difluorobenzene.
- Figure 3.15.** Molar absorption spectrum of $[WI(CNDipp)_6]I$ in 1,2-difluorobenzene.
- Figure 3.16.** Absorbance spectra acquired during irradiation of $W(CNDipp)_6$ (5 mol%), TMP (2 equiv), and 1-(2-iodobenzyl)-pyrrole substrate (50 mM) in DFB.
- Figure 3.17.** Absorbance spectra acquired during irradiation of $W(CNDipp)_6$ (5 mol%), TMP (2 equiv), and 1-(2-iodobenzyl)-pyrrole substrate (50 mM) in DFB with 0.2M TBAPF₆.

Figure 3.18. W(CNDipp)₆ (5 mol%), TMP (2 equiv) and 1-(2-iodobenzyl)-pyrrole substrate (50 mM) reactions in benzene, DFB, and DFB with 0.2M TBAPF₆ after 1 hour of irradiation.

Figure 3.19. Luminescence spectra acquired during irradiation of W(CNDipp)₆, TMP, and 1-(2-iodobenzyl)-pyrrole substrate in DFB (0.2M TBAI).

Figure 3.20. Luminescence spectra acquired during irradiation of 3 mM W(CNDipp)₆ in DFB. This concentration is representative of 5 mol% W(CNDipp)₆ BHAS photoredox conditions.

Figure 3.21. Luminescence spectra acquired during irradiation of 3 mM W(CNDipp)₆ in DFB (0.2M TBAPF₆). This concentration is representative of 5 mol% W(CNDipp)₆ BHAS photoredox conditions.

Figure 3.22. Luminescence spectra acquired during irradiation of 3 mM W(CNDipp)₆ with TMP in DFB. This concentration is representative of 5 mol% W(CNDipp)₆ BHAS photoredox conditions.

Figure 3.23. Luminescence spectra acquired during irradiation of 3 mM W(CNDipp)₆ with TMP in DFB (0.2M TBAPF₆).

Figure 3.24. Luminescence (620 nm) decay following laser excitation (532 nm, 8 ns) of W(CNDipp)₆ in DFB. Fit to a single-exponential function, $\tau = 63$ ns.

Figure 3.25. Change in absorbance spectrum of W(CNDipp)₆ in 1,2-difluorobenzene upon 532 nm sample irradiation.

Figure 3.26. Luminescence (620 nm) decay following laser excitation (532 nm, 8 ns) of W(CNDipp)₆ in DFB with TBAPF₆. Fit to a single-exponential function, $\tau = 62$ ns.

Figure 3.27. Change in absorbance spectrum of W(CNDipp)₆ in difluorobenzene with 0.2M TBAPF₆ upon 532 nm sample irradiation.

Figure 3.28. Plot of (τ_0/τ) versus 1-(2-iodobenzyl)-pyrrole concentration for W(CNDipp)₆.

Figure 3.29. Luminescence (620 nm) decay following laser excitation (532 nm, 8 ns) of W(CNDipp)₆ in DFB with 100 mM TMP.

Figure 3.30. Luminescence (620 nm) decay following laser excitation (532 nm, 8 ns) of W(CNDipp)₆ in DFB in the presence of IBP substrate.

Figure 3.31. Plot of (τ_0/τ) versus 1-(2-iodobenzyl)-pyrrole concentration for W(CNDipp)₆ with 0.2M TBAPF₆.

Figure 3.32. Luminescence (620 nm) decay following laser excitation (532 nm, 8 ns) of W(CNDipp)₆ in DFB (0.2 M TBAPF₆) with 100 mM TMP.

Figure 3.33. Luminescence (620 nm) decay following laser excitation (532 nm, 8 ns) of W(CNDipp)₆ in DFB (0.2M TBAPF₆) in the presence of IBP substrate.

Figure 3.34. Plot of (τ_0/τ) versus 1-(2-bromobenzyl)-pyrrole concentration for W(CNDipp)₆ in DFB.

Figure 3.35. Luminescence (620 nm) decay following laser excitation (532 nm, 8 ns) of W(CNDipp)₆ in DFB in the presence of BBP substrate.

Figure 3.36. Plot of (τ_0/τ) versus 1-(2-bromobenzyl)-pyrrole concentration for W(CNDipp)₆ in DFB with 0.2 M TBAPF₆.

Figure 3.37. Time dependent luminescence measurements for W(CNDipp)₆ in DFB (0.2M TBAPF₆) upon 532 nm excitation, 620 nm probe.

Figure 3.38. Plot of (τ_0/τ) versus 1-(2-iodobenzyl)-pyrrole concentration for $W(CNDipp)_6$ in DFB with 0.2 M TBAI.

Figure 4.1. Structures of gold(I) arylisocyanide $[Au(CNAr)_2]^+$ crystals (1a–2c).

Figure 4.2. UV-vis absorption spectra of gold(I) arylisocyanides at room temperature: (a) $[Au(CNDippPh^{OMe3})_2](BF_4)$ (1a), $[Au(CNDippPh^{NO2})_2](BF_4)$ (1b), $[Au(CNDippPh^{NPh2})_2](BF_4)$ (1c); $[Au(CNDippPh^{NHPH2})_2](OTf)_3$ (1d) (b) $[Au(CNDipp^{CC}Ph^{OMe})_2](BF_4)$ (2a), $[Au(CNDipp^{CC}Ph^{CN})_2](BF_4)$ (2b), $[Au(CNDipp^{CC}-1-Naph)_2](BF_4)$ (2c). All species are 4.37 μ M in DCM.

Figure 4.3. Overlay of $[Au(CNDippPh^{NPh2})_2](BF_4)$ (1c) UV-vis absorption spectra in ACN, DCM, THF, and toluene at room temperature.

Figure 4.4. 1H NMR of $[Au(CNDippPh^{OMe3})_2](BF_4)$ (1a).

Figure 4.5. 1H NMR of $[Au(CNDippPh^{NO2})_2](BF_4)$ (1b).

Figure 4.6. 1H NMR of $[Au(CNDippPh^{NPh2})_2](BF_4)$ (1c).

Figure 4.7. 1H NMR of $[Au(CNDipp^{CC}Ph^{OMe})_2](BF_4)$ (2a).

Figure 4.8. 1H NMR of $[Au(CNDipp^{CC}Ph^{CN})_2](BF_4)$ (2b).

Figure 4.9. 1H NMR of $[Au(CNDipp^{CC}-1-Naph)_2](BF_4)$ (2c).

Figure 4.10. Representation of $[Au(CNDippPh^{NO2})_2](BF_4)$ (1b) in the perpendicular geometry.

Figure 4.11. Visualized TDDFT spectra and geometry assignments for the optimized structures of $[Au(CNDippPh^{NO2})_2](BF_4)$ (1b).

Figure 4.12. Calculated TDDFT spectra for optimized $[Au(CNDippPh^{OMe3})_2](BF_4)$ (1a) structure.

Figure 4.13. Calculated TDDFT spectra for optimized $[Au(CNDippPh^{NO2})_2](BF_4)$ (1b) structure.

Figure 4.14. Calculated TDDFT spectra for optimized $[Au(CNDippPh^{NPh2})_2](BF_4)$ (1c) structure.

Figure 4.15. Calculated TDDFT spectra for optimized $[Au(CNDippPh^{NHPH2})_2](OTf)_3$ (1d).structure.

Figure 4.16. Calculated TDDFT spectra for optimized $[Au(CNDipp^{CC}Ph^{OMe})_2](BF_4)$ (2a).structure.

Figure 4.17. Calculated TDDFT spectra for optimized $[Au(CNDipp^{CC}Ph^{CN})_2](BF_4)$ (2b).structure.

Figure 4.18. Calculated TDDFT spectra for optimized $[Au(CNDipp^{CC}-1-naph)_2](BF_4)$ (2c).structure.

Figure 5.1. Structures of $[Fe(qpy)](BF_4)_2$ (Fe-qpy, left) and $[Co(qpy)](BF_4)_2$ (Co-qpy, right) showing the coordination geometry and ligand planarity.

Figure 5.2. Variable temperature 1H NMR (Evans method) of Fe-qpy in CD_3CN solution.

Figure 5.3. Zero-field ^{57}Fe Mössbauer spectra of Fe-qpy recorded at 80 K.

Figure 5.4. Solid-state Co-qpy and Fe-qpy infrared transmission spectra at 295 K.

Figure 5.5. Vis-NIR absorption spectra of Co-qpy (left) and Fe-qpy (right) in MeCN solution at 295 K.

Figure 5.6. Variable temperature UV-vis absorption spectra of Fe-qpy in MeCN solution.

Figure 5.7. 1H NMR (D_2O , 400 MHz) spectrum of Fe-qpy.

Figure 5.8. ^1H NMR (CD_3CN , 400 MHz) spectrum of Fe-qpy.

Figure 5.9. ^1H NMR (CD_3CN , 400 MHz) spectrum of Co-qpy.

Figure 5.10. Calculated Fe-qpy $S = 2$ absorption spectrum.

Figure 5.11. Calculated Fe-qpy $S = 0$ absorption spectrum.

Figure 5.12. Calculated Co-qpy $S = 3/2$ absorption spectrum.

Figure 5.13. Calculated Co-qpy $S = 1/2$ absorption spectrum.

LIST OF TABLES

- Table 1.1.** Ground and Excited-State Reduction Potentials of $W(CNAr)_6$ Complexes.
- Table 1.2.** Excited-State Decay Parameters for $W(CNAr)_6$ Complexes.
- Table 2.1.** Properties of $W(CNAr)_6$ and $Mo(CN^{tBu}Ar_3NC)_3$ Photocatalysts.
- Table 2.2.** One-Photon Photoredox Catalysis Mediated by $W(CNAr)_6$ Complexes.
- Table 2.3.** Stern-Volmer Quenching Constants and Reaction Driving Forces.
- Table 2.4.** Two-Photon Absorption (TPA) Cross Sections of $W(CNAr)_6$ Complexes.
- Table 2.5.** Two-Photon NIR Photoredox Catalysis Mediated by $W(CNDipp)_6$ and $W(CNDippPh^{OMe3})_6$ Complexes.
- Table 3.1.** Luminescence Quenching Kinetics of $W(CNDipp)_6$.
- Table 3.2.** $W(CNDipp)_6$ Photoredox in C_6H_6 and C_6D_6 .
- Table 3.3.** Photoredox Catalysis of 1-(2-indobenzyl)-pyrrole Conversion to Cyclized Product.
- Table 3.4.** Photoredox Catalysis of 1-(2-bromobenzyl)-pyrrole Conversion to Cyclized Product.
- Table 3.5.** Stern-Volmer Analysis of 1-(2-iodobenzyl)-pyrrole Quenching of $W(CNDipp)_6$ in 1,2-Difluorobenzene Solution.
- Table 3.6.** Stern-Volmer Analysis of 1-(2-iodobenzyl)-pyrrole Quenching of $W(CNDipp)_6$ in 1,2-Difluorobenzene Solution with 0.2M TBAPF₆.
- Table 3.7.** Stern-Volmer Analysis of 1-(2-bromobenzyl)-pyrrole Quenching of $W(CNDipp)_6$ in 1,2-Difluorobenzene Solution.
- Table 3.8.** Stern-Volmer Analysis of 1-(2-bromobenzyl)-pyrrole Quenching of $W(CNDipp)_6$ in 1,2-Difluorobenzene Solution with 0.2M TBAPF₆.
- Table 3.9.** Stern-Volmer Analysis of 1-(2-iodobenzyl)-pyrrole Quenching of $W(CNDipp)_6$ in 1,2-Difluorobenzene Solution with 0.2 M TBAI.
- Table 4.1.** Structural data for $[Au(CNAr)_2]^+$ Complexes.
- Table 4.2.** Absorption Data for 1a-1d and 2a-2c in DCM.
- Table 5.1.** Crystallographic Structure of M-qpy (M = Fe, Co).
- Table 5.2.** Electronic Spectra and Transition Assignments for M-qpy (M = Fe, Co) Complexes at 295 K.
- Table 5.3.** Optimized Geometry of M-qpy (M = Fe, Co).
- Table 5.4.** Calculated Electronic Transitions in $S = 2$ Fe-qpy.
- Table 5.5.** Calculated Electronic Transitions in $S = 0$ Fe-qpy.
- Table 5.6.** Calculated Electronic Transitions in $S = 3/2$ Co-qpy.
- Table 5.7.** Calculated Electronic Transitions in $S = 1/2$ Co-qpy.

1 Spectroscopy and Reactivity of Tungsten(0) Arylisocyanides

1.1. Conspectus

Photoredox catalysis utilizes light to drive selective and efficient electron transfer. Inspired by nature, photoredox systems have found utility in the efficient storage of solar energy in the form of renewable fuels and chemical feedstocks. Benefiting from a resurgence of interest, this field has grown tremendously over the past decade as transition metal photocatalysts mediate an abundance of synthetic organic transformations with high fidelity. Critical for the further advancement of this research area is the discovery of earth-abundant photocatalysts that can replace and/or complement established noble metal-based photosensitizers while maintaining benchmark activity and selectivity.

In this review, we report on one such promising class of molecules: homoleptic tungsten(0) complexes supported by monodentate arylisocyanide ligands. Originally reported by our group 40 years ago, we have recently established $W(CNAr)_6$ as a new family of highly modular photosensitizers with exceptional photophysical and photochemical properties. Taking advantage of their long-lived metal-to-ligand charge transfer (MLCT) excited states that are remarkably strong reductants with $E^\circ(W^{+/*}W^0) = -2.2$ to -3.0 V vs $Fe^{[+/0]}$, $W(CNAr)_6$ have now also found utility as photoredox catalysts. Owing to very large one- and two-photon absorption cross sections, catalysis can be driven by both visible and near-infrared excitation. In this review, we discuss the key design principles that led to the development of three generations of tungsten(0) photoreductants. Moreover, the mechanisms of $W(CNAr)_6$ -mediated photoredox reactions as well as potential two-photon imaging and 3D printing applications of these very bright luminophores are highlighted.

1.2. Introduction

A major goal of 21st century science is solar energy conversion of abundant small molecules to renewable fuels and chemical feedstocks.^{1,2} To make progress in this area, chemists have exploited the excited-state properties of transition metal complexes to mediate demanding chemical transformations to obtain energy-rich small molecules. These advances have found parallel utility in organic synthesis, where there is tremendous interest in catalyzing thermodynamically challenging reactions with visible light.^{3,4} To date, Ru and Ir polypyridyl photoreactions have dominated the field, as the complexes of these metals have long-lived, redox-active electronic excited states.⁵ However, despite these favorable properties, these noble metal photosensitizers have limited industrial utility due to their cost and adverse environmental impact.⁶

There is widespread ongoing work aimed at identifying earth-abundant transition metal photosensitizers that exhibit excited-state redox properties that are comparable to or better than their precious metal counterparts. Noteworthy developments over the past decade include efforts by Wenger,⁷⁻¹⁵ Wärnmark,¹⁶⁻²¹ Herbert,²² Milsman,^{23,24} Schelter,²⁵ Berkefeld,²⁶ Zysman-Colman,²⁷ and Meyer.²⁸ As many of these systems have been the subject of recent reviews,²⁹⁻³³ they will not be discussed further here.

In the 1970s, one of us (H.B.G.) began research on the electronic structures and reaction chemistry of homoleptic Group 6 (Cr, Mo, W) hexakis(arylisocyanide) complexes that feature low-lying metal-to-ligand charge transfer (MLCT) excited states. In this family, W(CNAr)₆ compounds (**Figure 1.1**) displayed exceptionally promising photophysical and photochemical properties; yet, despite their potential, these systems remained relatively unexplored for decades.

In this review, we detail the evolution of tungsten(0) arylicyanide photoactive complexes, with a focus on our group's work over the last 10 years to delineate key

design principles for readily tuning photophysical properties and improving outer-sphere electron transfer. After years of being recognized among the most powerful molecular photoreductants that can be generated with visible light, we also discuss how we established $W(CNAr)_6$ as dual visible- and NIR-light photoredox catalysts. Finally, we conclude with a perspective on how this newly established class of modular, earth-abundant photosensitizers may find use in applications for bioimaging and additive manufacturing.

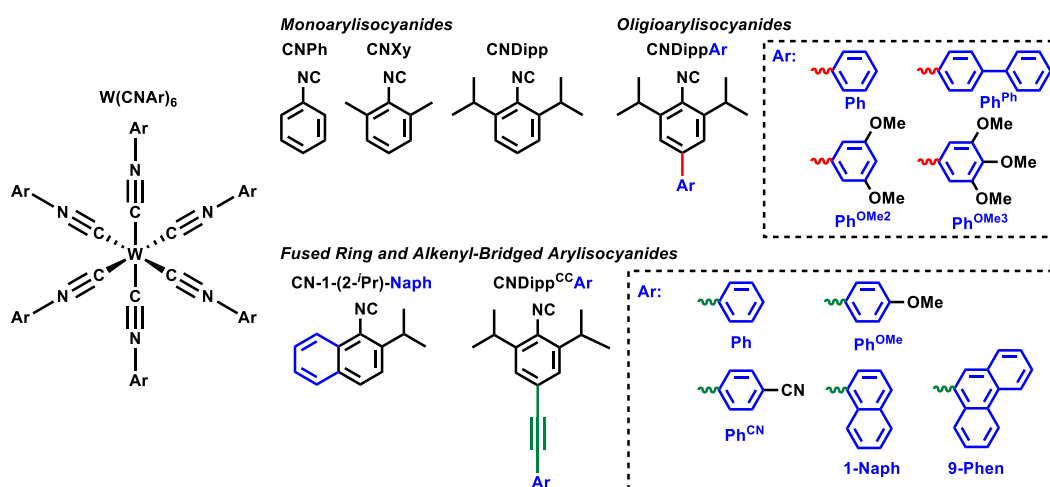


Figure 1.1. Scope of homoleptic tungsten(0) arylisocyanide $W(CNAr)_6$ complexes.

1.3. Fundamentals

Molecular photocatalysts can access a number of high-energy excited state configurations upon photon absorption (e.g. MLCT, ligand-to-metal charge transfer (LMCT), spin-flip, etc). Because the $W(CNAr)_6$ complexes that are the focus of this chapter possess MLCT excited states, we focus on the fundamentals of this type of excited state here. As explored in the following sections, $W(CNAr)_6$ coordination compounds feature very strong absorptions in the visible range with molar extinction coefficients on the order of $\sim 10^5 \text{ M}^{-1} \text{ cm}^{-1}$ that correspond to spin- and symmetry-allowed singlet MLCT (1MLCT) transitions. Facilitated by spin-orbit coupling, this initially populated 1MLCT state rapidly funnels down via intersystem

crossing to a lower energy, long-lived triplet MLCT ($^3\text{MLCT}$) state which supports photoluminescence and photochemical reactivity, described throughout this chapter.

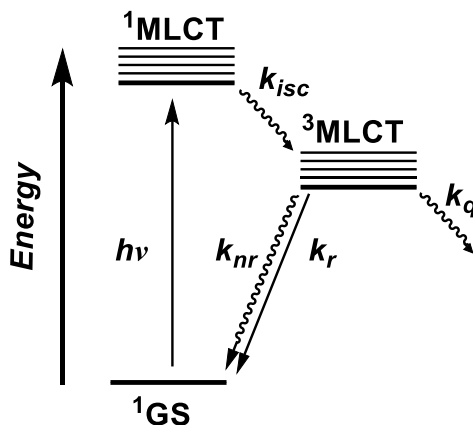


Figure 1.2. Qualitative Jablonski diagram for $\text{W}(\text{CNDipp})_6$.

Decay of the $^3\text{MLCT}$ state of electronically excited $^*\text{W}(\text{CNAr})_6$ (*denotes the lowest energy excited state) can occur through a number of interrelated competing pathways, the most prominent of which are depicted in the Jablonski diagram in **Figure 1.2**. In the absence of an exogenous quencher, emission of light from radiative decay (rate constant k_r) of $^*\text{W}(\text{CNAr})_6$ back to its ground state (^1GS) takes place with excited-state lifetimes (τ) of up to 1–4 μs and photoluminescence quantum yields (Φ_{PL}) of up to 0.4 in degassed room temperature solution. The remaining population of $^*\text{W}(\text{CNAr})_6$ can decay unproductively by nonradiative relaxation (rate constant k_{nr}) that dissipates the initial energy gained upon visible light excitation via thermal avenues. Because k_{nr} depends strongly on factors such as temperature and solvent polarity, nonradiative relaxation most strongly governs the excited-state dynamics of $^*\text{W}(\text{CNAr})_6$.

In addition to radiative and nonradiative decay processes, $^*\text{W}(\text{CNAr})_6$ can undergo deactivation via bimolecular reactivity with a quencher substrate (rate constant k_q). For example, $^*\text{W}(\text{CNAr})_6$ can facilitate excitation energy transfer to substrates such as anthracene, which may find use in the upconversion applications.³⁴ Alternatively,

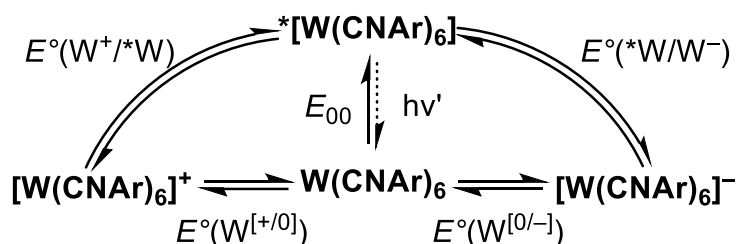
resulting from formal transfer of charge from the tungsten metal center onto the arylisocyanide ligands in the $^3\text{MLCT}$ state, $^*\text{W}(\text{CNAr})_6$ are both stronger oxidants and reductants when compared to their ground states. Combined with τ on the order of hundreds of nanoseconds to several microseconds, $^*\text{W}(\text{CNAr})_6$ are primed for intermolecular single-electron transfer chemistry.

In order to drive electron transfer, the reaction product $[\text{W}(\text{CNAr})_6]^{+/-}$ must be thermodynamically favorable relative to the excited state species $^*\text{W}(\text{CNAr})_6$. To a first approximation, the excited state redox potentials ($\text{W}^+/*\text{W}^0$ or $^*\text{W}^0/\text{W}^-$) can be calculated from the ground state redox couples ($\text{W}^{+/0}$ or $\text{W}^{0/-}$) and the zero-point energy (E_{00}) according to the Latimer diagram shown in **Scheme 1.1** and the Rehm-Weller equations (1) and (2). The standard reduction potentials $E^\circ(\text{W}^{+/0})$ or $E^\circ(\text{W}^{0/-})$ can be determined by cyclic voltammetry, while E_{00} can be estimated from the onset of emission in 77 K steady-state emission spectra.

$$E^\circ(\text{W}^+/*\text{W}) = E^\circ(\text{W}^{+/0}) - E_{00} \quad (1)$$

$$E^\circ(*\text{W}/\text{W}^-) = E^\circ(\text{W}^{0/-}) + E_{00} \quad (2)$$

Scheme 1.1



Performing this analysis for $\text{W}(\text{CNAr})_6$ reveals that they possess rich excited-state reductive chemistry. Combining their reductive power in the ground state of with the energy gained upon electronic excitation, we find that tungsten arylisocyanides are powerful photoreductants that access excited-state reduction potentials up to

$E^\circ(\text{W}^{+/*}\text{W}^0) = -3.0 \text{ V vs Fc}^{[+/0]}$. Thus, they are among the most powerful photoreductants that can be generated by visible light excitation.

As illustrated in this review, all of the above photophysical and photochemical properties of tungsten(0) arylisocyanides can be readily tuned by judicious design of highly modular arylisocyanide ligands.

1.4. First Generation: Monoarylisocyanides

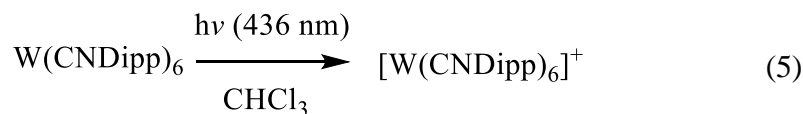
Investigation of the ground- and excited-state properties of Group 6 hexakis(arylisocyanide) complexes revealed remarkable photophysical and photochemical properties of $\text{W}(\text{CNAr})_6$ systems, including luminescent, highly reducing $^3\text{MLCT}$ excited states. The use of sterically encumbering isopropyl groups at the 2,6-positions of the diisopropylphenylisocyanide framework was identified as a key design element for complex photostability.

Preliminary Electronic Structure and Reactivity Investigations

Our inaugural 1976 examination of first-generation $\text{W}(\text{CNAr})_6$ complexes manifested as part of a systematic study aimed at evaluating the electronic structure of Group 6 hexakis(arylisocyanides). While $\text{M}(\text{CNAr})_6$ ($\text{M} = \text{Cr}, \text{Mo}, \text{W}$; $\text{Ar} = \text{Ph}, \text{Dipp}$) complexes are sterically encumbered analogues of $\text{M}(\text{CO})_6$ compounds, and thus possess a qualitatively similar electronic structure, the greater σ -donating and π -accepting ability of arylisocyanides endows the former with several benefits. One notable advantage is that $\text{M}(\text{CNAr})_6$ complexes have lower energy ligand-based π^* orbitals relative to their carbonyl congeners, leading to MLCT transitions that are red-shifted by $\sim 1.6 \text{ eV}$. This places the lowest energy MLCT absorption in the visible region and affords intensely pigmented complexes ($\epsilon_{\text{max}} \sim 65,000$ to $85,000 \text{ M}^{-1} \text{ cm}^{-1}$) ripe for photochemistry experiments.³⁵

Because of the significantly greater ligand field splitting imparted by arylisocyanide ligands, $\text{M}(\text{CNAr})_6$ complexes also possess higher energy metal-based $d\sigma^*$ orbitals,

and consequently, more photostable MLCT excited states. This difference is reflected in the ligand photosubstitution mechanisms operative for $M(\text{CO})_6$ versus $M(\text{CNAr})_6$ ($M = \text{Mo}, \text{W}$) coordination compounds; whereas $M(\text{CO})_6$ typically undergo a dissociative substitution process whereby electronic excitation promotes dissociation of a carbonyl ligand to generate an empty coordination site, photosubstitution of $M(\text{CNAr})_6$ is more consistent with a bimolecular excited state pathway. For example, irradiation of $\text{Mo}(\text{CNAr})_6$ and $\text{W}(\text{CNAr})_6$ in neat pyridine (Py) solution affords $M(\text{CNAr})_5(\text{Py})$ species with corresponding photosubstitution quantum yields (Φ_{PS}) of 0.055 and 0.011 for $\text{Ar} = \text{Ph}$ that decrease substantially to 0.022 and 0.0003 when $\text{Ar} = \text{Dipp}$ (equation 3). With incorporation of isopropyl groups, the increased steric hinderance protects the positively charged metal center in the $^3\text{MLCT}$ excited state from quenching via direct nucleophilic attack. Interestingly, $\Phi_{\text{PS}} = 0.23$ for $\text{Cr}(\text{CNAr})_6$ ($\text{Ar} = \text{Ph}, \text{Dipp}$) suggest these complexes follow the dissociative substitution trend, as might be expected on the basis of the weaker ligand field associated with first row transition metals.



Irradiation studies in degassed chloroform solution further demonstrated the ability of sterically encumbering CNDipp ligands to shield the tungsten center from nucleophilic attack. In this instance, irradiation of $\text{W}(\text{CNPh})_6$ was found to lead to the formation of the net two-electron oxidized, seven-coordinate product

$[\text{W}(\text{CNPh})_6(\text{Cl})]^+$, which features irreversible structural changes undesired in photosensitizer and photoredox applications (equation 4). In turn, similar irradiation of $\text{W}(\text{CNDipp})_6$ only yielded the one-electron oxidation product $[\text{W}(\text{CNDipp})_6]^+$ (equation 5). Thus, these results illustrate that steric encumbrance of the metal center through incorporation of *ortho* sterics on the arylisocyanide ligand is a vital design element to preserve in subsequent $\text{W}(\text{CNAr})_6$ generations, with an aim towards targeted outer-sphere reactivity.

Tungsten(0) Arylisocyanides – Powerful Photoreductants

Despite the great, early promise exhibited by $\text{W}(\text{CNAr})_6$ complexes, this family of photosensitizers remained relatively unexplored for several decades. With a resurgence of interest in developing earth-abundant photosensitizers, and the emergence of photoredox catalysis as a crucial branch of organic synthesis, we revisited $\text{W}(\text{CNAr})_6$ complexes, studying their photophysical and photochemical properties in greater detail.

For this investigation, comparative studies of $\text{W}(\text{CNDipp})_6$ and $\text{W}(\text{CNXy})_6$ ($\text{Xy} = \text{xylyl}$; 2,6-dimethylphenyl) further highlighted the importance of utilizing sterically encumbering arylisocyanides. Whereas the isopropyl groups of CNDipp favor a coplanar orientation of *trans* arylisocyanide π -systems, the smaller *ortho* methyl substituents of $\text{W}(\text{CNXy})_6$ allow *trans* CNXy ligands to adopt nearly orthogonal configurations. As a result of the greater conjugation across the octahedral molecular axes in the former, the lowest energy MLCT absorption maximum of $\text{W}(\text{CNDipp})_6$ occurs at $\lambda_{\text{abs}} = 465 \text{ nm}$ ($\epsilon = 9.1 \times 10^4 \text{ M}^{-1} \text{ cm}^{-1}$), whereas that of $\text{W}(\text{CNXy})_6$ is centered at $\lambda_{\text{abs}} = 381 \text{ nm}$ ($\epsilon = 1.3 \times 10^5 \text{ M}^{-1} \text{ cm}^{-1}$).³⁶

The emission spectra of $\text{W}(\text{CNDipp})_6$ and $\text{W}(\text{CNXy})_6$ are identical ($\lambda_{\text{em}} = 580 \text{ nm}$), indicating that ligand orientation does not influence $^3\text{MLCT}$ excited-state energies. However, $\tau(^3\text{MLCT})$ is four-fold longer in $\text{W}(\text{CNDipp})_6$ (73 ns) than in $\text{W}(\text{CNXy})_6$ (17 ns) when dissolved in degassed THF at room temperature. This demonstrates

that steric encumbrance about the metal center by CNDipp ligands better inhibit ³MLCT deactivation from metal-solvent interactions, consistent with previous irradiation studies in pyridine (*vide supra*). Presenting a high molar absorptivity, long-lived ³MLCT emission lifetime, and robust photostability, W(CNDipp)₆ was therefore a prime candidate for visible light-activated single electron transfer chemistry.

Table 1.1. Ground and Excited-State Reduction Potentials of W(CNAr)₆ Complexes^a

| W(CNAr) ₆ | $E(W^{[+0]})^b$ | E_{00}^c | $E(W^{+/*}W^0)^b$ |
|---|--------------------|------------|-------------------|
| W(CNDipp) ₆ | -0.72 ^d | 2.28 | -3.00 |
| W(CNDippPh) ₆ | -0.68 ^d | 2.12 | -2.80 |
| W(CNDippPh ^{OMe3}) ₆ | -0.65 ^d | 2.15 | -2.80 |
| W(CNDippPh ^{OMe2}) ₆ | -0.65 ^d | 2.14 | -2.79 |
| W(CNDippPh ^{Ph}) ₆ | -0.67 ^d | 2.08 | -2.75 |
| W(CN-1-(2- ⁱ Pr)-Naph) ₆ | -0.47 ^e | 2.02 | -2.49 |
| W(CNDipp ^{CC} Ph ^{OMe}) ₆ | -0.42 ^e | 2.01 | -2.43 |
| W(CNDipp ^{CC} Ph) ₆ | -0.39 ^e | 1.99 | -2.38 |
| W(CNDipp ^{CC} -1-Naph) ₆ | -0.37 ^e | 1.94 | -2.31 |
| W(CNDipp ^{CC} -9-Phen) ₆ | -0.36 ^e | 1.93 | -2.29 |
| W(CNDipp ^{CC} Ph ^{CN}) ₆ | -0.30 ^e | 1.89 | -2.19 |

^aTable reproduced from from Ref. 42. ^bV vs Fc^[+0]. ^cIn eV. ^dMeasurements performed in CH₂Cl₂ with 0.5 M [ⁿBu₄N][PF₆] supporting electrolyte. ^eMeasurements performed in THF with 0.1 M [ⁿBu₄N][PF₆] supporting electrolyte.

From electrochemical and emission measurements, the excited-state reduction potential of W(CNDipp)₆ was estimated to be $E^\circ(W^{+/*}W^0) = -3.0$ V vs Fc^[+0], making it one of the most powerful photoreductants that can be generated by visible light excitation. Interestingly, despite a driving force of $\Delta G_{ET} \approx -0.3$ eV for electron transfer (ET) from ^{*}W(CNDipp)₆ to anthracene [anth; $E^\circ(\text{anth}^{[0/1-]}) = -2.47$ vs Fc^[+0] in glyme], transient absorption measurements instead revealed the formation of the triplet excited state of anthracene (³anth) via diffusion-controlled excitation

energy transfer (EET), a process that is also thermodynamically favorable ($\Delta G_{\text{ET}} \approx -0.5$ eV). Hypothesizing that the predominance of EET over ET was a result from diffusional limitations of cage escape events, addition of 0.1 M $[\text{Bu}^n_4\text{N}][\text{PF}_6]$ electrolyte was used to bias the ET pathway. In doing so, diffusion-controlled ($k_q = 1.0 \times 10^{10} \text{ M}^{-1} \text{ s}^{-1}$) stoichiometric photoreduction of anthracene, benzophenone, and cobaltocenium was achieved. The determination that excited-state charge separation can be tuned by addition of a solvated electrolyte is also an important factor that enabled $\text{W}(\text{CNAr})_6$ -mediated photoredox catalysis (*vide infra*).

1.5. Second Generation: Tungsten Oligoarylisocyanides

Having established from structural variation of monoarylisocyanides the importance of sterically shielding *ortho* isopropyl groups on the photostability and ground- and excited-state properties of $\text{W}(\text{CNDipp})_6$, we then performed electronic modifications of the CNDipp ligand framework. Appending aryl groups *para* to the isocyanide functionality gave rise to a second generation of tungsten(0) oligoarylisocyanides $\text{W}(\text{CNDippAr})_6$ possessing greatly enhanced photophysical and photochemical properties, including Φ_{PL} of up to 0.4 and microsecond $\tau(^3\text{MLCT})$, all whilst maintaining highly reducing excited states with $E^\circ(\text{W}^+/*\text{W}^0) < -2.75 \text{ V vs Fc}^{[+/0]}$.

Enhanced Photophysical and Photochemical Properties

To introduce a diverse range of substituents at the 4-position of the CNDipp ligand framework, we developed a highly modular synthetic route for the preparation of 2,6-diisopropylarylisocyanide derivatives. The syntheses of these ligands proceed via a common *N*-formyl-4-halo-2,6-diisopropylaniline intermediate. Using this methodology, we prepared the oligoarylisocyanides CNDippPh and CNDippPh^{Ph} bearing radially extended biphenyl or terphenyl aromatic systems, respectively (**Figure 1.1**).³⁷ Oligoarylisocyanides CNDippPh^{OMe2} and CNDippPh^{OMe3} were

decorated with methoxy substituents to impart a greater solubility in organic solvents.

Maintaining the photostable $W(\text{CNDipp})_6$ primary coordination sphere enabled us to delineate the effect of CNAr electronic modification on the properties of ensuing $W(\text{CNDippAr})_6$ complexes. As for $W(\text{CNDipp})_6$, the *trans* CNDipp π -systems of $W(\text{CNDippAr})_6$ are nearly coplanar. In accordance with their extended aromatic systems, the latter display both red-shifted and more intense absorption profiles, with the most highly conjugated system $W(\text{CNDippPh}^{\text{Ph}})_6$ displaying the largest bathochromic shift of the lowest energy MLCT absorption maximum. An augmentation of ϵ_{max} for $W(\text{CNDippAr})_6$ complexes by 30–60% reflects an increase in orbital overlap between the ground- and excited-state wavefunctions.

In a similar fashion, within the same solvent the emission maxima of $W(\text{CNDippAr})_6$ complexes are red-shifted by 1000–1500 cm^{-1} relative to $W(\text{CNDipp})_6$. Consistent with emission from a $^3\text{MLCT}$ excited state, their luminescence profiles are highly solvent dependent, with the greatest stabilization and distortions occurring in more polar solvents. This solvent-dependent emission shift correlates with the number of ligand aryl groups, with the degree of λ_{max} red-shifting from toluene to THF solvent increasing in the order $W(\text{CNDipp})_6 < W(\text{CNDipp}^{\text{Ph}})_6 < W(\text{CNDippPh}^{\text{Ph}})_6$ ($60 \text{ cm}^{-1} < 230 \text{ cm}^{-1} < 650 \text{ cm}^{-1}$). The larger shifts in highly conjugated $W(\text{CNDippAr})_6$ species reflect increased excited-state dipoles that are better stabilized in polar media.

Table 1.2. Excited-State Decay Parameters for W(CNAr)₆ Complexes^a

| W(CNAr) ₆ | Toluene | | | | THF | | | |
|---|----------|-------------|-------------------|-------------------|----------|-------------|-------------------|-------------------|
| | τ^b | ϕ_{PL} | k_r^c | k_{nr}^c | τ^b | ϕ_{PL} | k_r^c | k_{nr}^c |
| W(CNDipp) ₆ | 0.12 | 0.03 | 2.3×10^5 | 8.0×10^6 | 0.08 | 0.01 | 1.6×10^5 | 1.3×10^7 |
| W(CNDippPh) ₆ | 1.73 | 0.41 | 2.4×10^5 | 3.4×10^5 | 1.32 | 0.21 | 1.6×10^5 | 6.0×10^5 |
| W(CNDippPh ^{OMe3}) ₆ | 1.83 | 0.41 | 2.2×10^5 | 3.2×10^5 | 1.56 | 0.25 | 1.6×10^5 | 4.8×10^5 |
| W(CNDippPh ^{OMe2}) ₆ | 1.65 | 0.42 | 2.6×10^5 | 3.5×10^5 | 1.20 | 0.21 | 1.8×10^5 | 6.6×10^5 |
| W(CNDippPh ^{Ph}) ₆ | 1.53 | 0.44 | 2.9×10^5 | 3.7×10^5 | 0.35 | 0.07 | 1.9×10^5 | 2.7×10^6 |
| W(CN-1-(2- ⁱ Pr)-Naph) ₆ | 3.83 | 0.25 | 6.5×10^5 | 2.0×10^5 | 2.15 | 0.11 | 5.3×10^5 | 4.1×10^5 |
| W(CNDipp ^{CC} Ph ^{OMe}) ₆ | 1.82 | 0.78 | 4.3×10^5 | 1.2×10^5 | 1.45 | 0.55 | 3.8×10^5 | 3.1×10^5 |
| W(CNDipp ^{CC} Ph) ₆ | 1.75 | 0.37 | 2.1×10^5 | 3.6×10^5 | 0.80 | 0.16 | 2.0×10^5 | 1.0×10^6 |
| W(CNDipp ^{CC} -1-Naph) ₆ | 1.45 | 0.30 | 2.0×10^5 | 4.8×10^5 | 0.22 | 0.05 | 2.1×10^5 | 4.3×10^6 |
| W(CNDipp ^{CC} -9-Phen) ₆ | 1.24 | 0.26 | 2.1×10^5 | 6.0×10^5 | 0.15 | 0.03 | 2.2×10^5 | 6.4×10^6 |
| W(CNDipp ^{CC} Ph ^{CN}) ₆ | 0.36 | 0.23 | 6.3×10^5 | 2.2×10^6 | 0.008 | 0.01 | 7.5×10^5 | 1.3×10^8 |

^aTable reproduced from Ref. 42. ^bIn μs . ^cIn s^{-1} .

In addition to their more favorable optical properties, W(CNDippAr)₆ exhibit photoluminescence quantum yields and excited-state lifetimes one order of magnitude larger than W(CNDipp)₆ (Table 1.2). For instance, in degassed room temperature toluene solution W(CNDippAr)₆ species have $\Phi_{PL} \approx 0.4$ and $\tau \approx 1.5$ – $1.8 \mu\text{s}$, compared to $\Phi_{PL} = 0.03$ and $\tau = 0.12 \mu\text{s}$ for W(CNDipp)₆. Determination of the radiative (k_r) and nonradiative (k_{nr}) decay rate constants reveals that while the former values are similar for W(CNAr)₆, k_{nr} of oligoarylisocyanide complexes were roughly one order of magnitude smaller than for W(CNDipp)₆, indicating that longer lifetimes and brighter luminescence arises from slower nonradiative decay.

In agreement with the greater distortions/³MLCT stabilization observed in steady-state luminescence spectra, *W(CNDippAr)₆ excited-state lifetimes diminish in more polar THF. Such solvents effects are most pronounced for MeCN-soluble W(CNDippPh^{OMe2/3})₆, with of Φ_{PL} = 0.01/0.02 and τ = 94/210 ns in this solvent. While k_r remain relatively constant in each solvent, k_{nr} vary by up to two orders of magnitude. Thus, nonradiative decay processes govern the excited-state dynamics of *W(CNAr)₆. In line with this, *W(CNAr)₆ are significantly longer lived at 77 K in toluene and 2-MeTHF glasses, exhibiting average luminescent lifetimes of 5.1–6.1 μs and 8.2–10.9 μs, respectively.

Building on these promising properties, the excited-state reduction potentials of W(CNDippAr)₆ complexes were evaluated. While W(CNAr)₆ ground-state potentials E°(W^[+/0]) remain largely unperturbed by aryl substitution, varying from –0.72 (Ar = Dipp) to –0.65 V (Ar = CNDippPh^{OMe2/3}), the zero-point energies (E₀₀) of oligoarylisocyanide complexes are red-shifted by ~0.1–0.2 eV. These effects are consistent with extension of the aryl π-systems in W(CNDippAr)₆ having the greatest effect on the ³MLCT energies via lowering the energy of the ligand-based π* LUMO (over W-based HOMO), as also reflected in the red-shifted absorption and emission profiles (*vide supra*). Gratifyingly, W(CNDippAr)₆ display all the aforementioned benefits while retaining highly reducing excited-states with E°(W⁺/*W⁰) < –2.75 V vs Fc^[+/0].

Single electron transfer to benzophenone (BP) [E°(BP^[0/1-]) = –2.30 V vs Fc^[+/0]] and acetophenone (AP) [E°(AP^[0/1-]) = –2.50 V] substrates were accessible with W(CNAr)₆ (Ar = Dipp, DippPh^{OMe2}) in THF solvent. In both cases, oxidative quenching of *W(CNDipp)₆ was faster than for functionalized *W(CNDippPh^{OMe2})₆. However, the slower reactivity of oligoarylisocyanide systems may serve advantageous for targeted photoredox applications; while bimolecular quenching of *W(CNDippPh^{OMe2})₆ (k_q = 2.1 × 10⁶ M⁻¹ cm⁻¹) is attenuated by two orders of magnitude relative to *W(CNDipp)₆ (k_q ~ 2.2 × 10⁸

$M^{-1} \text{ cm}^{-1}$), ~ 7 times higher concentration of AP substrate is required to quench 50% of the former. Nevertheless, the ability of $^*W(\text{CNAr})_6$ to reduce alkyl-aryl ketones, a substrate outside the potential range of electronically-excited $^*[\text{Ru}(\text{bpy})_3]^{2+}$ and $^*[\text{fac-Ir}(\text{ppy})_3]$, highlights the advantages of our tungsten arylisocyanide photoreductants.

Two-Photon Absorption

In addition to the enhancement of the photophysical and photochemical properties detailed above, the use of oligoarylisocyanides endowed $W(\text{CNDippAr})_6$ complexes with exceptional two-photon absorption (TPA) properties. That is, as an alternative to the use of one-photon of visible light to reach the long-lived, strongly luminescent, and highly reducing $^3\text{MLCT}$ excited state, $^*W(\text{CNAr})_6$ can instead be generated by simultaneous absorption (which differs from a consecutive, step-wise absorption mechanism) of two photons of roughly half the energy. This effectively shifts the excitation wavelength for $W(\text{CNAr})_6$ into the near-infrared (NIR) spectral region, whose lower energy and greater depth penetration, combined with the temporal and spatial resolution afforded by TPA, are highly advantageous for applications such two-photon biological imaging, photodynamic therapy, and photoredox catalysis.

To quantify the proclivity of $W(\text{CNAr})_6$ to undergo two-photon excitation, we measured the two-photon absorption (TPA) cross sections (δ) of $W(\text{CNAr})_6$ complexes via the two-photon luminescence (or two-photon excitation fluorescence) method, using fluorescein as a reference dye. Whereas in degassed room temperature 2-MeTHF solution $W(\text{CNDipp})_6$ does not display two-photon-induced emission after ns-pulsed 812 nm excitation (from a Nd:YAG laser), luminescence is observed following fs-pulsed 810 nm excitation (from a Ti:sapphire laser) of a similarly degassed toluene solution. This is likely due to the faster nonradiative decay and lower photoluminescence quantum yield of

W(CNDipp)₆ in more polar 2-MeTHF ($\Phi_{\text{PL}} = 0.01$, $k_{\text{nr}} = 1.3 \times 10^7 \text{ s}^{-1}$ in THF) versus toluene ($\Phi_{\text{PL}} = 0.03$, $k_{\text{nr}} = 8.0 \times 10^6 \text{ s}^{-1}$), rather than differences in the excitation source.³⁸ Importantly, *W(CNDipp)₆ (and *W(CNDippAr)₆) emission spectra obtained following one-photon and two-photon excitation are virtually identical, confirming the same long-lived ³MLCT photoreductant is generated in both cases. A TPA cross section of $\delta_{810} = 230 \text{ GM}$ (GM = Goeppert–Mayer; 1 GM = $10^{-50} \text{ cm}^4 \text{ s photon}^{-1} \text{ molecule}^{-1}$) was thus determined for W(CNDipp)₆

Analogous measurements on tungsten(0) oligoarylisocyanides reveal that W(CNDippAr)₆ (Ar = Ph, Ph^{OMe2}, Ph^{OMe3}, Ph^{Ph}) possess $\delta_{810/812} = 1000\text{--}2000 \text{ GM}$ that are comparable in 2-MeTHF/toluene solution and independent of the laser excitation source (**Table 2.4**).³⁸ These cross sections are larger than that of parent W(CNDipp)₆, as well as orders of magnitude greater than those of [Ru(bpy)₃]²⁺ ($\delta_{812} = 7 \text{ GM}$)³⁸ and *fac*-Ir(ppy)₃ ($\delta_{800} = 20 \text{ GM}$)⁴⁰ at similar wavelengths. Interestingly, determination of 800–1000 nm extended TPA spectra of W(CNDippAr)₆ (Ar = Ph, Ph^{OMe2}, Ph^{Ph}) reveal a blue-shift relative to the corresponding one-photon absorption spectra, suggesting that δ_{812} are not maxima and TPA cross sections are likely to be significantly larger at shorter wavelengths.

The exceptional TPA cross sections of tungsten(0) oligoarylisocyanides, which rival those of the best organic and inorganic chromophores, can be attributed to a number of important TPA design elements. Of key importance are the strong one-photon absorption cross sections (extinction coefficients, $\epsilon \sim 10^5 \text{ M}^{-1} \text{ cm}^{-1}$) near the TPA band, centrosymmetric geometries, and extended π -conjugation of these complexes enabled in large part by the use of arylisocyanide ligands. As described above, the bulky isopropyl groups of CNDippAr favor an approximately coplanar orientation of *trans* CNDipp aromatic systems in both solution and the solid state, resulting in maximized conjugation across the three octahedral molecular axes. The ensuing centrosymmetric geometry also promotes three-fold degeneracy of the MLCT excited-states. Finally, the degree of conjugation can be readily tuned by

installation of extended π -systems moieties *para* to the isocyanide. In particular, addition of one phenyl ring (or alkynyl-aryl unit in third generation $W(CNAr)_6$, *vide infra*) to $W(CNDipp)_6$ significantly enhances δ . Given that the different degrees of conjugation across $W(CNAr)_6$ shift both the one- and two-photon absorption spectra, single-point measurements at δ_{810} do not allow for a direct comparison of δ_{max} in the series. Therefore, future work is aimed at collecting extended TPA spectra of all three generations of $W(CNAr)_6$ complexes to better understand the interplay of the above factors on the corresponding δ and further develop TPA design principles for this family of photosensitizers. Moreover, these results establish $W(CNAr)_6$ among the most powerful photoreductants that can be generated by both visible *and* NIR excitation, making them an attractive dual platform for photoredox applications (*vide infra*).

Geometric Influence on Excited State Dynamics

Geometric insights to $W(CNAr)_6$ (Ar = Ph, Xy, Dipp, and DippPh^{OMe2}) excited states are elucidated from computational investigation and time-resolved vibrational spectroscopy. Optimized geometries were calculated using density functional theory and time dependent (TD-DFT) calculations, incorporating both relativistic effects and spin-orbit coupling to model the excited state absorption spectra. The evaluated optimized geometry of $W(CNAr)_6$ species were found to reproduce the bonding parameters of crystallographic structures.⁴¹

Three high-intensity MLCT transitions were calculated in the UV-visible absorption spectrum of $W(CNAr)_6$, matching experimental observation. *Trans* ligand aryl groups were rotated in the optimized structure to lend insight into the geometric dependence of these electronic transitions. From these TD-DFT analyses, the middle transition (380-420 nm) is assigned to orthogonally oriented *trans* ligands, whereas the higher energy (300-320 nm) and lower energy (450-550 nm) features correspond to transitions originating from coplanar *trans* ligands. These

calculations lend insight that experimental absorption spectra represent a superposition of these conformers in solution, stabilized as either the coplanar or orthogonal orientation through ligand steric effects.

Time-resolved infrared spectroscopy (TRIR) affords characterization of the $^*W(CNAr)_6$ excited state as shifts in the ligand $\nu(C=N)$ stretch. Nanosecond-timescale measurements observe two excited state absorption features (c.a. 1880 and 2020 cm^{-1}) and a significant ground state bleach feature (c.a. 1950 cm^{-1}), which results from splitting in the octahedral T_{1u} stretching mode. The TRIR decay lifetimes (60 ns) align well with the excited state emission lifetimes (75 ns), indicating that a single structural conformer is generated in the excited state whose torsional exchange outpaces the excited state decay. These vibrational peak shifts are assigned to charge transfer from tungsten to arylisocyanide ligand in the MLCT excited state.

1.6. Third Generation: Fused-Ring and Alkenyl-Bridged Arylisocyanides

After evaluating the synthetic modularity of $W(CNAr)_6$ species, we extended the conjugated π -system of arylisocyanide ligands with enforced structural rigidity to target tailored 3MLCT excited state lifetimes and $E(W^+/*W^0)$ photoredox potentials. The influence of these extended aromatic systems on excited state reactivity and catalysis are assessed.

Extending π -System Conjugation

Our combined insights from experiment and calculation illustrate that 3MLCT energies rely on ligand π -system aromaticity. To extend these synthetic insights, we introduced intraligand structural rigidity *via* alkenyl-bridged functionalities to reinforce π^* orbital delocalization and incorporate naphthyl substituents to investigate orthogonal functionalization. The alkenyl-bridged arylisocyanides are

notated herein as $W(\text{CNDipp}^{\text{CC}}\text{Ar})_6$ and the naphthyl-substituted species as $W(\text{CN-1-(2-}^i\text{Pr)-Naph})_6$ (**Figure 1.1**).⁴²

Matching previous insights in oligoarylisocyanides, the aryl diisopropyl functionalization orients *trans* ligands to be coplanar about the metal center to optimize aromaticity and ³MLCT absorption intensities. This extended ligand conjugation further red-shifts the absorption maxima λ_{max} from $W(\text{CNDipp})_6$ (21500 cm^{-1}) > $W(\text{CNDippAr})_6$ (20100 cm^{-1}) > $W(\text{CNDipp}^{\text{CC}}\text{Ar})_6$ (18900 cm^{-1}) in toluene. The addition of naphthyl substituents enables orthogonal ligand conjugation, with an absorption maximum of $W(\text{CN-1-(2-}^i\text{Pr)-Naph})_6$ at 19600 cm^{-1} in toluene.

Matching these absorption shifts, the emission spectra originating from ³MLCT states red-shift with extended ligand aromaticity. The emission maxima λ_{max} shift from $W(\text{CNDipp})_6$ (17300 cm^{-1}) > $W(\text{CNDippAr})_6$ (16100 cm^{-1}) > $W(\text{CNDipp}^{\text{CC}}\text{Ar})_6$ (15300 cm^{-1}) in toluene. This emission shift increases in polar THF solvent for extended ligand systems, with an additional red-shift of 375 cm^{-1} in $W(\text{CNDippAr})_6$ and a red-shift of 570 cm^{-1} in $W(\text{CNDipp}^{\text{CC}}\text{Ar})_6$. These insights reveal that the conjugated systems observe enhanced excited state dipole stabilization in polar solvent environments.

Emission lifetimes from ³MLCT are comparable between $W(\text{CNDippAr})_6$ and $W(\text{CNDipp}^{\text{CC}}\text{Ar})_6$, ranging 0.3–1.7 μs in toluene. These emission lifetimes are outlived by the orthogonal $W(\text{CN-1-(2-}^i\text{Pr)-Naph})_6$ species, which represents the longest excited state lifetime for our library of $W(\text{CNAr})_6$ species at 3.83 μs . These excited state emission lifetimes rely heavily on solvent polarity, indicating a reliance of excited state distortions on solvent environment. The excited state lifetimes shorten 15-77% for $W(\text{CNDippAr})_6$ species and shorten 20-98% for $W(\text{CNDipp}^{\text{CC}}\text{Ar})_6$ when the solvent is exchanged for polar THF. The excited state decay lifetimes are governed by nonradiative decay rates (k_{nr}) which increase in

polar solvents (10-60% increase from toluene to THF). The photoluminescence quantum yields for $W(\text{CNDipp}^{\text{CC}}\text{Ar})_6$ depend on the π -accepting ability of the secondary aryl group, observing a decrease for $\text{Ar} = 1\text{-Naph}, 9\text{-Phen},$ and Ph^{CN} substituents ($\Phi_{\text{PL}} = 0.23\text{-}0.30$) and accessing much larger values for $\text{Ar} = \text{Ph}^{\text{OMe}}$ substituent ($\Phi_{\text{PL}} = 0.78$). These values vary more significantly than those for $W(\text{CNDippAr})_6$ ($\Phi_{\text{PL}} = 0.41\text{-}0.44$).

With these proposed excited state shifts, the excited state reduction potentials of $W(\text{CNDipp}^{\text{CC}}\text{Ar})_6$ were evaluated to compare with our precedent work. The electrochemically reversible $W^{[+/0]}$ couples are less negative in the alkenyl-bridged ligands, ranging $E^\circ = -0.47$ to -0.30 V vs $\text{Fc}^{[+/0]}$ in $W(\text{CNDipp}^{\text{CC}}\text{Ar})_6$. This feature shifts cathodically with a decrease in electron-withdrawing character of the distal aromatic system. The E_{00} energies span a small range of 1.93 to 2.01 eV. Resulting from these constituent properties, the excited state reduction potentials for $W(\text{CNDipp}^{\text{CC}}\text{Ar})_6$ species span $E(W^+/*W^0) = -2.19$ to -2.43 V vs $\text{Fc}^{[+/0]}$. Alongside these species, $W(\text{CN-1-(2-}^i\text{Pr)-Naph})_6$ was evaluated to $E(W^+/*W^0) = -2.49$ V vs $\text{Fc}^{[+/0]}$, corresponding to the anodically shifted $E^\circ(W^{[+/0]}) = -0.47$ V vs $\text{Fc}^{[+/0]}$. The modular tunability of these systems highlights their utility for directed applications in organic synthesis.

Photoredox Catalysis for Synthetic Chemistry

After three generations of insight tuning the excited state properties of $W(\text{CNAr})_6$ complexes, we explored application of these species for targeted applications in synthetic organic chemistry. $W(\text{CNAr})_6$ ($\text{Ar} = \text{Dipp}, \text{DippPh}^{\text{OMe}3}, \text{DippPh}^{\text{OMe}2}, \text{DippPh}^{\text{Ph}}, \text{Dipp}^{\text{CC}}\text{Ph}^{\text{OMe}}$) were irradiated with 1-(2-iodobenzyl)-pyrrole (IBP) and/or 1-(2-bromobenzyl)-pyrrole (BBP) in d_6 -benzene to generate the cyclized 5*H*-pyrrolo[2,1-*a*]isoindol product *via* base-promoted homolytic aromatic substitution (BHAS) catalysis in presence of excess 2,2,6,6-tetramethylpyridine. These substrates were selected as generalizable challenging substrates for synthetic

organic transformations, with IBP [$E^0(\text{Ph-I}^{0/-}) = -2.64 \text{ V vs Fc}^{+/0}$] and BBP [$E^0(\text{Ph-Br}^{0/-}) = -2.84 \text{ V vs Fc}^{+/0}$]. Turnover numbers up to 17 (for Ar = DippPh^{OMe2}) illustrate that these species are competent catalytic photoredox agents, amenable to activation with visible light (445 nm) irradiation (**Table 2.2**). The quenching rates (k_q) of *W(CNAr)₆ by IBP/BBP were interrogated using Stern-Volmer quenching kinetics to evaluate diffusion-limited reactivity (**Table 2.3**).³⁹

We proposed that cage escape limited our overall photoredox activity (**Figure 3.1**). Adapting insights from our prior work mediating EET versus ET,³⁶ the reaction solvent (d₆-benzene) was exchanged for 1,2-difluorobenzene (DFB) and solvated electrolyte [ⁿBu₄N][PF₆] was added to enhance charge separation in *W(CNDipp)₆. This work demonstrated that the overall reaction yield was enhanced in DFB solvent conditions, increasing from 11 TON to 17 TON after 1-hr irradiation (**Table 3.3**). Luminescence was rapidly quenched in our reaction conditions that employed a solvated electrolyte, which terminated our primary reaction mechanism (<5 min). Stern-Volmer analyses were used to assign the quenching rate of this reaction, evaluating a five-fold increase when the d₆-benzene solvent ($k_q = 6.2 \times 10^7 \text{ M}^{-1} \text{ s}^{-1}$) is exchanged for DFB ($k_q = 3.1 \times 10^8 \text{ M}^{-1} \text{ s}^{-1}$), and an additional enhancement reflecting an order-of-magnitude enhancement with the addition of 0.2 M [ⁿBu₄N][PF₆] ($k_q = 6.4 \times 10^8 \text{ M}^{-1} \text{ s}^{-1}$).⁴³ These insights illustrate that rate-limiting charge separation can be improved with increasingly polar solvent conditions.

Two-Photon Absorption and Reactivity

Motivated by these modular photophysical properties, we evaluated the TPA cross-sections of W(CNDipp^{CC}Ar)₆ complexes at 810 nm (**Table 2.4**). The TPA values of W(CNDipp^{CC}Ar)₆ species are exceptionally high over the range 800-1000 nm, with TPA cross-sections (δ_{810}) measured between 480–1100 GM.³⁹ The luminescence spectra of all W(CNAr)₆ complexes were identical upon one-photon and two-

photon (810 nm) irradiation in toluene, indicating relaxation from the same $^3\text{MLCT}$ state which could be adapted to drive excited state reactivity.

Informed by these TPA absorption measurements, we evaluated whether $\text{W}(\text{CNAr})_6$ complexes could mediate two-photon photoredox catalysis upon NIR irradiation. We prepared the BHAS reaction conditions with IBP substrate optimized for one-photon reactivity and studied $\text{W}(\text{CNAr})_6$, Ar = Dipp and $\text{DippPh}^{\text{OMe}3}$ under 810 nm irradiation (**Table 2.5**). After 12-h of irradiation, $\text{W}(\text{CNDipp})_6$ afforded 56% conversion (TON = 5) and $\text{W}(\text{CNDippPh}^{\text{OMe}3})_6$ afforded 33% conversion (TON = 3), indicating photocatalysis upon 810 nm fs-pulsed irradiation.³⁹ This demonstrates successful utility of NIR irradiation to drive excited state reduction of challenging substrates.

Catalyst Deactivation

Despite the impressive reducing power of these catalysts, the modest catalyst turnover values remain one focal area for improvement. Enhancing catalyst stability relies on identifying and inhibiting these possible deactivation pathways. We have identified that the primary deactivation product for these complexes in benzene solvent is a $\text{WI}_2(\text{CNAr})_5$ oxidative addition product, accessed *via* adverse metal-centered substitution.³⁹ Our subsequent studies in 1,2-difluorobenzene solvent indicating modest activity of this previous deactivation product in polar solvent conditions.⁴³

1.7. Summary and Outlook

In summation, we reflect upon the research advancements from our group that afford earth-abundant photosensitizers with photocatalytic properties that outperform commercial noble-metal photosensitizers. Diagnostic elements about these complexes that enable their high competency as photosensitizers are long-lived $^3\text{MLCT}$ excited state lifetimes, robust photostability, and exceptionally high

molar extinction coefficients. Through synthetic modulation, we demonstrated ease of accessing a sterically encumbered metal center to shield from solvent deactivation, ligand functionalization to red-shift the lowest $^3\text{MLCT}$ energy, and elongation of the $^3\text{MLCT}$ excited state lifetime for photochemical applications.

Multiphotonic reactivity is a developing frontier for inorganic chemistry, and this work represents one thrust in a new focus of catalysts designed for modular synthetic and photophysical studies. Design principles that guided our studies for two-photon absorption include exceptionally high one-photon absorption cross sections, excited state centrosymmetry, and long-lived $^3\text{MLCT}$ excited state lifetimes. Of note, these are many of the same design principles motivate single-photon photochemistry.

Efforts in two-photon sensitization reflect an area ripe for continued development. Interest in two-photon photoredox chemistry stems from the simultaneous and divergent goals to drive thermodynamically challenging reactions while applying steadily lower photon energies. Visible-light absorbing photocatalysts mediate a limited scope of excited-state redox potentials; thus the simultaneous absorption of two or more photons (with fixed energies of 300 kJ mol^{-1})⁸ serves to circumvent this and drive increasingly challenging reactions while maintaining high substrate selectivity. We remain optimistic that near-infrared irradiation is useful to drive photoredox chemistry in colored substrates, whose absorption profiles obstruct sensitization of visible-light photosensitizers.

Identifying photosensitizers with large two-photon absorption cross-sections empowers diverse functionality in bioimaging, photodynamic therapy, and additive manufacturing applications. Long irradiation wavelengths afford minimal scattering and deep penetration depth, useful for penetrative bioimaging with confocal or epifluorescence microscopy. Also utilizing this penetrative irradiation, photodynamic therapy harnesses light for localized oxygen sensitization to supply

targeted cell death. Finally, with the popularization of 3D printing, two-photon polymerization and lithography enable applications in additive manufacturing to fabricate highly detailed objects.

1.8. References.

- (1) Gray, H. B. Powering the Planet with Solar Fuel. *Nature Chemistry* **2009**, *1* (1), 7–7.
- (2) Lewis, N. S.; Nocera, D. G. Powering the Planet: Chemical Challenges in Solar Energy Utilization. *Proc Natl Acad Sci USA* **2006**, *103* (43), 15729.
- (3) Prier, C. K.; Rankic, D. A.; MacMillan, D. W. C. Visible Light Photoredox Catalysis with Transition Metal Complexes: Applications in Organic Synthesis. *Chem. Rev.* **2013**, *113* (7), 5322–5363.
- (4) Shaw, M. H.; Twilton, J.; MacMillan, D. W. C. Photoredox Catalysis in Organic Chemistry. *J. Org. Chem.* **2016**, *81* (16), 6898–6926.
- (5) Koike, T.; Akita, M. Visible-Light Radical Reaction Designed by Ru- and Ir-Based Photoredox Catalysis. *Inorg. Chem. Front.* **2014**, *1* (8), 562–576.
- (6) Khalil, M.; Gunlazuardi, J.; Ivandini, T. A.; Umar, A. Photocatalytic Conversion of CO₂ Using Earth-Abundant Catalysts: A Review on Mechanism and Catalytic Performance. *Renewable and Sustainable Energy Reviews* **2019**, *113*, 109246.
- (7) Sinha, N.; Pfund, B.; Wegeberg, C.; Prescimone, A.; Wenger, O. S. Cobalt(III) Carbene Complex with an Electronic Excited-State Structure Similar to Cyclometalated Iridium(III) Compounds. *J. Am. Chem. Soc.* **2022**, *144* (22), 9859–9873.
- (8) Glaser, F.; Kerzig, C.; Wenger, O. S. Multi-Photon Excitation in Photoredox Catalysis: Concepts, Applications, Methods. *Angewandte Chemie International Edition* **2020**, *59* (26), 10266–10284.

- (9) Büldt, L. A.; Wenger, O. S. Chromium(0), Molybdenum(0), and Tungsten(0) Isocyanide Complexes as Luminophores and Photosensitizers with Long-Lived Excited States. *Angew. Chem. Int. Ed.* **2017**, *56* (21), 5676–5682.
- (10) Glaser, F.; Wenger, O. S. Red Light-Based Dual Photoredox Strategy Resembling the Z-Scheme of Natural Photosynthesis. *JACS Au* **2022**, *2* (6), 1488–1503.
- (11) Wegeberg, C.; Wenger, O. S. Luminescent Chromium(0) and Manganese(I) Complexes. *Dalton Trans.* **2022**, *51* (4), 1297–1302.
- (12) Wegeberg, C.; Häussinger, D.; Wenger, O. S. Pyrene-Decoration of a Chromium(0) Tris(Diisocyanide) Enhances Excited State Delocalization: A Strategy to Improve the Photoluminescence of 3d⁶ Metal Complexes. *J. Am. Chem. Soc.* **2021**, *143* (38), 15800–15811.
- (13) Herr, P.; Kerzig, C.; Larsen, C. B.; Häussinger, D.; Wenger, O. S. Manganese(I) Complexes with Metal-to-Ligand Charge Transfer Luminescence and Photoreactivity. *Nature Chemistry* **2021**, *13* (10), 956–962.
- (14) Bilger, J. B.; Kerzig, C.; Larsen, C. B.; Wenger, O. S. A Photorobust Mo(0) Complex Mimicking [Os(2,2'-Bipyridine)₃]²⁺ and Its Application in Red-to-Blue Upconversion. *J. Am. Chem. Soc.* **2021**, *143* (3), 1651–1663.
- (15) Kübler, J. A.; Pfund, B.; Wenger, O. S. Zinc(II) Complexes with Triplet Charge-Transfer Excited States Enabling Energy-Transfer Catalysis, Photoinduced Electron Transfer, and Upconversion. *JACS Au* **2022**, *2* (10), 2367–2380.
- (16) Ilic, A.; Schwarz, J.; Johnson, C.; de Groot, L. H. M.; Kaufhold, S.; Lomoth, R.; Wärnmark, K. Photoredox Catalysis *via* Consecutive ²LMCT- and

³MLCT-Excitation of an Fe(III/II)-N-Heterocyclic Carbene Complex. *Chem. Sci.* **2022**, *13* (32), 9165–9175.

(17) Schwarz, J.; Ilic, A.; Johnson, C.; Lomoth, R.; Wärnmark, K. High Turnover Photocatalytic Hydrogen Formation with an Fe(III) N-Heterocyclic Carbene Photosensitiser. *Chem. Commun.* **2022**, *58* (35), 5351–5354.

(18) Chábera, P.; Kjaer, K. S.; Prakash, O.; Honarfar, A.; Liu, Y.; Fredin, L. A.; Harlang, T. C. B.; Lidin, S.; Uhlig, J.; Sundström, V.; Lomoth, R.; Persson, P.; Wärnmark, K. Fe^{II} Hexa N-Heterocyclic Carbene Complex with a 528 Ps Metal-to-Ligand Charge-Transfer Excited-State Lifetime. *J. Phys. Chem. Lett.* **2018**, *9* (3), 459–463.

(19) Kaufhold, S.; Rosemann, N. W.; Chábera, P.; Lindh, L.; Bolaño Losada, I.; Uhlig, J.; Pascher, T.; Strand, D.; Wärnmark, K.; Yartsev, A.; Persson, P. Microsecond Photoluminescence and Photoreactivity of a Metal-Centered Excited State in a Hexacarbene–Co(III) Complex. *J. Am. Chem. Soc.* **2021**, *143* (3), 1307–1312.

(20) Kjær, K. S.; Kaul, N.; Prakash, O.; Chábera, P.; Rosemann, N. W.; Honarfar, A.; Gordivska, O.; Fredin, L. A.; Bergquist, K.-E.; Häggström, L.; Ericsson, T.; Lindh, L.; Yartsev, A.; Styring, S.; Huang, P.; Uhlig, J.; Bendix, J.; Strand, D.; Sundström, V.; Persson, P.; Lomoth, R.; Wärnmark, K. Luminescence and Reactivity of a Charge-Transfer Excited Iron Complex with Nanosecond Lifetime. *Science* **2019**, *363* (6424), 249–253.

(21) Chábera, P.; Liu, Y.; Prakash, O.; Thyraug, E.; Nahhas, A. E.; Honarfar, A.; Essén, S.; Fredin, L. A.; Harlang, T. C. B.; Kjær, K. S.; Handrup, K.; Ericson, F.; Tatsuno, H.; Morgan, K.; Schnadt, J.; Häggström, L.; Ericsson, T.; Sobkowiak, A.; Lidin, S.; Huang, P.; Styring, S.; Uhlig, J.; Bendix, J.; Lomoth, R.; Sundström, V.; Persson, P.; Wärnmark, K. A Low-Spin Fe(III) Complex with

100-Ps Ligand-to-Metal Charge Transfer Photoluminescence. *Nature* **2017**, *543* (7647), 695–699.

(22) Braun, J. D.; Lozada, I. B.; Kolodziej, C.; Burda, C.; Newman, K. M. E.; van Lierop, J.; Davis, R. L.; Herbert, D. E. Iron(II) Coordination Complexes with Panchromatic Absorption and Nanosecond Charge-Transfer Excited State Lifetimes. *Nat. Chem.* **2019**, *11* (12), 1144–1150.

(23) Zhang, Y.; Lee, T. S.; Favale, J. M.; Leary, D. C.; Petersen, J. L.; Scholes, G. D.; Castellano, F. N.; Milsmann, C. Delayed Fluorescence from a Zirconium(IV) Photosensitizer with Ligand-to-Metal Charge-Transfer Excited States. *Nature Chemistry* **2020**, *12* (4), 345–352.

(24) Zhang, Y.; Petersen, J. L.; Milsmann, C. A Luminescent Zirconium(IV) Complex as a Molecular Photosensitizer for Visible Light Photoredox Catalysis. *J. Am. Chem. Soc.* **2016**, *138* (40), 13115–13118.

(25) Qiao, Y.; Schelter, E. J. Lanthanide Photocatalysis. *Acc. Chem. Res.* **2018**, *51* (11), 2926–2936.

(26) Leis, W.; Argüello Cordero, M. A.; Lochbrunner, S.; Schubert, H.; Berkefeld, A. A Photoreactive Iron(II) Complex Luminophore. *J. Am. Chem. Soc.* **2022**, *144* (3), 1169–1173.

(27) Pal, A. K.; Li, C.; Hanan, G. S.; Zysman-Colman, E. Blue-Emissive Cobalt(III) Complexes and Their Use in the Photocatalytic Trifluoromethylation of Polycyclic Aromatic Hydrocarbons. *Angew. Chem. Int. Ed.* **2018**, *57* (27), 8027–8031.

(28) Aydogan, A.; Bangle, R. E.; Cadranet, A.; Turlington, M. D.; Conroy, D. T.; Cauët, E.; Singleton, M. L.; Meyer, G. J.; Sampaio, R. N.; Elias, B.; Troian-Gautier, L. Accessing Photoredox Transformations with an Iron(III)

Photosensitizer and Green Light. *J. Am. Chem. Soc.* **2021**, *143* (38), 15661–15673.

(29) Glaser, F.; Wenger, O. S. Recent Progress in the Development of Transition-Metal Based Photoredox Catalysts. *Coordination Chemistry Reviews* **2020**, *405*, 213129.

(30) Larsen, C. B.; Wenger, O. S. Photoredox Catalysis with Metal Complexes Made from Earth-Abundant Elements. *Chem. Eur. J.* **2018**, *24* (9), 2039–2058.

(31) Chábera, P.; Lindh, L.; Rosemann, N. W.; Prakash, O.; Uhlig, J.; Yartsev, A.; Wärnmark, K.; Sundström, V.; Persson, P. Photofunctionality of Iron(III) N-Heterocyclic Carbenes and Related d^5 Transition Metal Complexes. *Coordination Chemistry Reviews* **2021**, *426*, 213517.

(32) Wenger, O. S. Photoactive Complexes with Earth-Abundant Metals. *J. Am. Chem. Soc.* **2018**, *140* (42), 13522–13533.

(33) Hockin, B. M.; Li, C.; Robertson, N.; Zysman-Colman, E. Photoredox Catalysts Based on Earth-Abundant Metal Complexes. *Catal. Sci. Technol.* **2019**, *9* (4), 889–915.

(34) Glaser, F.; Kerzig, C.; Wenger, O. S. Sensitization-Initiated Electron Transfer *via* Upconversion: Mechanism and Photocatalytic Applications. *Chem. Sci.* **2021**, *12* (29), 9922–9933.

(35) Gray, H. B.; Mann, K. R.; Lewis, N. S.; Thich, J. A.; Richman, R. M. Photochemistry of Metal-Isocyanide Complexes and Its Possible Relevance to Solar Energy Conversion. In *Inorganic and Organometallic Photochemistry; Advances in Chemistry*; American Chemical Society, **1978**; Vol. 168, pp 44–56.

(36) Sattler, W.; Ener, M. E.; Blakemore, J. D.; Rachford, A. A.; LaBeaume, P. J.; Thackeray, J. W.; Cameron, J. F.; Winkler, J. R.; Gray, H. B. Generation of

Powerful Tungsten Reductants by Visible Light Excitation. *J. Am. Chem. Soc.* **2013**, *135* (29), 10614–10617.

(37) Sattler, W.; Henling, L. M.; Winkler, J. R.; Gray, H. B. Bespoke Photoreductants: Tungsten Arylisocyanides. *J. Am. Chem. Soc.* **2015**, *137* (3), 1198–1205.

(38) Takematsu, K.; Wehlin, S. A. M.; Sattler, W.; Winkler, J. R.; Gray, H. B. Two-Photon Spectroscopy of Tungsten(0) Arylisocyanides Using Nanosecond-Pulsed Excitation. *Dalton Trans.* **2017**, *46* (39), 13188–13193.

(39) Edkins, R. M.; Bettington, S. L.; Goeta, A. E.; Beeby, A. Two-Photon Spectroscopy of Cyclometalated Iridium Complexes. *Dalton Trans.* **2011**, *40* (47), 12765.

(40) Kvapilová, H.; Sattler, W.; Sattler, A.; Sazanovich, I. V.; Clark, I. P.; Towrie, M.; Gray, H. B.; Záliš, S.; Vlček, A. Electronic Excited States of Tungsten(0) Arylisocyanides. *Inorg. Chem.* **2015**, *54* (17), 8518–8528.

(41) Fajardo, J.; Schwan, J.; Kramer, W. W.; Takase, M. K.; Winkler, J. R.; Gray, H. B. Third-Generation W(CNAr)₆ Photoreductants (CNAr = Fused-Ring and Alkynyl-Bridged Arylisocyanides). *Inorg. Chem.* **2021**, *60* (6), 3481–3491.

(42) Fajardo, J.; Barth, A. T.; Morales, M.; Takase, M. K.; Winkler, J. R.; Gray, H. B. Photoredox Catalysis Mediated by Tungsten(0) Arylisocyanides. *J. Am. Chem. Soc.* **2021**, *143* (46), 19389–19398.

(43) Barth, A. T.; Morales, M.; Winkler, J. R.; Gray, H. B. Photoredox Catalysis Mediated by Tungsten(0) Arylisocyanides in 1,2-Difluorobenzene. *Inorg. Chem.* **2022**, *61* (19), 7251–7255.

2 Photoredox Catalysis Mediated by Tungsten(0) Arylisocyanides

Reprinted with permission from *J. Am. Chem. Soc.* **2021**, 143, 46, 19389–19398.

Copyright 2021 American Chemical Society.

2.1. Abstract

$W(CNAr)_6$ (CNAr = arylisocyanide) photoreductants catalyze base-promoted homolytic aromatic substitution (BHAS) of 1-(2-iodobenzyl)-pyrrole in deuterated benzene. Moderate to high efficiencies correlate with $W(CNAr)_6$ excited-state reduction potentials upon one-photon 445-nm excitation, with 10 mol % loading of the most powerful photoreductants $W(CNDipp)_6$ (CNDipp = 2,6-diisopropylphenylisocyanide) and $W(CNDippPh^{OMe3})_6$ (CNDippPh^{OMe3} = 4-(3,4,5-trimethoxyphenyl)-2,6-diisopropylphenylisocyanide) affording nearly complete conversion. Stern-Volmer quenching experiments indicated that catalysis is triggered by substrate reductive dehalogenation. Taking advantage of the large two-photon absorption (TPA) cross sections of $W(CNAr)_6$ complexes, we found that photocatalysis can be driven with femtosecond-pulsed 810-nm excitation. For both one- and two-photon excitation, photocatalysis was terminated by the formation of seven-coordinate W^{II} -diiodo [$WI_2(CNAr)_5$] complexes. Notably, we discovered that $W(CNDipp)_6$ can be regenerated by chemical reduction of $WI_2(CNDipp)_5$ with excess ligand present in solution.

2.2. Introduction

Owing in part to low reorganization energies for electron transfers from relatively long-lived metal-to-ligand charge transfer (MLCT) excited states, Ru^{II} polypyridines, cyclometalated Ir^{III} 2-phenylpyridines (ppy), and their derivatives

have been widely employed in photoredox catalytic cycles.^{1–3} Complexes of earth-abundant metals, most notably Cu^{I} α -diimines/phosphines,⁴ Zr^{IV} bis(pyrrolyl)pyridines,⁵ Ce^{III} guanidinate(s)-amide(s),⁶ and W^{VI} Schiff base dioxos,⁷ also have shown great promise as redox photosensitizers.

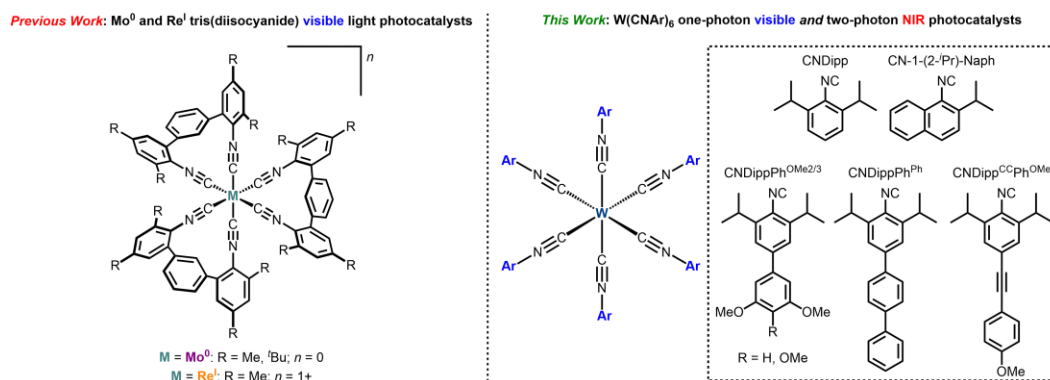


Figure 2.1. $[\text{M}(\text{CN}^{\text{R}}\text{Ar}_3\text{NC})_3]^n$ (refs. 15,16) and $\text{W}(\text{CNAr})_6$ homoleptic arylisocyanide photocatalysts.

In work over many years, we have demonstrated that homoleptic tungsten(0) arylisocyanides (**Figure 2.1**) are stronger photoreductants than the aforementioned Ru^{II} and Ir^{III} complexes; and, notably, $\text{W}(\text{CNAr})_6$ complexes possess intense visible absorptions ($\epsilon_{\lambda, \text{max}} \sim 10^4\text{--}10^5 \text{ M}^{-1} \text{ cm}^{-1}$) attributable to transitions to MLCT excited states with E° ($\text{W}^+/*\text{W}^0$) = -2.2 to -3.0 V vs $\text{Fc}^{[+0]}$ (* denotes the lowest energy MLCT excited state; Fc = ferrocene).^{8–12} With microsecond lifetimes (τ) and large photoluminescence quantum yields (ϕ_{PL}), these $*\text{W}(\text{CNAr})_6$ reagents efficiently reduce thermodynamically challenging substrates, including anthracene⁹ and acetophenone.¹⁰

Of direct relevance to our work, Wenger and co-workers have investigated Cr^0 and Mo^0 tris(diisocyanides) $\text{M}(\text{CN}^{\text{R}}\text{Ar}_3\text{NC})_3$ ($R = \text{Me}, \text{tBu}$; **Figure 2.1**); these complexes have remarkably robust, long-lived excited states with formal potentials [E° ($\text{Cr}^+/*\text{Cr}^0$) = -2.43 V vs $\text{Fc}^{[+0]}$ and E° ($\text{Mo}^+/*\text{Mo}^0$) $\approx -2.6 \text{ V}$ vs

$\text{Fc}^{[+/0]}$] more negative than that of $\text{fac-}^*\text{Ir}(\text{ppy})_3$ ($E^\circ(\text{Ir}^{4+}/^*\text{Ir}^{3+}) = -2.1$ V vs $\text{Fc}^{[+/0]}$).¹³⁻¹⁵ Notably, $\text{Mo}(\text{CN}^{\text{R}}\text{Ar}_3\text{NC})_3$ complexes photocatalyze the rearrangement of acyl cyclopropanes to 2,3-dihydrofurans (R = Me) as well as intramolecular base-promoted homolytic aromatic substitution (BHAS) of aryl iodides (R = ^tBu), reactions that are out of the potential range of $\text{fac-}^*\text{Ir}(\text{ppy})_3$. It also is of interest that the photocatalytic performance of isoelectronic $[\text{Re}(\text{CN}^{\text{Me}}\text{Ar}_3\text{NC})_3]^+$ (**Figure 2.1**) for dehalogenation of halobenzenes is similar to that of $\text{fac-}^*\text{Ir}(\text{ppy})_3$.¹⁶

In light of these findings, we decided to try our $\text{W}(\text{CNAr})_6$ complexes as photoreductants in BHAS catalytic cycles. While $\text{W}(\text{CNAr})_6$ and $\text{Mo}(\text{CN}^{\text{R}}\text{Ar}_3\text{NC})_3$ possess comparable ground- and excited-state properties (**Table 2.1**), employing monodentate arylisocyanides loomed as potentially problematic, given that seven-coordinate M^{II} arylisocyanides such as $[\text{MX}(\text{CNPh})_6]^+$ (M = Mo, W; X = Cl, I) are products of $\text{M}(\text{CNPh})_6$ oxidation.¹⁷⁻¹⁹ Furthermore, Wenger and co-workers noted that deactivation via formation of higher coordinate complexes likely was responsible for the lower efficiencies of $\text{Mo}(\text{CN}^{\text{Me}}\text{Ar}_3\text{NC})_3$ versus $\text{Mo}(\text{CN}^{\text{tBu}}\text{Ar}_3\text{NC})_3$ in photoredox catalysis, with the less sterically shielded complex being more susceptible to nucleophilic attack on the Mo^{I} center by the iodide generated upon substrate reductive dehalogenation.¹⁵

That said, several observations suggested that $\text{W}(\text{CNAr})_6$ complexes might be competent photoredox catalysts. One was that photosubstitution quantum yields (ϕ_{PS}) for CNAr displacement upon 436-nm irradiation of $\text{W}(\text{CNAr})_6$ in neat pyridine solution decreased greatly upon increasing the ligand sterics from phenylisocyanide (Ar = Ph, $\phi_{\text{PS}} = 0.011$) to 2,6-diisopropylphenylisocyanide (CNDipp, $\phi_{\text{PS}} = 0.003$), indicating that associative pyridine substitution occurs in the $^*\text{W}(\text{CNAr})_6$ reaction.^{17,18} Additionally, although 436-nm irradiation of $\text{W}(\text{CNPh})_6$ in CHCl_3 solution afforded the W^{II} seven-coordinate product $[\text{WCl}(\text{CNPh})_6]^+$, similar irradiation of $\text{W}(\text{CNDipp})_6$ instead yielded the six-

coordinate cation $[\text{W}(\text{CNDipp})_6]^+$.^{17,18} Taken together, these findings indicate that the use of bulky 2,6-isopropyl-substituted monodentate arylisocyanides likely would provide enough steric protection to enable efficient BHAS photocatalysis.

In prior work we demonstrated that three $\text{W}(\text{CNAr})_6$ photoreductants exhibit extremely large two-photon absorption (TPA) cross sections ($\delta > 10^3 \text{ GM}$).²⁰ In the context of photoredox catalysis, near-infrared (NIR) two-photon excitation can be used to generate reactive $\text{W}(\text{CNAr})_6$ MLCT excited states without competitive absorption or photoreactivity by the substrate. Also of great interest is the emerging technology of two-photon photochemistry in nano- to microscale 3D printing, wherein multiphoton-triggered free-radical polymerization creates cross-linked polymeric materials with extremely high spatial resolution ($< 100 \text{ nm}$).²¹ However, a current challenge for the advancement of this field is discovery of new photoinitiators with large TPA cross-sections.^{21a} Herein, we report large δ values for eight additional $\text{W}(\text{CNAr})_6$ photoreductants and demonstrate their capacity to generate organic radicals upon two-photon ultrafast laser excitation. Of note, $\text{W}(\text{CNAr})_6$ complexes are capable of driving both one-photon visible and two-photon NIR BHAS photoredox catalysis.

2.3. Results and Discussion

$\text{W}(\text{CNAr})_6$ One-Photon Photoredox Catalysis. In addition to the parent complex, $\text{W}(\text{CNDipp})_6$, five representative photoreductants from two subsequent generations of $\text{W}(\text{CNAr})_6$ compounds were investigated. From the oligoarylisocyanide series, we elected to explore $\text{W}(\text{CNDippPh}^{\text{OMe}2})_6$ and $\text{W}(\text{CNDippPh}^{\text{OMe}3})_6$, as the methoxy substituents impart greater solubility in a variety of solvents. We also studied $\text{W}(\text{CNDippPh}^{\text{Ph}})_6$ to see how a more radially extended aromatic system affects reactivity. And finally, we included $\text{W}(\text{CNDipp}^{\text{CCPh}^{\text{OMe}}})_6$ and $\text{W}(\text{CN-1-(2-}i\text{Pr)-Naph})_6$ in our investigation, as they are very strong photoreductants with among the longest excited-state lifetimes of all

W(CNAr)₆ complexes. Relevant properties of the W(CNAr)₆ photocatalysts are set out in **Table 2.1**.

Previously reported ground-state electrochemical data for all W(CNAr)₆ complexes in this study were collected under slightly different conditions. For consistency in comparisons of ground-state W^[+/0] and excited-state W^{+/*}W⁰ formal potentials, we acquired cyclic voltammograms (CVs) for W(CNDipp)₆, W(CNDippPh^{OMe3})₆, and W(CNDippPh^{Ph})₆ under conditions analogous to those for W(CNDipp^{CC}Ph^{OMe})₆ and W(CN-1-(2-ⁱPr)-Naph)₆. The full CVs of these complexes are typical of W(CNAr)₆ compounds,^{12,19,22} with reversible W^[+/0] couples exhibiting scan-rate dependences indicating diffusion-controlled processes. The revised ground-state and excited-state formal potentials are in **Table 2.1**. Because E° (W^[+/0]) values range from -0.42 to -0.56 V vs Fc^[+/0], strong sacrificial reductants would be needed for regeneration of W(CNAr)₆ in some photocatalytic cycles. For that reason, we chose to explore BHAS organic reactions, as they simplify photoredox cycles by obviating the need for sacrificial reductants.

As a starting point, we examined the intramolecular photoreaction of BHAS substrate 1-(2-iodobenzyl)-pyrrole (50 mM) in the presence of ca. 5 mol % W(CNAr)₆ and 2 equivalents (equiv) of 2,2,6,6-tetramethylpiperidine (TMP) in C₆D₆ (**Table 2.2**). Under similar conditions, Mo(CN^RAr₃NC)₃ efficiently catalyzed the reaction upon irradiation at 470 nm (14 W) for 1 h (**Table 2.2**, entry 12).¹⁵ Compared to this benchmark, 445-nm irradiation (6 W) of the parent complex W(CNDipp)₆ for 1 h afforded 62% conversion to the cyclized product (by ¹H NMR spectroscopy; **Table 2.2**, entry 2). This conversion corresponds to a turnover number (TON) of 11, demonstrating that W(CNDipp)₆ is a photocatalyst for the BHAS reaction. A colorless crystalline solid, identified as 2,2,6,6-tetramethylpiperidinium iodide [H-TMP][I], precipitated from solution within seconds of commencing irradiation. After 1-h irradiation, W(CNDipp)₆ was no

longer present in the reaction mixture, as confirmed by ^1H NMR and UV–visible spectroscopic data. Accordingly, sample luminescence and further conversion were not observed at longer irradiation times (**Figure 2.2**). Instead, free CNDipp and a new set of isopropyl resonances corresponding to a diamagnetic deactivation product (*vide infra*) appeared in the ^1H NMR spectrum.²³

Table 2.1. Properties of $\text{W}(\text{CNAr})_6$ and $\text{Mo}(\text{CN}^{t\text{Bu}}\text{Ar}_3\text{NC})_3$ Photocatalysts^a

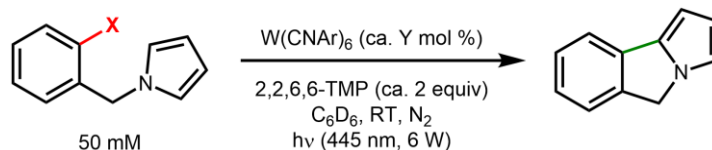
| Photocatalyst | λ_{max}^e | $\epsilon_{\lambda,\text{max}}^f$ | λ_{exc}^e | $\epsilon_{\lambda,\text{exc}}^f$ | τ^g | ϕ_{PL} | E^\bullet ($\text{W}^{[+0]}$) ^h | E^\bullet ($\text{W}^{+/*}\text{W}^0$) ^h |
|---|--------------------------|-----------------------------------|--------------------------|-----------------------------------|----------|--------------------|---|--|
| $\text{W}(\text{CNDipp})_6^b$ | 465 | 9.5×10^4 | 445 | 8.0×10^4 | 0.12 | 0.03 | −0.56 | −2.84 |
| $\text{W}(\text{CNDippPh}^{\text{OMe}_3})_6^b$ | 495 | 1.3×10^5 | 445 | 6.7×10^4 | 1.83 | 0.41 | −0.53 | −2.68 |
| $\text{W}(\text{CNDippPh}^{\text{Ph}})_6^b$ | 506 | 1.6×10^5 | 445 | 7.5×10^4 | 1.53 | 0.44 | −0.52 | −2.60 |
| $\text{W}(\text{CN-1-(2-}^i\text{Pr)-Naph})_6^c$ | 509 | 5.7×10^4 | 445 | 4.6×10^4 | 3.83 | 0.25 | −0.47 | −2.49 |
| $\text{W}(\text{CNDipp}^{\text{CCPh}^{\text{OMe}}})_6^c$ | 518 | 1.6×10^5 | 445 | 5.7×10^4 | 1.82 | 0.78 | −0.42 | −2.43 |
| $\text{Mo}(\text{CN}^{t\text{Bu}}\text{Ar}_3\text{NC})_3^d$ | 400 | 3.0×10^4 | 470 | 2.7×10^4 | 1.29 | 0.20 | −0.46 | −2.7 |

^aCollected from deaerated room temperature toluene solutions. ^bData from ref. 10.

^cData from ref. 12. ^dData from ref. 15 (λ_{max} , $\epsilon_{\lambda,\text{max}}$, and $\epsilon_{\lambda,\text{exc}}$ were estimated from the plot in **Figure 2.2** of this reference; τ is the weighted average lifetime). ^enm.

^f $\text{M}^{-1} \text{cm}^{-1}$. ^g μs . ^hV vs $\text{Fc}^{[+0]}$. Ground-state electrochemical measurements performed in tetrahydrofuran (THF) with 0.1 M [$n\text{Bu}_4\text{N}$][PF_6] supporting electrolyte.

Table 2.2. One-Photon Photoredox Catalysis Mediated by W(CNAr)₆ Complexes^a



| Entry | W(CNAr) ₆ | X | Y | Irrad Time (h) | Conversion (%) ^b | TON |
|-------|--|----|-----|----------------|-----------------------------|-----|
| 1 | W(CNDipp) ₆ | I | 2.5 | 1 | 28 | 11 |
| 2 | W(CNDipp) ₆ | I | 5 | 1 | 62 | 11 |
| 3 | W(CNDipp) ₆ | I | 10 | 4 | 98 | 8 |
| 4 | W(CNDipp) ₆ | Br | 10 | 12 | 14 | 1 |
| 5 | W(CNDippPh ^{OMe3}) ₆ | I | 2.5 | 1 | 42 | 15 |
| 6 | W(CNDippPh ^{OMe3}) ₆ | I | 5 | 4 | 85 | 16 |
| 7 | W(CNDippPh ^{OMe3}) ₆ | I | 10 | 4 | 98 | 9 |
| 8 | W(CNDippPh ^{OMe2}) ₆ | I | 5 | 4 | 88 | 17 |
| 9 | W(CNDippPh ^{Ph}) ₆ | I | 5 | 12 | 84 | 15 |
| 10 | W(CN-1-(2- ^t Pr)-Naph) ₆ | I | 5 | 12 | 42 | 7 |
| 11 | W(CNDipp ^{CC} Ph ^{OMe}) ₆ | I | 5 | 12 | 24 | 4 |
| 12 | Mo(CN ^t BuAr ₃ NC) ₃ ^d | I | 5 | 1 | 100 | 20 |
| 13 | <i>fac</i> -Ir(ppy) ₃ ^{d,e} | I | 5 | 1 | 4 | 1 |
| 14 | W(CNAr) ₆ | I | 5 | <i>c</i> | 0 | 0 |
| 15 | None | I | 0 | 4 | 0 | 0 |

^aReactions performed in J-Young NMR tubes. Irradiation with a high-power blue diode laser. Reported results are from single run experiments. ^bSubstrate conversion calculated by relative integration of the ¹H NMR benzylic resonances of the product and starting material. ^cSample stored in the dark at room temperature (RT) for 4 h. ^dData from ref. 15. Irradiation with a 470 nm LED operating at 14 W. ^eSimilar conversion observed when irradiated at 405 nm instead of 470 nm.

We next explored the photoredox activities of second and third generation W(CNAr)₆ complexes. Interestingly, despite being a slightly weaker photoreductant, W(CNDippPh^{OMe3})₆ was able to drive the BHAS reaction to 85% completion (TON = 16) after 4-h irradiation (**Table 2.2**, entry 6). We found that W(CNDippPh^{OMe2})₆, which has virtually identical ground- and excited-state properties as W(CNDippPh^{OMe3})₆,¹⁰ catalyzed the reaction with similar efficiency

(Table 2.2, entry 8). As occurs during $W(CNDipp)_6$ photocatalysis, $[H-TMP][I]$ precipitated upon progression of the reaction, $W(CNDippPh^{OMe2/3})_6$ complexes were no longer present after 4-h irradiation, and deactivation products appeared (isopropyl resonances attributable to such products were observed in the 1H NMR spectrum).

In contrast to biarylisocyanide photocatalysis, 445-nm irradiation of a BHAS reaction containing ca. 5 mol % $W(CNDippPh^{Ph})_6$ for 4 h only reached 53% conversion (TON = 9; Figure 2.2). However, after 12-h irradiation, conversion to product was about the same as that for $W(CNDippPh^{OMe2/3})_6$ (Figure 2.2; Table 2.2, entry 9). Following this trend, reactions with photoreductants $W(CN-1-(2-^iPr)-Naph)_6$ and $W(CNDipp^{CC}Ph^{OMe})_6$ reached 28% (TON = 5) and 13% (TON = 2) conversion after 4-h irradiation (Figure 2.2); the yields increased to 42% (TON = 7; Table 2.2, entry 10) and 24% (TON = 4; entry 11) after 12 h. Importantly, $W(CNDippPh^{Ph})_6$, $W(CN-1-(2-^iPr)-Naph)_6$, and $W(CNDipp^{CC}Ph^{OMe})_6$ were still present at the 12-h irradiation point (as determined by 1H NMR, UV-vis, and the luminescence of photoredox samples), suggesting that photocatalyst decomposition did not limit conversion.

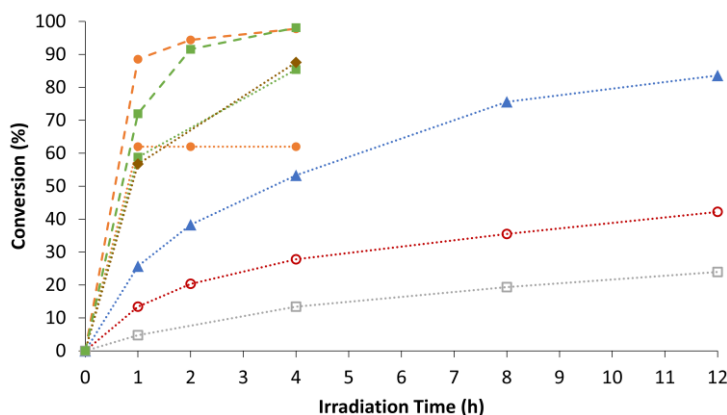


Figure 2.2. Time profiles of the BHAS photoredox reaction catalyzed by $W(CNAr)_6$ employing one-photon 445-nm excitation. Dotted and dashed lines, which are provided as guides for the eye only, represent ca. 5 and 10 mol %

W(CNAr)₆ photocatalyst loading, respectively. Color/marker code: W(CNDipp)₆ (orange; solid circle), W(CNDippPh^{OMe3})₆ (green; solid square), W(CNDippPh^{OMe2})₆ (brown; diamond), W(CNDippPh^{Ph})₆ (blue; triangle), W(CN-1-(2-ⁱPr)-Naph)₆ (red; open circle), W(CNDipp^{CCPh^{OMe}})₆ (gray; open square).

Although their efficiencies were somewhat lower than that for Mo(CN^{*t*Bu}Ar₃NC)₃ at a similar catalyst loading, all investigated W(CNAr)₆ complexes were active photoredox catalysts. Owing in part to more negative excited-state potentials, they performed better than *fac*-Ir(ppy)₃ (**Table 2.2**, entry 13).¹⁵ We emphasize that monitoring substrate solutions in the absence of W(CNAr)₆ or light confirmed that both components were essential for photocatalysis (**Table 2.2**, entries 14 and 15).

Given the favorable results obtained with W(CNDipp)₆ and W(CNDippPh^{OMe3})₆, we investigated the effect of photocatalyst loading on reaction conversion. Decreasing the W(CNAr)₆ loading by half reduced the conversion by half, albeit with comparable TONs (CNDipp: **Table 2.2**, entry 1; CNDippPh^{OMe3}: entry 5).²⁴ Alternatively, doubling the loading to ca. 10 mol % afforded near quantitative substrate conversion (CNDipp: 98%, **Table 2.2**, entry 3; CNDippPh^{OMe3}: 98%, entry 7). Consistent with the high yield achieved with ca. 5 mol % W(CNDippPh^{OMe3})₆, a substantial amount of photocatalyst was present (by ¹H NMR spectroscopy) upon reaction termination.

Encouraged by the above results with 1-(2-iodobenzyl)-pyrrole, we turned our attention to the analogous bromo substrate, 1-(2-bromobenzyl)-pyrrole. Subjecting this substrate to photoredox catalysis conditions with ca. 10 mol % W(CNDipp)₆ loading yielded 14% conversion after 12-h irradiation (**Table 2.2**, entry 4). For comparison, *Mo(CN^{*t*Bu}Ar₃NC)₃, a ca. 100 mV weaker photoreductant, only reached 7% conversion after 18-h irradiation.¹⁵ These results are consistent with reductive dehalogenation by *W(CNAr)₆ as the initial step in

the photodriven BHAS reaction (*vide infra*), as aryl bromides are more difficult to reduce than aryl iodides. Moreover, there was a substantial amount of $W(CNDipp)_6$ remaining after 12-h irradiation, indicating that performance was not limited by catalyst decomposition.

To gain further insight into the above trends among conversion efficiency, irradiation time, and $E^\circ (W^+/*W^0)$, we conducted Stern-Volmer quenching experiments using $W(CNDipp)_6$, $W(CNDippPh^{OMe3})_6$, and $W(CN-1-(2-^iPr)-Naph)_6$ as representative complexes. Although we previously collected photophysical and photochemical data for $W(CNAr)_6$ in toluene and THF solution, we performed Stern-Volmer experiments in benzene solution to mimic the photoredox catalysis conditions as closely as possible and minimize side reactions with intermediate aryl radicals. As the steady-state absorption and luminescence spectra of $W(CNDipp)_6$, $W(CNDippPh^{OMe3})_6$, and $W(CN-1-(2-^iPr)-Naph)_6$ in benzene and toluene are nearly identical, we anticipated the excited-state dynamics would also be very similar in the two solvents. Indeed, transient absorption (TA) spectra showed that $*W(CNAr)_6$ reagents were generated in benzene solution following excitation, and data obtained from time-resolved luminescence decays and TA bleach recoveries ($*W(CNDipp)_6$: 116 ns; $*W(CNDippPh^{OMe3})_6$: 1.76 μ s; $*W(CN-1-(2-^iPr)-Naph)_6$: 3.65 μ s) confirmed that the lifetimes were comparable to those in toluene solution (**Table 2.1**).

Substrate 1-(2-iodobenzyl)-pyrrole quenched the luminescences of $*W(CNDipp)_6$, $*W(CNDippPh^{OMe3})_6$, and $*W(CN-1-(2-^iPr)-Naph)_6$ with varying rate constants (k_q) 6.2×10^7 , 1.3×10^7 , and $2.2 \times 10^6 \text{ M}^{-1} \text{ s}^{-1}$ (**Table 2.3**). Notably, these k_q values are in line with electron-transfer driving forces (ΔG°_{ET}) for reduction of the iodoarene substrate (approximated as $E^\circ (Ph-I^{0/-}) \sim -2.64 \text{ V}$ vs $Fc^{[+/0]}$ for iodobenzene;²⁵ **Table 2.3**). In photoreactions in solutions with 50 mM quencher, the longer lifetimes of $*W(CNDippPh^{OMe3})_6$ and $*W(CN-1-(2-^iPr)-Naph)_6$ account for relatively high initial quenching yields (ϕ_q ; **Table 2.3**).

We also found that 1-(2-bromobenzyl)-pyrrole quenched the luminescence of $^*W(CNDipp)_6$ in benzene solution: k_q ($8.6 \times 10^6 \text{ M}^{-1} \text{ s}^{-1}$) was nearly an order of magnitude smaller than that for 1-(2-iodobenzyl)-pyrrole, as expected for a reaction with lower driving force [$^*W(CNDipp)_6$: $E^\circ (W^+/*W^0) = -2.84 \text{ V}$ vs $Fc^{[+/0]}$; aryl bromide substrate: approximated as $E^\circ (Ph-Br^{[0/-]}) \sim -2.84 \text{ V}$ vs $Fc^{[+/0]}$ for bromobenzene;²⁵ **Table 2.3**]. Unsurprisingly, ϕ_q for the bromo substrate was much lower than that for 1-(2-iodobenzyl)-pyrrole (**Table 2.3**).

The $W(CNAr)_6$ version of Wenger's mechanism for $Mo(CN^{tBu}Ar_3NC)_3$ -mediated BHAS photoredox catalysis is shown in **Figure 2.3**. Following 445-nm excitation of $W(CNAr)_6$, $^*W(CNAr)_6$ rapidly reduced the substrate. The quenching reaction generated $[W(CNAr)_6]^+$ along with halide and the corresponding organic aryl radical. After intramolecular cyclization of the latter, which likely occurred very rapidly, reduction of $[W(CNAr)_6]^+$ by the pyrrole-based radical regenerated the starting W^0 photocatalyst. In the final step, deprotonation of the tricyclic organic cation by TMP yielded the cyclized product and $[H-TMP][X]$, closing the productive cycle. The consumption of $W(CNAr)_6$ during turnover suggests that a decomposition reaction competed with reduction of $[W(CNAr)_6]^+$ by the pyrrole-based radical. Moreover, conversion efficiencies did not track with ϕ_q , indicating that there were additional loss pathways.

Table 2.3. Stern-Volmer Quenching Constants and Reaction Driving Forces^a

| $W(CNAr)_6$ | Quencher | k_q^b | ϕ_q^c | Conversion ^d | $E^\circ (Ph-X^{[0/-]})^{f,g}$ | $E^\circ (W^+/*W^0)^f$ | $\Delta G^\circ_{ET}^h$ |
|-------------------------|----------|-------------------|------------|-------------------------|--------------------------------|------------------------|-------------------------|
| $W(CNDipp)_6$ | | 6.2×10^7 | 0.27 | 62% | -2.64 | -2.84 | -0.20 |
| $W(CNDipp)_6$ | | 8.6×10^6 | 0.05 | 3% ^e | -2.84 | -2.84 | 0 |
| $W(CNDippPh^{OMe3})_6$ | | 1.3×10^7 | 0.54 | 59% | -2.64 | -2.68 | -0.04 |
| $W(CN-1-(2-Pr)-Naph)_6$ | | 2.2×10^6 | 0.30 | 13% | -2.64 | -2.49 | +0.15 |

^aStern-Volmer quenching experiments performed in deaerated room temperature benzene solutions. ^b $\text{M}^{-1} \text{s}^{-1}$. ^cInitial quenching yields for a substrate concentration of 50 mM. ^dAfter 1-h irradiation (445 nm, 6 W) of photoredox reactions with ca. 5 mol % $\text{W}(\text{CNAr})_6$ loading. ^eca. 10 mol % $\text{W}(\text{CNDipp})_6$ loading. ^fV vs $\text{Fc}^{[+0]}$. ^gReduction potentials for iodobenzene and bromobenzene reported in V vs SCE in ref. 25 were converted to V vs $\text{Fc}^{[+0]}$ using the approximation $E^\circ(\text{Fc}^{[+0]}) = +0.4$ V vs SCE. ^heV.

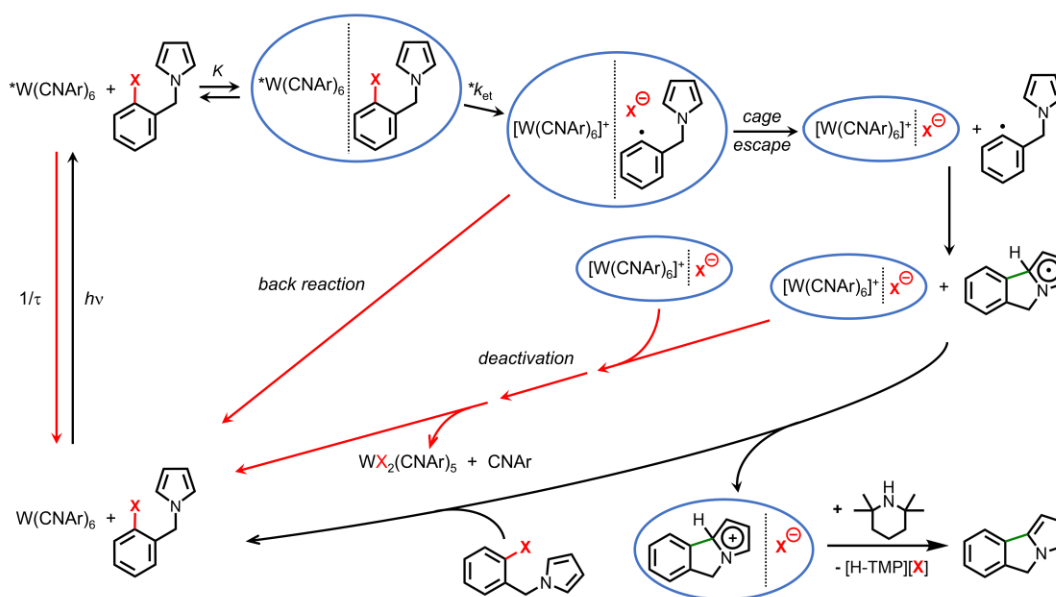


Figure 2.3. Proposed mechanism of BHAS photoredox catalysis in benzene solution mediated by $\text{W}(\text{CNAr})_6$ complexes (adapted from ref. 15). Productive catalysis pathways are shown as black arrows; unproductive back-reaction and deactivation pathways are indicated with red arrows. Electron-transfer quenching of $^*\text{W}(\text{CNAr})_6$ involves formation of a precursor complex (equilibrium constant K) followed by concerted electron transfer and C–X bond cleavage (rate constant $^*k_{\text{et}}$). The observed quenching rate constant is $k_{\text{q}} = K^*k_{\text{et}}$. Ion-pair separation from solvent cages (blue ellipses) is unfavorable in benzene; only the neutral organic radical is likely to escape the solvent cage after quenching.

Given that ground-state $W(CNAr)_6^{[+/0]}$ formal potentials range from -0.42 to -0.56 V vs $Fe^{[+/0]}$, the ΔG°_{ET} values associated with reduction of $[W(CNAr)_6]^+$ by the intermediate tricyclic organic radical also will vary, leading to different rates of $W(CNAr)_6$ regeneration, which in turn likely account for different rates of photocatalyst deactivation via nucleophilic attack of $[W(CNAr)_6]^+$ by the halide anion liberated in the reductive dehalogenation step (*vide infra*).

The BHAS reactions photocatalyzed by $W(CNAr)_6$ complexes are consistent with our amended version of Wenger's mechanism. Under a uniform set of reaction conditions (**Figure 2.2**), two differences are apparent among the $W(CNAr)_6$ complexes: (i) conversion rates tend to decrease as the $*W(CNAr)_6$ reducing power decreases; and (ii) conversion yields are highly variable. The initial 1-(2-iodobenzyl)-pyrrole quenching yields for $W(CNDipp)_6$, $W(CNDippPh^{OMe3})_6$, and $W(CN-1-(2-*i*Pr)-Naph)_6$ are $> 25\%$ and bear no relationship to conversion rates. Slow conversion in the presence of efficient quenching is a hallmark of competition between back reaction and cage escape after quenching. Back reaction is unexpected since reduction of aryl iodides is believed to involve concerted electron transfer and C–I bond cleavage.²⁵ Of relevance here, however, is the report by Savéant that less than unit product-formation quantum yields for concerted C–X bond cleavage can occur during phototriggered reductions of aryl halide substrates.²⁶ Competition between back reaction and cage escape after quenching can rationalize our observation that slower conversion rates correlate with higher back-reaction driving forces (increasing $E^{\circ}(W^{[+/0]})$).

Low cage-escape efficiency likely is responsible for the twenty-fold reduction in product conversion with 1-(2-bromobenzyl)-pyrrole compared to the aryl iodide. A factor of 5.5 was expected on the basis of ϕ_q . In contrast to aryl iodides, reduction of aryl chlorides and bromides is thought to proceed via a two-step mechanism with an intermediate radical anion.²⁵ It is likely, then, that the large reduction in product conversion with the aryl bromide substrate is due to less

efficient quenching coupled with rapid back reaction between $[\text{W}(\text{CNAr})_6]^+$ and $[\text{Ar-Br}]^{[0/-]}$ prior to radical escape from the solvent cage..

The variations in conversion efficiencies and $\text{W}(\text{CNAr})_6$ consumption during catalysis indicate that a $[\text{W}(\text{CNAr})_6]^+$ decomposition pathway competes with productive reaction between the cation and the intermediate aryl radical. $\text{W}(\text{CNDipp})_6$ reaches limiting 62% conversion and full W^0 consumption after 1 h (or less) of irradiation, indicative of a high radical cage-escape yield and rapid $[\text{W}(\text{CNDipp})_6]^+$ decomposition. Doubling the $\text{W}(\text{CNDipp})_6$ loading leads to higher conversion because more time is required to deplete the $\text{W}(\text{CNDipp})_6$ complex. $\text{W}(\text{CmijkNDippPh}^{\text{OMe}3})_6$, $\text{W}(\text{CNDippPh}^{\text{OMe}2})_6$, and $\text{W}(\text{CNDippPh}^{\text{Ph}})_6$ achieve higher conversions (> 80%) than $\text{W}(\text{CNDipp})_6$, albeit more slowly, consistent with diminished radical cage-escape yields after quenching, but more favorable competition between $[\text{W}(\text{CNAr})_6]^+$ decomposition and reduction. Low radical cage-escape efficiency after quenching slows photocatalysis with $\text{W}(\text{CN-1-(2-}^i\text{Pr)-Naph})_6$ and $\text{W}(\text{CNDipp}^{\text{CC}}\text{Ph}^{\text{OMe}})_6$ to the point that limiting conversion is not reached after 12 h of irradiation.

Two-Photon Photoredox Catalysis. All investigated $\text{W}(\text{CNAr})_6$ complexes displayed photoluminescence upon femtosecond-pulsed 810-nm excitation; and $^*\text{W}(\text{CNAr})_6$ emission spectra obtained following one- or two-photon excitation were virtually identical (**Figure 2.4**), confirming that the same long-lived excited triplet ($^3\text{MLCT}$) photoreductant was generated in both cases. In 2-methyl THF solution, $\text{W}(\text{CNDippPh}^{\text{OMe}2/3})_6$ and $\text{W}(\text{CNDippPh}^{\text{Ph}})_6$ exhibited very large two-photon absorption cross sections [$\delta = 1000\text{--}2000 \text{ GM}$ ($1 \text{ GM} = 10^{-50} \text{ cm}^4 \text{ s photon}^{-1} \text{ molecule}^{-1}$)] upon excitation at 812 nm.²⁰ We have extended this work to include TPA cross sections for all three generations of $\text{W}(\text{CNAr})_6$ complexes in toluene solution (810-nm excitation; **Table 2.4**). As δ values for $[\text{Ru}(\text{bpy})_3]^{2+}$ ($\text{bpy} = 2,2'$ -bipyridine; $\delta_{812} = 7 \text{ GM}$)²⁰ and *fac*- $\text{Ir}(\text{ppy})_3$ ($\delta_{800} = 20 \text{ GM}$)²⁷ are orders of magnitude smaller at similar wavelengths, our scalable tungsten complexes have

the potential to displace ruthenium and iridium photosensitizers in two-photon biological imaging, photodynamic therapy, and photoredox catalysis applications (*vide infra*).

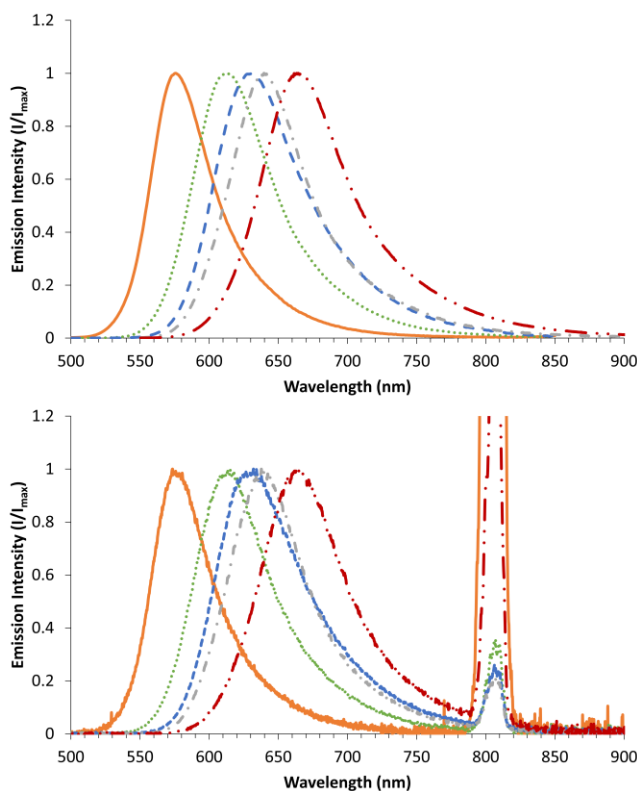


Figure 2.4. Stacked luminescence spectra collected upon one-photon (top) and two-photon (810 nm; bottom) excitation of $W(CNDipp)_6$ (orange; solid trace), $W(CNDippPh^{OMe3})_6$ (green; dotted trace), $W(CNDippPh^{Ph})_6$ (blue; dashed trace), $W(CNDipp^{CC}Ph^{OMe})_6$ (gray; dotted-dashed trace), and $W(CN-1-(2-Pr)-Naph)_6$ (red; double dotted-dashed trace) in room temperature toluene solution. For the bottom spectra, the signal at 810 nm corresponds to scattered excitation light from the femtosecond-pulsed Ti:Sapphire laser.

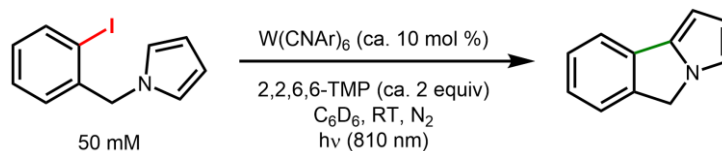
Table 2.4. Two-Photon Absorption (TPA) Cross Sections of $W(CNAr)_6$ Complexes^a

| W(CNAr)₆ | δ₈₁₀ (GM) |
|---|-----------------------------|
| W(CNDipp) ₆ | 230 ± 14 |
| W(CNDippPh) ₆ | 1000 ± 220 |
| W(CNDippPh ^{OMe2}) ₆ | 1100 ± 130 |
| W(CNDippPh ^{OMe3}) ₆ | 970 ± 96 |
| W(CNDippPh ^{Ph}) ₆ | 1900 ± 280 |
| W(CNDipp ^{CC} Ph ^{OMe}) ₆ | 1100 ± 70 |
| W(CNDipp ^{CC} Ph) ₆ | 1100 ± 160 |
| W(CNDipp ^{CC} -1-Naph) ₆ | 1100 ± 180 |
| W(CNDipp ^{CC} -9-Phen) ₆ | 1100 ± 160 |
| W(CNDipp ^{CC} Ph ^{CN}) ₆ | 480 ± 50 |
| W(CN-1-(2- ⁱ Pr)-Naph) ₆ | 180 ± 40 |

^aCollected from complexes in deaerated room temperature toluene solution: fs-pulsed 810-nm excitation (Ti:Sapphire laser); the δ₈₁₀ values are an average of three measurements.

In our exploration of two-photon BHAS photocatalysis, we employed conditions that were optimal for one-photon reactions, namely ca. 10 mol % loading of W(CNDipp)₆ or W(CNDippPh^{OMe3})₆. We found that both complexes catalyzed BHAS of 1-(2-iodobenzyl)-pyrrole upon fs-pulsed 810-nm irradiation, with 56% (TON = 5) and 33% (TON = 3) conversion observed for W(CNDipp)₆ and W(CNDippPh^{OMe3})₆ after 12-h irradiation in C₆D₆ solution, respectively (**Table 2.5**). Owing to differences in laser power and two-photon cross sections, the W(CNDippPh^{OMe3})₆ excitation rate was 1.7 times that for W(CNDipp)₆. The higher W(CNDipp)₆ conversion efficiency with a nearly two-fold lower excitation rate is consistent with a lower cage-escape yield for W(CNDippPh^{OMe3})₆.

Table 2.5. Two-Photon NIR Photoredox Catalysis Mediated by $W(CNDipp)_6$ and $W(CNDippPh^{OMe3})_6$ Complexes^a



| $W(CNAr)_6$ | Irrad Time (h) | Conversion (%) ^b | TON |
|------------------------|----------------|-----------------------------|-----|
| $W(CNDipp)_6$ | 12 | 56 | 5 |
| $W(CNDippPh^{OMe3})_6$ | 12 | 33 | 3 |

^aIrradiation with a fs-pulsed Ti:Sapphire laser. ^bSubstrate conversion calculated by relative integration of the ¹H NMR benzylic resonances of the product and starting material.

In related work, Rovis and co-workers reported that Os^{II} polypyridines function as NIR photoredox catalysts.^{28,29} Interestingly, the reactive Os^{II} MLCT states can be generated via one-photon $S_0 \rightarrow T_1$ NIR excitation. It also is worth noting that photoredox³⁰ and photoisomerization³¹ reactions can be triggered by triplet fusion NIR-to-visible upconversion.

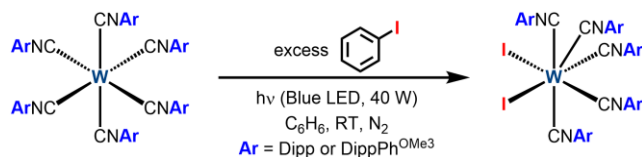
$WI_2(CNAr)_5$ Deactivation Products. We observed that $W(CNAr)_6$ complexes were consumed during catalytic photoredox reactions involving haloaryl substrates. Concomitantly, new sets of diamagnetic isopropyl resonances appeared in ¹H NMR spectra. While one set of resonances was assignable to uncomplexed CNAr, we suspected that the other set belonged to an uncharged, C₆D₆-soluble tungsten complex. We therefore set out to synthesize and characterize one or more deactivation products and establish whether such species could re-enter photocatalytic cycle.

On pursuing the aforementioned products, we found that stoichiometric photoreduction of iodobenzene by $^*W(CNDipp)_6$ in room temperature benzene

solution proceeded over the course of several hours with loss of sample luminescence to yield a new diamagnetic tungsten arylisocyanide complex (**Scheme 2.1**). Of relevance is that the UV–vis and ^1H NMR spectra of this new compound matched those acquired at the termination of $\text{W}(\text{CNDipp})_6$ -mediated photoredox catalysis. Following crystallization by slow evaporation of a concentrated benzene solution, seven-coordinate $\text{WI}_2(\text{CNDipp})_5$ was isolated in 95% yield (XRD structure; **Figure 2.5**).

The geometry of $\text{WI}_2(\text{CNDipp})_5$ in the solid state approximates a capped octahedron, where one CNDipp serves as the capping ligand to the tris(CNDipp) face, and the uncapped face is occupied by the remaining CNDipp and two iodide ligands. In this regard, its structure is analogous to that of $\text{WI}_2(\text{CO})(\text{CN}^t\text{Bu})_4$,³² wherein the carbonyl ligand caps the tris(CN^tBu) face of the octahedron. Interestingly, as in $\text{WI}_2(\text{CO})(\text{CN}^t\text{Bu})_4$, the weakly bound isocyanide (based on its relatively long W–C bond) in $\text{WI}_2(\text{CNDipp})_5$ resides in the uncapped face. It is worth noting that while the related compounds $\text{MoX}_2(\text{CN-}p\text{-tolyl})_5$ ($\text{X} = \text{Cl}, \text{Br}$) have been reported,³³ complexes of the composition $\text{MX}_2(\text{CNR})_5$ ($\text{M} = \text{Mo}, \text{W}$; $\text{X} = \text{halide}$; $\text{R} = \text{alkyl or aryl}$) have seldom been spectroscopically or structurally characterized.³⁴ Seven-coordinate M^{II} ($\text{M} = \text{Mo}, \text{W}$) homoleptic isocyanides $[\text{M}(\text{CNR})_7][\text{X}]_2$,^{19,35} mixed halide-isocyanides $[\text{MX}(\text{CNR})_6][\text{X}]$,^{19,35[c,h],36} and mixed halide-isocyanide-carbonyls $\text{MX}_2(\text{CO})_{5-y}(\text{CNR})_y$ ($y = 2-4$)^{35h,37} are more common. The W–I and W–C bond lengths in $\text{WI}_2(\text{CNDipp})_5$ fall within the range observed for structurally characterized coordination compounds of this latter type.

Scheme 2.1. Synthesis of $\text{WI}_2(\text{CNAr})_5$ Complexes



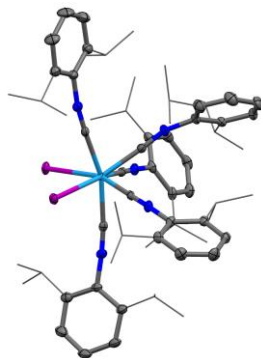


Figure 2.5. Structure of crystalline $WI_2(CNDipp)_5$ with thermal ellipsoids set at 50% probability. Isopropyl groups are presented as wireframes and hydrogen atoms omitted for clarity. Atom color code: W, teal; I, purple; N, blue; C, gray.

In room temperature C_6D_6 solution, $WI_2(CNDipp)_5$ displayed a single set of 1H and ^{13}C NMR resonances for the CNDipp ligands, suggesting that the isocyanides exchange rapidly on the NMR timescale. Such fluxionality is typical of related seven-coordinate (halide-)isocyanide M^{II} complexes ($M = Mo, W$).^{35c} $WI_2(CNDipp)_5$ also exhibited a broad, intense $\nu(CN)$ stretch centered at 2050 cm^{-1} , intermediate between that of uncomplexed CNDipp (2114 cm^{-1}) and $W(CNDipp)_6$ (1938 cm^{-1}), consistent with attenuated π -back-donation from the W^{II} center. Although $WI_2(CNDipp)_5$ absorbs fairly strongly in the region 300–500 nm ($\epsilon_{\lambda, \text{max}} \sim 10^4\text{ M}^{-1}\text{ cm}^{-1}$), the complex did not luminesce when excited at 445 nm, as expected from the observed loss of $W(CNAr)_6$ luminescence during photoredox catalysis.

As with $W(CNDipp)_6$, photoreduction of iodobenzene by $*W(CNDippPh^{OMe3})_6$ in benzene solution formed a product (~95% isolated yield) with UV–vis and 1H NMR spectroscopic signatures reminiscent of those observed in the corresponding post-photoredox catalysis reaction mixtures. Despite numerous attempts, single crystals of the product suitable for XRD analysis could not be grown. However, because it shares similar $^1H/^{13}C$ NMR, UV–vis, IR, and CV data with

$\text{WI}_2(\text{CNDipp})_5$, we suggest that this new complex is $\text{WI}_2(\text{CNDippPh}^{\text{OMe}_3})_5$ (**Scheme 2.1**).

CVs of $\text{WI}_2(\text{CNDipp})_5$ displayed quasi-reversible oxidation and irreversible reduction waves at -0.07 and -2.31 V vs $\text{Fc}^{+/0}$, respectively (**Figure 2.6**), with relative integration revealing that twice the amount of charge was passed in the latter. We therefore assign these as 1-electron $\text{W}^{[3+/2+]}$ and 2-electron $\text{W}^{[2+/0]}$ redox events. In this regard, the electrochemical behavior mirrors that of related $[\text{M}(\text{CNPh})_7]^{2+}$ ($\text{M} = \text{Mo}, \text{W}$) and $[\text{MoI}(\text{CNPh})_6]^+$ complexes.^{19,22,38} Of interest is that oxidation and reduction of $\text{WI}_2(\text{CNDipp})_5$ occurred at more negative potentials, in line with replacement of uncharged π -accepting arylisocyanides by anionic iodide ligands to yield an overall neutral complex. Extrapolation of $[\text{M}(\text{CNPh})_7]^{2+}$ and $[\text{MoI}(\text{CNPh})_6]^+$ formal potentials also indicated that $E^\circ(\text{W}^{[3+/2+]})$ and $E_{\text{p,c}}^\circ(\text{W}^{[2+/0]})$ will be similar to those experimentally determined for $\text{WI}_2(\text{CNDipp})_5$.

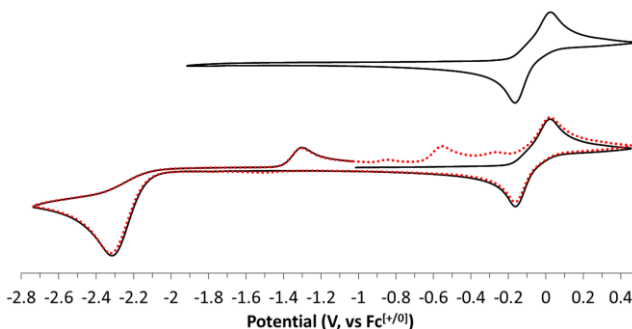


Figure 2.6. Cyclic voltammograms of $\text{WI}_2(\text{CNDipp})_5$ at a scan rate of 100 mV s^{-1} in THF with $0.1 \text{ M } [\text{nBu}_4\text{N}][\text{PF}_6]$ supporting electrolyte (vs $\text{Fc}^{+/0}$). Cycles 1 and 2 (lower CVs) are depicted as solid black and dotted red traces, respectively.

Scanning cathodically from the $\text{WI}_2(\text{CNDipp})_5$ $\text{W}^{[2+/0]}$ feature produced oxidation waves in the return scan that could not be reliably assigned (**Figure 2.6**, bottom). At more negative potentials, an irreversible cathodic event at -3.3 V (vs $\text{Fc}^{+/0}$) attributable to CNDipp-based reduction was observed. The CVs of

$WI_2(CNDippPh^{OMe3})_5$ are analogous to those of $WI_2(CNDipp)_5$, displaying quasi-reversible $W^{[3+/2+]}$ and irreversible $W^{[2+/0]}$ features at -0.06 and -2.35 V, respectively.

Attempts to regenerate $W(CNDipp)_6$ from $WI_2(CNDipp)_5$ electrochemically were unsuccessful,³⁹ as CVs of $WI_2(CNDipp)_5$ collected in the presence of excess $CNDipp$ (up to 51 equiv) did not reveal a well-defined $W(CNDipp)_6^{[+/0]}$ wave upon scanning cathodically of the irreversible $W^{[2+/0]}$ couple. However, $Na(Hg)$ reduction of $WI_2(CNDipp)_5$, followed by addition of $CNDipp$, regenerated $W(CNDipp)_6$ (supported by UV-vis and 1H NMR data).

2.4. Conclusion

In summary, $W(CNAr)_6$ complexes catalyze 1-(2-iodobenzyl)-pyrrole BHAS upon either one-photon (visible) or two-photon excitation, with the latter representing a unique approach to NIR photoredox catalysis. Our proposed photochemical model (**Figure 2.3**) suggests that the rate of catalysis is slowed by charge recombination within the solvent cage, owing to limited ion-pair separation in low dielectric solvents. Overall catalytic turnover is limited by deactivation pathways, among them the production of $WI_2(CNAr)_5$. Such pathways could be disfavored by more polar solvents or the addition of salts,⁹ to promote escape of $[W(CNAr)_6]^+$ from iodide in the solvent cage. Finally, owing to exceptional TPA cross sections and excited-state reduction potentials, $W(CNAr)_6$ complexes might define an important new class of photoinitiators for 3D lithography applications.

2.5. References

- (1) Prier, C. K.; Rankic, D. A.; MacMillan, D. W. C. Visible Light Photoredox Catalysis with Transition Metal Complexes: Applications in Organic Synthesis. *Chem. Rev.* **2013**, *113*, 5322–5363.
- (2) Koike, T.; Akita, M. Visible-Light Radical Reaction Designed by Ru- and Ir-Based Photoredox Catalysis. *Inorg. Chem. Front.* **2014**, *1*, 562–576.
- (3) Shaw, M. H.; Twilton, J.; MacMillan, D. W. C. Photoredox Catalysis in Organic Chemistry. *J. Org. Chem.* **2016**, *81*, 6898–6926.
- (4) (a) Hernandez-Perez, A. C.; Collins, S. K. Heteroleptic Cu-Based Sensitizers in Photoredox Catalysis. *Acc. Chem. Res.* **2016**, *49*, 1557–1565. (b) Reiser, O. Shining Light on Copper: Unique Opportunities for Visible-Light-Catalyzed Atom Transfer Radical Addition Reactions and Related Processes. *Acc. Chem. Res.* **2016**, *49*, 1990–1996. (c) Larsen, C. B.; Wenger, O. S. Photoredox Catalysis with Metal Complexes Made from Earth-Abundant Elements. *Chem. – Eur. J.* **2018**, *24*, 2039–2058. (d) He, J.; Chen, C.; Fu, G. C.; Peters, J. C. Visible-Light-Induced, Copper-Catalyzed Three-Component Coupling of Alkyl Halides, Olefins, and Trifluoromethylthiolate To Generate Trifluoromethyl Thioethers. *ACS Catal.* **2018**, *8*, 11741–11748.
- (5) (a) Zhang, Y.; Petersen, J. L.; Milsmann, C. A Luminescent Zirconium(IV) Complex as a Molecular Photosensitizer for Visible Light Photoredox Catalysis. *J. Am. Chem. Soc.* **2016**, *138*, 13115–13118. (b) Zhang, Y.; Lee, T. S.; Favale, J. M.; Leary, D. C.; Petersen, J. L.; Scholes, G. D.; Castellano, F. N.; Milsmann, C. Delayed Fluorescence from a Zirconium(IV) Photosensitizer with Ligand-to-Metal Charge-Transfer Excited States. *Nat. Chem.* **2020**, *12*, 345–352.
- (6) Qiao, Y.; Schelter, E. J. Lanthanide Photocatalysis. *Acc. Chem. Res.* **2018**, *51*, 2926–2936.

- (7) Yu, D.; To, W.-P.; Tong, G. S. M.; Wu, L.-L.; Chan, K.-T.; Du, L.; Phillips, D. L.; Liu, Y.; Che, C.-M. Luminescent Tungsten(VI) Complexes as Photocatalysts for Light-Driven C–C and C–B Bond Formation Reactions. *Chem. Sci.* **2020**, *11*, 6370–6382.
- (8) Mann, K. R.; Cimolino, M.; Geoffroy, G. L.; Hammond, G. S.; Orio, A. A.; Albertin, G.; Gray, H. B. Electronic Structures and Spectra of Hexakisphenylisocyanide Complexes of Cr(0), Mo(0), W(0), Mn(I), and Mn(II). *Inorg. Chim. Acta* **1976**, *16*, 97–101.
- (9) Sattler, W.; Ener, M. E.; Blakemore, J. D.; Rachford, A. A.; LaBeaume, P. J.; Thackeray, J. W.; Cameron, J. F.; Winkler, J. R.; Gray, H. B. Generation of Powerful Tungsten Reductants by Visible Light Excitation. *J. Am. Chem. Soc.* **2013**, *135*, 10614–10617.
- (10) Sattler, W.; Henling, L. M.; Winkler, J. R.; Gray, H. B. Bespoke Photoreductants: Tungsten Arylisocyanides. *J. Am. Chem. Soc.* **2015**, *137*, 1198–1205.
- (11) Kvapilová, H.; Sattler, W.; Sattler, A.; Sazanovich, I. V.; Clark, I. P.; Towrie, M.; Gray, H. B.; Zálíš, S.; Vlček, A. Electronic Excited States of Tungsten(0) Arylisocyanides. *Inorg. Chem.* **2015**, *54*, 8518–8528.
- (12) Fajardo, J.; Schwan, J.; Kramer, W. W.; Takase, M. K.; Winkler, J. R.; Gray, H. B. Third-Generation W(CNAr)₆ Photoreductants (CNAr = Fused-Ring and Alkynyl-Bridged Arylisocyanides). *Inorg. Chem.* **2021**, *60*, 3481–3491.
- (13) Büldt, L. A.; Guo, X.; Vogel, R.; Prescimone, A.; Wenger, O. S. A Tris(Diisocyanide)Chromium(0) Complex Is a Luminescent Analog of Fe(2,2'-Bipyridine)₃²⁺. *J. Am. Chem. Soc.* **2017**, *139*, 985–992.

- (14) Büldt, L. A.; Guo, X.; Prescimone, A.; Wenger, O. S. A Molybdenum(0) Isocyanide Analogue of Ru(2,2'-Bipyridine)₃²⁺: A Strong Reductant for Photoredox Catalysis. *Angew. Chem. Int. Ed.* **2016**, *55*, 11247–11250.
- (15) Herr, P.; Glaser, F.; Büldt, L. A.; Larsen, C. B.; Wenger, O. S. Long-Lived, Strongly Emissive, and Highly Reducing Excited States in Mo(0) Complexes with Chelating Isocyanides. *J. Am. Chem. Soc.* **2019**, *141*, 14394–14402.
- (16) Larsen, C. B.; Wenger, O. S. Photophysics and Photoredox Catalysis of a Homoleptic Rhenium(I) Tris(Diisocyanide) Complex. *Inorg. Chem.* **2018**, *57*, 2965–2968.
- (17) Mann, K. R.; Gray, H. B.; Hammond, G. S. Excited-State Reactivity Patterns of Hexakisarylisocyano Complexes of Chromium(0), Molybdenum(0), and Tungsten(0). *J. Am. Chem. Soc.* **1977**, *99*, 306–307.
- (18) Gray, H. B.; Mann, K. R.; Lewis, N. S.; Thich, J. A.; Richman, R. M. Photochemistry of Metal-Isocyanide Complexes and Its Possible Relevance to Solar Energy Conversion. In *Inorganic and Organometallic Photochemistry*; American Chemical Society, 1978; Vol. 168, 44–56.
- (19) Klendworth, D. D.; Welters, W. W.; Walton, R. A. Redox Chemistry of Hexakis(Phenyl Isocyanide) Complexes of Molybdenum and Tungsten: The Synthesis of the Seven-Coordinate Cations [M(CNPh)₇]²⁺ and Their Electrochemistry and Substitution Reactions. *Organometallics* **1982**, *1*, 336–343.
- (20) Takematsu, K.; Wehlin, S. A. M.; Sattler, W.; Winkler, J. R.; Gray, H. B. Two-Photon Spectroscopy of Tungsten(0) Arylisocyanides Using Nanosecond-Pulsed Excitation. *Dalton Trans.* **2017**, *46*, 13188–13193.
- (21) (a) Arnoux, C.; Konishi, T.; Van Elslande, E.; Poutougnigni, E.-A.; Mulatier, J.-C.; Khrouz, L.; Bucher, C.; Dumont, E.; Kamada, K.; Andraud, C.;

Baldeck, P.; Banyasz, A.; Monnereau, C. Polymerization Photoinitiators with Near-Resonance Enhanced Two-Photon Absorption Cross-Section: Toward High-Resolution Photoresist with Improved Sensitivity. *Macromolecules* **2020**, *53*, 9264–9278. (b) Skliutas, E.; Lebedevaite, M.; Kabouraki, E.; Baldacchini, T.; Ostrauskaite, J.; Vamvakaki, M.; Farsari, M.; Juodkazis, S.; Malinauskas, M. Polymerization Mechanisms Initiated by Spatio-Temporally Confined Light. *Nanophotonics* **2021**, *10*, 1211–1242.

(22) Klendworth, D. D.; Welters, W. W.; Walton, R. A. Homoleptic Phenyl Isocyanide Complexes of Molybdenum and Tungsten: Zerovalent Six-Coordinate versus Divalent Seven-Coordinate. *J. Organomet. Chem.* **1981**, *213*, C13–C16.

(23) Performing the photoredox catalysis in the presence of increasing equivalents of TMP or excess free CNDipp did not improve the conversion or TON.

(24) Decreasing the W(CNDipp)₆ loading below 2.5 mol % led to further decreases in conversion, but with similar TONs.

(25) Pause, L.; Robert, M.; Savéant, J.-M. Can Single-Electron Transfer Break an Aromatic Carbon–Heteroatom Bond in One Step? A Novel Example of Transition between Stepwise and Concerted Mechanisms in the Reduction of Aromatic Iodides. *J. Am. Chem. Soc.* **1999**, *121*, 7158–7159.

(26) Robert, M.; Savéant, J.-M. Photoinduced Dissociative Electron Transfer: Is the Quantum Yield Theoretically Predicted to Equal Unity? *J. Am. Chem. Soc.* **2000**, *122*, 514–517.

(27) Edkins, R. M.; Bettington, S. L.; Goeta, A. E.; Beeby, A. Two-Photon Spectroscopy of Cyclometalated Iridium Complexes. *Dalton Trans.* **2011**, *40*, 12765–12770.

(28) Ravetz, B. D.; Tay, N. E. S.; Joe, C. L.; Sezen-Edmonds, M.; Schmidt, M. A.; Tan, Y.; Janey, J. M.; Eastgate, M. D.; Rovis, T. Development of a Platform for Near-Infrared Photoredox Catalysis. *ACS Cent. Sci.* **2020**, *6*, 2053–2059.

(29) For other examples of red-light-driven photoredox catalysis, see the following and references cited therein: Mei, L.; Gianetti, T. Helical Carbenium Ion-Based Organic Photoredox Catalyst: A Versatile and Sustainable Option in Red-Light-Induced Reactions. *Synlett* **2021**, *32*, 337–334.

(30) Ravetz, B. D.; Pun, A. B.; Churchill, E. M.; Congreve, D. N.; Rovis, T.; Campos, L. M. Photoredox Catalysis Using Infrared Light via Triplet Fusion Upconversion. *Nature* **2019**, *565*, 343–346.

(31) Bilger, J. B.; Kerzig, C.; Larsen, C. B.; Wenger, O. S. A Photorobust Mo(0) Complex Mimicking [Os(2,2'-Bipyridine)₃]²⁺ and Its Application in Red-to-Blue Upconversion. *J. Am. Chem. Soc.* **2021**, *143*, 1651–1663.

(32) Dewan, J. C.; Roberts, M. M.; Lippard, S. J. Geometric Isomerism in Seven-Coordinate Tungsten(II) Mixed Carbonyl-Iodide-*tert*-Butyl Isocyanide Complexes. *Inorg. Chem.* **1983**, *22*, 1529–1533.

(33) Bonati, F.; Minghetti, G. Molybdenum(II)-Isocyanide Complexes. *Inorg. Chem.* **1970**, *9*, 2642–2644.

(34) The structure of the related complex [ReI₂(CN^{*t*}Bu)₅][I₃] is available in the Cambridge Crystallographic Data Centre (CCDC deposition number 1993025).

(35) (a) Novotny, M.; Lippard, S. J. Heptakis(Alkyl Isocyanide)Molybdenum(II) Complexes. *J. Chem. Soc., Chem. Commun.* **1973**, *6*, 202. (b) Lewis, D. L.; Lippard, S. J. Structure of Heptakis(*tert*-Butyl Isocyanide)Molybdenum(II) Hexafluorophosphate, a Seven-Coordinate Complex with C_{2v} Monocapped Trigonal Prismatic Geometry. *J. Am. Chem. Soc.* **1975**, *97*,

2697–2702. (c) Lam, C. T.; Novotny, M.; Lewis, D. L.; Lippard, S. J. Synthesis and Characterization of Seven-Coordinate Molybdenum(II) and Tungsten(II) Isocyanide Complexes. *Inorg. Chem.* **1978**, *17*, 2127–2133. (d) Brant, P.; Cotton, F. A.; Sekutowski, J. C.; Wood, T. E.; Walton, R. A. Dimolybdenum Tetraacetate and the Octachlorodimolybdate(II) Anion as Reagents for Preparing Mononuclear Molybdenum(II) Complexes: Geometry of the Hepta(Methylisocyano)Molybdenum(II) Cation. *J. Am. Chem. Soc.* **1979**, *101*, 6588–6593. (e) Szalda, D. J.; Dewan, J. C.; Lippard, S. J. Structural Studies of Three Seven-Coordinate Isocyanide Complexes of Molybdenum(II) and Tungsten(II). *Inorg. Chem.* **1981**, *20*, 3851–3857. (f) Mialki, W. S.; Wild, R. E.; Walton, R. A. Seven-Coordinate Alkyl Isocyanide and Mixed-Alkyl Isocyanide-Phosphine Complexes of Tungsten(II). *Inorg. Chem.* **1981**, *20*, 1380–1384. (g) Dewan, J. C.; Lippard, S. J. Structure of a Homoleptic Seven Coordinate Molybdenum(II) Aryl Isocyanide Complex, $[\text{Mo}(\text{CNPh})_7](\text{PF}_6)_2$. *Inorg. Chem.* **1982**, *21*, 1682–1684. (h) Giandomenico, C. M.; Hanau, L. H.; Lippard, S. J. Improved Synthesis of Seven-Coordinate Molybdenum(II) and Tungsten(II) Isocyanide Complexes: Dealkylation of Coordinated *tert*-Butyl Isocyanide. *Organometallics* **1982**, *1*, 142–148.

(36) Lewis, D. F.; Lippard, S. J. Synthesis and Structure of Iodohexakis(*tert*-Butyl Isocyanide)Molybdenum(II) Iodide. *Inorg. Chem.* **1972**, *11*, 621–626.

(37) (a) Dreyer, E. B.; Lam, C. T.; Lippard, S. J. Synthesis and Structure of Diiododicarbonyltris(*tert*-Butyl Isocyanide)Tungsten(II), an Example of the 4:3 Piano Stool Seven-Coordinate Geometry. *Inorg. Chem.* **1979**, *18*, 1904–1908. (b) Ditri, T. B.; Moore, C. E.; Rheingold, A. L.; Figueroa, J. S. Oxidative Decarbonylation of *m*-Terphenyl Isocyanide Complexes of Molybdenum and Tungsten: Precursors to Low-Coordinate Isocyanide Complexes. *Inorg. Chem.* **2011**, *50*, 10448–10459.

(38) Caravana, Carl.; Giandomenico, C. M.; Lippard, S. J. Electrochemical Studies of Seven-Coordinated Isocyanide Complexes of Molybdenum(II) and Tungsten(II). *Inorg. Chem.* **1982**, *21*, 1860–1863.

(39) Attempts to generate $WI_2(CNDipp)_5$ (i) electrochemically from $W(CNDipp)_6$ in the presence of tetrabutylammonium iodide or (ii) chemically by treatment of $W(CNDipp)_6$ with I_2 in C_6D_6 were also unsuccessful.

3 Photoredox Catalysis Mediated by Tungsten(0) Arylisocyanides in 1,2-Difluorobenzene

Reprinted with permission from *Inorg. Chem.* **2022**, *61*, 19, 7251–7255.

Copyright 2022 American Chemical Society.

3.1. Abstract

We have studied the photochemical cyclization of 1-(2-iodobenzyl)-pyrrole (IBP) and 1-(2-bromobenzyl)-pyrrole (BBP) to 5*H*-pyrrolo[2,1-*a*]isoindol catalyzed by W(CNDipp)₆ (CNDipp = 2,6-diisopropylphenylisocyanide) in 1,2-difluorobenzene (DFB). Irradiation (445 nm) of W(CNDipp)₆ (5 mol%) in DFB solution converted 78% of IBP (50 mM) to product after 1 h (16 turnovers). Addition of tetra-*n*-butyl ammonium hexafluorophosphate (TBAPF₆) (0.2 M) to the DFB solution led to rapid photoinduced disappearance of W(CNDipp)₆ but, remarkably, did not inhibit photochemical cyclization of IBP, indicating that IBP cyclization was driven by a nonluminescent photocatalyst.

3.2. Introduction

A goal of renewable energy science is replacement of rare metal (Ru, Rh, Ir, Pt) photosensitizers and catalysts with ones containing only earth-abundant elements.^{1–17} To achieve this goal, we have synthesized and fully characterized tungsten(0) arylisocyanides whose metal-to-ligand charge-transfer (MLCT) excited states (*W(CNAr)₆) are exceptionally strong photoreductants ($E^\circ(\text{W}^+/*\text{W}^0) = -2.2$ to -3.0 V vs Fc^[+/0]).^{18–22} We have shown that [*W(CNAr)₆] complexes reduce challenging substrates such as anthracene and acetophenone,²⁰ and that their intense visible absorption features and synthetic modularity make them attractive candidates for one- and two-photon photoredox catalysis.²⁴

Base-promoted homolytic aromatic substitution (BHAS)^{25,26} transformations provide a convenient test of photoredox reactivity.²³ In prior work we examined the photochemical conversion of 1-(2-iodobenzyl)-pyrrole (IBP) and 1-(2-bromobenzyl)-pyrrole (BBP) to 5*H*-pyrrolo[2,1-*a*]isoindol catalyzed by $W(CNAr)_6$ in C_6D_6 solution (**Figure 3.1**).²⁴ With $W(CNDipp)_6$ (CNDipp = 2,6-diisopropylphenylisocyanide) at 5 mol % loading, 1 h of irradiation (6W diode laser, 445 nm) afforded 62% conversion to the cyclized product, corresponding to a turnover number (TON) of 11. Longer irradiation times did not increase turnovers; ¹H NMR, UV-visible absorption and luminescence spectra confirmed the conversion of $W(CNDipp)_6$ into photochemically unreactive $WI_2(CNDipp)_5$. Our proposed mechanism for $W(CNAr)_6$ catalyzed IDP or BBP cyclization included two critical unproductive pathways stemming from tight ion pairs in benzene solution (**Figure 3.1**).

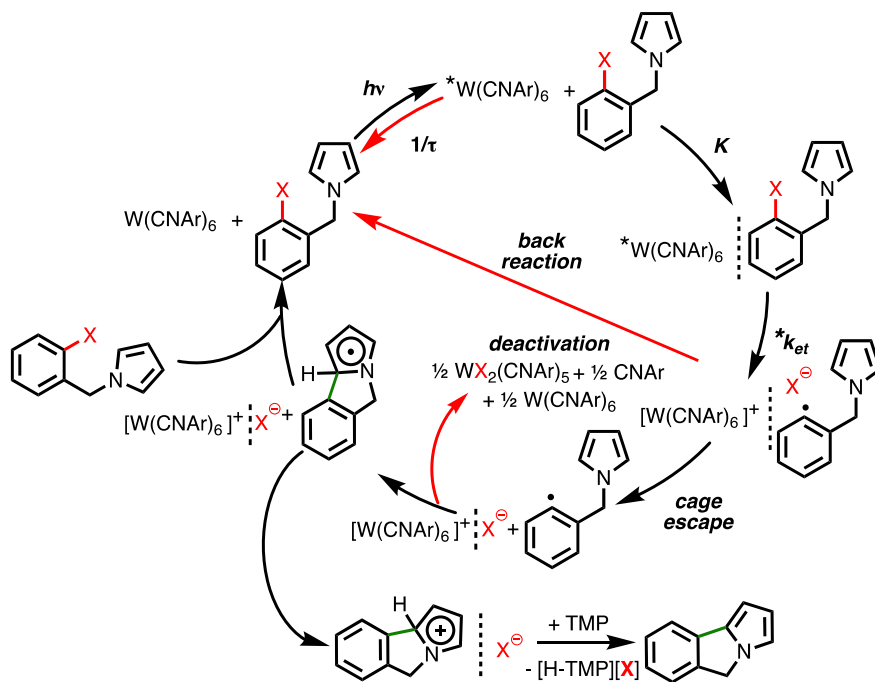


Figure 3.1. Mechanism for BHAS photoredox catalysis mediated by $W(CNAr)_6$ in benzene solution. Red arrows indicate unproductive pathways.²⁴ Abbreviations

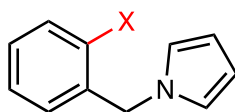
include X = Br, I; TMP = 2,2,6,6-tetramethylpiperidine ; concerted electron transfer k_{et} ; and equilibrium constant K . Ion pairing represented by dashed lines.

We suggested that a more polar solvent and/or the addition of electrolyte could favor ion-pair separation and limit the unproductive pathways in BHAS photocatalysis with $W(CNAr)_6$.²⁴ We selected 1,2-difluorobenzene (DFB, $\epsilon_0 = 13.38$ ²⁷) as solvent, and tetra-*n*-butyl ammonium hexafluorophosphate (TBAPF₆) and tetra-*n*-butyl ammonium iodide (TBAI) as electrolytes to test this hypothesis.

3.3. Results and Discussion

The first step in the photocatalytic process is electron-transfer (ET) quenching of $^*W(CNDipp)_6$ by IBP or BBP. The specific rate (k_{obsd}) of $^*W(CNDipp)_6$ luminescence decay in DFB solutions varies linearly with IDB or BBP concentration. The second-order rate constants extracted from the kinetics (k_q , **Table 3.1**) reveal that DFB produces substantial increases in quenching rates for both the iodo- and bromo-aromatic substrates (**Table 3.1**). Addition of TBAI (0.2 M) and TBAPF₆ (0.2 M) leads to further rate enhancements. These observations are consistent with increased reaction driving force, owing to stabilization of the ET products in the more polar solvent environment. The larger ET rate constants in DFB also produce substantial increases in yields of quenching products (**Table 3.1**).

Table 3.1. Luminescence Quenching Kinetics of $W(CNDipp)_6$ ^a



| Solvent | X | [Electrolyte] | k_q ($M^{-1}s^{-1}$) ^b | Φ_q (%) ^c |
|---------|----|--------------------------|---------------------------------------|---------------------------|
| Benzene | I | - | 6.2×10^7 | 26 |
| DFB | I | - | 3.1×10^8 | 49 |
| DFB | I | 0.2 M TBAI | 3.5×10^8 | 51 |
| DFB | I | 0.2 M TBAPF ₆ | 6.4×10^8 | 66 |
| Benzene | Br | - | 8.6×10^6 | 5 |

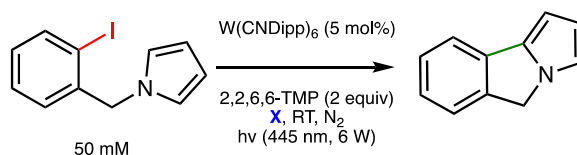
| | | | | |
|-----|----|--------------------------|-------------------|----|
| DFB | Br | - | 7.0×10^7 | 19 |
| DFB | Br | 0.2 M TBAPF ₆ | 8.1×10^7 | 20 |

^aQuenching experiments performed in deaerated solutions at room temperature.

^bFrom the slopes of k_{obsd} vs. [substrate] plots. ^cQuenching yield with 50 mM substrate.

We then examined the photochemical cyclization reactions of IDB and BBP catalyzed by W(CNDipp)₆ in DFB solution. All reactions were performed in the presence of IBP or BBP (50 mM) and a 2-fold excess (100 mM) of 2,2,6,6-tetramethylpiperidine (TMP) to scavenge protons produced in the cyclization reaction. Quantitative product analyses were performed using No-D ¹H NMR in DFB.²⁸ The method was tested by comparing photolysis yields evaluated in C₆H₆ and C₆D₆. Both solvents afforded virtually identical conversion yields and TON values (**Table 3.2**).

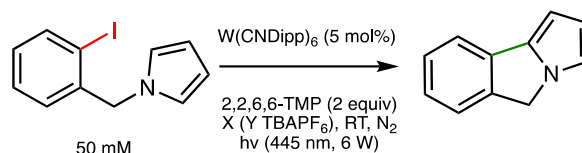
Table 3.2. W(CNDipp)₆ Photoredox in C₆H₆ and C₆D₆. To evaluate the effectiveness of measuring substrate alkane peaks in deuterated versus protonated solvents, the same reaction mixture was prepared in d₆-benzene and benzene solvents. Integration of the methylene feature presented comparable conversions in both photoredox reactions, as determined by ¹H NMR.



| Entry | Solvent [X] | Time (min) | Conversion (%) | TON |
|-------|-------------------------------|------------|----------------|-----|
| 1 | C ₆ D ₆ | 5 | 34 | 7 |
| 2 | C ₆ D ₆ | 30 | 62 | 9 |
| 3 | C ₆ D ₆ | 60 | 66 | 10 |
| 4 | C ₆ D ₆ | 120 | 67 | 10 |
| 5 | C ₆ H ₆ | 30 | 63 | 10 |
| 6 | C ₆ H ₆ | 60 | 66 | 11 |

7 C₆H₆ 120 66 11

Table 3.3. Photoredox Catalysis of 1-(2-iodobenzyl)-pyrrole Conversion to Cyclized Product



| Solvent (X) | [Electrolyte] (Y) | Irrad. Time (min) | Conversion (%) | TON |
|-------------------------------|--------------------------|-------------------|----------------|-----|
| C ₆ D ₆ | - | 5 | 34 | 7 |
| C ₆ D ₆ | - | 60 | 62 | 11 |
| DFB | - | 5 | 62 | 13 |
| DFB | - | 60 | 78 | 16 |
| DFB | - | 120 | 81 | 17 |
| DFB | 0.2 M TBAI | 5 | 68 | 9 |
| DFB | 0.2 M TBAI | 60 | 83 | 10 |
| DFB | 0.2 M TBAI | 120 | 87 | 11 |
| DFB | 0.2 M TBAPF ₆ | 5 | 44 | 8 |
| DFB | 0.2 M TBAPF ₆ | 60 | 67 | 13 |
| DFB | 0.2 M TBAPF ₆ | 120 | 74 | 14 |

The most striking difference between W(CNDipp)₆ catalyzed IBP cyclization in DFB and C₆D₆ is the conversion rate. Product quantification from ¹H NMR afforded comparable reactivity in DFB after 5 min to that in C₆D₆ after 1-h irradiation (Table 3.3). Although direct kinetics comparisons are difficult, owing to variations in excitation conditions, the reactions clearly proceed much more rapidly in DFB than in C₆D₆. A likely explanation for this observation is that the more polar solvent (DFB $\epsilon_0 = 13.38^{27}$, benzene $\epsilon_0 = 2.26^{29}$) favors cage escape of the ET quenching products, thereby inhibiting the unproductive back reaction. As with reactions conducted in C₆D₆, the luminescence (**Figure 3.2**), UV-visible (**Figure 3.16** and **3.17**), and ¹H NMR signatures of W(CNDipp)₆ disappeared after 1-h irradiation in DFB. At lower loadings, however, the catalyst remained active for more than 120 min (**Figure 3.3**).

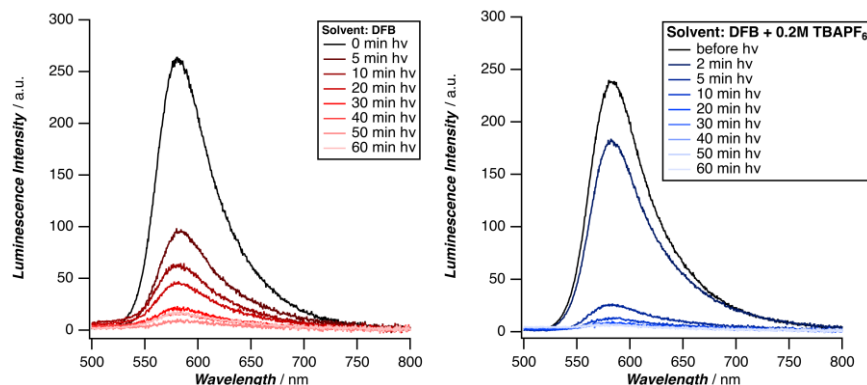


Figure 3.2. Luminescence spectra of 5 mol% W(CNDipp)₆ catalyst, 2 equivalents TMP, and 50 mM IBP in DFB (left). Same conditions with added 0.2 M TBAPF₆ (right).

We also examined the effect of dissolved electrolyte on W(CNDipp)₆ photoreactions in DFB solution. The presence of TBAI/TBAPF₆ (0.2 M) produced a modest reduction in the rate of W(CNDipp)₆-catalyzed IBP photocyclization (Table 1). More remarkable, however, was the loss of W(CNDipp)₆ luminescence after just 10 min of irradiation (**Figure 3.2**), indicating that IBP cyclization in TBAPF₆ was driven by a nonluminescent photocatalyst. UV-visible spectra and ¹H NMR confirm the rapid disappearance of W(CNDipp)₆ from solution.

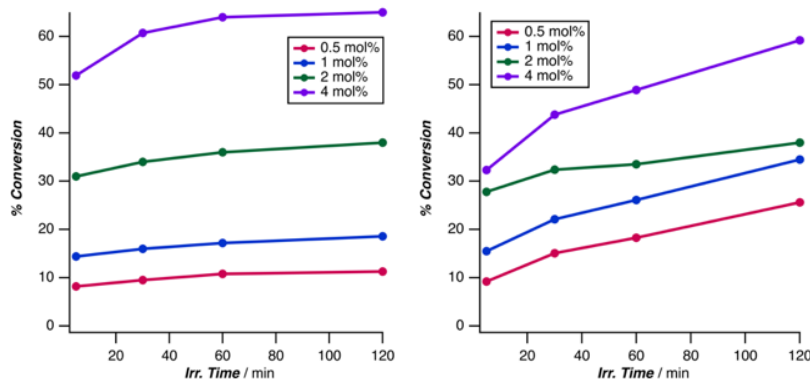
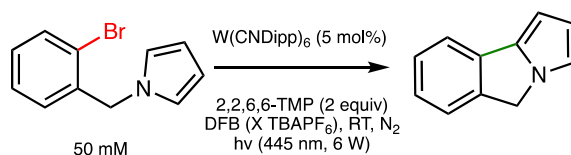


Figure 3.3. Catalyst loading dependence of substrate conversion to cyclized product: W(CNDipp)₆ photocatalyst with, 100 mM TMP, and 50 mM IBP in DFB solution (left). Percent conversion values with addition of 0.2 M TBAPF₆ (right).

The high molar extinction coefficient of W(CNDipp)₆ ($\epsilon_{445\text{nm}} = \sim 55,000 \text{ M}^{-1} \text{ cm}^{-1}$, **Figure 3.10**) prohibited penetration of light into the bulk of the reaction mixture, as demonstrated by precipitation of [H-TMP][I] on the entrance surface of the sample tube. At 5 mol% loading, >95% of the excitation light was absorbed in the first 10 μm of sample. It seemed likely that lowering the catalyst loading would involve more of the sample in catalysis and lead to higher TON values.

Lower catalyst loadings (4, 2, 1, and 0.5 mol%) had little impact on irradiations in DFB. Conversion to substrate ceased after 1-2 h of irradiation (**Figure 3.3**) with TONs in the range of 16-22. With 0.2 M TBAPF₆ in DFB, however, conversion to product was initially slower, but continued to increase roughly linearly with time after 2 h of irradiation (**Figure 3.3**). Moreover, lower catalyst loadings produced higher TON values: after 2-h irradiation at 0.5 mol% catalyst loading the TON was 51; after 24 h the TON was 179, corresponding to 89% substrate conversion.

Table 3.4. Photoredox Catalysis of 1-(2-bromobenzyl)-pyrrole Conversion to Cyclized Product



| [TBAPF ₆] | Irrad. Time (h) | Conversion (%) | TON |
|-----------------------|-----------------|----------------|-----|
| - | 1 | 6.0 | 1.5 |
| - | 2 | 9.0 | 1.9 |
| - | 24 | 16.8 | 3.5 |
| 0.2 M | 1 | 8.4 | 1.5 |
| 0.2 M | 2 | 12.4 | 2.2 |
| 0.2 M | 24 | 27.7 | 5.0 |

We extended our work in DFB/TBAPF₆ solutions to include the BBP substrate. In our prior study, we found that ca. 10 mol% W(CNDipp)₆ loading in C₆D₆ afforded 14% substrate conversion (1.2 TON) after 12-h irradiation.²⁴ Experiments in DFB with ca. 5 mol% catalyst loading gave 6% conversion (1.5 TON) after 1-h irradiation, and 16.8% conversion (3.5 TON) after 24-h irradiation. Upon addition of 0.2 M TBAPF₆, we found 8.4% conversion (1.5 TON) after 1-h irradiation and 27.7% conversion (5.0 TON) after 24-h irradiation. In both studies, W(CNDipp)₆ luminescence persisted after 1-h irradiation, indicating greatly reduced catalyst degradation.

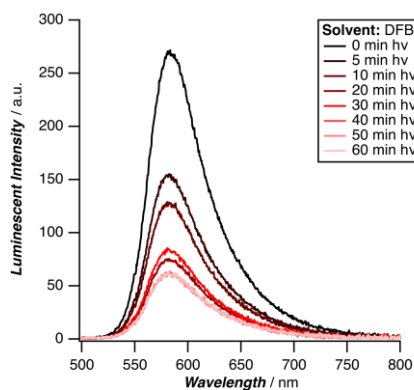


Figure 3.4. Luminescence spectra acquired during irradiation of W(CNDipp)₆, TMP and 1-(2-bromobenzyl)-pyrrole substrate in DFB.

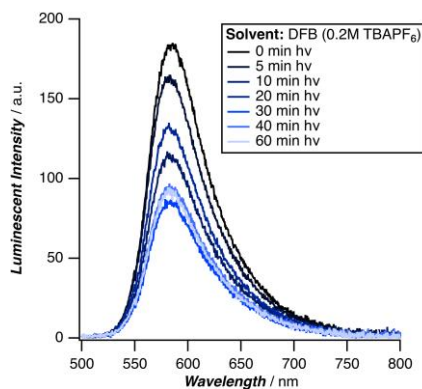


Figure 3.5. Luminescence spectra acquired during irradiation of $W(\text{CNDipp})_6$, TMP and 1-(2-bromobenzyl)-pyrrole substrate in DFB with 0.2 M TBAPF_6 .

Nonluminescent Photocatalyst

The nonluminescent species formed in irradiations of $W(\text{CNDipp})_6$ in DFB with 0.2 M TBAPF_6 appears to be an efficient photocatalyst for the BHAS reaction. In prior work, we identified $W\text{I}_2(\text{CNDipp})_5$ as the deactivation product of photocatalysis in C_6D_6 . This seven-coordinate W(II) complex, or a related six-coordinate W(II) species, $[W(\text{CNDipp})_6]^+$, could be a photocatalyst in DFB. Irradiation of $[W(\text{CNDipp})_6]\text{I}$ in DFB with IBP (50 mM) led to rapid (5 min) formation of $W\text{I}_2(\text{CNDipp})_5$, the liberation of CNDipp , and only trace product formation (**Figure 3.6**), thereby eliminating the six-coordinate W(II) complex as a candidate for the nonluminescent photocatalyst. After 1-h irradiation of $W\text{I}_2(\text{CNDipp})_5$ with IBP in DFB, however, we found 4% conversion to cyclized product (1 TON); and the conversion was 12% (3 TON) after 1-h irradiation with 0.2 M TBAPF_6 in solution. Although $W\text{I}_2(\text{CNDipp})_5$ appears to catalyze IBP cyclization, the activity is markedly lower than that of the species formed by irradiation of $W(\text{CNDipp})_6$ in DFB with TBAPF_6 .

We propose that this nonluminescent species $W\text{I}_2(\text{CNDipp})_5$ can engage in photocatalysis through irradiative loss of I^\cdot . This radical combines with the substrate iodine to generate I_2 , and subsequently, the substrate cyclizes. This radical initiation pathway would sensibly be facilitated in solvent conditions of higher dielectric and in the presence of electrolyte.

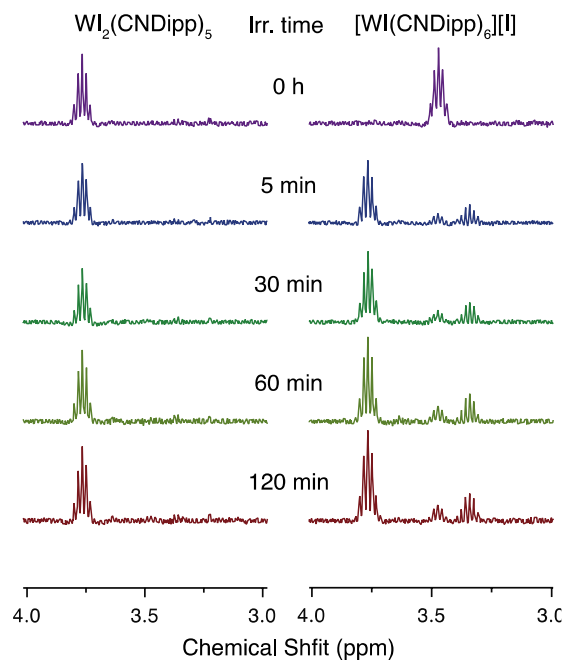


Figure 3.6. ^1H NMR spectra (methine resonances) of $\text{WI}_2(\text{CNDipp})_5$ (left) and $[\text{WI}(\text{CNDipp})_6]\text{I}$ (right) after irradiation with 1-(2-iodobenzyl)-pyrrole in DFB solution.

3.4. Conclusion

We have shown that substrate conversion to cyclized product was enhanced when $\text{W}(\text{CNDipp})_6$ -mediated photoredox catalysis of BHAS reactions was run in a solvent (DFB) more polar than benzene. Although the reaction was somewhat slower with addition of 0.2 M TBAPF_6 , catalytic activity continued well beyond a TON value of 20, reaching 179 TON after 24-h irradiation in DFB solution. There is another advantage of employing DFB as the BHAS reaction solvent, namely, that photogeneration of $\text{WI}_2(\text{CNDipp})_5$ does not terminate catalysis, in striking contrast to the outcome in benzene.

3.5. Experimental Methods

General Considerations

All manipulations were conducted using standard Schlenk or glovebox techniques under inert atmosphere (N₂ or Ar). Solvents are deoxygenated and dried by sparging with N₂ gas and subsequent passage through an activated alumina column on the solvent purification system by SG Water USA, LLC. Non-halogenated solvents were tested with sodium benzophenone ketyl in tetrahydrofuran (THF) to confirm absence of oxygen and water. Deuterated solvents were purchased from Cambridge Isotope Laboratories, Inc., degassed, and dried over activated 3 Å molecular sieves.

W(CNDipp)₆, 1-(2-iodobenzyl)-pyrrole, 1-(2-bromobenzyl)-pyrrole, and WI₂(CNDipp)₅, were prepared according to literature methods.^{1,2} 2,2,6,6-Tetramethylpiperidine (TMP) was purified by vacuum distillation, degassed using freeze-pump-thaw (three cycles), and dried over activated 3 Å molecular sieves. Iodine (I₂) was sublimed prior to introduction into the glovebox. Tetra-*n*-butyl ammonium hexafluorophosphate (TBAPF₆, ≥99.0%) and tetra-*n*-butyl ammonium iodide (TBAI, 98%) were used as received from Sigma-Aldrich. All other reagents were purchased from commercial vendors and used without further purification.

NMR Spectroscopy

NMR measurements were performed at room temperature, obtained using a Varian 400 MHz spectrometer. ¹H and ¹³C chemical shifts were reported in ppm relative to tetramethylsilane, using residual proton and ¹³C resonances from solvent as an internal standard.

NMR spectra obtained in proteo solvents were generated using the ¹H proton gradient shim in the aromatic region of the associated spectrum. Spectra were subsequently processed using signal suppression in MestResNova (suppressed at 6.93 ppm). Peak features were referenced using addition of tetramethylsilane in samples of 1,2-difluorobenzene.

IR Spectroscopy

IR spectra were obtained using a ThermoFisher iD5 ATR spectrometer in an argon-filled glovebox.

UV-Visible Spectroscopy

UV-Visible absorption measurements were performed under an N₂ atmosphere at room temperature using a Cary 50 UV-visible spectrophotometer. Samples were prepared in anhydrous, degassed solvents using the nitrogen-filled glovebox, placed in the cell of a 1 cm path length fused quartz cuvette (Starna Cells), and isolated from atmosphere by a high-vacuum Teflon valve (Kontes). All samples were stored in the dark before measurement and were referenced to a blank solvent background.

Luminescence Spectroscopy

Steady-state and time-resolved luminescence measurements were carried out in the Beckman Institute Laser Resource Center (BILRC) at Caltech, and performed under an N₂ atmosphere at room temperature. Samples were prepared using anhydrous, degassed solvents inside of an N₂-filled glovebox and placed into J. Young NMR tubes. All samples were stored in the dark before measurement.

Steady State

Steady state emission spectra were recorded on a modified Jobin Yvon Spec Fluorolog-3-11. Sample excitation employed a xenon arc lamp with wavelength selection using a monochromator. Luminescence was collected at 90° to the excitation direction and directed by a bifurcated optical fiber bundle to two Ocean Optics QEPro CCD spectrometers spanning 300 to 930 nm. Spectra were corrected for instrument response.

Time Resolved

To collect time-resolved measurements, laser excitation was provided by 8 ns pulses from a Q-switched Nd:YAG laser operating at 10 Hz (Spectra-Physics Quanta-Ray PRO series). The second harmonic was used to provide 532 nm laser pulses.

After colinear transmission through the sample, the scattered excitation light was rejected using short and long pass filters. Probe wavelengths were selected for detection by a double monochromator (Instruments SA DH-10) with 1 mm slits. All instruments and electronics were controlled by software written in LabVIEW (National Instruments). Also, see reference 3.

Time-resolved Stern-volmer measurements were performed in 1 cm quartz cuvettes with automated stirring. Luminescence decay traces were fit to a single exponential.

Initial quenching yields (Φ_q) were calculated according to the equation

$$\Phi_q = \frac{1}{1 + \frac{1}{\tau_0 k_q [Q]}}$$

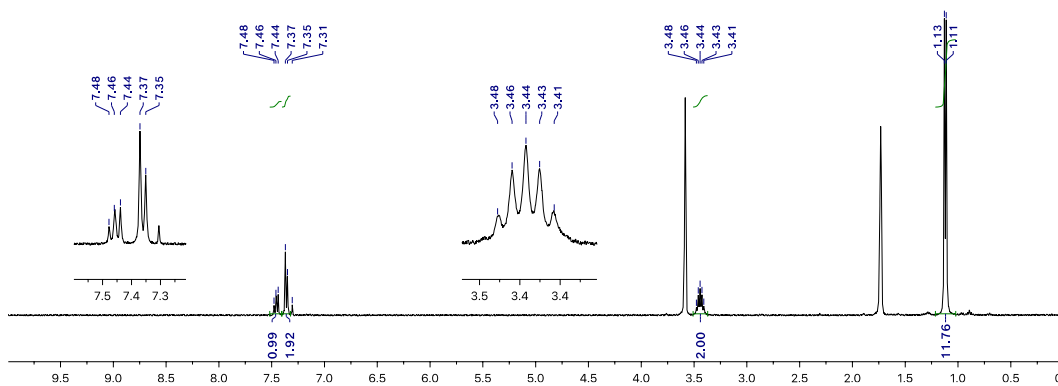
where τ_0 is the lifetime of $^*W(CNDipp)_6$ in reaerated solutions of 1,2-difluorobenzene, k_q is the bimolecular quenching constant from the corresponding Stern-Volmer plot, and [Q] is the initial quencher (1-(2-iodobenzyl)-pyrrole or 1-(2-bronobenzyl)-pyrrole). Initial quenching yields were calculated at 50 mM substrate concentration to reflect BHAS photoredox catalytic conditions.

3.5.1. Synthetic Details and Characterization Data

[WI(CNDipp)₆]I. A solution of W(CNDipp)₆ (1.0 equiv, 0.0157 g, 0.0120 mmol) in benzene (2 mL) is prepared in a 20 mL scintillation vial. To this, a solution of I₂ (1.1 equiv, 0.0017 g, 0.0135 mmol) dissolved in 1 mL benzene is added via pipette. This solution is allowed to stir for 1 hour in the dark, generating an orange microcrystalline powder with clear supernatant. The powder is collected using a celite-plugged filter pipette and washed with three 1 mL benzene washes. The product is triturated with a minimal volume of THF, generating an orange residue under reduced pressure in 64.5% yield (0.0111 g).

Elem Anal. For [WI(CNDipp)₆]I • C₆H₆ (%) found (calc'd): C, 62.05 (61.54); H, 6.77 (6.64); N, 5.64 (5.13).

Figure 3.7. ¹H NMR spectrum of [WI(CNDipp)₆]I. Trace benzene at δ(ppm) = 7.31.



¹H NMR (400 MHz, d₈-THF): δ(ppm) 1.13-1.11 (d, 72H, Ar-CH-2(CH₃)) , 3.48-3.41 (br q, 12H, Ar-CH-2(CH₃)), 7.37-7.35 (d, 6H, Ar CH-CH-CH), 7.48-7.44 (t, 12H, Ar CH-CH-CH)

Figure 3.8. ¹³C{¹H} NMR spectrum (101 MHz, d₈-THF) of [WI(CNDipp)₆]I.

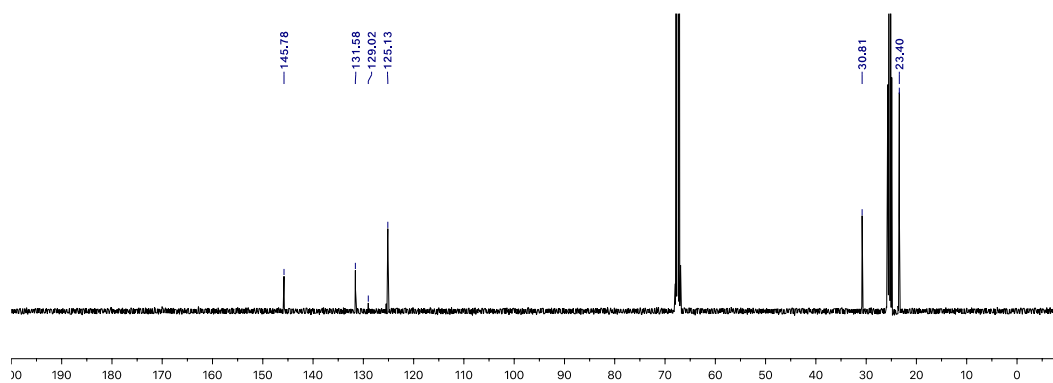
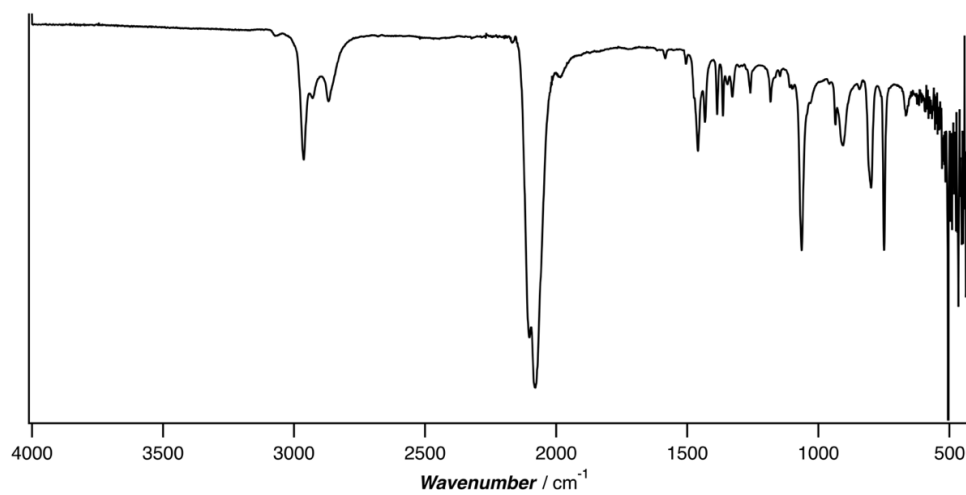


Figure 3.9. ATR-IR spectrum of $[\text{WI}(\text{CNDipp})_6]\text{I}$, deposited as a thin film from THF.



3.5.2. UV-Visible Spectra

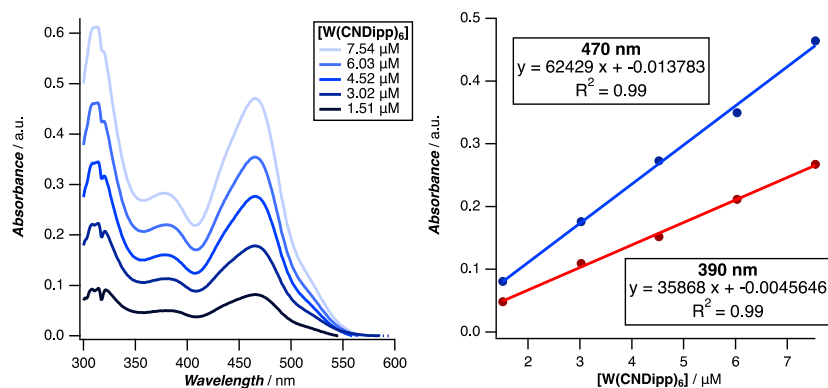


Figure 3.10. Beer's law test of W(CNDipp)₆ absorbance in 1,2-difluorobenzene.

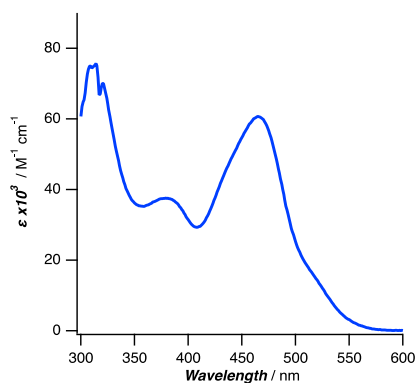


Figure 3.11. Molar absorption spectrum of W(CNDipp)₆ in 1,2-difluorobenzene. Spectrum is identical to prior measurements in THF¹⁹, toluene, and benzene²⁴.

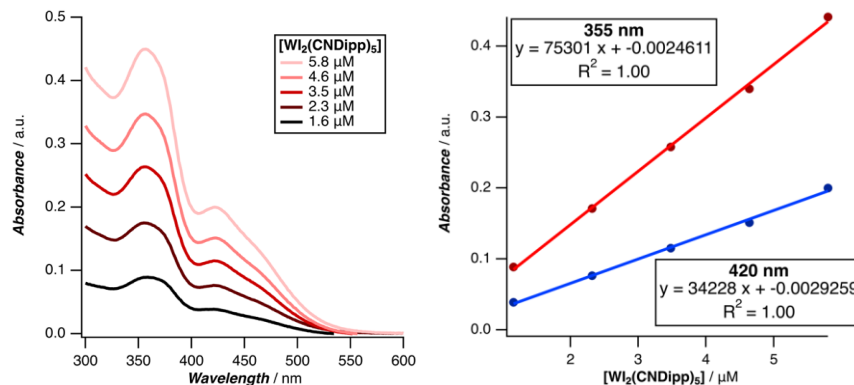


Figure 3.12. Beer's law test of $WI_2(CNDipp)_5$ absorbance in 1,2-difluorobenzene.

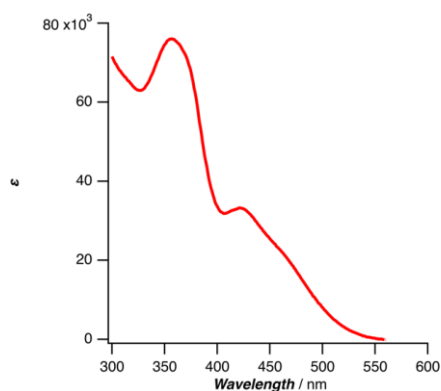


Figure 3.13. Molar absorption spectrum of $WI_2(CNDipp)_5$ in 1,2-difluorobenzene.

Spectrum is identical to prior measurements in benzene and THF²⁴.

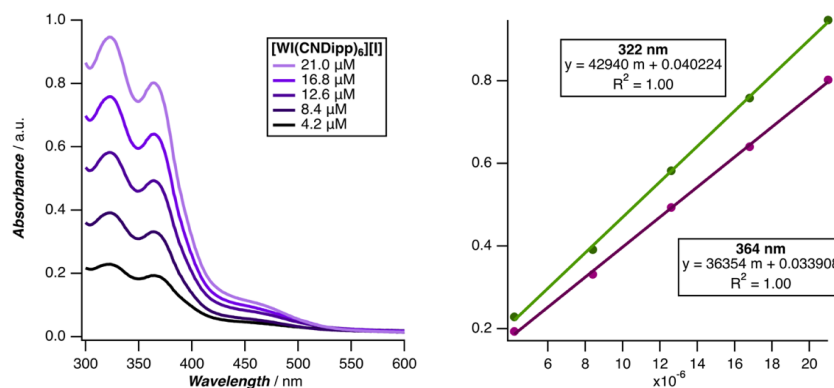


Figure 3.14. Beer's law test of $[WI(CNDipp)_6]I$ absorbance in 1,2-difluorobenzene.

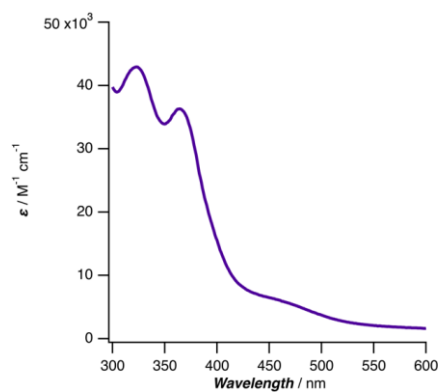


Figure 3.15. Molar absorption spectrum of [WI(CNDipp)₆]I in 1,2-difluorobenzene.

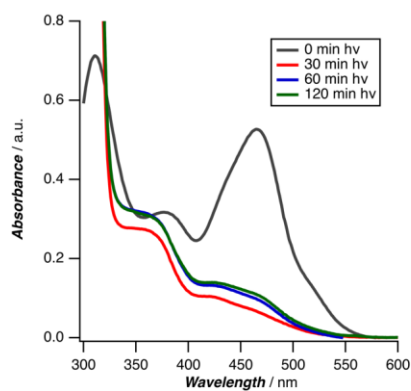


Figure 3.16. Absorbance spectra acquired during irradiation of W(CNDipp)₆ (5 mol%), TMP (2 equiv), and 1-(2-iodobenzyl)-pyrrole substrate (50 mM) in DFB.

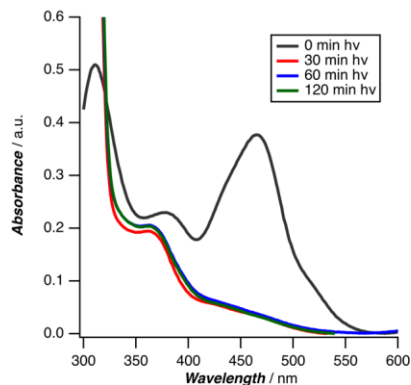


Figure 3.17. Absorbance spectra acquired during irradiation of W(CNDipp)₆ (5 mol%), TMP (2 equiv), and 1-(2-iodobenzyl)-pyrrole substrate (50 mM) in DFB with 0.2M TBAPF₆.



Figure 3.18. W(CNDipp)₆ (5 mol%), TMP (2 equiv), and 1-(2-iodobenzyl)-pyrrole substrate (50 mM) reactions in benzene (left), DFB (center), and DFB with 0.2M TBAPF₆ (right) after 1 hour of irradiation.

Luminescence Spectroscopy

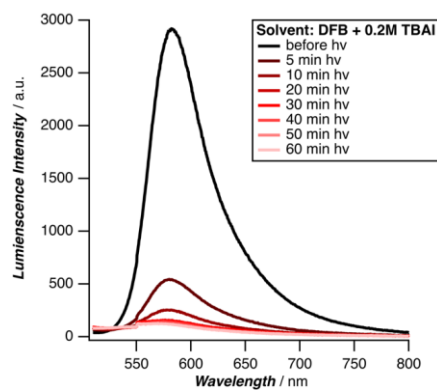


Figure 3.19. Luminescence spectra acquired during irradiation of W(CNDipp)₆, TMP, and 1-(2-iodobenzyl)-pyrrole substrate in DFB (0.2M TBAI).

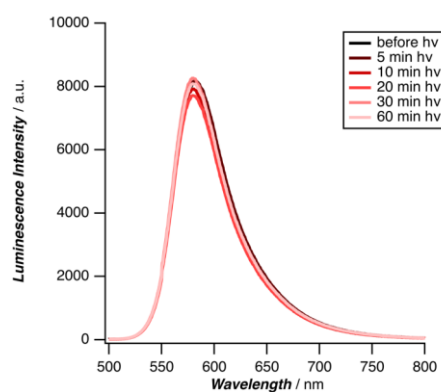


Figure 3.20. Luminescence spectra acquired during irradiation of 3 mM W(CNDipp)₆ in DFB. This concentration is representative of 5 mol% W(CNDipp)₆ BHAS photoredox conditions.

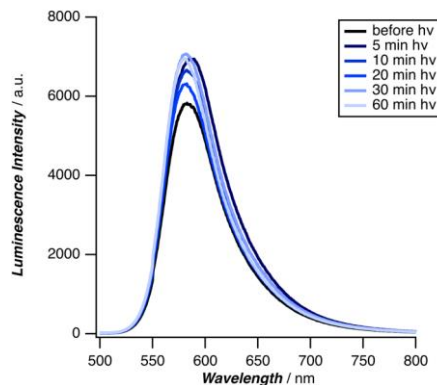


Figure 3.21. Luminescence spectra acquired during irradiation of 3 mM W(CNDipp)₆ in DFB (0.2M TBAPF₆). This concentration is representative of 5 mol% W(CNDipp)₆ BHAS photoredox conditions.

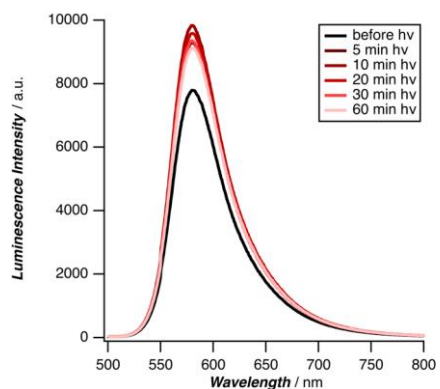


Figure 3.22. Luminescence spectra acquired during irradiation of 3 mM W(CNDipp)₆ with TMP in DFB. This concentration is representative of 5 mol% W(CNDipp)₆ BHAS photoredox conditions.

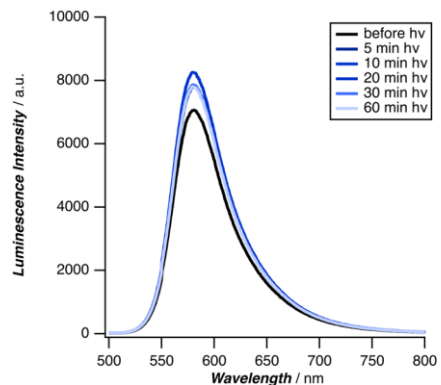


Figure 3.23. Luminescence spectra acquired during irradiation of 3mM W(CNDipp)₆ with TMP in DFB (0.2M TBAPF₆). This concentration is representative of 5 mol% W(CNDipp)₆ BHAS photoredox conditions.

Time-resolved luminescence

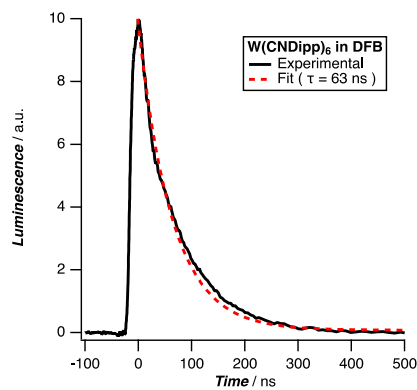


Figure 3.24. Luminescence (620 nm) decay following laser excitation (532 nm, 8 ns) of W(CNDipp)₆ in DFB. Fit to a single-exponential function, $\tau = 63$ ns.

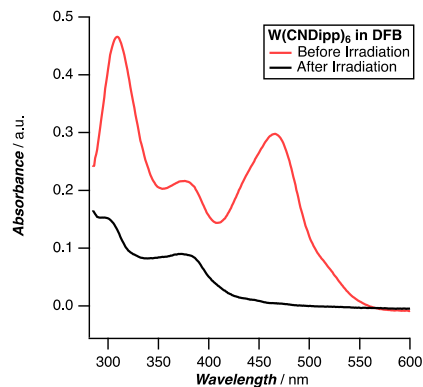


Figure 3.25. Change in absorbance spectrum of W(CNDipp)₆ in 1,2-difluorobenzene upon 532 nm sample irradiation.

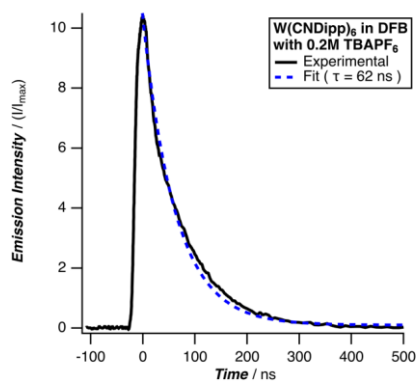


Figure 3.26. Luminescence (620 nm) decay following laser excitation (532 nm, 8 ns) of W(CNDipp)₆ in DFB with TBAPF₆. Fit to a single-exponential function, $\tau = 62$ ns.

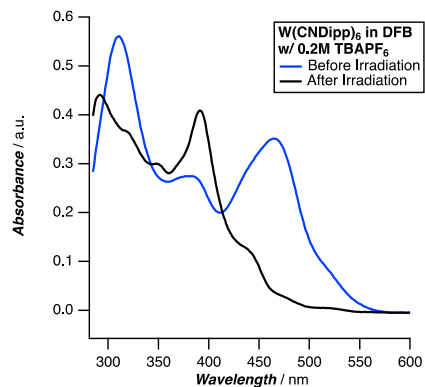


Figure 3.27. Change in absorbance spectrum of W(CNDipp)₆ in difluorobenzene with 0.2M TBAPF₆ upon 532 nm sample irradiation.

3.5.3. Stern-Volmer Quenching Experiments

1-(2-Iodobenzyl)-pyrrole Quenching of $W(\text{CNDipp})_6$ in 1,2-Difluorobenzene Solution

Table 3.5. Stern-Volmer Analysis of 1-(2-iodobenzyl)-pyrrole Quenching of $W(\text{CNDipp})_6$ in 1,2-Difluorobenzene solution ($\lambda_{\text{ex}} = 532 \text{ nm}$, $\lambda_{\text{obs}} = 620 \text{ nm}$).

| Entry | [$W(\text{CNDipp})_6$] (μM) | Solvent | [TMP] (mM) | [1-2-iodobenzyl]- pyrrole] (mM) | Lifetime (ns) |
|----------------|---|---------|---------------|---------------------------------------|------------------|
| 1 ^a | --- | Toluene | --- | --- | 122 |
| 2 ^b | 3.4 | Benzene | --- | --- | 116 |
| 3 | 9.2 | DFB | --- | --- | 63 |
| 4 | 9.2 | DFB | 98.9 | --- | 65 |
| 5 | 9.2 | DFB | --- | 12.5 | 51 |
| 6 | 9.2 | DFB | --- | 25.0 | 43 |
| 7 | 9.2 | DFB | --- | 37.5 | 39 |
| 8 | 9.2 | DFB | --- | 50.0 | 31 |

^a Data from ref. 20 ^b Data from ref. 25

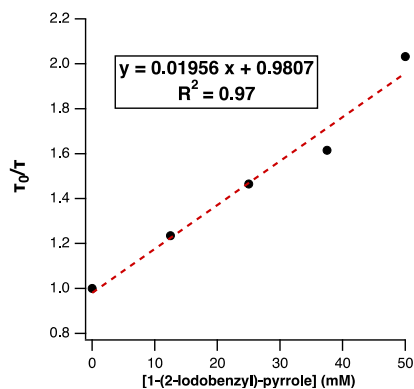


Figure 3.28. Plot of (τ_0/τ) versus 1-(2-iodobenzyl)-pyrrole concentration for $W(\text{CNDipp})_6$. From the slope of the linear fit, the bimolecular quenching constant was determined to be $k_q = 3.1 \times 10^8 \text{ M}^{-1}\text{s}^{-1}$.

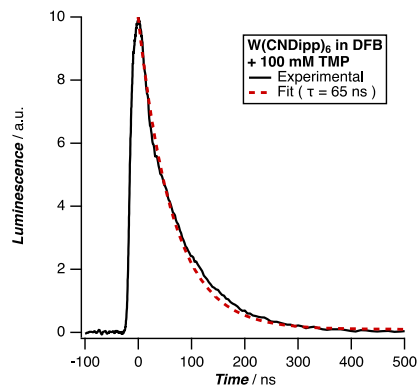


Figure 3.29. Luminescence (620 nm) decay following laser excitation (532 nm, 8 ns) of W(CNDipp)₆ in DFB with 100 mM TMP. Fit to a single-exponential function, $\tau = 65$ ns.

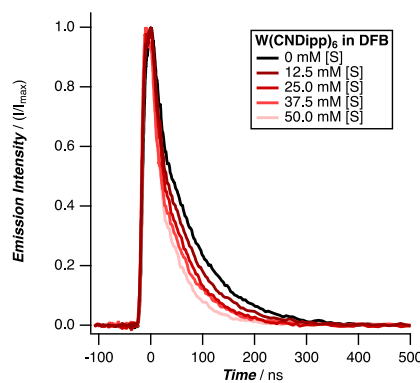


Figure 3.30. Luminescence (620 nm) decay following laser excitation (532 nm, 8 ns) of W(CNDipp)₆ in DFB in the presence of IBP substrate. Each trace is fit to a single-exponential function.

1-(2-Iodobenzyl)-pyrrole Quenching of W(CNDipp)₆ in 1,2-Difluorobenzene Solution with 0.2M TBAPF₆

Table 3.6. Stern-Volmer Analysis of 1-(2-iodobenzyl)-pyrrole Quenching of W(CNDipp)₆ in 1,2-Difluorobenzene solution with 0.2M TBAPF₆ ($\lambda_{\text{ex}} = 532 \text{ nm}$, $\lambda_{\text{obs}} = 620 \text{ nm}$).

| Entry | [W(CNDipp) ₆] (μM) | Solvent | [TMP] (mM) | [1-2-iodobenzyl)-pyrrole] (mM) | Lifetime (ns) |
|----------------|--|--------------------------------|---------------|-----------------------------------|------------------|
| 1 ^a | --- | Toluene | --- | --- | 122 |
| 2 ^b | 3.4 | Benzene | --- | --- | 116 |
| 3 | 9.4 | DFB (0.2M TBAPF ₆) | --- | --- | 62 |
| 4 | 9.4 | DFB (0.2M TBAPF ₆) | 98.9 | --- | 66 |
| 5 | 9.4 | DFB (0.2M TBAPF ₆) | --- | 12.5 | 47 |
| 6 | 9.4 | DFB (0.2M TBAPF ₆) | --- | 25.0 | 33 |
| 7 | 9.4 | DFB (0.2M TBAPF ₆) | --- | 37.5 | 26 |
| 8 | 9.4 | DFB (0.2M TBAPF ₆) | --- | 50.0 | 22 |

^a Data from ref. 20 ^b Data from ref. 25, $\lambda_{\text{obs}} = 580 \text{ nm}$

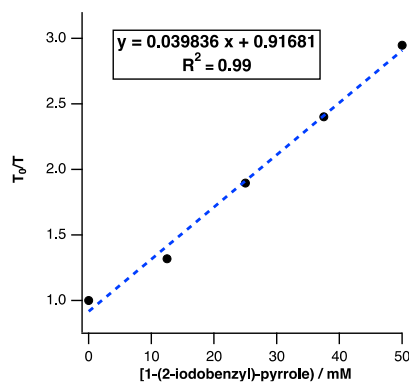


Figure 3.31. Plot of (τ_0/τ) versus 1-(2-iodobenzyl)-pyrrole concentration for W(CNDipp)₆ with 0.2M TBAPF₆. From the slope of the linear fit, the bimolecular quenching constant was determined to be $k_q = 6.4 \times 10^8 \text{ M}^{-1}\text{s}^{-1}$.

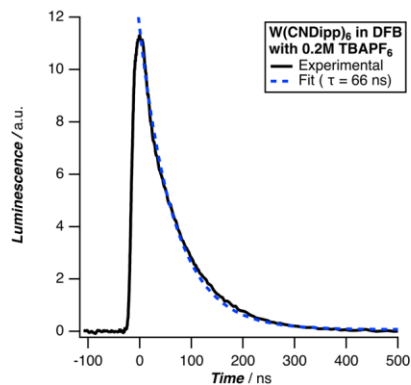


Figure 3.32. Luminescence (620 nm) decay following laser excitation (532 nm, 8 ns) of W(CNDipp)₆ in DFB (0.2 M TBAPF₆) with 100 mM TMP. Fit to a single-exponential function, $\tau = 66$ ns.

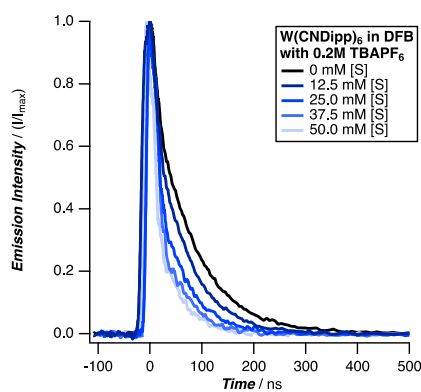


Figure 3.33. Luminescence (620 nm) decay following laser excitation (532 nm, 8 ns) of W(CNDipp)₆ in DFB (0.2M TBAPF₆) in the presence of IBP substrate. Each trace is fit to a single-exponential function.

1-(2-Bromobenzyl)-pyrrole Quenching of W(CNDipp)₆ in 1,2-Difluorobenzene Solution

Table 3.7. Stern-Volmer Analysis of 1-(2-bromobenzyl)-pyrrole Quenching of W(CNDipp)₆ in 1,2-Difluorobenzene solution ($\lambda_{\text{ex}} = 532 \text{ nm}$, $\lambda_{\text{obs}} = 620 \text{ nm}$).

| Entry | [W(CNDipp) ₆] (μM) | Solvent | [TMP] (mM) | [1-2-bromobenzyl)-pyrrole] (mM) | Lifetime (ns) |
|-------|---|---------|------------|---------------------------------|---------------|
| 1 | 9.4 | DFB | --- | --- | 65 |
| 2 | 9.4 | DFB | 98.9 | --- | 65 |
| 3 | 9.4 | DFB | --- | 25.0 | 58 |
| 4 | 9.4 | DFB | --- | 50.0 | 56 |
| 5 | 9.4 | DFB | --- | 100.0 | 45 |
| 6 | 9.4 | DFB | --- | 150.0 | 39 |

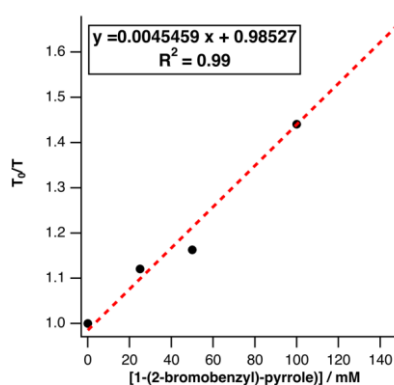


Figure 3.34. Plot of (τ_0/τ) versus 1-(2-bromobenzyl)-pyrrole concentration for W(CNDipp)₆ in DFB. From the slope of the linear fit, the bimolecular quenching constant was determined to be $k_q = 7.0 \times 10^7 \text{ M}^{-1}\text{s}^{-1}$.

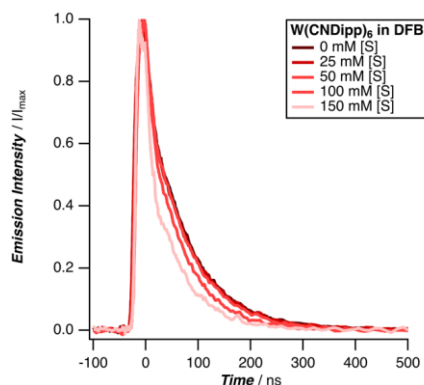


Figure 3.35. Luminescence (620 nm) decay following laser excitation (532 nm, 8 ns) of $W(CNDipp)_6$ in DFB in the presence of BBP substrate. Each trace is fit to a single-exponential function. In the figure, $[S] = 1-(2\text{-bromobenzyl})\text{-pyrrole}$.

1-(2-Bromobenzyl)-pyrrole Quenching of $W(CNDipp)_6$ in 1,2-Difluorobenzene Solution with 0.2M TBAPF₆

Table 3.8. Stern-Volmer Analysis of 1-(2-bromobenzyl)-pyrrole Quenching of $W(CNDipp)_6$ in 1,2-Difluorobenzene solution with 0.2M TBAPF₆ ($\lambda_{ex} = 532$ nm, $\lambda_{obs} = 620$ nm).

| Entry | $[W(CNDipp)_6]$ (μM) | Solvent | $[TMP]$ (mM) | $[1\text{-}2\text{-bromobenzyl}\text{-pyrrole}]$ (mM) | Lifetime (ns) |
|-------|--------------------------------------|---------|-----------------|--|------------------|
| 1 | 8.6 | DFB | --- | --- | 63 |
| 2 | 8.6 | DFB | 98.9 | --- | 63 |
| 3 | 8.6 | DFB | --- | 25.0 | 56 |
| 4 | 8.6 | DFB | --- | 50.0 | 55 |
| 5 | 8.6 | DFB | --- | 100.0 | 45 |
| 6 | 8.6 | DFB | --- | 150.0 | 35 |

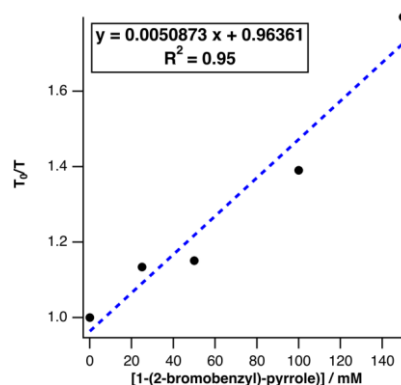


Figure 3.36. Plot of (τ_0/τ) versus 1-(2-bromobenzyl)-pyrrole concentration for $W(\text{CNDipp})_6$ in DFB with 0.2 M TBAPF_6 . From the slope of the linear fit, the bimolecular quenching constant was determined to be $k_q = 8.1 \times 10^7 \text{ M}^{-1}\text{s}^{-1}$.

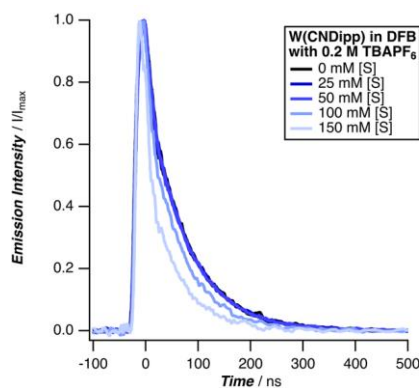


Figure 3.37. Time dependent luminescence measurements for $W(\text{CNDipp})_6$ in DFB (0.2M TBAPF_6) upon 532 nm excitation, 620 nm probe. Each spectra are fit to one exponential. In the figure, $[\text{S}] = 1-(2\text{-bromobenzyl})\text{-pyrrole}$.

1-(2-Iodobenzyl)-pyrrole Quenching of W(CNDipp)₆ in 1,2-Difluorobenzene Solution with 0.2M TBAI

Table 3.9. Stern-Volmer analysis of 1-(2-iodobenzyl)-pyrrole Quenching of W(CNDipp)₆ in 1,2-Difluorobenzene solution with 0.2 M TBAI ($\lambda_{\text{ex}} = 532 \text{ nm}$, $\lambda_{\text{obs}} = 650 \text{ nm}$).

| Entry | [W(CNDipp) ₆] (μM) | Solvent | [TMP] (mM) | [1-2-iodobenzyl)-pyrrole] (mM) | Lifetime (ns) |
|----------------|--|-----------------|---------------|-----------------------------------|------------------|
| 1 ^a | --- | Toluene | --- | --- | 122 |
| 2 ^b | 3.4 | Benzene | --- | --- | 116 |
| 3 | 6.0 | DFB (0.2M TBAI) | --- | --- | 59 |
| 4 | 6.0 | DFB (0.2M TBAI) | 98.9 | --- | 59 |
| 5 | 6.0 | DFB (0.2M TBAI) | --- | 6.3 | 54 |
| 6 | 6.0 | DFB (0.2M TBAI) | --- | 12.5 | 49 |
| 7 | 6.0 | DFB (0.2M TBAI) | --- | 25.0 | 41 |
| 8 | 6.0 | DFB (0.2M TBAI) | --- | 37.5 | 30 |
| 9 | 6.0 | DFB (0.2M TBAI) | --- | 50.0 | 26 |

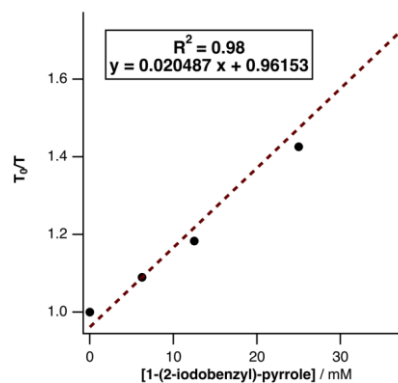


Figure 3.38. Plot of (τ_0/τ) versus 1-(2-iodobenzyl)-pyrrole concentration for W(CNDipp)₆ in DFB with 0.2 M TBAI. From the slope of the linear fit, the bimolecular quenching constant was determined to be $k_q = 3.5 \times 10^8 \text{ M}^{-1}\text{s}^{-1}$.

3.6. References

- (1) Shing Cheung, K. P.; Sarkar, S.; Gevorgyan, V. Visible Light-Induced Transition Metal Catalysis. *Chem. Rev.* **2021**.
- (2) Shaw, M. H.; Twilton, J.; MacMillan, D. W. C. Photoredox Catalysis in Organic Chemistry. *J. Org. Chem.* **2016**, *81* (16), 6898–6926.
- (3) Prier, C. K.; Rankic, D. A.; MacMillan, D. W. C. Visible Light Photoredox Catalysis with Transition Metal Complexes: Applications in Organic Synthesis. *Chem. Rev.* **2013**, *113* (7), 5322–5363.
- (4) Gray, H. B. Powering the Planet with Solar Fuel. *Nature Chemistry* **2009**, *1* (1), 7–7.
- (5) Lewis, N. S.; Nocera, D. G. Powering the Planet: Chemical Challenges in Solar Energy Utilization. *Proc Natl Acad Sci USA* **2006**, *103* (43), 15729.
- (6) Hunter, B. M.; Gray, H. B.; Müller, A. M. Earth-Abundant Heterogeneous Water Oxidation Catalysts. *Chem. Rev.* **2016**, *116* (22), 14120–14136.
- (7) Hernandez-Perez, A. C.; Collins, S. K. Heteroleptic Cu-Based Sensitizers in Photoredox Catalysis. *Acc. Chem. Res.* **2016**, *49* (8), 1557–1565.
- (8) Reiser, O. Shining Light on Copper: Unique Opportunities for Visible-Light-Catalyzed Atom Transfer Radical Addition Reactions and Related Processes. *Acc. Chem. Res.* **2016**, *49* (9), 1990–1996.
- (9) Larsen, C. B.; Wenger, O. S. Photoredox Catalysis with Metal Complexes Made from Earth-Abundant Elements. *Chem. Eur. J.* **2018**, *24* (9), 2039–2058.
- (10) He, J.; Chen, C.; Fu, G. C.; Peters, J. C. Visible-Light-Induced, Copper-Catalyzed Three-Component Coupling of Alkyl Halides, Olefins, and

Trifluoromethylthiolate To Generate Trifluoromethyl Thioethers. *ACS Catal.* **2018**, *8* (12), 11741–11748.

(11) Zhang, Y.; Petersen, J. L.; Milsmann, C. A Luminescent Zirconium(IV) Complex as a Molecular Photosensitizer for Visible Light Photoredox Catalysis. *J. Am. Chem. Soc.* **2016**, *138* (40), 13115–13118.

(12) Zhang, Y.; Lee, T. S.; Favale, J. M.; Leary, D. C.; Petersen, J. L.; Scholes, G. D.; Castellano, F. N.; Milsmann, C. Delayed Fluorescence from a Zirconium(IV) Photosensitizer with Ligand-to-Metal Charge-Transfer Excited States. *Nature Chemistry* **2020**, *12* (4), 345–352.

(13) Qiao, Y.; Schelter, E. J. Lanthanide Photocatalysis. *Acc. Chem. Res.* **2018**, *51* (11), 2926–2936.

(14) Büldt, L. A.; Guo, X.; Vogel, R.; Prescimone, A.; Wenger, O. S. A Tris(Diisocyanide)Chromium(0) Complex Is a Luminescent Analog of Fe(2,2'-Bipyridine)₃²⁺. *J. Am. Chem. Soc.* **2017**, *139* (2), 985–992.

(15) Büldt, L. A.; Guo, X.; Prescimone, A.; Wenger, O. S. A Molybdenum(0) Isocyanide Analogue of Ru(2,2'-Bipyridine)₃²⁺: A Strong Reductant for Photoredox Catalysis. *Angewandte Chemie International Edition* **2016**, *55* (37), 11247–11250.

(16) Bilger, J. B.; Kerzig, C.; Larsen, C. B.; Wenger, O. S. A Photorobust Mo(0) Complex Mimicking [Os(2,2'-Bipyridine)₃]²⁺ and Its Application in Red-to-Blue Upconversion. *J. Am. Chem. Soc.* **2021**, *143* (3), 1651–1663.

(17) Yu, D.; To, W.-P.; Tong, G. S. M.; Wu, L.-L.; Chan, K.-T.; Du, L.; Phillips, D. L.; Liu, Y.; Che, C.-M. Luminescent Tungsten(VI) Complexes as Photocatalysts for Light-Driven C–C and C–B Bond Formation Reactions. *Chem. Sci.* **2020**, *11* (25), 6370–6382.

- (18) Wegeberg, C.; Häussinger, D.; Wenger, O. S. Pyrene-Decoration of a Chromium(0) Tris(Diisocyanide) Enhances Excited State Delocalization: A Strategy to Improve the Photoluminescence of $3d^6$ Metal Complexes. *J. Am. Chem. Soc.* **2021**, *143* (38), 15800–15811.
- (19) Fajardo, J.; Schwan, J.; Kramer, W. W.; Takase, M. K.; Winkler, J. R.; Gray, H. B. Third-Generation $W(CNAr)_6$ Photoreductants (CNAr = Fused-Ring and Alkynyl-Bridged Arylisocyanides). *Inorg. Chem.* **2021**, *60* (6), 3481–3491.
- (20) Sattler, W.; Henling, L. M.; Winkler, J. R.; Gray, H. B. Bespoke Photoreductants: Tungsten Arylisocyanides. *J. Am. Chem. Soc.* **2015**, *137* (3), 1198–1205.
- (21) Sattler, W.; Ener, M. E.; Blakemore, J. D.; Rachford, A. A.; LaBeaume, P. J.; Thackeray, J. W.; Cameron, J. F.; Winkler, J. R.; Gray, H. B. Generation of Powerful Tungsten Reductants by Visible Light Excitation. *J. Am. Chem. Soc.* **2013**, *135* (29), 10614–10617.
- (22) Kvapilová, H.; Sattler, W.; Sattler, A.; Sazanovich, I. V.; Clark, I. P.; Towrie, M.; Gray, H. B.; Zálíš, S.; Vlček, A. Electronic Excited States of Tungsten(0) Arylisocyanides. *Inorg. Chem.* **2015**, *54* (17), 8518–8528.
- (23) Mann, K. R.; Cimolino, M.; Geoffroy, G. L.; Hammond, G. S.; Orio, A. A.; Albertin, G.; Gray, H. B. Electronic Structures and Spectra of Hexakisphenylisocyanide Complexes of Cr(0), Mo(0), W(0), Mn(I), and Mn(II). *Inorganica Chimica Acta* **1976**, *16*, 97–101.
- (24) Herr, P.; Glaser, F.; Büldt, L. A.; Larsen, C. B.; Wenger, O. S. Long-Lived, Strongly Emissive, and Highly Reducing Excited States in Mo(0) Complexes with Chelating Isocyanides. *J. Am. Chem. Soc.* **2019**, *141* (36), 14394–14402.

- (25) Fajardo, J.; Barth, A. T.; Morales, M.; Takase, M. K.; Winkler, J. R.; Gray, H. B. Photoredox Catalysis Mediated by Tungsten(0) Arylisocyanides. *J. Am. Chem. Soc.* **2021**.
- (26) Studer, A.; Curran, D. P. Organocatalysis and C-H Activation Meet Radical- and Electron-Transfer Reactions. *Angewandte Chemie International Edition* **2011**, *50* (22), 5018–5022.
- (27) Studer, A.; Curran, D. P. The Electron Is a Catalyst. *Nature Chemistry* **2014**, *6* (9), 765–773.
- (28) Mansingh, A.; McLay, D. B. Dielectric Relaxation of Dihalobenzenes. III. Pure Liquids. *J. Chem. Phys.* **1971**, *54* (8), 3322–3325.
- (29) Hoye, T. R.; Eklov, B. M.; Ryba, T. D.; Voloshin, M.; Yao, L. J. No-D NMR (No-Deuterium Proton NMR) Spectroscopy: A Simple Yet Powerful Method for Analyzing Reaction and Reagent Solutions. *Org. Lett.* **2004**, *6* (6), 953–956.
- (30) Mardolcar, U. V.; de Castro, C. A. N.; Santos, F. J. V. Dielectric Constant Measurements of Toluene and Benzene. *Fluid Phase Equilibria* **1992**, *79*, 255–264.

4 SYNTHESSES AND STRUCTURES OF GOLD(I) ARYLISOCYANIDES

4.1. Abstract

We have synthesized and characterized seven $[\text{Au}(\text{CNAr})_2]^+$ compounds with expanded π -aryl networks (Ar = DippPh^{OMe3}, DippPh^{NO2}, DippPh^{NPh2}, CNDippPh^{NHPh2}, Dipp^{CC}Ph^{OMe}, Dipp^{CC}Ph^{CN}, and Dipp^{CC}-1-naph). Electronic structures and absorption spectra of the complexes are reported.

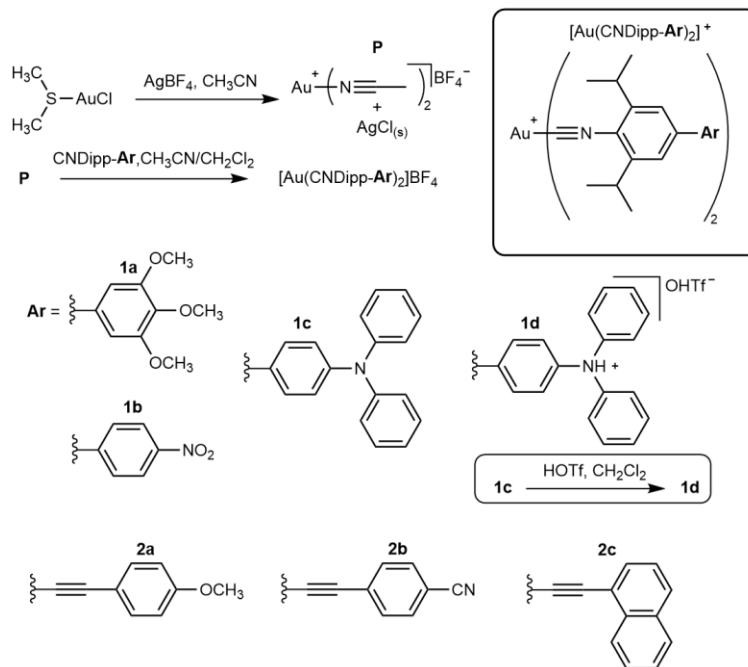
4.2. Introduction

Transition metal complexes are functionally diverse platforms for energy conversion, optical imaging, and photoredox catalysis, owed to their tunable spectroscopic and photophysical properties.¹⁻⁵ Gold complexes form a special class where aurophilic ($\text{Au}^{\text{I}}\cdots\text{Au}^{\text{I}}$) interactions⁶⁻⁷ drive aggregation, forming supramolecular nanowires and other extended structures.⁸⁻¹³ The spectroscopic properties of gold(I) complexes depend on both solvent ligation and aurophilic interactions.^{8,10,13-15} Many have been used to treat rheumatoid arthritis¹⁶⁻¹⁷ and cancer,¹⁸⁻²⁰ and some regulate blood glucose levels.²¹

Here we report the syntheses and spectroscopic properties of two-coordinate Au(I) arylisocyanides, representing an extension of our body of work on $\text{W}(\text{CNAr})_6$ complexes.²²⁻³⁰ We found that the brightly luminescent W(0) molecules exhibit exceptionally large one-photon and two-photon absorption cross sections, making them candidates for optical imaging applications.²³⁻²⁴ Perhaps not surprisingly, as Au(I) arylisocyanides are coordinatively unsaturated, they exhibit striking solvatochromic spectroscopic behavior.

4.3. Results and Discussion

Syntheses. All ligands were synthesized by literature methods.^{21,23} Compounds [Au(CNDippPh^{OMe3})₂](BF₄) (**1a**), [Au(CNDippPh^{NO2})₂](BF₄) (**1b**), [Au(CNDippPh^{NPh2})₂](BF₄) (**1c**), [Au(CNDippPh^{NHPh2})₂](OTf)₃ (**1d**), [Au(CNDipp^{CC}Ph^{OMe})₂](BF₄) (**2a**), [Au(CNDipp^{CC}Ph^{CN})₂](BF₄) (**2b**), and [Au(CNDipp^{CC}-1-naph)₂](BF₄) (**2c**) are shown in **Scheme 4.1**. The intermediate in the syntheses of these compounds (except for **1d**) was [Au(MeCN)₂](BF₄), denoted precursor (**P**), prepared by one-pot silver-salt metathesis and ligand exchange involving Me₂SAuCl, AgBF₄, and excess acetonitrile. Following filtration to remove AgCl, a solution of arylisocyanide (in either acetonitrile, DCM, or an acetonitrile/DCM mixture) was added to the filtrate containing **P**, affording complexes **1a-1c**, **2a**, and **2c**. In the synthesis of **2b**, the filtrate was added dropwise to a solution of the arylisocyanide to disfavor side reactions. Except for **1d**, solvent was removed *in vacuo*, and then the Au(I) complexes were washed with diethyl ether. Yields were generally high (~75-95%) for the two-step syntheses. To prepare **1d**, **1c** was dissolved in a DCM solution containing excess triflic acid, displacing [BF₄]⁻ to yield a triflate salt.



Scheme 4.1. Synthesis and structures of gold(I) isocyanides **1a-1d** and **2a-2c**.

For protein-bound complexes, concentrated solutions (4-5 mM) of **1a**, **1c**, and **2a** in acetonitrile were added to ~5 mL of aqueous bovine serum albumin (BSA)-containing solutions (50 μM BSA, 0.1 M phosphate buffer, pH = 7). Acetonitrile was added (~1-1.5 mL) to this mixture to solubilize the complex well before protein denaturation. The mixture was syringe injected into a 30 kDa MWCO centrifuge filter run at 3000 RPM three times, and then washed with aqueous 0.1 M phosphate buffer between each filtration step. After the final filtration step, the remaining protein/complex residue was re-diluted with 0.1 M phosphate buffer solution and collected for spectroscopic experiments.

Crystal Structures. The geometric parameters of structures reported in this study are set out in **Table 4.1**. Except for **1d**, single crystals of all complexes were obtained *via* diethyl ether vapor diffusion into either acetonitrile or DCM. Images of these structures are depicted in **Figure 4.1**. Generally, complexes adopted a linear geometry with C–Au–C bond angles close to 180° (ranging 175 - 179°). Au–C

bond lengths were minimally perturbed through substitution of CNDipp ligands, lengthening 1.96 to 1.98 in the following order: **2c** < **1b** < **1c** < **2a** < **2b** < **1a**. Steric bulk was responsible for large dihedral angles between opposite diisopropylphenyl groups (~40-70°) in structures **1a**, **1b**, **2a**, and **2c**. Interestingly, dihedral angles between opposing diisopropylphenyl groups in **1c** and **2b** were much lower (~12-17°). For each complex with alkynyl-bridged ligands (**2a-2c**), the aromatic group was independently locked into a planar conformation with a dihedral angle of nearly zero across each alkyne (~4-10°). For complexes **1a-1c**, aromatic networks were less planar, with larger dihedral angles (~33-42°). Nevertheless, geometric optimizations indicated that the molecules would adopt a planar geometry in solution.

Table 4.1. Structural data for [Au(CNAr)₂]⁺ Complexes

| Cation | $d(\text{Au}-\text{C})_{\text{avg}}$ (Å) | $d(\text{N}-\text{C})_{\text{avg}}$ (Å) | $\angle(\text{C}-\text{Au}-\text{C})$ (°) | Intraligand Dihedral $\chi[\text{Ar}(1),\text{Dipp}$ $(2)]_{\text{avg}}$ (°) | Interligand Dihedral $\chi[\text{Dipp}(1),\text{Di}$ $\text{pp}(2)]_{\text{avg}}$ (°) |
|-----------|---|--|--|---|--|
| 1a | 1.975(3) | 1.148(3) | 175.66(19) | 42.640 | 59.576 |
| 1b | 1.965(2) | 1.146(3) | 179.10(9) | 33.260 | 78.92 |
| 1c | 1.968(4) | 1.142(4) | 176.6(2) | 33.611 | 16.956 |
| 2a | 1.9694(19) | 1.140(2) | 178.82(10) | 4.229 | 72.863 |
| 2b | 1.971(4) | 1.140(6) | 174.2(3) | 10.626 | 11.8445 |
| 2c | 1.961(2) | 1.398(2) | 178.31(9) | 10.626 | 43.479 |

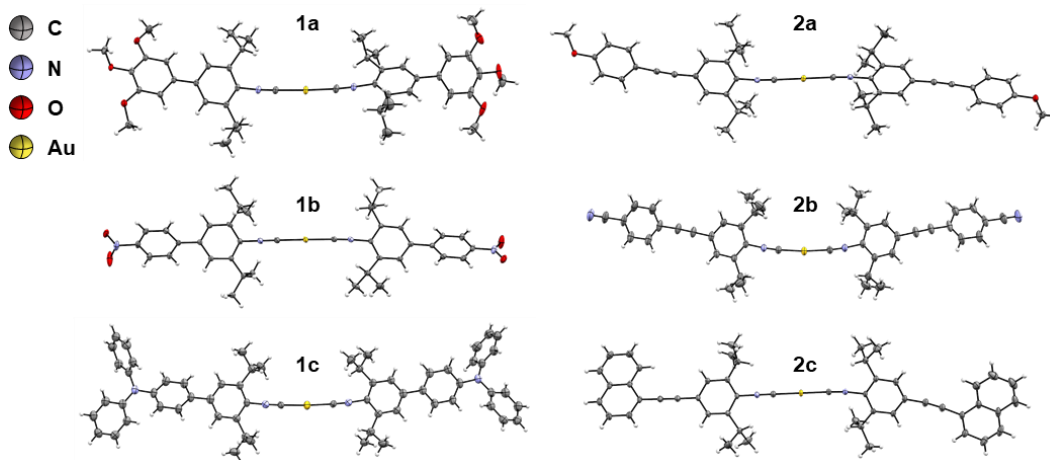


Figure 4.1. Structures of gold(I) arylisocyanide $[\text{Au}(\text{CNAr})_2]^+$ crystals (**1a–2c**). Counter-ions and solvent molecules were removed for clarity. The **1b** crystal was twinned (the unit cell contains two molecules; one molecule was removed for clarity).

Absorption Spectra

UV-vis absorption spectra were obtained for all complexes in DCM solution at room temperature; luminescence spectra were collected in DCM both at room temperature and 77 K (all spectroscopic data are given in **Table 4.2**). A system at $\sim 300\text{--}340$ nm in the absorption spectra of **1a–1d** (**Figure 4.2**) likely is attributable to intraligand transitions. An additional peak at 413 nm in the spectrum of **1d** can be assigned to $n \rightarrow \pi^*$ transitions in the tertiary amine groups. In support of this assignment, the 413-nm peak disappeared upon protonation of the amines (**1c** to **1d**). Though triflic acid was in molar excess, residual absorption features in the $\sim 380\text{--}470$ nm region suggested an equilibrium between **1c** and **1d**, albeit one that highly favors the quaternary amine form. Absorption spectra for **2a–2c** exhibited peaks that can be assigned to the same transitions as in **1a–1d**.

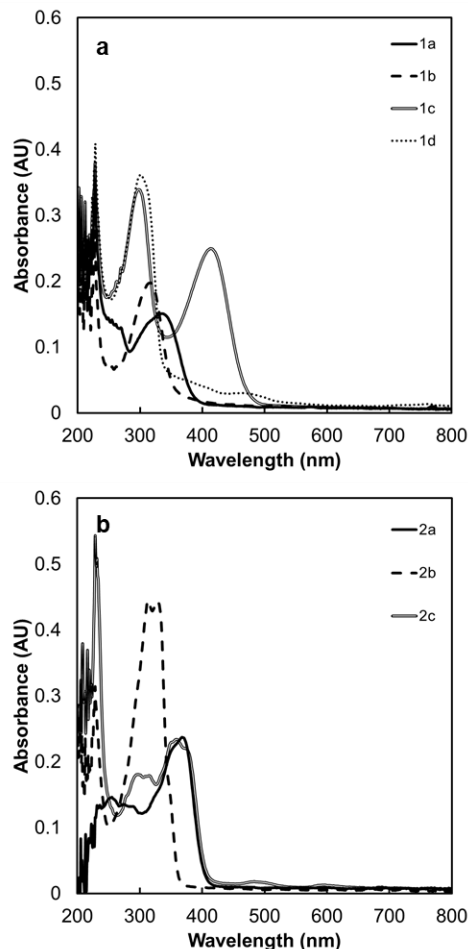


Figure 4.2. UV-vis absorption spectra of gold(I) arylisocyanides at room temperature: (a) $[\text{Au}(\text{CNDippPh}^{\text{OMe}_3})_2](\text{BF}_4)$ (**1a**), $[\text{Au}(\text{CNDippPh}^{\text{NO}_2})_2](\text{BF}_4)$ (**1b**), $[\text{Au}(\text{CNDippPh}^{\text{NPh}_2})_2](\text{BF}_4)$ (**1c**); $[\text{Au}(\text{CNDippPh}^{\text{NHPH}_2})_2](\text{OTf})_3$ (**1d**) (b) $[\text{Au}(\text{CNDipp}^{\text{CCPh}^{\text{OMe}}})_2](\text{BF}_4)$ (**2a**), $[\text{Au}(\text{CNDipp}^{\text{CCPh}^{\text{CN}}})_2](\text{BF}_4)$ (**2b**), $[\text{Au}(\text{CNDipp}^{\text{CC-1-Naph}})_2](\text{BF}_4)$ (**2c**). All species are $4.37 \mu\text{M}$ in DCM.

Solvatochromic Behavior. Absorption spectra for **1c** (21.84 and $4.37 \mu\text{M}$) in acetonitrile (ACN), dichloromethane (DCM), tetrahydrofuran (THF), and toluene solutions are shown in **Figure 4.3**. The positions of absorption maxima in DCM and toluene did not depend on **1c** concentration. However, spectra in both ACN and THF exhibited red shifts upon increasing **1c** concentrations. This effect was larger for **1c** in ACN. Most solutions exhibited two primary absorption features, although

an additional peak at 298 nm was observed for **1c** at lower concentrations in ACN. The concentration-dependent spectral changes in ACN can be attributed to molecular aggregation driven by aurophilic interactions.

In addition to concentration-dependent absorptions, **1c** also exhibited solvatochromic behavior in ACN, DCM, THF, and toluene (**Figure 4.3**). The higher wavelength absorption band exhibited very pronounced solvatochromism, consistent with an $n \rightarrow \pi^*$ assignment (*vide supra*). With DCM as exception, increases in absorption energy occurred with increases in solvent polarity³⁵ in the order: (DCM <) toluene < THF < ACN. Notably, the 298 nm feature did not display solvatochromic behavior.

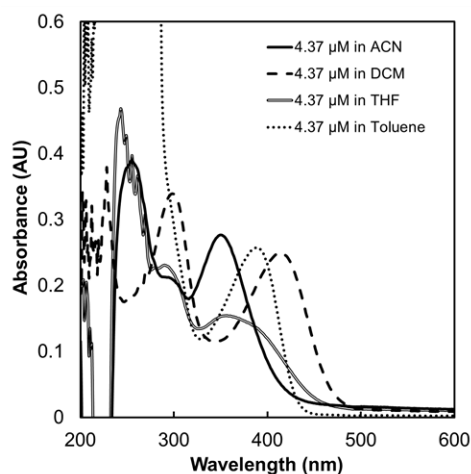


Figure 4.3. Overlay of Au(CNDippPh^{NPh2})₂(BF₄) (**1c**) UV-vis absorption spectra in ACN, DCM, THF, and toluene at room temperature.

Absorption Spectra of Protein Complexes. As expected from their solvatochromic behavior in organic solvents, **1a**, **1c**, and **2a** exhibited shifts in absorption spectra when bound to BSA in aqueous solution. Importantly, these complexes may find use in biological imaging or in drug delivery in aqueous media using cyclodextrin⁴³ as carrier.

4.4. Experimental Section

General Considerations. All manipulations were conducted using standard Schlenk or glovebox techniques under inert atmosphere (N_2). Solvents are deoxygenated and dried by sparging with N_2 gas and passage through an activated alumina column on the solvent purification system by SG Water USA, LLC. Dichloromethane- d_2 and acetonitrile- d_3 were obtained from Cambridge Isotope Laboratories, Inc., degassed following a freeze-pump-thaw Schlenk procedure, and dried over 3 Å molecular sieves.

Chloro(dimethylsulfide)gold(I) and silver tetrafluoroborate were obtained from Sigma Aldrich. Sodium phosphate monobasic was obtained from Fisher Scientific. Sodium phosphate dibasic was obtained from Mallinckrodt. Amicon Ultra 15 30 kDa nominal molecular weight limit (NMWL) centrifuge filters were obtained from Merck Millipore. Water used throughout experiments was purified using a Barnstead E-pure filtration system. A Beckman GS-6R refrigerated centrifuge was also utilized in some cases.

Spectroscopy. UV-vis absorption spectra for complexes were collected in custom 1-cm pathlength quartz cuvettes under an N_2 atmosphere in a Cary 50 spectrometer. All samples were prepared with dry, degassed solvents in an N_2 -filled glovebox isolated from the atmosphere using high-vacuum Teflon valves. In the reported spectra of all complexes, a previously obtained blank spectrum was subtracted automatically.

Infrared (IR) spectra were obtained from solid powders of precursor CNAr and Au-complex materials using a Bruker Alpha Platinum ATR spectrometer in a glovebox with a N_2 atmosphere.

Nuclear magnetic resonance (NMR) spectra were obtained at room temperature using a Varian 400 MHz spectrometer. 1H NMR chemical shifts are reported in

parts per million (ppm) relative to tetramethylsilane, using solvent response as an internal reference.

X-ray Crystallography. Low-temperature diffraction data (ϕ - and ω -scans) for the structures of all compounds were collected on a Bruker AXS KAPPA APEX II diffractometer coupled to a PHOTON 100 CMOS detector with graphite monochromated Mo K_α radiation ($\lambda = 0.71073 \text{ \AA}$) or a Bruker AXS D8 VENTURE KAPPA diffractometer coupled to a PHOTON II CPAD detector with Mo K_α radiation ($\lambda = 0.71073 \text{ \AA}$) or Cu K_α radiation ($\lambda = 1.54178 \text{ \AA}$) from an I μ S micro-source. The structures were solved by direct methods using SHELXS³¹ and refined against F^2 on all data by full-matrix least squares with SHELXL-2017³² using established refinement techniques.³³ All non-hydrogen atoms were refined anisotropically. All hydrogen atoms were included in the model at geometrically calculated positions and refined using a riding model. The isotropic displacement parameters of all hydrogen atoms were fixed to 1.2 times the U value of the atoms they are linked to (1.5 times for methyl groups). Unless otherwise noted, all disordered atoms were refined with the help of similarity restraints on the 1,2- and 1,3-distances and displacement parameters as well as enhanced rigid bond restraints for anisotropic displacement parameters. In general, for all complexes, the highest electron density maxima were located near the Au atoms. $[\text{Au}(\text{CNDippPh}^{\text{OMe}3})_2](\text{BF}_4)$ crystallized in the orthorhombic space group $Pna2_1$ with one molecule in the asymmetric unit along with one molecule of acetonitrile. $[\text{BF}_4]^-$ was disordered over two positions. $[\text{Au}(\text{CNDippPh}^{\text{NO}2})_2](\text{BF}_4)$ crystallized in the triclinic space group $P-1$ with two molecules in the asymmetric unit. The crystal was non-merohedrally twinned. Two independent orientation matrices for the unit cell were determined using the program CELL_NOW,³⁴ and data reduction was performed with SAINT,³⁵ with full account of twinning. The program TWINABS³⁶ was used for absorption correction and scaling; it also was used to set up the HKLF5 format file for structure refinement. The twin ratio was refined.

[Au(CNDippPh^{NPh2})₂](BF₄) crystallized in the monoclinic space group *P2₁/n* with half a molecule in the asymmetric unit along with a molecule of acetonitrile, which was disordered over two positions. [Au(CNDipp^{CC}Ph^{OMe})₂](BF₄) crystallized in the monoclinic space group *C2/c* with half a molecule in the asymmetric unit. [Au(CNDipp^{CC}Ph^{CN})₂](BF₄) crystallized in the orthorhombic space group *Fddd* with half a molecule in the asymmetric unit along with acetonitrile and diethyl ether. One of the isopropyl groups was disordered over two positions, and one of the [BF₄]⁻ anions was disordered with diethyl ether. Acetonitrile and diethyl ether were refined with the help of direct distance restraints on the C–C, C–O, and C–N distances (1.54(4) Å, 1.43(4) Å, and 1.15(4) Å, respectively). [Au(CNDipp^{CC}-1-naph)₂](BF₄) crystallized in the monoclinic space group *P2₁/n* with one molecule in the asymmetric unit.

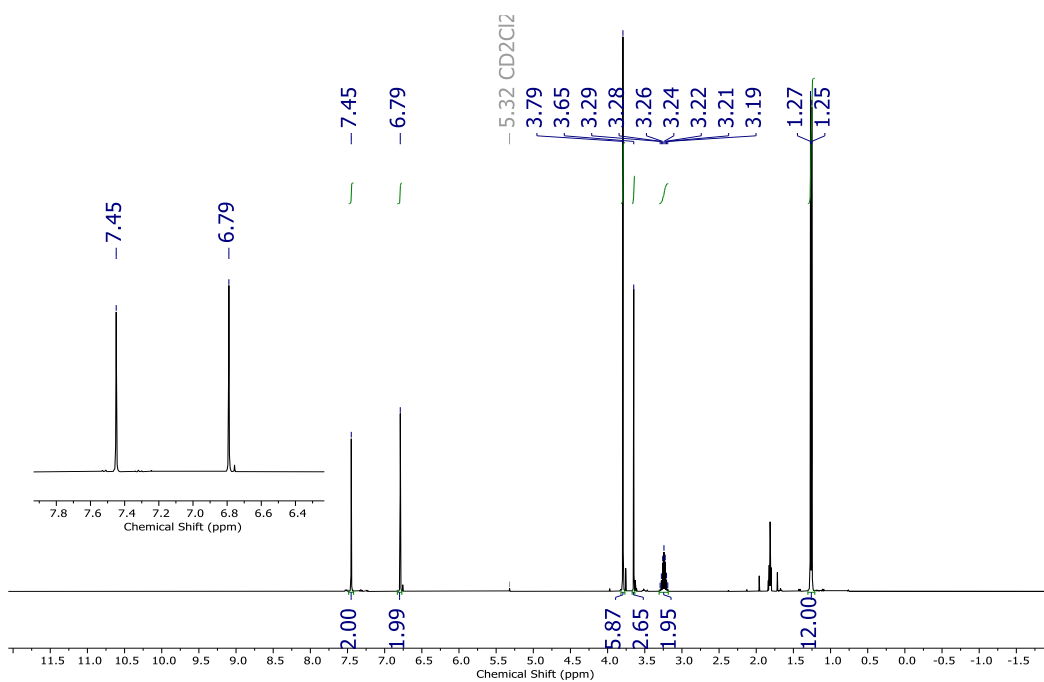


Figure 4.4. ¹H NMR of Au(CNDippPhOMe₃)₂(BF₄) (**1a**). ¹H NMR (400 MHz, CD₂Cl₂): δ 7.58 (s, 4H), 6.92 (s, 4H), 3.92 (s, 12H), 3.78 (s, 6H), 3.40 – 3.33 (m, 4H), 1.39 (d, *J* = 6.9 Hz, 24H).

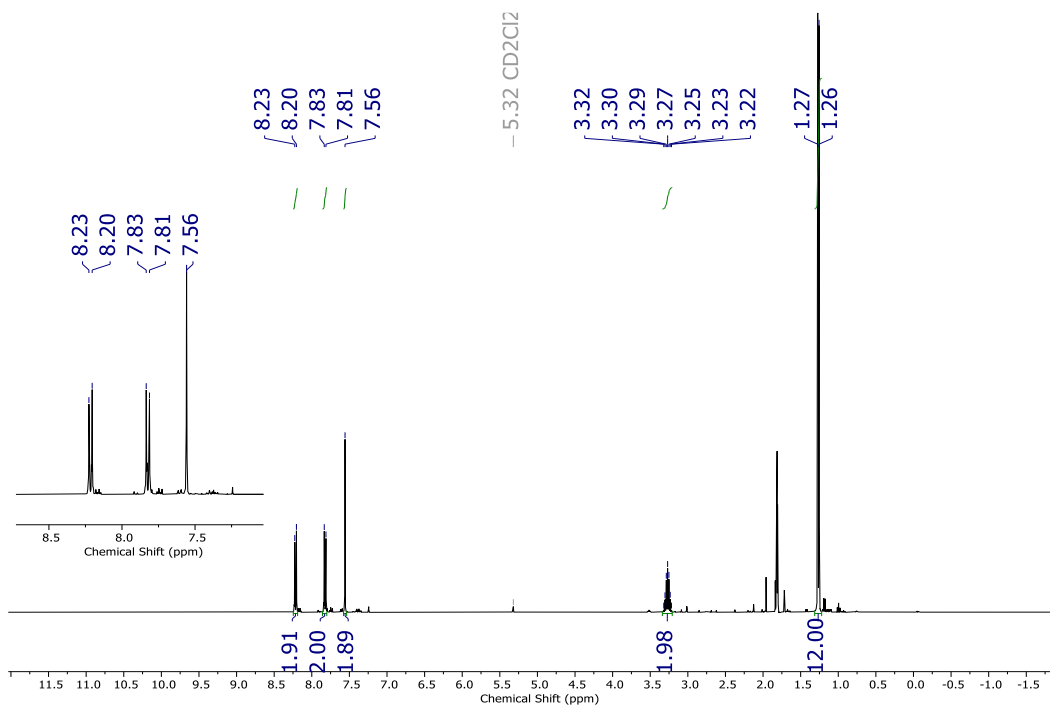


Figure 4.5. ^1H NMR of $\text{Au}(\text{CNDippPhNO}_2)_2(\text{BF}_4)$ (**1b**). ^1H NMR (400 MHz, CD_2Cl_2): δ 8.22 (d, $J = 9.2$ Hz, 4H), 7.82 (d, $J = 9.2$ Hz, 4H), 7.56 (s, 4H), 3.32 – 3.22 (m, 4H), 1.26 (d, $J = 6.8$ Hz, 24H).

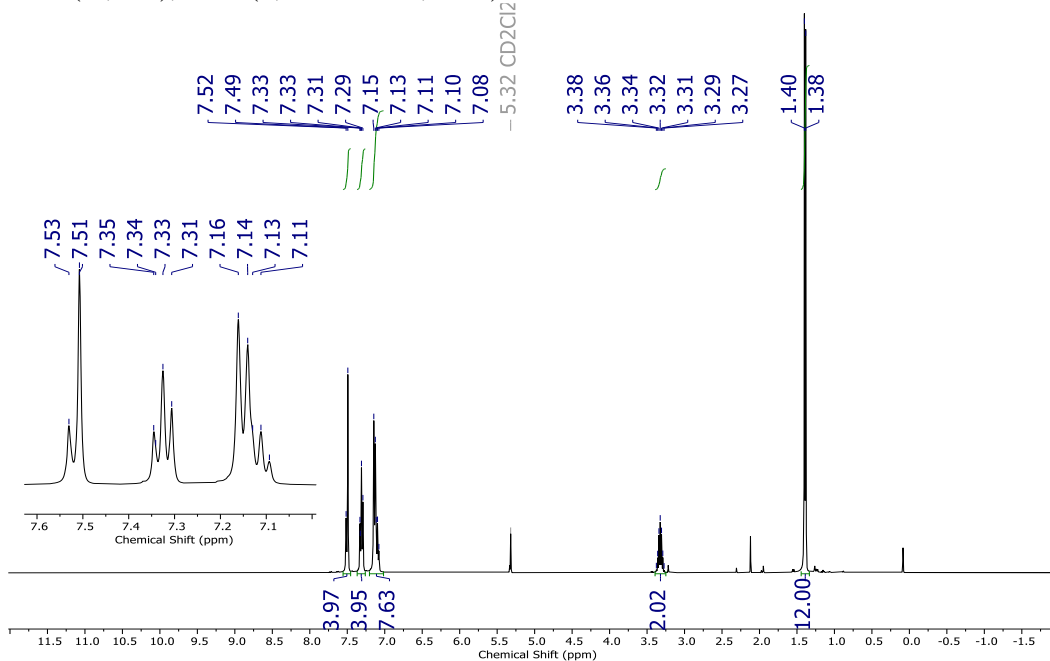


Figure 4.6. ^1H NMR of $\text{Au}(\text{CNDippPhNPh}_2)_2(\text{BF}_4)$ (**1c**). ^1H NMR (400 MHz, CD_2Cl_2): δ 7.51 (d, $J = 8.9$ Hz, 8H), 7.33 (t, $J = 7.4$ Hz, 8H), 7.16 – 7.09 (m, 16H), 3.37 – 3.20 (m, 4H), 1.41 (d, $J = 6.7$ Hz, 24H).

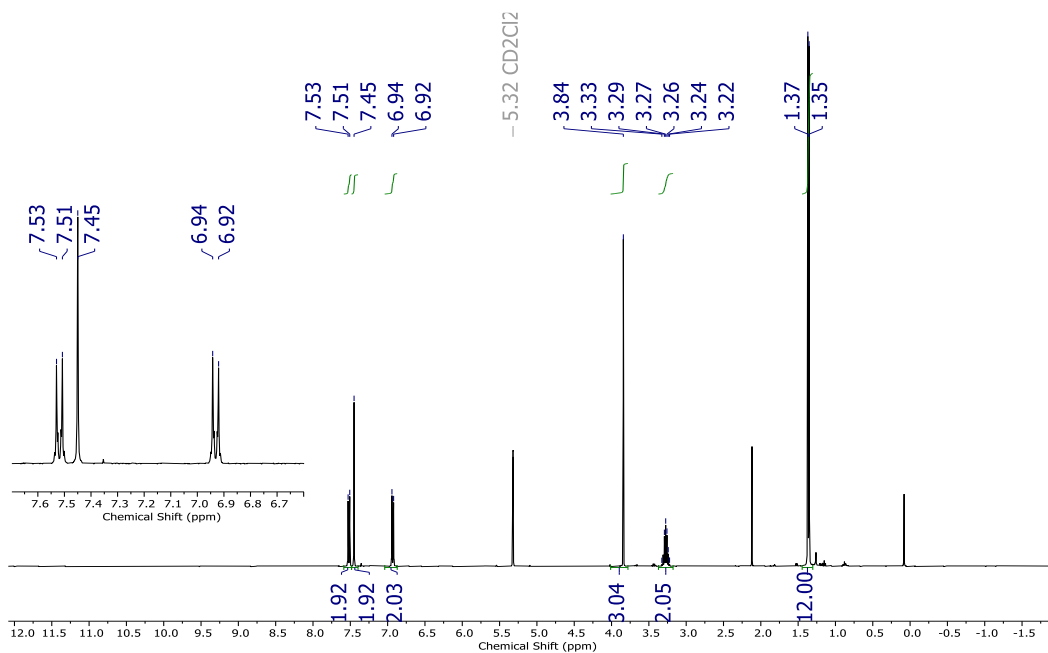


Figure 4.7. ^1H NMR of $\text{Au}(\text{CNDippCCPhOMe})_2(\text{BF}_4)$ (**2a**). ^1H NMR (400 MHz, CD_2Cl_2): δ 7.52 (d, $J = 8.6$ Hz, 4H), 7.45 (s, 4H), 6.93 (d, $J = 8.6$ Hz, 4H), 3.86 (s, 6H), 3.32 – 3.25 (m, 4H), 1.37 (d, $J = 6.7$ Hz, 24H).

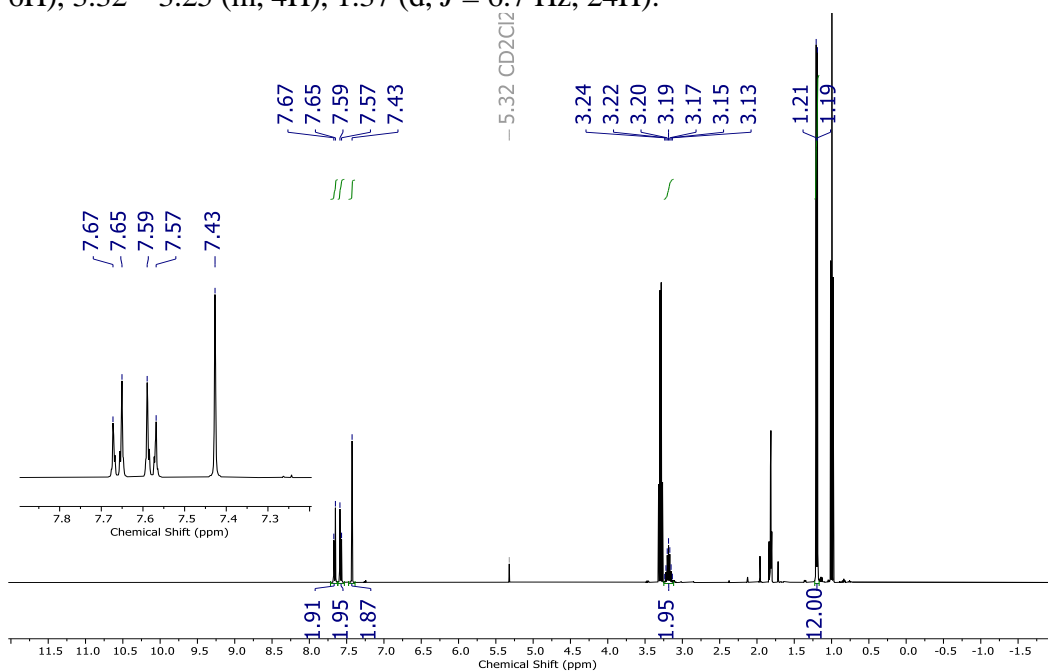


Figure 4.8. ^1H NMR of $\text{Au}(\text{CNDippCCPhCN})_2(\text{BF}_4)$ (**2b**). ^1H NMR (400 MHz, CD_2Cl_2): δ 7.80 (d, $J = 8.7$ Hz, 4H), 7.73 (d, $J = 8.7$ Hz, 4H), 7.58 (s, 4H), 3.39 – 3.30 (m, 4H), 1.35 (d, $J = 6.9$ Hz, 24H).

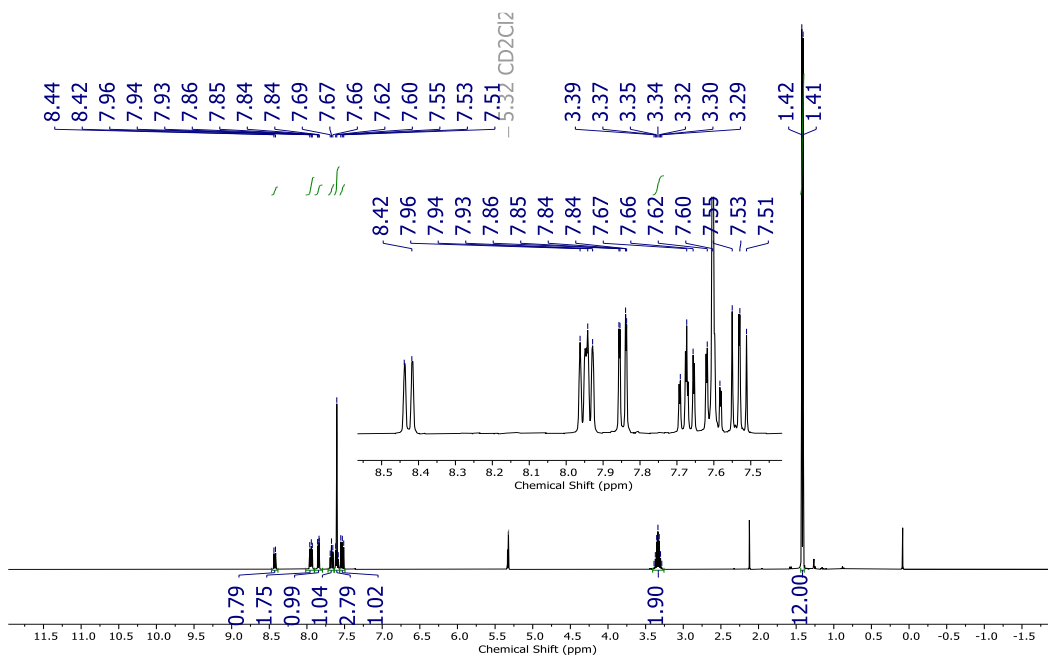


Figure 4.9. ^1H NMR of $\text{Au}(\text{CNDippCC-1-Naph})_2(\text{BF}_4)$ (**2c**). ^1H NMR (400 MHz, CD_2Cl_2): δ 8.43 (d, $J = 8.8$ Hz, 2H), 7.94 (t, $J = 6.2$ Hz, 4H), 7.84 (dd, $J = 3.2$, 1.2 Hz, 2H), 7.67 (dtd, $J = 1.3$, 1.4 Hz, 2H), 7.60 (dtd, $J = 1.3$, 2.2 Hz, 6H), 7.53 (sds, $J = 1.1$ Hz, 2H), 3.40 – 3.30 (m, 4H), 1.41 (d, $J = 6.9$ Hz, 24H).

Table 4.2. Absorption data for 1a-1d and 2a-2c in DCM: absorption at room temperature; luminescence at room temperature and 77 K.

| Species | Absorption | |
|-----------|--|---|
| | λ_{abs} // nm | $(\epsilon // \times 10^4 \text{ dm}^3 \text{ mol}^{-1} \text{ cm}^{-1})$ |
| 1a | ~310 (<i>shoulder</i>), 336 (3.45) | |
| 1b | 317 (4.52) | |
| 1c | 298 (7.76), 413 (5.71) | |
| 1d | 301 (8.28), ~315 (<i>shoulder</i>), ~380 (<i>shoulder</i>), 463 (0.69) | |
| 2a | 254 (3.34), 274 (3.09), 289 (3.02), ~325 (<i>shoulder</i>), ~350 (<i>shoulder</i>), 368 (5.42) | |
| 2b | ~295 (<i>shoulder</i>), 313 (10.17), 327 (10.16), ~350 (<i>shoulder</i>) | |
| 2c | 277 (3.35), 297 (4.14), 314 (4.09), 350 (5.25), 359 (5.35), 483 (0.41), 596 (0.29) | |

TDDFT Calculations. Equilibrium geometries of all complexes were optimized from single crystal data (except for **1d**, which was optimized after simulated protonation of **1c**). Ligand dihedral angles were more planar in TDDFT optimized geometries than those in single crystal structures. Solvent molecules were not included in the calculations, but counterions were included alongside the metal, requisite for convergence. The calculated electronic structure for **1a**, along with selected absorption and emission transitions, are shown in **Figure 4.12** (results for other complexes were similar). The HOMO is primarily ligand π , and the LUMO is ligand π^* . According to TDDFT, the main absorption appears upon excitation to a singlet $\pi \rightarrow \pi^*$ ($^1LL/LMCT$) state.

In the TDDFT model, the other major absorption feature can be assigned to transitions to singlet and triplet excited states (typically ~85-95% for the singlet and ~60-90% for the triplet) from $5d_z^2/6s$ (HOMO-10 for **1a** in **Figure 4.12**) to the LUMO. Although there is substantial mixing of singlet and triplet MLCT states, there is little evidence of 3MLCT emission, as lifetimes for most complexes were short (< 20 ns). Our observation of decreased MLCT emission intensity at low temperature (77 K) is consistent with delayed fluorescence. Note, however, that decreased MLCT transition oscillator strengths also were obtained in calculations performed on **1a** and **1b** structures with perpendicularly oriented ligands. Ligand steric bulk could have caused the complexes to adopt a less planar conformation at low temperature, as observed in all single crystal structures (main text **Figure 4.1**). There is greatly reduced delocalization in both HOMO and LUMO for out-of-plane arylisocyanide ligands, which also could account for lower oscillator strengths.

Input Parameters

Calculations were performed using ORCA^{37,38} version 5.0 on the Resnick High Performance Computing Center, supported by the Resnick Sustainability Institute at Caltech. Representative inputs for density functional theory (DFT) optimization

calculations are provided in this document under **Representative Input Files**. Starting geometries for structural optimizations use the coordinates from single-crystal structural analysis. Optimization calculations were carried out using a BP86³⁹⁻⁴¹ exchange functional. All calculations were performed to consider the relativistic effect using the scalar relativistic Douglas-Kroll-Hess (DKH) Hamiltonian. The segmented all-electron relativistically contracted (SARC) basis set (SARC-DKH-TZVPP) was used to describe Au⁴², while the basis set DKH-def2-SVP was employed on ligand atoms. One [BF₄]⁻ counterion proximal to the Au site was necessary for structural convergence. The structure of **1d** was generated through modelling protonation of crystallographic **1c** and subsequent optimization.

For TDDFT calculations, functionals BP86 (0%), B3LYP (20%), PBE0 (25%) and CAM-B3LYP (33%) were used to explore the influence of Hartree-Fock exchange on resulting spectral fit. Calculations were employed using the conductor-like polarizable continuum (CPCM) model, employing a $\epsilon = 9.08$ dielectric constant for dichloromethane.⁴³ UV-Vis spectra visualizations were generated using QMForge, employing a 3000 cm⁻¹ FWHM thermal broadening. Molecular orbitals are visualized in Avogadro with a c=0.20 isosurface value.

Representative Input Files***Geometry Optimization***

```
! BP86 def2-SVP def2/J RIJCOSX Opt TightSCF KDIIS SOSCF SlowConv LargePrint
printbasis
! defgrid3
%basis
NewGTO Au "def2-TZVPP" end
end
%scf
MaxIter 12000
end
%pal
nprocs 16
end
%maxcore 12000
* xyz 0 1
input_coordinates
*
```

TDDFT

```
! PBE0 DKH DKH-def2-SVP SARC/J RIJCOSX TightSCF CPCM(CH2Cl2) KDIIS
SOSCF LargePrint printbasis
! defgrid3
%rel
picturechange true
end
%basis
NewGTO Au "SARC-DKH-TZVPP" end
end
%scf
MaxIter 12000
end
%pal
nprocs 16
end
%tddft
nroots 30
maxdim 5
tda true
DOSOC True
triplets true
end
%maxcore 12000
* xyz 0 1
input_coordinates
```

Optimized Geometries

[Au(CNDippPh^{OMe3})₂](BF₄) (1a)

| | | | |
|----|-------------------|-------------------|-------------------|
| Au | -0.03274083837015 | -0.34865493762062 | -1.76407274454952 |
| C | 1.90875566718401 | -0.05380560279946 | -1.84640365046864 |
| N | 3.06954826869920 | 0.13734887570013 | -1.76123538948897 |
| C | 4.41569321755585 | 0.33181575266943 | -1.52435867272284 |
| C | 5.24727299139275 | 0.77399476689954 | -2.59447351445586 |
| C | 4.66875532007713 | 0.98754698750634 | -3.99136739795916 |
| H | 3.61475498544749 | 1.31577699885825 | -3.85807341960242 |
| C | 4.63917473697139 | -0.34707261238850 | -4.77217743962879 |
| H | 5.66885007223038 | -0.72673706080834 | -4.93843085945830 |
| H | 4.15987989098567 | -0.21013535004757 | -5.76356012058312 |
| H | 4.07596606844285 | -1.13171949292392 | -4.22832483528034 |
| C | 5.38586623080348 | 2.08358321389575 | -4.79711083527838 |
| H | 5.44246574854102 | 3.03771259579526 | -4.23545527532256 |
| H | 4.84168115984184 | 2.27638811942008 | -5.74384905592657 |
| H | 6.41926373186913 | 1.78780629053230 | -5.07409105354110 |
| C | 6.60411933141608 | 0.97343276422578 | -2.30743747744993 |
| H | 7.26465298043959 | 1.35032479723417 | -3.10076639782943 |
| C | 7.14439938306034 | 0.75504054393123 | -1.01647216149523 |
| C | 8.58687973353225 | 0.98521596910901 | -0.74553856178115 |
| C | 9.55184537461459 | 0.73664368364435 | -1.74883343063530 |
| H | 9.23066921190816 | 0.32887380211782 | -2.71565998593097 |
| C | 10.92047991510341 | 0.94590543369491 | -1.49068467357224 |
| O | 11.92017675043322 | 0.69105046012809 | -2.38614843656105 |
| C | 11.57585612701939 | 0.16765673945289 | -3.65803950805976 |
| H | 11.06416576731223 | -0.81731451414641 | -3.57510696702300 |
| H | 12.52679066062752 | 0.03231833627932 | -4.20622497125369 |
| H | 10.92360274709526 | 0.86325203474627 | -4.23309399502721 |
| C | 11.34905429039473 | 1.42531541330016 | -0.22384962883253 |
| O | 12.66767367092191 | 1.58712142716513 | 0.08545885640870 |
| C | 13.36653488003190 | 2.63236254904072 | -0.59361094144155 |
| H | 13.40934558690491 | 2.45714314216762 | -1.68916923657793 |
| H | 14.39515152042304 | 2.63672205171005 | -0.18516085202020 |
| H | 12.89779344693722 | 3.62230231634694 | -0.39647865278944 |
| C | 10.37470672439310 | 1.68462585148631 | 0.77897543733068 |
| O | 10.86582617436974 | 2.16070872853213 | 1.95463328288664 |
| C | 9.95915836480625 | 2.40358934776952 | 3.01758221606225 |
| H | 9.21158140613986 | 3.18719169064663 | 2.75847161848528 |
| H | 10.56853097998705 | 2.75837168610467 | 3.86957153522363 |
| H | 9.41780514501246 | 1.47945501687538 | 3.32109688475209 |
| C | 9.00937236632425 | 1.45200156213418 | 0.52016520516506 |
| H | 8.25772524061059 | 1.68467659681061 | 1.28494349154458 |
| C | 6.27248223505867 | 0.32071916245330 | 0.00944213877262 |
| H | 6.68272886902250 | 0.12303395968325 | 1.0095986501570 |
| C | 4.90416681430711 | 0.09704537172081 | -0.20226173043757 |
| C | 3.98073661677498 | -0.42389728313837 | 0.88944353862878 |
| H | 2.97413706565229 | 0.01707982784023 | 0.72989547582386 |
| C | 3.81926770177672 | -1.95927509818263 | 0.77196442997879 |
| H | 3.50026249235899 | -2.26806891490721 | -0.24469751893353 |
| H | 3.04000714093443 | -2.29149988820416 | 1.48482709559880 |
| H | 4.77508019433958 | -2.47779229814790 | 0.99809189008166 |
| C | 4.40337914495349 | -0.03230870481676 | 2.31353900015206 |
| H | 3.58730886655432 | -0.31454445449170 | 3.00668520367210 |
| H | 4.57012129926778 | 1.06031137033246 | 2.40896689287405 |
| H | 5.32626502624520 | -0.55662080928359 | 2.64253462216454 |
| C | -1.97288100827003 | -0.64190929372447 | -1.65291575670016 |
| N | -3.11940983531653 | -0.83359611332781 | -1.45310254409351 |
| C | -4.43313362754393 | -1.04171894147148 | -1.08314421402740 |
| C | -5.37992384009678 | -1.41514707611982 | -2.08132881698556 |
| C | -4.95858513784754 | -1.54313359738193 | -3.54343328232429 |
| H | -3.89921227725072 | -1.88101539962649 | -3.54595663951503 |
| C | -5.76855361772411 | -2.58602545309166 | -4.33148390314071 |

| | | | |
|---|--------------------|-------------------|-------------------|
| H | -5.77146192674986 | -3.57291403251426 | -3.82643627674933 |
| H | -5.33264741032050 | -2.72076139575172 | -5.34216809642650 |
| H | -6.82354096428881 | -2.27214998453223 | -4.47495225836768 |
| C | -5.00196287051264 | -0.16300681532031 | -4.23997116007763 |
| H | -6.04010627557921 | 0.22857837621979 | -4.27019353488805 |
| H | -4.63396582490900 | -0.23959064151328 | -5.28399879658921 |
| H | -4.37623533440601 | 0.58526976119212 | -3.71348329982643 |
| C | -6.69924674398779 | -1.62920316682253 | -1.66084908314926 |
| H | -7.44574080726333 | -1.95375775271852 | -2.39917893026365 |
| C | -7.09378925860245 | -1.49081703437102 | -0.30765808400988 |
| C | -8.50078929398775 | -1.73461267036030 | 0.10420499609784 |
| C | -9.56733985532455 | -1.41628182163133 | -0.76746805408479 |
| H | -9.34911276980541 | -0.95503603718013 | -1.73895004203353 |
| C | -10.90208213787408 | -1.65107990582923 | -0.38085037288164 |
| O | -11.98888583281939 | -1.37073391621185 | -1.15159613748500 |
| C | -11.78156283810512 | -0.78596463340743 | -2.42501965042098 |
| H | -11.27591257615546 | 0.20345837147943 | -2.35189052808275 |
| H | -12.78485743313729 | -0.64264810267038 | -2.86802962032881 |
| H | -11.18280917854264 | -1.44415901647090 | -3.09528760871793 |
| C | -11.19260830528400 | -2.20159509108847 | 0.89704124925637 |
| O | -12.49671202703714 | -2.35097689826105 | 1.26965352480061 |
| C | -12.97714691374838 | -3.69072591863643 | 1.39805826152728 |
| H | -12.89121915932999 | -4.24235606322776 | 0.43517010642110 |
| H | -14.04675403354215 | -3.61459411248012 | 1.67207477144253 |
| H | -12.43603549893085 | -4.24860815719969 | 2.19109865287223 |
| C | -10.11717240203333 | -2.52014690218162 | 1.76922697527428 |
| O | -10.48058003654475 | -3.04485539955340 | 2.97530220553071 |
| C | -9.46527247270004 | -3.34058039604190 | 3.92203888990025 |
| H | -8.76356889014706 | -4.12102046869368 | 3.55102008635025 |
| H | -9.98220324510951 | -3.72174203648719 | 4.82219084102259 |
| H | -8.88137836334981 | -2.43413527868561 | 4.19694193875587 |
| C | -8.78558816396680 | -2.28581798836068 | 1.37435460340031 |
| H | -7.95760569731293 | -2.56278755855976 | 2.03896189719006 |
| C | -6.11176284281966 | -1.12312864763510 | 0.64184249271962 |
| H | -6.40862396904106 | -0.98778872351819 | 1.69129201245594 |
| C | -4.77277156256360 | -0.88878089504936 | 0.29624696256045 |
| C | -3.73178747979716 | -0.43815947994135 | 1.31067260338393 |
| H | -2.75144292620472 | -0.86662782254326 | 1.01320617125075 |
| C | -3.57492119024225 | 1.10170009846150 | 1.27562773604373 |
| H | -3.36743664544335 | 1.47592830077563 | 0.25208568264684 |
| H | -2.72005140881119 | 1.38768128814755 | 1.91839320873051 |
| H | -4.49699175997721 | 1.60348739233190 | 1.63840035798357 |
| C | -3.99696954383182 | -0.92222889326482 | 2.74440971805515 |
| H | -4.87524890368969 | -0.42254500833271 | 3.20682056228641 |
| H | -3.10780336346729 | -0.68421878751800 | 3.35992476829563 |
| H | -4.15758985468660 | -2.01916756899492 | 2.78625082235525 |
| B | 0.15619552037025 | -0.45631633774397 | 1.70541394132143 |
| F | -0.75998847865113 | 0.16274038231672 | 2.56858436888426 |
| F | 1.16016273698717 | -1.12484852198049 | 2.42145609596581 |
| F | -0.53549960517095 | -1.39060391591853 | 0.85999936513010 |
| F | 0.75323204975849 | 0.53139627696907 | 0.84853210255435 |

[Au(CNDippPh^{NO2})₂](BF₄) (**1b**)

| | | | |
|----|--------------|-------------|-------------|
| Au | -0.011515826 | 0.690323356 | 1.447683464 |
| C | 1.952068348 | 0.698008327 | 1.425293670 |
| N | 3.105273557 | 0.573075171 | 1.211157309 |
| C | -1.967442803 | 0.570160292 | 1.271843916 |
| N | -3.124890997 | 0.392819810 | 1.395031897 |
| C | 4.410587591 | 0.332564285 | 0.823896609 |
| C | 5.461955313 | 1.023686745 | 1.492575092 |
| C | 5.154735263 | 2.034316826 | 2.594642846 |
| H | 4.224426729 | 1.690970908 | 3.097401015 |
| C | 4.860781061 | 3.424043278 | 1.982388381 |
| H | 5.758880383 | 3.824178970 | 1.467501890 |
| H | 4.570464337 | 4.144857966 | 2.774036860 |

| | | | |
|---|---------------|--------------|--------------|
| H | 4.038002311 | 3.384533567 | 1.240651713 |
| C | 6.248703819 | 2.122473490 | 3.672053357 |
| H | 6.492770766 | 1.127264604 | 4.095051392 |
| H | 5.909356380 | 2.772269051 | 4.503707197 |
| H | 7.186209746 | 2.567870998 | 3.278890431 |
| C | 6.770124196 | 0.761231298 | 1.062429173 |
| H | 7.606826831 | 1.254331351 | 1.576764678 |
| C | 7.046124685 | -0.146083372 | 0.012797542 |
| C | 8.446271169 | -0.401594221 | -0.417268187 |
| C | 9.412805134 | 0.635907422 | -0.404661643 |
| H | 9.117643006 | 1.651613611 | -0.102081687 |
| C | 10.732360603 | 0.402542400 | -0.807644261 |
| H | 11.490300530 | 1.197399835 | -0.814458358 |
| C | 11.092428561 | -0.886319046 | -1.226619561 |
| N | 12.493134589 | -1.142897271 | -1.652971383 |
| O | 13.280469702 | -0.194577226 | -1.611941187 |
| O | 12.773748438 | -2.286520886 | -2.018214406 |
| C | 10.166555767 | -1.939181284 | -1.253784591 |
| H | 10.497876738 | -2.933614035 | -1.581984488 |
| C | 8.849847745 | -1.689947473 | -0.850656869 |
| H | 8.125928754 | -2.518240696 | -0.844434491 |
| C | 5.966849481 | -0.805511991 | -0.616954537 |
| H | 6.168700091 | -1.489103003 | -1.453510410 |
| C | 4.630701360 | -0.595910148 | -0.239446629 |
| C | 3.477149491 | -1.345596710 | -0.889943958 |
| H | 2.580505046 | -0.691542450 | -0.866166300 |
| C | 3.712171363 | -1.703819087 | -2.366319521 |
| H | 4.014593522 | -0.820100474 | -2.964889954 |
| H | 2.762262585 | -2.091752711 | -2.783008529 |
| H | 4.484247771 | -2.492602959 | -2.494650574 |
| C | 3.130024780 | -2.611716488 | -0.068915590 |
| H | 3.970114081 | -3.337867217 | -0.091247207 |
| H | 2.226339819 | -3.084617870 | -0.498662792 |
| H | 2.909599393 | -2.375208423 | 0.991241496 |
| C | -4.465749923 | 0.163692542 | 1.624515360 |
| C | -5.012951628 | -1.094812707 | 1.239290580 |
| C | -4.122859299 | -2.197901401 | 0.678055182 |
| H | -3.303058444 | -1.699301649 | 0.116420709 |
| C | -3.474160542 | -2.991158162 | 1.838889894 |
| H | -2.927084066 | -2.334913861 | 2.545087502 |
| H | -2.761725859 | -3.740926206 | 1.437575559 |
| H | -4.251950908 | -3.534090336 | 2.415874318 |
| C | -4.846194329 | -3.130615372 | -0.307921824 |
| H | -4.117931479 | -3.827547449 | -0.769265842 |
| H | -5.344738742 | -2.569279785 | -1.124498891 |
| H | -5.610632039 | -3.757510732 | 0.196931239 |
| C | -6.381894763 | -1.288539963 | 1.475147181 |
| H | -6.830190846 | -2.257639726 | 1.214494074 |
| C | -7.189664149 | -0.296403567 | 2.075317107 |
| C | -8.637231960 | -0.538665024 | 2.311217726 |
| C | -9.409387893 | -1.286639242 | 1.386761193 |
| H | -8.938458918 | -1.669814295 | 0.469335380 |
| C | -10.773131827 | -1.516243449 | 1.600324950 |
| H | -11.388726747 | -2.083348935 | 0.889236813 |
| C | -11.373188699 | -0.994421560 | 2.755402724 |
| N | -12.821108530 | -1.234027383 | 2.989115000 |
| O | -13.316731367 | -0.757372242 | 4.012608924 |
| O | -13.430336672 | -1.893300229 | 2.143370654 |
| C | -10.643406295 | -0.252492570 | 3.695388953 |
| H | -11.154794786 | 0.125708203 | 4.590752669 |
| C | -9.281124518 | -0.028321984 | 3.466760574 |
| H | -8.696235005 | 0.527698351 | 4.214440531 |
| C | -6.594856359 | 0.930294176 | 2.448125903 |
| H | -7.222880875 | 1.714765570 | 2.892880915 |
| C | -5.234169602 | 1.197068380 | 2.235877970 |

| | | | |
|---|--------------|--------------|--------------|
| C | -4.580541631 | 2.498898519 | 2.685755553 |
| H | -3.765892103 | 2.720028638 | 1.961669767 |
| C | -5.536705588 | 3.703025601 | 2.675159780 |
| H | -6.316732856 | 3.620438597 | 3.460567762 |
| H | -6.044789129 | 3.826526459 | 1.696877244 |
| H | -4.970824545 | 4.632635264 | 2.885657394 |
| C | -3.925126481 | 2.309087177 | 4.075580953 |
| H | -3.403284120 | 3.239436600 | 4.379444684 |
| H | -3.184502425 | 1.486157911 | 4.088878077 |
| H | -4.698733962 | 2.085377782 | 4.839366966 |
| B | -0.303315949 | -1.398641985 | -1.096016575 |
| F | 0.370192661 | -0.133437338 | -1.212862577 |
| F | -1.684765249 | -1.200022875 | -1.325381589 |
| F | -0.129947744 | -1.858760228 | 0.248898085 |
| F | 0.250212109 | -2.314088752 | -1.990053995 |

[Au(CNDippPh^{NPh2})₂](BF₄) (1c)

| | | | |
|----|--------------------|-------------------|-------------------|
| Au | -0.20431953094603 | 0.46522146350901 | 1.22232200445131 |
| C | -2.14895614335614 | 0.41119268923127 | 0.94320817523112 |
| N | -3.29575702252629 | 0.26447008952545 | 0.70885939733563 |
| C | -4.60415257072050 | -0.03539125309315 | 0.38768530278102 |
| C | -4.91559081259172 | -1.38363188482261 | 0.03065139773655 |
| C | -3.84419104005265 | -2.46411182956857 | 0.05917017023398 |
| H | -2.88057433729744 | -2.00363089235342 | -0.24499384352853 |
| C | -3.65003830631369 | -2.99086721410515 | 1.50213729588748 |
| H | -3.45664494706979 | -2.17007860742428 | 2.22301479076024 |
| H | -2.77424981723738 | -3.66798427485890 | 1.51966533833232 |
| H | -4.55099264614683 | -3.53990698857839 | 1.84949077708935 |
| C | -4.09273459658336 | -3.62756399817752 | -0.91261490611275 |
| H | -4.94951116435554 | -4.26451395546387 | -0.60417683534294 |
| H | -3.18616868100212 | -4.26310300387732 | -0.92972884375246 |
| H | -4.27956155359822 | -3.27036404732668 | -1.94603832425886 |
| C | -6.25009994302842 | -1.65058581487504 | -0.30727398883174 |
| H | -6.50980896150175 | -2.67046758871523 | -0.62349115980291 |
| C | -7.25762604306561 | -0.65609245222658 | -0.29176952126992 |
| C | -8.65732769188154 | -0.98356317638724 | -0.65109835798820 |
| C | -9.20126047076447 | -2.27131658074930 | -0.41357706093794 |
| H | -8.58756633996630 | -3.03664634189083 | 0.08543283284912 |
| C | -10.52215430875554 | -2.58510077015992 | -0.74327868555454 |
| H | -10.91820649038125 | -3.58583110468083 | -0.51804018380804 |
| C | -11.36612275650596 | -1.62053990928060 | -1.34884553099156 |
| N | -12.70072306602276 | -1.93515987291699 | -1.69432989950484 |
| C | -13.03924185188051 | -3.24566829107645 | -2.14554641205148 |
| C | -12.21907991490518 | -3.91950834268727 | -3.08007937381348 |
| H | -11.31542290587566 | -3.42310241281189 | -3.46367516185134 |
| C | -12.55768045891207 | -5.20886761893270 | -3.51619113661746 |
| H | -11.90904416702604 | -5.71957447439820 | -4.24494486766135 |
| C | -13.72280451056211 | -5.83993144754413 | -3.04554520113545 |
| H | -13.98821531688411 | -6.84910840148756 | -3.39518619356224 |
| C | -14.54565048451325 | -5.16784761258192 | -2.12460834490988 |
| H | -15.45769082142301 | -5.65274228504232 | -1.74284120230282 |
| C | -14.20723953221070 | -3.88497556580397 | -1.66954573199302 |
| H | -14.84623013194008 | -3.36737650165745 | -0.93891046859601 |
| C | -13.72432058379657 | -0.94710237337750 | -1.59649002063554 |
| C | -14.69019309984157 | -0.81520551258685 | -2.62104210774630 |
| H | -14.63726409938604 | -1.47380185483127 | -3.50049554837469 |
| C | -15.70485280666371 | 0.14743224267422 | -2.51604394952884 |
| H | -16.44820227216895 | 0.23806515604534 | -3.32346289391911 |
| C | -15.76720849933343 | 1.00236261784287 | -1.40150553378695 |
| H | -16.56155587377843 | 1.76026790955728 | -1.32564772052807 |
| C | -14.80497896774950 | 0.87722373231024 | -0.38375343688275 |
| H | -14.84791680774148 | 1.53276470574169 | 0.50011318254873 |
| C | -13.79585633976628 | -0.09292131481887 | -0.47134196504360 |
| H | -13.05566371229800 | -0.19901155458974 | 0.33550491215601 |
| C | -10.83181184220051 | -0.33170100997088 | -1.59929639659343 |

| | | | |
|---|--------------------|-------------------|-------------------|
| H | -11.45771742533877 | 0.42768505815693 | -2.08989521198520 |
| C | -9.51424497558124 | -0.02539242520563 | -1.24940079264361 |
| H | -9.12487613988994 | 0.97486274921964 | -1.49355969598192 |
| C | -6.89151550496577 | 0.66209304535940 | 0.07792939891384 |
| H | -7.66991949686966 | 1.43625378107355 | 0.12601956206733 |
| C | -5.57725545737686 | 1.00611205863025 | 0.41899697054909 |
| C | -5.17358601276780 | 2.43620862557956 | 0.77000411697685 |
| H | -4.32851062417454 | 2.36625132978113 | 1.48945296201411 |
| C | -6.28875715114498 | 3.24220934903554 | 1.45676887967213 |
| H | -5.89485898139051 | 4.22109249695908 | 1.79776329598249 |
| H | -6.69672312564829 | 2.71151707422059 | 2.34061938800198 |
| H | -7.13179123390515 | 3.45707276137159 | 0.76744379990481 |
| C | -4.6798919453955 | 3.17122566909591 | -0.48519946152071 |
| H | -3.80678036093865 | 2.62804745712845 | -0.96046822706082 |
| H | -4.29067703570540 | 4.18821986489224 | -0.22189121652961 |
| H | -5.45181990993287 | 3.27556250788629 | -1.24339117419354 |
| C | 1.74269315852854 | 0.49371541834399 | 1.48835326368634 |
| N | 2.91121657430132 | 0.38436526607765 | 1.60765473511495 |
| C | 4.26632981509347 | 0.13192456307613 | 1.67820896187484 |
| C | 4.77838021392991 | -0.99120182461646 | 0.95799271301837 |
| C | 3.86205411785380 | -1.84754919408426 | 0.09581703868203 |
| H | 2.86758569476662 | -1.89371394145880 | 0.58781213010677 |
| C | 3.64492620247299 | -1.18137631836468 | -1.28487093931026 |
| H | 3.29563799415459 | -0.13258021318609 | -1.19130829964669 |
| H | 2.86887698760365 | -1.74734413353937 | -1.83551233276002 |
| H | 4.58631523492900 | -1.17226107162710 | -1.87439345511543 |
| C | 4.32882520421192 | -3.30144304061063 | -0.07223842472531 |
| H | 5.24151165852397 | -3.38599685082090 | -0.70048880673770 |
| H | 3.51942522737220 | -3.86878073684881 | -0.57129925065086 |
| H | 4.53349743731284 | -3.78525180183156 | 0.90475626477305 |
| C | 6.15602458654034 | -1.22968018990566 | 1.06525471378367 |
| H | 6.57041004973608 | -2.10921711372977 | 0.55312127095284 |
| C | 7.01808386218204 | -0.40863100221641 | 1.83149253114464 |
| C | 8.4695917446240 | -0.69509270301063 | 1.91289304379974 |
| C | 9.16401109402171 | -1.31209508918460 | 0.84161702790773 |
| H | 8.62692945765897 | -1.54833881856816 | -0.08956429208544 |
| C | 10.53354285351677 | -1.57992796841764 | 0.90896873988852 |
| H | 11.04417908853581 | -2.03370832945221 | 0.04735330409931 |
| C | 11.27863592852864 | -1.25590486493467 | 2.07053683549595 |
| N | 12.66258968701449 | -1.53514117492561 | 2.14893658009071 |
| C | 13.20047246494555 | -2.69786726729648 | 1.52083957333686 |
| C | 12.53887240239348 | -3.94348058880894 | 1.62468498553342 |
| H | 11.60367895499846 | -4.01306983251305 | 2.19977058697551 |
| C | 13.07320474259857 | -5.08098040206778 | 1.00188117464401 |
| H | 12.54634988524900 | -6.04364767287351 | 1.09313912217508 |
| C | 14.27928166892548 | -5.00260627498649 | 0.28321044212708 |
| H | 14.69843627486801 | -5.89889704695302 | -0.19856171508565 |
| C | 14.94462458672935 | -3.76767314098170 | 0.18747722718473 |
| H | 15.88665163763577 | -3.69053546139381 | -0.37760765767034 |
| C | 14.41012571313173 | -2.62073536649411 | 0.79263626619106 |
| H | 14.92643734951206 | -1.65341065813780 | 0.70454688931167 |
| C | 13.53723885044151 | -0.66059944982821 | 2.85865482621596 |
| C | 14.53963415648967 | -1.18639353743056 | 3.70645563887006 |
| H | 14.63035063828898 | -2.27640940032956 | 3.82313520283908 |
| C | 15.40845342687216 | -0.32500532883753 | 4.39229899960719 |
| H | 16.1825945501985 | -0.75077208215651 | 5.04970901308345 |
| C | 15.28600588776628 | 1.06934588299966 | 4.25897808431235 |
| H | 15.96601502683960 | 1.74196821644462 | 4.80334037047517 |
| C | 14.28672525682105 | 1.59522439650485 | 3.42097596599642 |
| H | 14.18616562777469 | 2.68503788320274 | 3.29852595381017 |
| C | 13.42327974392520 | 0.74223270819581 | 2.71807126024228 |
| H | 12.65441360838788 | 1.15766220690976 | 2.04992460142689 |
| C | 10.59450284717251 | -0.64572509661267 | 3.15173102374206 |
| H | 11.14385300340707 | -0.40581117128939 | 4.07355040010501 |
| C | 9.22795154484630 | -0.36761202611810 | 3.06528095846157 |

| | | | |
|---|-------------------|-------------------|-------------------|
| H | 8.72519623804610 | 0.07308198264468 | 3.93979570422694 |
| C | 6.45521371133835 | 0.69562364112094 | 2.51846569576971 |
| H | 7.11795154976196 | 1.36019744948888 | 3.09008120481518 |
| C | 5.08701858512063 | 0.99125885982385 | 2.46602057718696 |
| C | 4.47347826445385 | 2.15200705606861 | 3.24535801781310 |
| H | 3.59547805749081 | 2.50521573777343 | 2.66151077958521 |
| C | 5.41983608084248 | 3.35263482847815 | 3.41255337766157 |
| H | 4.87621975878919 | 4.20358180554371 | 3.87085375742597 |
| H | 5.82974846802723 | 3.69291354383101 | 2.44022133710490 |
| H | 6.27447227964905 | 3.11926964447815 | 4.08128077477875 |
| C | 3.94717825430320 | 1.66274046100185 | 4.61485515973024 |
| H | 3.22166989313406 | 0.83185929155166 | 4.50583529772551 |
| C | 3.44051033688284 | 2.48789587830481 | 5.15679501838418 |
| H | 4.78265701614225 | 1.29844150017020 | 5.24823254909555 |
| B | 0.05379299276812 | -2.71260525724967 | -0.15859706611515 |
| F | 1.05234986096084 | -3.10549469484120 | -1.06185736163553 |
| F | -0.82888562916452 | -3.76739552021719 | 0.11731353943242 |
| F | -0.67918479489337 | -1.60290065961855 | -0.70420737608196 |
| F | 0.66131338676847 | -2.26134770159639 | 1.06354640943841 |

[Au(CNDippPh^{NHPh2})₂](OTf)₃ (**1d**)

| | | | |
|----|-------------------|-------------------|-------------------|
| Au | -0.18460718519759 | -0.55732642548889 | 3.54366166302165 |
| C | 1.75298520078649 | -0.65190705053558 | 3.86591764998905 |
| N | 2.92936203646477 | -0.62380531396184 | 3.93938677106206 |
| C | 4.30802611603901 | -0.51684317442173 | 3.95850850632013 |
| C | 4.90489763389047 | 0.57635602465331 | 3.26082319406875 |
| C | 4.05596707121070 | 1.62338913143857 | 2.55756684045876 |
| H | 3.14969891983080 | 1.12505857307224 | 2.15696883879150 |
| C | 3.56984229152988 | 2.68725749572714 | 3.57097871043562 |
| H | 3.05592054539393 | 2.23079040234296 | 4.44064792599650 |
| H | 2.84148001362557 | 3.35908259045256 | 3.07770488393168 |
| H | 4.41816865553956 | 3.29270435181765 | 3.95483166685962 |
| C | 4.74877005592763 | 2.27755251168674 | 1.35278285405508 |
| H | 5.58249426906460 | 2.94973843299445 | 1.65006534129085 |
| H | 4.00856715360047 | 2.88782673755477 | 0.80088335037029 |
| H | 5.13985461212033 | 1.52040585870169 | 0.64359239476768 |
| C | 6.30755838791850 | 0.64382977231810 | 3.29005877219149 |
| H | 6.79716528563354 | 1.45408577957815 | 2.73143884169483 |
| C | 7.09561554734697 | -0.31055484736562 | 3.97005904152067 |
| C | 8.57855333560564 | -0.19906348201486 | 3.96721869500042 |
| C | 9.21457883496767 | 1.06792515612066 | 3.99158477758952 |
| H | 8.60741920414080 | 1.98311749856118 | 4.04603911093095 |
| C | 10.60995243116404 | 1.18184219532705 | 3.97922090737813 |
| H | 11.07850141054693 | 2.17915578554513 | 3.99357050220265 |
| C | 11.38941330993911 | 0.01563552568424 | 3.95037900413135 |
| N | 12.88448153872219 | 0.17890853571671 | 3.92051101333747 |
| C | 13.43300681501839 | 0.57681650008609 | 2.57394252715045 |
| C | 12.79900119601066 | 0.16316118688829 | 1.39645842767685 |
| H | 11.87652630418242 | -0.43347649438022 | 1.42783988510135 |
| C | 13.36257589193466 | 0.54477156503562 | 0.16553600022299 |
| H | 12.87624388269572 | 0.23031640608906 | -0.76977449650226 |
| C | 14.52818715781326 | 1.32762178916548 | 0.12807302699793 |
| H | 14.95797598129247 | 1.62679452898512 | -0.83939435274373 |
| C | 15.14386604569005 | 1.73551362005465 | 1.32461267284494 |
| H | 16.05388475658967 | 2.35303232826522 | 1.29961332317385 |
| C | 14.59884450662442 | 1.35719341729012 | 2.56171504179326 |
| H | 15.08801787654354 | 1.66416969538317 | 3.50027078714648 |
| C | 13.63821396802978 | -0.94816926612060 | 4.57756251624078 |
| C | 14.24193172997414 | -1.94692594673398 | 3.80430794576795 |
| H | 14.20253987707291 | -1.91648458410095 | 2.70640033213720 |
| C | 14.92090161814609 | -2.98530992915729 | 4.46689527109615 |
| H | 15.40441369591271 | -3.77616694559155 | 3.87446212985294 |
| C | 14.99335943098399 | -3.00774811088601 | 5.86948418688678 |
| H | 15.53424343405569 | -3.81929112085501 | 6.37848689141863 |
| C | 14.38337913346189 | -1.99046141899791 | 6.62452128352985 |

| | | | |
|---|--------------------|-------------------|-------------------|
| H | 14.44396038951481 | -2.00053708765985 | 7.72285361917942 |
| C | 13.69508995659151 | -0.95085354671833 | 5.97937778206300 |
| H | 13.20675297194225 | -0.15874291041557 | 6.56974176061880 |
| C | 10.80213158020081 | -1.25490254829536 | 3.93325597408997 |
| H | 11.41829046681486 | -2.16486620403038 | 3.91739088680727 |
| C | 9.40218231949211 | -1.35059720566388 | 3.93876435997280 |
| H | 8.94197424783278 | -2.34862397461003 | 3.89863660029792 |
| C | 6.45377899256928 | -1.37208914139744 | 4.64804189096721 |
| H | 7.05761014463344 | -2.10054233417949 | 5.20745432757780 |
| C | 5.05697013129344 | -1.50464864553252 | 4.66236961568346 |
| C | 4.35944429985589 | -2.67226488901477 | 5.35442091481545 |
| H | 3.37249268712733 | -2.29699079915916 | 5.70207557939572 |
| C | 5.10904688219843 | -3.19377405972657 | 6.59174732967676 |
| H | 4.48872508998902 | -3.94563036563494 | 7.11908404255551 |
| H | 5.33977871922854 | -2.38117659636897 | 7.30983403201745 |
| H | 6.06025942117362 | -3.69855627698394 | 6.32200954626655 |
| C | 4.08994858063649 | -3.81120978415917 | 4.34224903497159 |
| H | 3.50619721303571 | -3.46202083789224 | 3.46721198818606 |
| H | 3.52044269580289 | -4.63098308332129 | 4.82523290931468 |
| H | 5.04329979192685 | -4.23478532234627 | 3.96376734052463 |
| C | -2.11163953204400 | -0.42642771185755 | 3.17126789251199 |
| N | -3.21921225958075 | -0.24749213039530 | 2.80795765631482 |
| C | -4.45544446679360 | 0.04854466356756 | 2.26189543866328 |
| C | -4.49943317302024 | 0.99243155721394 | 1.19075215084991 |
| C | -3.24505155578308 | 1.70686536004064 | 0.71450980403377 |
| H | -2.39368798508413 | 0.99896910915343 | 0.80067415725497 |
| C | -3.29230182645868 | 2.15314781316348 | -0.75478187199673 |
| H | -3.56255504995478 | 1.31849207578014 | -1.43387090392963 |
| H | -2.28286173544478 | 2.50849652064944 | -1.03840400953940 |
| H | -4.00358289416087 | 2.99021210740220 | -0.92381266905801 |
| C | -2.92582190480707 | 2.90704620585936 | 1.64062369291147 |
| H | -3.70361352419915 | 3.69470382326405 | 1.55257885684068 |
| H | -1.94364227231931 | 3.32640677450998 | 1.34893371020096 |
| H | -2.86297461578865 | 2.60985839052808 | 2.70720399545101 |
| C | -5.76571394317611 | 1.25302132770819 | 0.64189542637557 |
| H | -5.83321755410318 | 1.98957386147585 | -0.17137844609139 |
| C | -6.93924602124771 | 0.63122141982048 | 1.12181965169399 |
| C | -8.25767983184760 | 0.94084249403490 | 0.50760564780109 |
| H | -8.37166214543550 | 1.19565785979143 | -0.88258420533050 |
| H | -7.48057463622549 | 1.13460615044918 | -1.52408581362666 |
| C | -9.60785037904578 | 1.49385032439511 | -1.46823305247768 |
| H | -9.66781502739059 | 1.69197083570006 | -2.55060240991635 |
| C | -10.75409901597367 | 1.53269186975474 | -0.65999159432756 |
| N | -12.06119524909780 | 1.87193466617308 | -1.32337138516053 |
| C | -12.22661680416414 | 3.33563605528971 | -1.64317628190578 |
| C | -11.63548397506012 | 4.31229257125732 | -0.83301880686898 |
| H | -11.01766747387663 | 4.03376064983748 | 0.03222898157636 |
| C | -11.83720026857591 | 5.66461273781975 | -1.16290273869150 |
| H | -11.37840664217702 | 6.44541507284689 | -0.53835514905289 |
| C | -12.60752395845735 | 6.01714928949671 | -2.28331065839552 |
| H | -12.75430570563628 | 7.07740221501078 | -2.53733937206330 |
| C | -13.18657523031776 | 5.01774399445500 | -3.08516687866608 |
| H | -13.78612010624785 | 5.28956020542907 | -3.96650083284889 |
| C | -13.00157148732944 | 3.66334455370755 | -2.76578334079653 |
| H | -13.46623590547892 | 2.87915912939145 | -3.38508959364727 |
| C | -13.26483948044624 | 1.25249520409651 | -0.66211442565276 |
| C | -14.07854178920594 | 2.01040972841946 | 0.18840826975863 |
| H | -13.87376524023980 | 3.07479137397456 | 0.37015859075902 |
| C | -15.18170756578929 | 1.38112144296586 | 0.79274372037580 |
| H | -15.83393280434429 | 1.96304434368931 | 1.46071518862620 |
| C | -15.45746372460043 | 0.02760985914723 | 0.53767018410127 |
| H | -16.32778298789879 | -0.45359045964347 | 1.00801695929555 |
| C | -14.62850602245090 | -0.71171943335992 | -0.32446392594711 |
| H | -14.84517847749680 | -1.76997549360606 | -0.53244270913799 |
| C | -13.51883701118683 | -0.10106421632323 | -0.92985708356372 |

| | | | |
|---|--------------------|-------------------|-------------------|
| H | -12.86148515287801 | -0.68175965425955 | -1.59705581000895 |
| C | -10.68682236287316 | 1.28104235747276 | 0.71535065046918 |
| H | -11.58944012645398 | 1.30670409516743 | 1.34185137548432 |
| C | -9.43867603085693 | 0.99032909036934 | 1.28714746374169 |
| H | -9.38298927944175 | 0.81762323645421 | 2.37187496913449 |
| C | -6.84008020215086 | -0.29272251643519 | 2.18742909844610 |
| H | -7.74324730393378 | -0.81044433847869 | 2.54023619030875 |
| C | -5.60764260126303 | -0.61201206675536 | 2.77781108129377 |
| C | -5.49258789085906 | -1.59334100791339 | 3.94088465370162 |
| H | -4.49902232029315 | -2.08366922701074 | 3.84977905594276 |
| C | -6.55312226918120 | -2.70657717778736 | 3.91789742880943 |
| H | -6.33342785636036 | -3.45297738002508 | 4.70706744333078 |
| H | -6.57477020563914 | -3.23830029263607 | 2.94531135302016 |
| H | -7.57222142455960 | -2.31690963091490 | 4.12289401202229 |
| C | -5.50985533319736 | -0.83229016748025 | 5.28789229777671 |
| H | -4.71556592820048 | -0.06104537316926 | 5.34046638313120 |
| H | -5.35650349915808 | -1.53529322610476 | 6.13164493989068 |
| H | -6.48431475662261 | -0.32359969395176 | 5.44042181878766 |
| H | 13.06838502462861 | 0.99935556350032 | 4.52591614455506 |
| H | -12.00982880068673 | 1.41018916252802 | -2.24947029259412 |
| B | 0.56374492399209 | 1.38127545726951 | 0.88913335017331 |
| F | -0.03847277961076 | 2.43943853989897 | 0.20047504201905 |
| F | 0.73899480647516 | 1.74542107181275 | 2.27110106346110 |
| F | 1.80735382405679 | 1.03802263498567 | 0.34811003660815 |
| F | -0.30512037168081 | 0.23196039756526 | 0.86298804761823 |

[Au(CNDipp^{CC}Ph^{OMe})₂](BF₄) (**2a**)

| | | | |
|----|--------------------|-------------------|-------------------|
| Au | -0.04214648590868 | 0.86636149190466 | -1.03459853215671 |
| C | -1.98772989182724 | 0.61140713851565 | -1.14696384346869 |
| N | -3.13910613501244 | 0.35570487298871 | -1.10990396806900 |
| C | -4.46805117093426 | 0.00365574270186 | -0.99350611639394 |
| C | -5.37565596186139 | 0.42034466837217 | -2.01524344643384 |
| C | -4.89474111134979 | 1.28655138439114 | -3.17723603673271 |
| H | -3.84634102614633 | 0.98471705577603 | -3.39215560828024 |
| C | -5.69974031301637 | 1.08515402954493 | -4.47173001203281 |
| H | -5.75307778889236 | 0.01640330836421 | -4.76166839091426 |
| H | -5.22397633589145 | 1.64163774350748 | -5.30448411405632 |
| H | -6.73763778951619 | 1.46763424042071 | -4.37992173356687 |
| C | -4.86964623153479 | 2.77680691593318 | -2.76435904267625 |
| H | -5.89457134407864 | 3.13767476190073 | -2.53839069180374 |
| H | -4.45831664664502 | 3.40204588317626 | -3.58348467387112 |
| H | -4.24718899826033 | 2.94627360333014 | -1.86304469789328 |
| C | -6.71312079936304 | 0.03572668492704 | -1.87901010141186 |
| H | -7.44759340236540 | 0.32990204848557 | -2.64093386470917 |
| C | -7.15739233580830 | -0.74031176003553 | -0.77373619052644 |
| C | -8.52364414949138 | -1.11978015301844 | -0.66269192779834 |
| C | -9.70897270919584 | -1.45092344383719 | -0.56403073204973 |
| C | -11.07344098657217 | -1.83689592556975 | -0.44539254776646 |
| C | -12.03155542232443 | -1.45308236530818 | -1.41911271601982 |
| H | -11.70774724034360 | -0.84676426179139 | -2.27806295762567 |
| C | -13.37579114056762 | -1.83022327538955 | -1.30782214367374 |
| H | -14.08675022447592 | -1.51303556708818 | -2.08284146909892 |
| C | -13.79947411661412 | -2.60965526182665 | -0.20696513186054 |
| O | -15.07601035069422 | -3.02861247548825 | -0.00325445317194 |
| C | -16.07465544921471 | -2.67286623667193 | -0.94860652063338 |
| H | -16.19824943570756 | -1.56942012785602 | -1.02372102731379 |
| H | -17.01939334160456 | -3.11631694583651 | -0.58352263103159 |
| H | -15.85047108354607 | -3.08046099892861 | -1.95958106803750 |
| C | -12.85482883630305 | -3.00067799025093 | 0.77335397227576 |
| H | -13.20476668078181 | -3.60697369601670 | 1.62172535300421 |
| C | -11.51982046408505 | -2.62252986143899 | 0.65710731272315 |
| H | -10.79326535168711 | -2.93110856465606 | 1.42312249870443 |
| C | -6.21642621582803 | -1.13514908118384 | 0.21281163853304 |
| H | -6.56433389501199 | -1.74168971207431 | 1.06033957558057 |
| C | -4.86338412761859 | -0.77950170520444 | 0.13537290298942 |

| | | | |
|---|-------------------|-------------------|-------------------|
| C | -3.86916209432295 | -1.16317351797920 | 1.22232040356125 |
| H | -2.85415373496205 | -1.19622868251550 | 0.77912087984333 |
| C | -4.12265429451289 | -2.55041561755763 | 1.83439158408535 |
| H | -3.24915096167178 | -2.82394779526864 | 2.45676837297519 |
| H | -4.23323295096796 | -3.32920637071847 | 1.05243614447771 |
| H | -5.02861043373738 | -2.57308073008316 | 2.47705142261198 |
| C | -3.82575615787204 | -0.06886961272041 | 2.31426193809623 |
| H | -3.60452402330699 | 0.92973927975141 | 1.88741133455688 |
| H | -3.01983223898086 | -0.30219917191452 | 3.03617328666822 |
| H | -4.79416961027767 | -0.00678485315571 | 2.85497726931538 |
| C | 1.90454500272447 | 1.09778753978578 | -0.89624837745718 |
| N | 3.06590157354827 | 1.15310575302541 | -0.69470298884672 |
| C | 4.41228260366456 | 1.15402503261657 | -0.39340110621706 |
| C | 5.25782876381222 | 2.09778339361202 | -1.05350870942454 |
| C | 4.69172351065014 | 3.04244427404164 | -2.11131847436416 |
| H | 3.65065603511565 | 3.28362444235967 | -1.80385251964831 |
| C | 5.45307450058295 | 4.37377696702113 | -2.22117061458495 |
| H | 5.54454582577929 | 4.87868951548275 | -1.23840916723402 |
| H | 4.91926402774294 | 5.06005131127610 | -2.90932883255999 |
| H | 6.47485117659384 | 4.23570120793998 | -2.63210185793562 |
| C | 4.61432479586644 | 2.33200432477072 | -3.48292203095229 |
| H | 5.62974071249291 | 2.06778005668973 | -3.84468499135752 |
| H | 4.14175676397711 | 2.99276341641973 | -4.23866922277652 |
| H | 4.02151794287080 | 1.39684283683245 | -3.43220529142383 |
| C | 6.61507931804404 | 2.08577493650469 | -0.71730817833537 |
| H | 7.30391210780281 | 2.79467149471414 | -1.19633522601460 |
| C | 7.13775614641451 | 1.17689271047990 | 0.24292125606731 |
| C | 8.52254904700738 | 1.18907350516508 | 0.56726350823064 |
| C | 9.72343523246610 | 1.20016421415400 | 0.85387586867286 |
| C | 11.10741746123590 | 1.20317454155287 | 1.18465957789741 |
| C | 12.00797381568541 | 2.10688668830662 | 0.56354508805255 |
| H | 11.62323052198264 | 2.81495017147338 | -0.18538774112032 |
| C | 13.37122916608085 | 2.11435194030993 | 0.88460531009016 |
| H | 14.03573299304277 | 2.82975207086093 | 0.38125732936376 |
| C | 13.87283751608317 | 1.20746282165066 | 1.84630688170976 |
| O | 15.17404655764140 | 1.13073625289151 | 2.23042462484049 |
| C | 16.11755746053530 | 2.01291123679225 | 1.63971697721272 |
| H | 16.18743717321718 | 1.86641493809405 | 0.53871298011795 |
| H | 17.09526468478079 | 1.77284686553930 | 2.09680572448183 |
| H | 15.87302126744925 | 3.07859593188151 | 1.84703391324705 |
| C | 12.98627935290673 | 0.29940156782079 | 2.47532850627078 |
| H | 13.39662171255617 | -0.39756656140460 | 3.22075121384363 |
| C | 11.63199305668547 | 0.29686944066320 | 2.15180831962003 |
| H | 10.95117651870425 | -0.41189055251934 | 2.64579892545468 |
| C | 6.25645832610308 | 0.26214043526932 | 0.87623343346199 |
| H | 6.66519374931706 | -0.43217269967815 | 1.62328505752563 |
| C | 4.88728839551382 | 0.22215329404306 | 0.58121258335702 |
| C | 3.95656646707886 | -0.79475986913859 | 1.22670276055007 |
| H | 2.92647864375834 | -0.38641291428463 | 1.22271185040024 |
| C | 4.29599384206464 | -1.10321445105907 | 2.69409723145892 |
| H | 3.46186299178678 | -1.68398648128059 | 3.13238052419396 |
| H | 4.40807850269934 | -0.17575151481093 | 3.29196922134699 |
| H | 5.22782954592772 | -1.69887015332830 | 2.79960018334765 |
| C | 3.91081980944821 | -2.08737084553987 | 0.37893075077695 |
| H | 3.62973300290709 | -1.87992951636171 | -0.67290556725606 |
| H | 3.14599883574063 | -2.77187940775976 | 0.79317898512171 |
| H | 4.89712285429521 | -2.59848327883421 | 0.37860316042830 |
| B | 0.05627030199702 | -1.27136090271882 | 1.60108567488580 |
| F | -0.82401346157370 | -2.34411336215200 | 1.78498333901645 |
| F | -0.70074487617031 | -0.05054513226291 | 1.52095425649413 |
| F | 0.99468167768489 | -1.17570494142165 | 2.63589635280801 |
| F | 0.75031683736971 | -1.42383110509290 | 0.35034877723838 |

[Au(CNDipp^{CC}Ph^{CN})₂](BF₄) (**2b**)

Au 0.00292263553406 -0.04347253389926 -0.00773934574295

| | | | |
|---|--------------------|-------------------|-------------------|
| C | -1.96103887268601 | -0.06620348233515 | -0.07543348123316 |
| N | -3.13683835385018 | -0.06230794275165 | 0.01708063365173 |
| C | -4.49558338383403 | -0.06216199763949 | 0.26303061874829 |
| C | -4.92900374589012 | -0.27951585721053 | 1.60840725556891 |
| C | -3.92760351230591 | -0.56443678141348 | 2.71761025249749 |
| H | -3.00761970259715 | 0.02222003102754 | 2.51079426970981 |
| C | -3.51967423039054 | -2.05815396530396 | 2.70107360020138 |
| H | -4.37779993479185 | -2.70786284915892 | 2.97445479746941 |
| H | -2.69608540098053 | -2.20824307190328 | 3.42541580652995 |
| H | -3.15522472353005 | -2.38119389892092 | 1.70432410176056 |
| C | -4.40316601118512 | -0.14751773175246 | 4.11755356006349 |
| H | -5.22597421800507 | -0.79061550717703 | 4.49688175474885 |
| H | -4.74575403427171 | 0.90717851050011 | 4.14129581836123 |
| H | -3.54896930626846 | -0.24435427830129 | 4.81530109623437 |
| C | -6.31234860861321 | -0.25653468247488 | 1.83212791447453 |
| H | -6.69477844655234 | -0.41147901138613 | 2.85008918749252 |
| C | -7.23783685129146 | -0.03316268564163 | 0.78033400298609 |
| C | -6.75635446661882 | 0.17983273761819 | -0.53866242463155 |
| H | -7.48397868866537 | 0.35973647811056 | -1.34149118519571 |
| C | -5.38691273520545 | 0.17171261395863 | -0.82659289670780 |
| C | -4.85298361715822 | 0.36147808176260 | -2.24413899241133 |
| H | -3.86809170596849 | 0.86925451126819 | -2.15158852193075 |
| C | -4.60456858129807 | -1.01036425011797 | -2.91401308260414 |
| H | -3.92005383987628 | -1.64575091247229 | -2.31705928408662 |
| H | -4.15410983630399 | -0.87683005192979 | -3.91896289163702 |
| H | -5.55784281820365 | -1.56520256498854 | -3.03656388480755 |
| C | -5.74407487819061 | 1.25383050235021 | -3.12401921649768 |
| H | -6.71325813110109 | 0.76818122794862 | -3.36218426463982 |
| H | -5.24013972651687 | 1.45617359364272 | -4.09058695101964 |
| H | -5.95781322517429 | 2.22835931025551 | -2.64063844648294 |
| | | | |
| C | -8.63708154092370 | -0.01584891721793 | 1.04444753880540 |
| C | -9.84903150549239 | -0.00672288436421 | 1.27442562537766 |
| C | -11.24665735589082 | 0.00557726156121 | 1.54481741008933 |
| C | -11.73167908478012 | -0.20197832458959 | 2.86599347190047 |
| H | -11.01302321301872 | -0.37233884479572 | 3.68058387548300 |
| C | -13.10169863738786 | -0.19056359590954 | 3.13259426763067 |
| H | -13.46825505237017 | -0.35173207572466 | 4.15674335206734 |
| C | -14.03114034130292 | 0.02901711675524 | 2.08461237237074 |
| C | -15.44026548718612 | 0.04037652334394 | 2.35676641363327 |
| N | -16.59420000777528 | 0.04789525772291 | 2.57767779219656 |
| C | -13.55718774632308 | 0.23716904232854 | 0.76461490332963 |
| H | -14.27746268148857 | 0.40783786789207 | -0.04860270341561 |
| C | -12.18683795643587 | 0.22540670090830 | 0.50012124089489 |
| H | -11.82206243283406 | 0.38718261905238 | -0.52451031156260 |
| C | 1.96589875181170 | -0.01741236665798 | 0.08292187609561 |
| N | 3.12975089978991 | -0.01216056074962 | 0.27407408935672 |
| C | 4.46253453735386 | 0.00584250833312 | 0.63514424528044 |
| C | 4.77972293593978 | 0.30832071974847 | 1.99623431682302 |
| C | 3.68784633322575 | 0.66157972018141 | 2.99488121291487 |
| H | 2.78498509628244 | 0.06567507237552 | 2.74433089039271 |
| C | 3.29439875480538 | 2.15253678479803 | 2.85269983119257 |
| H | 4.12878460227193 | 2.81586555695697 | 3.16415103145939 |
| H | 2.40968801303150 | 2.34793784950588 | 3.48882328075576 |
| C | 3.02425020572054 | 2.41651043708004 | 1.80957396957767 |
| H | 4.03728045823101 | 0.32951627863439 | 4.45339784954335 |
| H | 4.82918738411067 | 0.99274681873949 | 4.86268645311022 |
| H | 4.36860507824115 | -0.72252582689895 | 4.57067264007702 |
| H | 3.12682209845896 | 0.47026618783551 | 5.06746859126109 |
| C | 6.13863517210780 | 0.30131125531808 | 2.33911482794619 |
| H | 6.43267396512734 | 0.52024723649655 | 3.37456915519039 |
| C | 7.15018974267652 | 0.01373753100511 | 1.38697266197401 |
| C | 6.78285341592290 | -0.28273824541209 | 0.04742882255627 |
| H | 7.57588052006869 | -0.51167102478901 | -0.67716863238888 |
| C | 5.44323085537096 | -0.29492260000605 | -0.35699996278915 |

| | | | |
|---|-------------------|-------------------|-------------------|
| C | 5.03272677419365 | -0.57443302575545 | -1.80059861109108 |
| H | 4.04050324406993 | -1.07480390719439 | -1.76175356553582 |
| C | 4.85119637170693 | 0.75198371910306 | -2.57506164296458 |
| H | 4.12074377290453 | 1.42378072127300 | -2.08133326943252 |
| H | 4.48911094036043 | 0.55483824339412 | -3.60497403276079 |
| H | 5.81440543516807 | 1.29819790731697 | -2.64907853804558 |
| C | 5.99109086626087 | -1.52165489880906 | -2.54148393781465 |
| H | 6.98009700846220 | -1.05275747086626 | -2.72557170200185 |
| H | 5.57098413445456 | -1.78515517203739 | -3.53306676894259 |
| H | 6.15646600470002 | -2.46338805375644 | -1.98038914518499 |
| C | 8.52139173795180 | 0.01563465344592 | 1.77124162908445 |
| C | 9.70896585504707 | 0.02796646469227 | 2.10489090348639 |
| C | 11.07810959476098 | 0.03445049882607 | 2.49479292203491 |
| C | 11.44872089223715 | 0.32597685378412 | 3.83698743021044 |
| H | 10.66359218110462 | 0.54699839094234 | 4.57439333919408 |
| C | 12.79070410462658 | 0.33278462882584 | 4.22064679289940 |
| H | 13.06863441560411 | 0.55895083446507 | 5.26027451474790 |
| C | 13.80580857919614 | 0.04807596312801 | 3.27254369306866 |
| C | 15.18611014890244 | 0.05553445345608 | 3.66563661583497 |
| N | 16.31620765515789 | 0.06403985597927 | 3.98693650280360 |
| C | 13.44612169361960 | -0.24382659627978 | 1.93250064562398 |
| H | 14.23274254766568 | -0.46505979667461 | 1.19661374797816 |
| C | 12.10362831829479 | -0.25013637340452 | 1.55087586626466 |
| H | 11.82737620531488 | -0.47687794431928 | 0.51098425861629 |
| B | -0.14086696368502 | 0.06162678254193 | 3.44093550041441 |
| F | 0.67137922475141 | 0.87905718327944 | 4.23765355078964 |
| F | -1.01827523946632 | -0.70593511218979 | 4.21824381075501 |
| F | 0.68514307360689 | -0.80728970054658 | 2.64516949417794 |
| F | -0.89714941352004 | 0.87721719125811 | 2.52714863878873 |

[Au(CNDipp^{CC}-1-naph)₂](BF₄) (2c)

| | | | |
|----|-------------------|-------------------|-------------------|
| Au | 0.33278563714518 | -1.03420577282296 | -1.87580492725728 |
| C | 2.27148347802383 | -1.30610080978472 | -1.70750160358881 |
| N | 3.42608870347736 | -1.41882664788650 | -1.49301537639946 |
| C | 4.76096890945282 | -1.52183634407270 | -1.15948920639688 |
| C | 5.12962205405230 | -1.33442304882208 | 0.20904366468999 |
| C | 4.07817445118444 | -1.09300835808809 | 1.28210002546487 |
| H | 3.22501726991444 | -0.55072292898269 | 0.82656831288831 |
| C | 4.56745310205502 | -0.21920924694813 | 2.44760663943525 |
| H | 5.29536236755172 | -0.74641962519463 | 3.10070493883582 |
| H | 3.69486288475139 | 0.06606522765030 | 3.06599312450423 |
| H | 5.03820169718167 | 0.71813161508260 | 2.08757722856880 |
| C | 3.51777062011750 | -2.44191580886413 | 1.79163228272623 |
| H | 3.13553255241442 | -3.07014067182419 | 0.96230032729970 |
| H | 2.66807763555560 | -2.25462363730872 | 2.47586292511185 |
| H | 4.29873263674006 | -3.02039309881192 | 2.32946775918251 |
| C | 6.49457747761172 | -1.42773448533179 | 0.51139053725085 |
| H | 6.82598976729943 | -1.28442458708367 | 1.54888199619616 |
| C | 7.46911902522284 | -1.69778413003533 | -0.48454844624859 |
| C | 8.84649632078955 | -1.78482583151032 | -0.13823940898676 |
| C | 10.03839844109026 | -1.85828127197393 | 0.17581549532517 |
| C | 11.40395775018825 | -1.93759699718604 | 0.56916005646330 |
| C | 11.75170500040782 | -1.74488344928157 | 1.91815315209135 |
| H | 10.95501386893132 | -1.53492703208585 | 2.64678165476008 |
| C | 13.09907288278716 | -1.81683136448086 | 2.34294010347084 |
| H | 13.33910578874963 | -1.66111310754741 | 3.40578953259682 |
| C | 14.11180056587074 | -2.08118330194868 | 1.42881182987954 |
| H | 15.16116144366083 | -2.13720963849591 | 1.75910225944020 |
| C | 13.81492764535778 | -2.28472191214056 | 0.04750390724025 |
| C | 14.84156306244543 | -2.55738169765965 | -0.90785514315783 |
| H | 15.88519981067290 | -2.60976683409861 | -0.55901630352321 |
| C | 14.53691030750914 | -2.75278718987434 | -2.24754244719237 |
| H | 15.33898104705496 | -2.96201562149608 | -2.97207882947884 |
| C | 13.18696456936511 | -2.68293975489544 | -2.68763850830347 |
| H | 12.95125814025119 | -2.83853562693725 | -3.75182072945552 |

| | | | |
|---|--------------------|-------------------|-------------------|
| C | 12.16499888615972 | -2.41960242967606 | -1.78380374399040 |
| H | 11.11958699702445 | -2.36495192398620 | -2.12260974809251 |
| C | 12.44446131666545 | -2.21446629617894 | -0.40218656597307 |
| C | 7.05121422677951 | -1.87352000839351 | -1.83139367637628 |
| H | 7.81379864365512 | -2.07435110683243 | -2.59587688921106 |
| C | 5.70402098939960 | -1.78956064810542 | -2.19814938086984 |
| C | 5.23794015493351 | -2.01391882195442 | -3.63469818891923 |
| H | 4.34548638130365 | -1.36867626602171 | -3.78841912043770 |
| C | 6.27873081482394 | -1.60916087819566 | -4.69170126135605 |
| H | 6.63733469983690 | -0.57093906563503 | -4.54142896215157 |
| H | 5.83369371861743 | -1.67299026725704 | -5.70520326553270 |
| H | 7.16155986925488 | -2.28186316349958 | -4.68492846730055 |
| C | 4.78658933503525 | -3.48011348304713 | -3.83213230950869 |
| H | 5.64085566062614 | -4.17478981626840 | -3.69304691456391 |
| H | 4.38544944414261 | -3.63010694221146 | -4.85560125806427 |
| H | 3.99572233375196 | -3.77102968911439 | -3.11212181517695 |
| C | -1.60565817612049 | -0.74410412253395 | -2.02289751301230 |
| N | -2.76039749379282 | -0.50840588390341 | -1.96662620792600 |
| C | -4.08714176271698 | -0.18630539842678 | -1.76465214044670 |
| C | -4.98293309294987 | -0.24194576603499 | -2.87436290683209 |
| C | -4.49633515612807 | -0.70550035322564 | -4.24532161353065 |
| H | -3.43708114254505 | -0.38018049475292 | -4.33810387529348 |
| C | -4.51365331497411 | -2.24974263213552 | -4.32884649799552 |
| H | -3.91536995696354 | -2.71481858361168 | -3.51991616654573 |
| H | -4.09820602543668 | -2.59271079122154 | -5.29877099023915 |
| H | -5.55100334992792 | -2.63508375485606 | -4.24444010493692 |
| C | -5.26887071874688 | -0.07917549423158 | -5.41810343712720 |
| H | -6.31666059021403 | -0.44200652594113 | -5.46698493737147 |
| H | -4.78803200962864 | -0.35412748226212 | -6.37862952051449 |
| H | -5.29210293869562 | 1.02727509384896 | -5.35245981372741 |
| C | -6.31679184789695 | 0.10622349023054 | -2.63644473454951 |
| H | -7.04416106037253 | 0.08305928628259 | -3.45914666815379 |
| C | -6.76410447383423 | 0.50143971495876 | -1.34665961311500 |
| C | -8.12691996437967 | 0.85334491756336 | -1.13797696510372 |
| C | -9.31186909531267 | 1.15470476309324 | -0.96529830169711 |
| C | -10.68114343477313 | 1.49928402555479 | -0.78649559341181 |
| C | -11.56637750386342 | 1.42853059758758 | -1.87695897844548 |
| H | -11.17922182765159 | 1.10596316152851 | -2.85465923691334 |
| C | -12.93301374115138 | 1.76356150449444 | -1.73197366324882 |
| H | -13.60092179941077 | 1.69805030766690 | -2.60445859538647 |
| C | -13.43011295073032 | 2.17195596877165 | -0.50017971405696 |
| H | -14.49426746450237 | 2.43295793338661 | -0.38664228160270 |
| C | -12.57576048886505 | 2.26189672766156 | 0.63979586372849 |
| C | -13.06757551716181 | 2.68004666164031 | 1.91423590957318 |
| H | -14.13466010583186 | 2.93703450310139 | 2.00864511137907 |
| C | -12.22388277746828 | 2.76284718082191 | 3.01294208325169 |
| H | -12.61716645514829 | 3.08692924057997 | 3.98881555698672 |
| C | -10.84832906384345 | 2.42935967592809 | 2.88072052660940 |
| H | -10.18340230445332 | 2.49728779810507 | 3.75554948607167 |
| C | -10.33841999206927 | 2.01894454155629 | 1.65505458316571 |
| H | -9.27386506755325 | 1.76106886617430 | 1.55176722790916 |
| C | -11.17803321423730 | 1.92340988040490 | 0.50834475649706 |
| C | -5.83372276006106 | 0.54548187980198 | -0.27536902708146 |
| H | -6.18437045234922 | 0.85948063325542 | 0.71709934918791 |
| C | -4.48564332723728 | 0.20555911261739 | -0.44780800117400 |
| C | -3.49081954693981 | 0.20265615418256 | 0.70375927795126 |
| H | -2.49829972176165 | 0.49856728253229 | 0.30291086662154 |
| C | -3.33245123849189 | -1.22812009891381 | 1.27464510130732 |
| H | -4.27068893275275 | -1.56607028268442 | 1.76346632703243 |
| H | -2.5091597773840 | -1.22613007511471 | 2.01500856596251 |
| H | -3.07621812676940 | -1.96621191605242 | 0.48731882327204 |
| C | -3.82095623181863 | 1.19921655042295 | 1.82535401140933 |
| H | -3.98305090732904 | 2.22441222798040 | 1.43398832405107 |
| H | -2.96174904239681 | 1.23048151755741 | 2.52309607731913 |
| H | -4.71988005357607 | 0.90172123905834 | 2.40675648581184 |

| | | | |
|---|-------------------|-------------------|------------------|
| B | 0.34250681539030 | 0.17066702963180 | 1.30580947730865 |
| F | -0.57670254266549 | 0.13118544974658 | 2.36340377017543 |
| F | -0.25784496257059 | 0.82186140281986 | 0.17141334560835 |
| F | 1.51851245676696 | 0.84256663509451 | 1.66274916289693 |
| F | 0.66971142775784 | -1.16913531062062 | 0.90271287044366 |

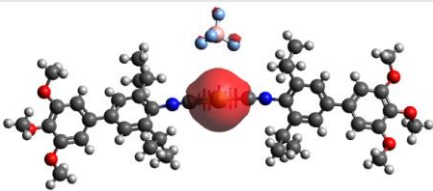
Crystallographic Versus Optimized Structure (1a)

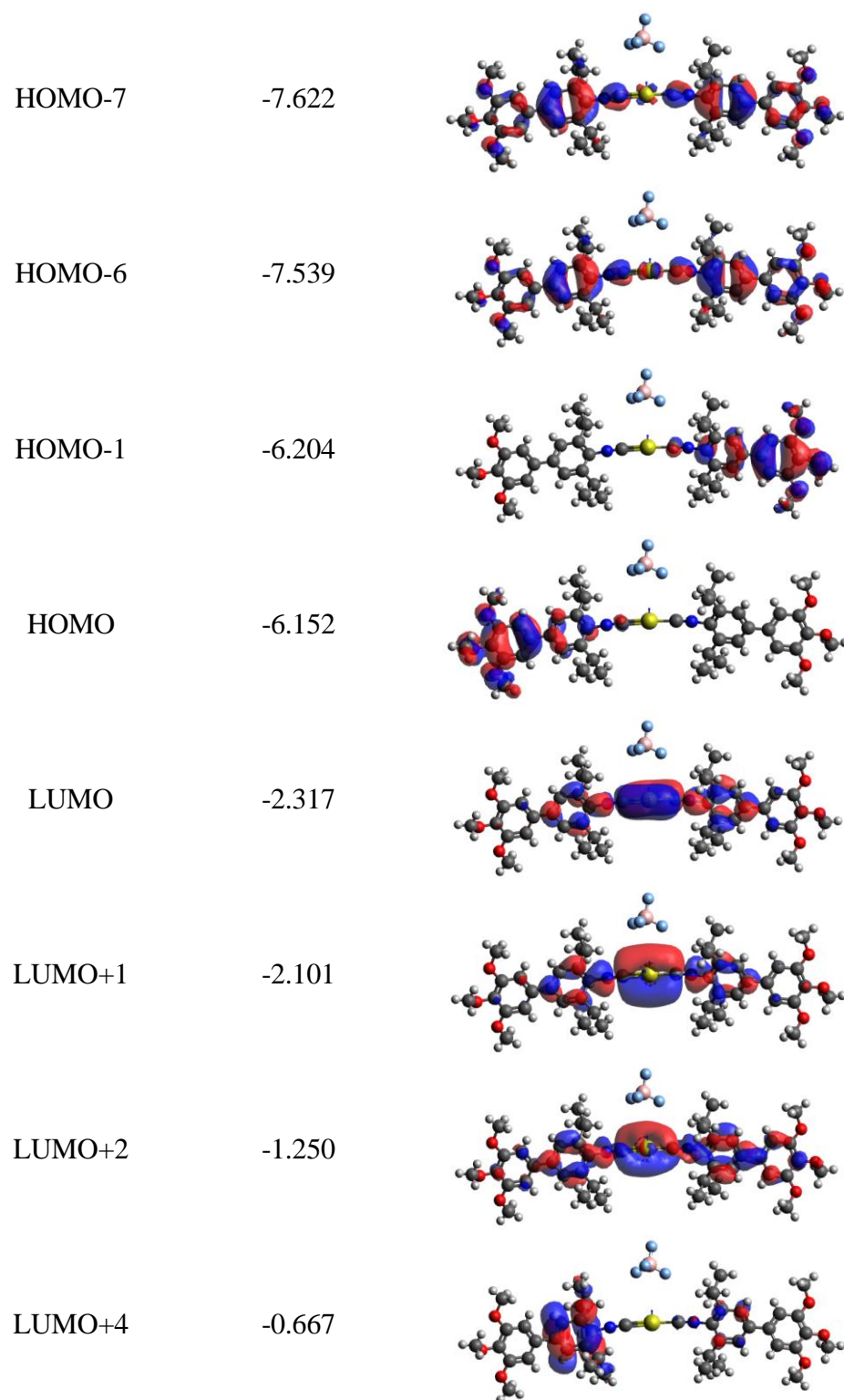
Singlets

| Energy (cm ⁻¹) | Wavelength (nm) | Osc. Strength | Primary Contribution |
|----------------------------|-----------------|---------------|------------------------|
| 27496.0 | 363.7 | 0.80615577 | 74.0% HOMO → LUMO |
| 36424.6 | 274.5 | 0.44061973 | 79.2% HOMO-1 → LUMO+2 |
| 37174.9 | 269.0 | 0.43965491 | 72.8% HOMO-6 → LUMO |
| 38734.8 | 258.2 | 0.36942546 | 37.4% HOMO-7 → LUMO+1 |
| 38909.8 | 257.0 | 0.21342751 | 30.1% HOMO-7 → LUMO |
| 28028.4 | 356.8 | 0.1331127 | 78.5% HOMO-1 → LUMO |
| 36139.3 | 276.7 | 0.11034077 | 80.3% HOMO → LUMO+2 |
| 42336.9 | 236.2 | 0.08622359 | 92.5% HOMO-10 → LUMO+1 |
| 29786.2 | 335.7 | 0.08572887 | 92.5% HOMO-1 → LUMO+1 |
| 38482.7 | 259.9 | 0.08278591 | 26.2% HOMO → LUMO+4 |
| 37981.6 | 263.3 | 0.07452327 | 35.2% HOMO-6 → LUMO+1 |
| 41212.1 | 242.6 | 0.06895094 | 94.2% HOMO-10 → LUMO |

Triples

| Energy (cm ⁻¹) | Wavelength (nm) | Primary Contribution |
|----------------------------|-----------------|----------------------|
| 37962.4 | 263.4 | 86.9% HOMO-10 → LUMO |

| Orbital | Energy (eV) | Visualization |
|---------|-------------|--|
| HOMO-10 | -8.600 |  |



Perpendicular Geometric Representation (1b)

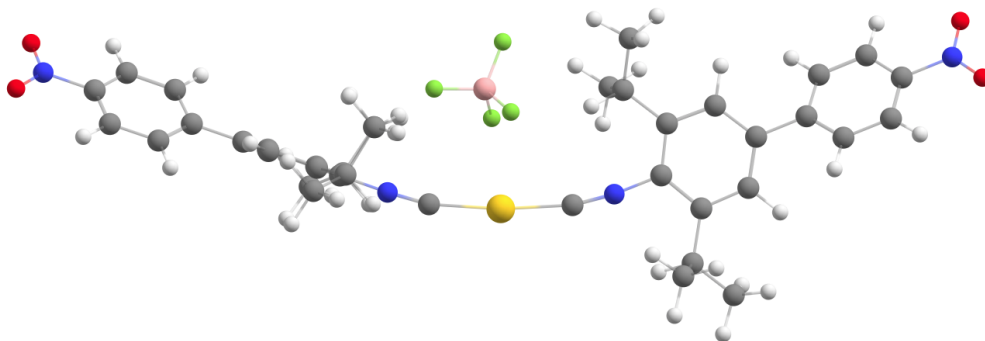


Figure 4.10. Representation of $[\text{Au}(\text{CNDippPh}^{\text{NO}_2})_2](\text{BF}_4)$ (**1b**) in the perpendicular geometry.

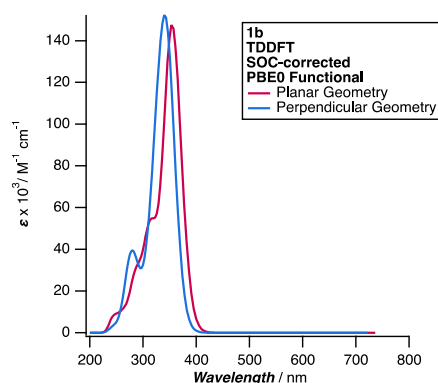


Figure 4.11. Visualized TDDFT spectra and geometry assignments for the optimized structures of $[\text{Au}(\text{CNDippPh}^{\text{NO}_2})_2](\text{BF}_4)$ (**1b**).

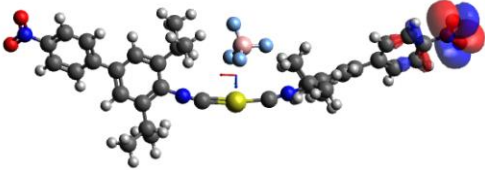
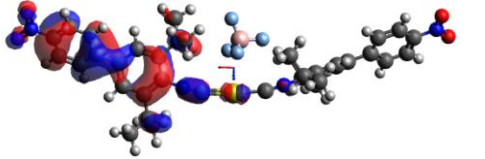
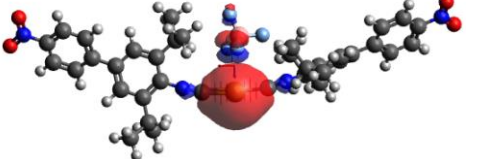
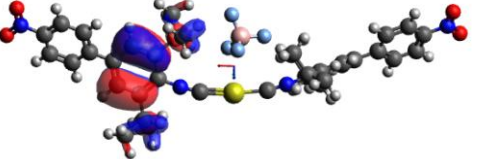
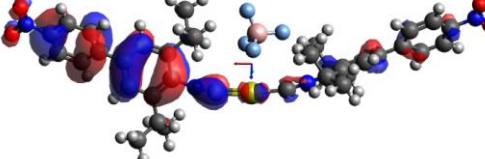
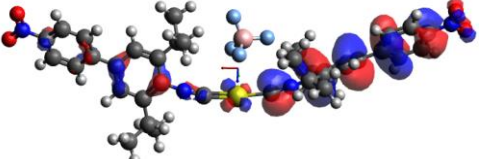
Singlets

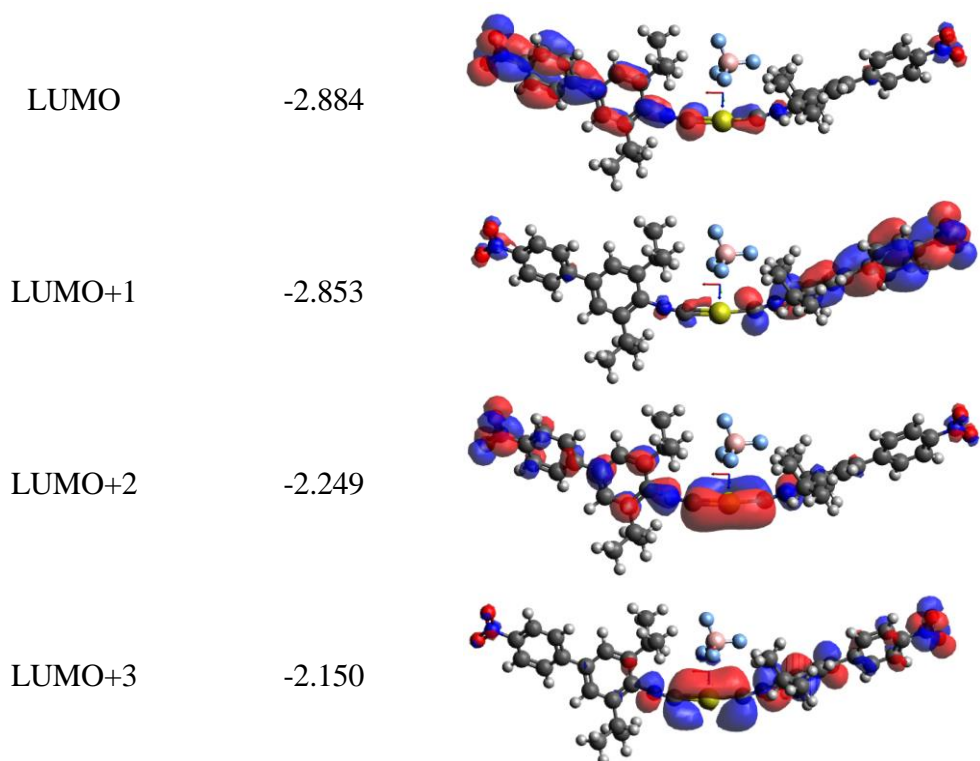
| Energy (cm^{-1}) | Wavelength (nm) | Osc. Strength | Primary Contribution |
|--------------------------------|--------------------|------------------|-----------------------------------|
| 29822.3 | 335.3 | 2.49054868 | 36.6% HOMO \rightarrow LUMO |
| 30644.0 | 326.3 | 0.22880428 | 50.1% HOMO-1 \rightarrow LUMO+1 |
| 35142.9 | 284.6 | 0.13823568 | 47.2% HOMO-1 \rightarrow LUMO+2 |
| 35361.0 | 282.8 | 0.12046967 | 53.1% HOMO \rightarrow LUMO+2 |
| 36775.7 | 271.9 | 0.05078102 | 60.0% HOMO-6 \rightarrow LUMO+1 |
| 35926.8 | 278.3 | 0.05007867 | 53.3% HOMO-6 \rightarrow LUMO |
| 36040.1 | 277.5 | 0.04213809 | 64.0% HOMO-1 \rightarrow LUMO+3 |
| 32126.1 | 311.3 | 0.04111561 | 86.3% HOMO-3 \rightarrow LUMO |
| 36945.0 | 270.7 | 0.03923792 | 81.9% HOMO-3 \rightarrow LUMO+2 |
| 31738.3 | 315.1 | 0.03878347 | 35.4% HOMO-9 \rightarrow LUMO+1 |

| | | | |
|---------|-------|------------|-----------------------|
| 35136.9 | 284.6 | 0.03821389 | 69.6% HOMO-3 → LUMO+1 |
| 40041.1 | 249.7 | 0.03444583 | 86.3% HOMO-8 → LUMO |
| 35634.3 | 280.6 | 0.03081026 | 53.3% HOMO-6 → LUMO |

Triplets

| Energy (cm ⁻¹) | Wavelength (nm) | Primary Contribution |
|----------------------------|-----------------|----------------------|
| 33462.7 | 298.8 | 43.1% HOMO-6 → LUMO |

| Orbital | Energy (eV) | Visualization |
|---------|-------------|--|
| HOMO-9 | -8.798 |  |
| HOMO-8 | -8.431 |  |
| HOMO-6 | -8.087 |  |
| HOMO-3 | -7.508 |  |
| HOMO-1 | -7.177 |  |
| HOMO | -7.149 |  |



Assignment of TDDFT Excitations

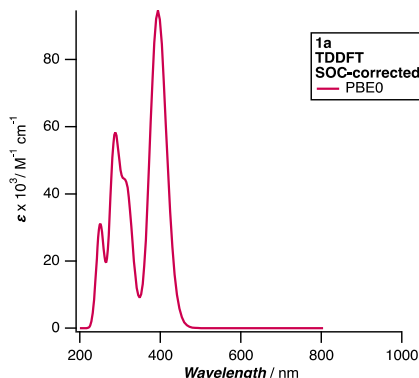
 $[\text{Au}(\text{CNDippPh}^{\text{OMe}_3})_2](\text{BF}_4)$ (**1a**)

Figure 4.12. Calculated TDDFT spectra for optimized $[\text{Au}(\text{CNDippPh}^{\text{OMe}_3})_2](\text{BF}_4)$ (**1a**) structure.

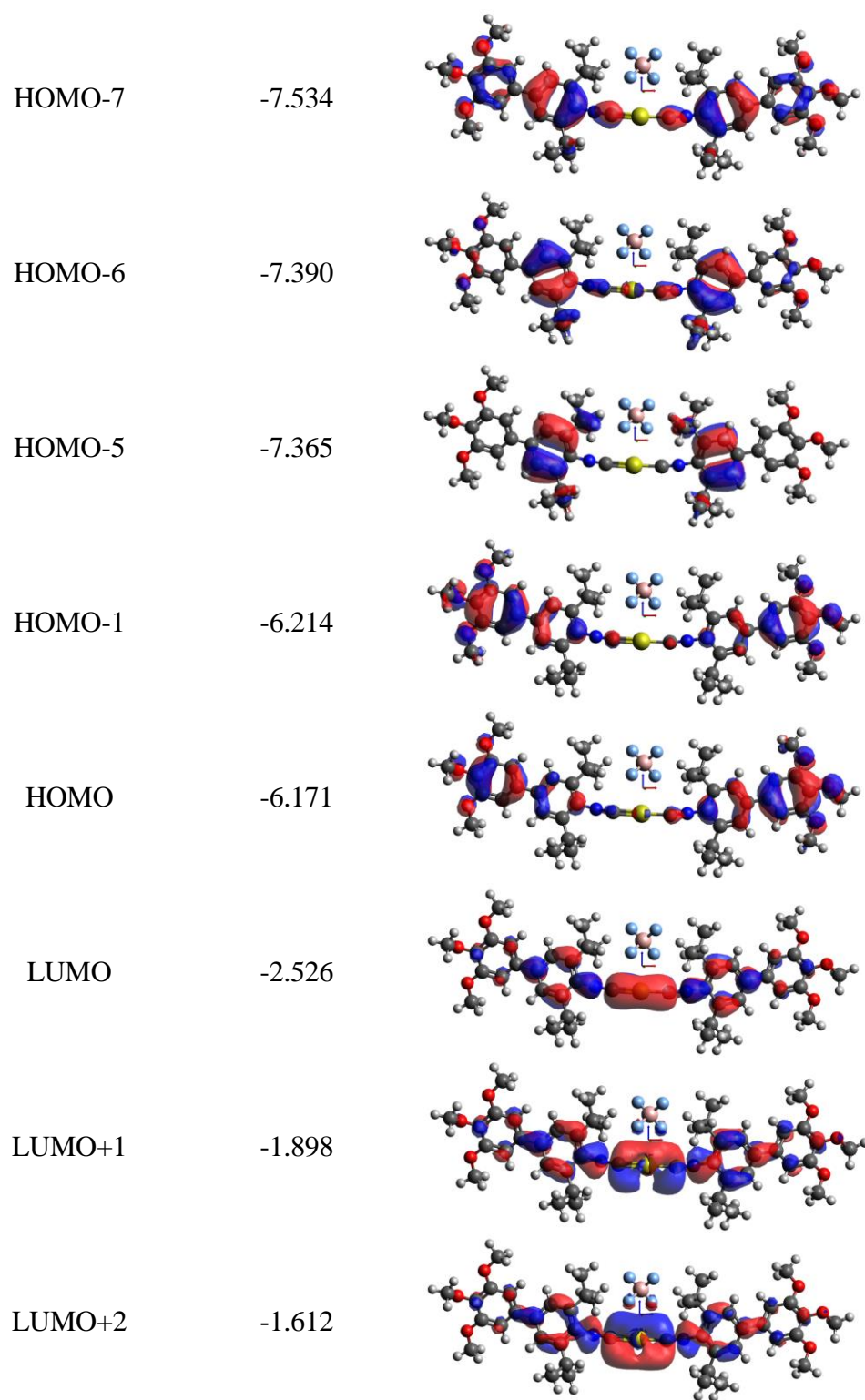
Singlets

| Energy (cm ⁻¹) | Wavelength (nm) | Osc. Strength | Primary Contribution |
|----------------------------|-----------------|---------------|------------------------|
| 25833.1 | 387.1 | 1.35635446 | 95.1% HOMO → LUMO |
| 34536.0 | 289.6 | 0.60158535 | 57.5% HOMO-6 → LUMO |
| 33537.2 | 298.2 | 0.28367586 | 43.4% HOMO-1 → LUMO+2 |
| 31367.3 | 318.8 | 0.25915778 | 89.8% HOMO-1 → LUMO+1 |
| 39804.8 | 251.2 | 0.16249507 | 20.7% HOMO-7 → LUMO+1 |
| 39502.0 | 253.2 | 0.12742263 | 23.1% HOMO-7 → LUMO+1 |
| 33625.8 | 297.4 | 0.10847615 | 39.2% HOMO-1 → LUMO+2 |
| 33640.6 | 297.3 | 0.08359671 | 81.0% HOMO-5 → LUMO |
| 40740.2 | 245.5 | 0.06544745 | 47.9% HOMO-10 → LUMO+1 |
| 36221.2 | 276.1 | 0.04396424 | 96.2% HOMO-10 → LUMO |

Triplets

| Energy (cm ⁻¹) | Wavelength (nm) | Primary Contribution |
|----------------------------|-----------------|----------------------|
| 33886.8 | 295.1 | 92.2% HOMO-10 → LUMO |

| Orbital | Energy (eV) | Visualization |
|---------|-------------|---------------|
| HOMO-10 | -8.120 | |



[Au(CNDippPh^{NO2})₂](BF₄)(1b)

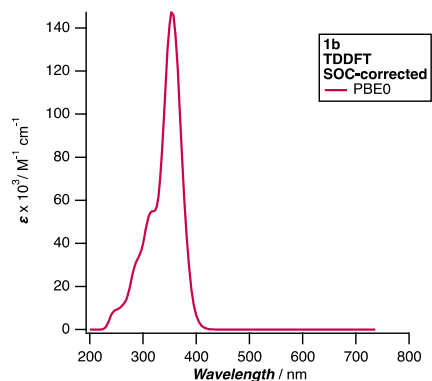


Figure 4.13. Calculated TDDFT spectra for optimized [Au(CNDippPh^{NO2})₂](BF₄) (**1b**) structure.

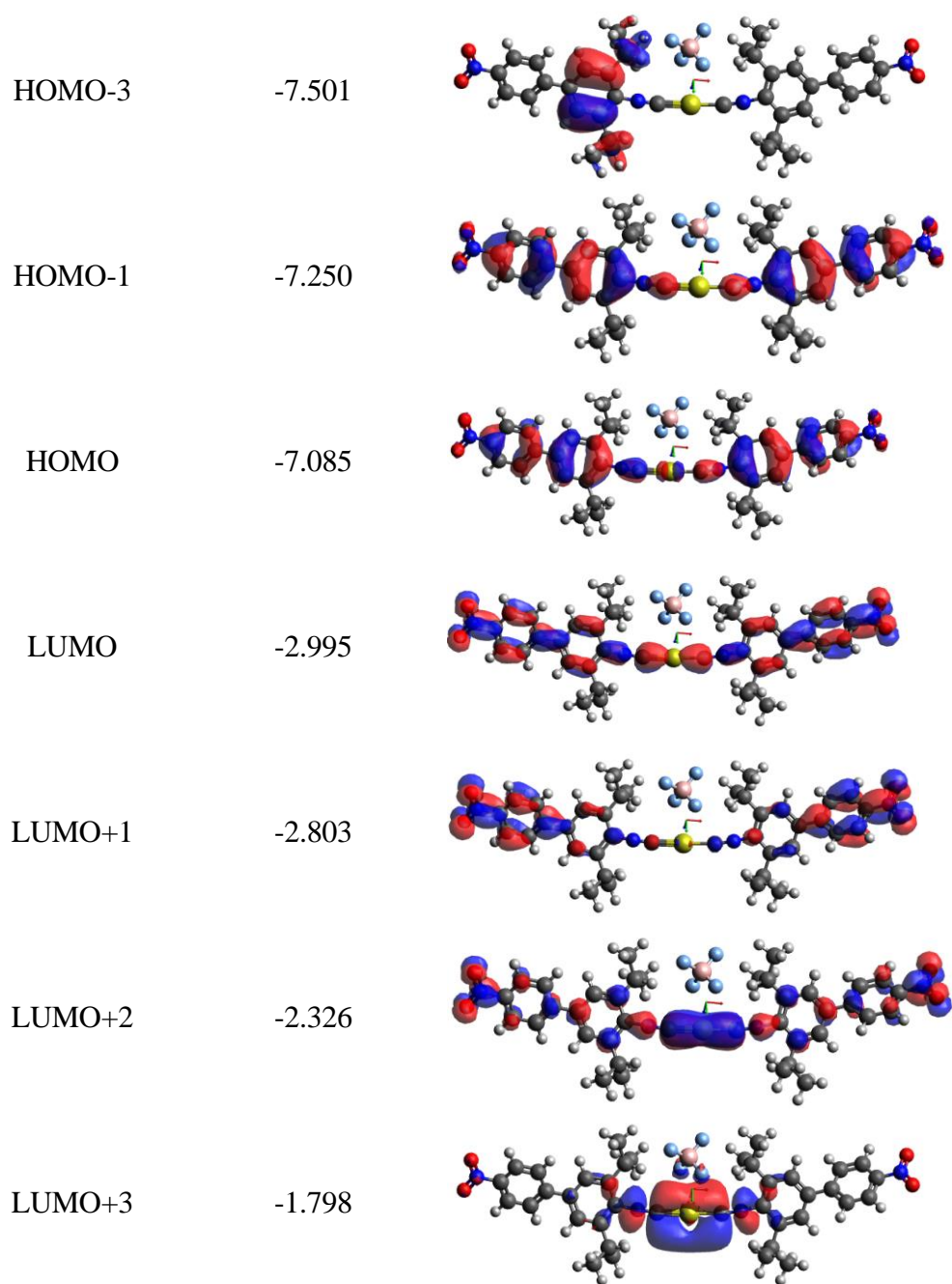
Singlets

| Energy (cm ⁻¹) | Wavelength (nm) | Osc. Strength | Primary Contribution |
|----------------------------|-----------------|---------------|-----------------------|
| 28954.6 | 345.4 | 2.5333443 | 86.6% HOMO → LUMO |
| 34713.2 | 288.1 | 0.24329856 | 76.7% HOMO → LUMO+2 |
| 30653.3 | 326.2 | 0.0962766 | 48.9% HOMO → LUMO+1 |
| 33068.2 | 302.4 | 0.09054963 | 78.2% HOMO-1 → LUMO+1 |
| 39555.2 | 252.8 | 0.08494233 | 76.1% HOMO-7 → LUMO |
| 40398.8 | 247.5 | 0.05862561 | 70.7% HOMO-6 → LUMO+3 |
| 31923.8 | 313.2 | 0.05751884 | 51.9% HOMO-3 → LUMO |
| 34598.0 | 289.0 | 0.04351976 | 67.6% HOMO-6 → LUMO |

Triplets

| Energy (cm ⁻¹) | Wavelength (nm) | Primary Contribution |
|----------------------------|-----------------|----------------------|
| 32630.2 | 306.5 | 60.4% HOMO-7 → LUMO |

| Orbital | Energy (eV) | Visualization |
|---------|-------------|---------------|
| HOMO-7 | -8.096 | |
| HOMO-6 | -8.096 | |



[Au(CNDippPh^{NPh2})₂](BF₄) (1c)

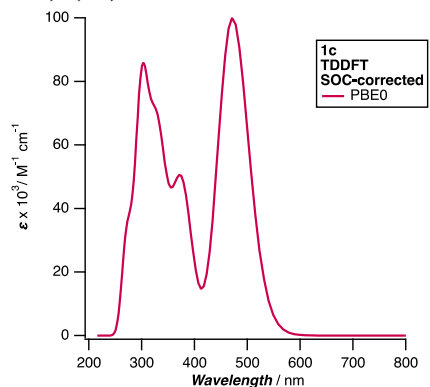


Figure 4.14. Calculated TDDFT spectra for optimized [Au(CNDippPh^{NPh2})₂](BF₄) (**1c**) structure.

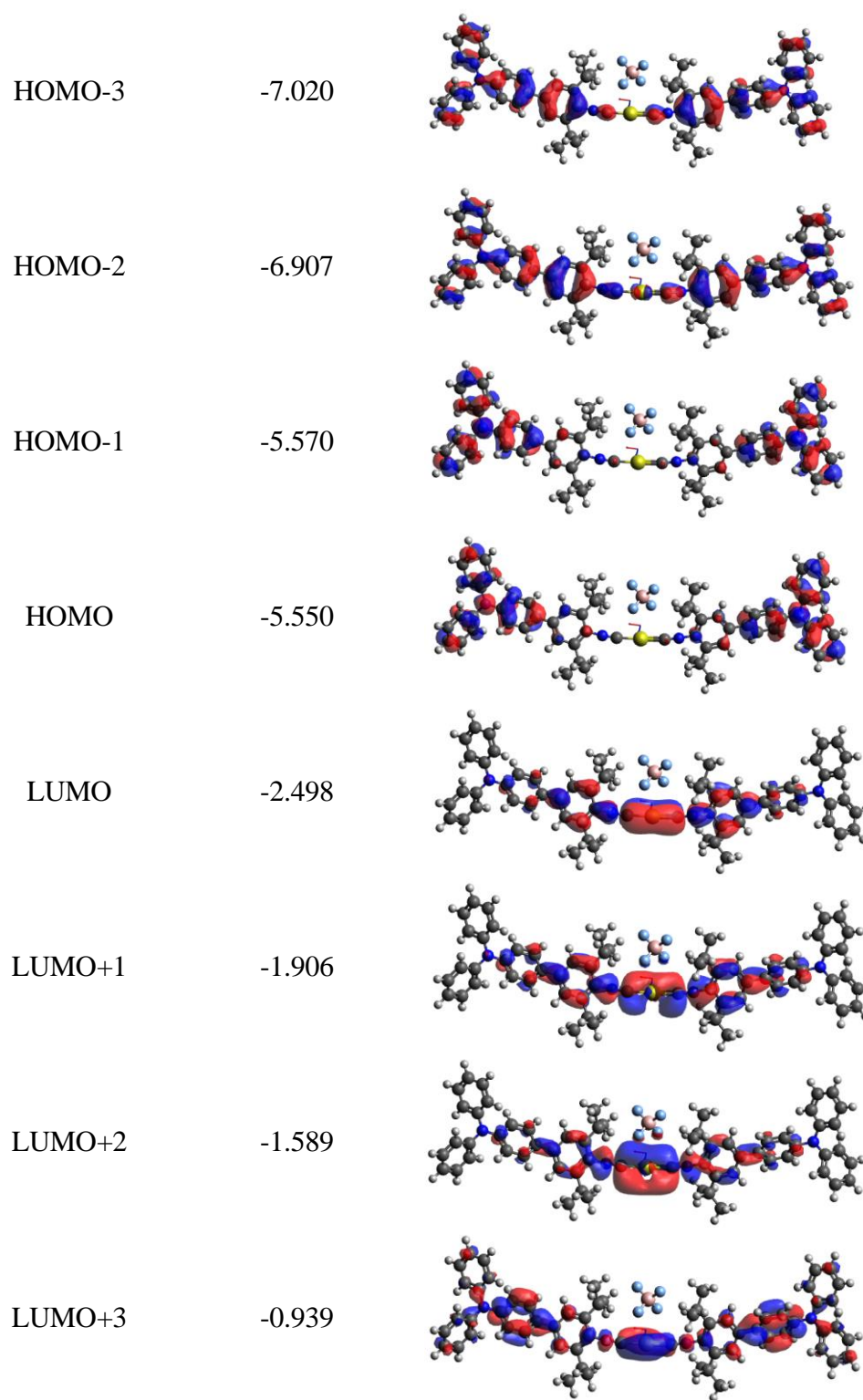
Singlets

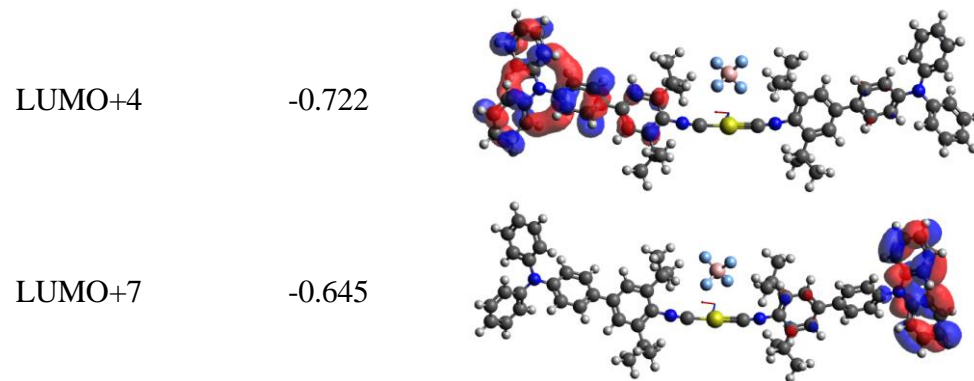
| Energy (cm ⁻¹) | Wavelength (nm) | Osc. Strength | Primary Contribution |
|----------------------------|-----------------|---------------|-----------------------|
| 21480.1 | 465.5 | 1.42102967 | 94.7% HOMO → LUMO |
| 31509.7 | 317.4 | 0.97812523 | 85.8% HOMO-2 → LUMO |
| 26606.4 | 375.8 | 0.46365622 | 94.6% HOMO → LUMO+1 |
| 29049.5 | 344.2 | 0.44452372 | 93.1% HOMO-1 → LUMO+2 |
| 33378.4 | 299.6 | 0.32324627 | 70.8% HOMO → LUMO+3 |
| 33084.4 | 302.3 | 0.21640855 | 46.4% HOMO → LUMO+7 |
| 36737.2 | 272.2 | 0.17401234 | 58.3% HOMO-3 → LUMO+1 |
| 33163.5 | 301.5 | 0.0598479 | 58.4% HOMO-3 → LUMO |
| 31566.5 | 316.8 | 0.05579271 | 42.7% HOMO → LUMO+4 |
| 22101.3 | 452.5 | 0.04311672 | 96.4% HOMO-1 → LUMO |
| 36325.5 | 275.3 | 0.04216259 | 91.2% HOMO-16 → LUMO |

Triplets

| Energy (cm ⁻¹) | Wavelength (nm) | Primary Contribution |
|----------------------------|-----------------|----------------------|
| 33985.8 | 294.3 | 84.9% HOMO-16 → LUMO |

| Orbital | Energy (eV) | Visualization |
|---------|-------------|---------------|
| HOMO-16 | -8.092 | |





[Au(CNDippPh^{NHPh2})₂](OTf)₃ (1d**)**

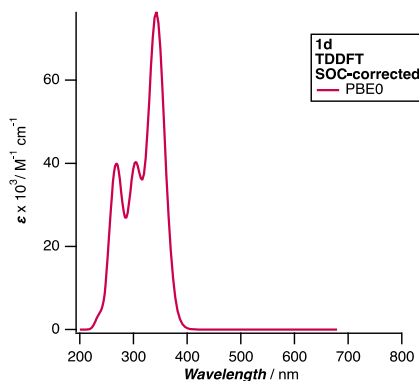


Figure 4.15. Calculated TDDFT spectra for optimized [Au(CNDippPh^{NHPh2})₂](OTf)₃ (**1d**) structure.

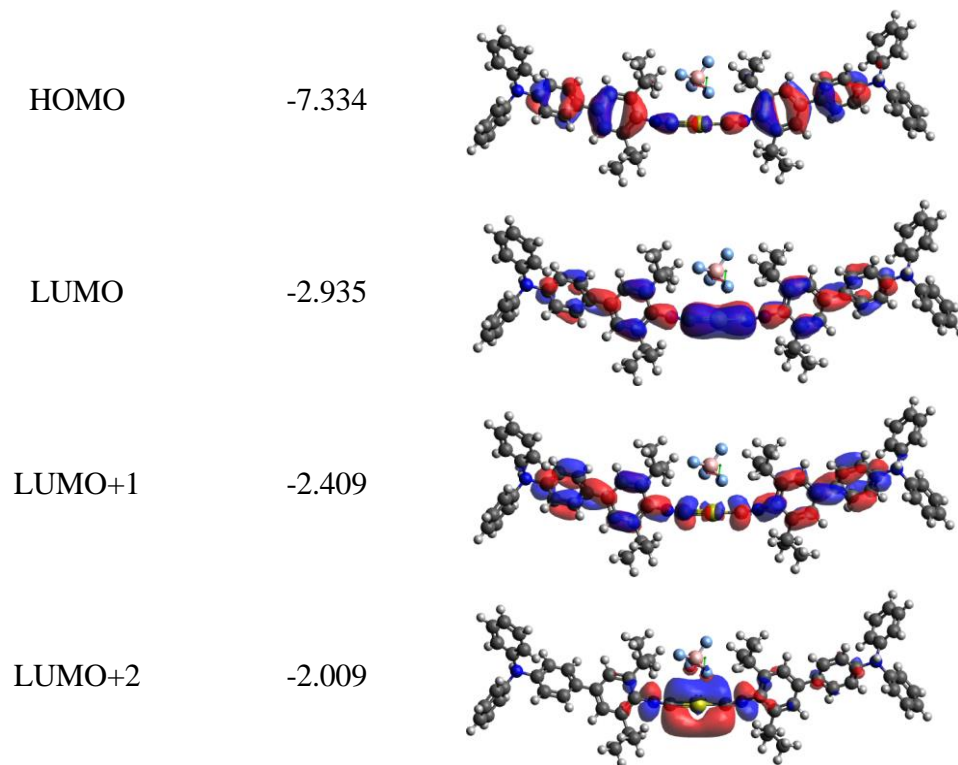
Singlets

| Energy (cm ⁻¹) | Wavelength (nm) | Osc. Strength | Primary Contribution |
|----------------------------|-----------------|---------------|------------------------|
| 30722.1 | 325.5 | 2.39200824 | 94.2% HOMO → LUMO |
| 38408.5 | 260.4 | 0.39350232 | 48.6% HOMO-1 → LUMO+2 |
| 36858.1 | 271.3 | 0.26704834 | 44.9% HOMO-1 → LUMO+1 |
| 33306.1 | 300.2 | 0.14106205 | 78.1% HOMO-1 → LUMO |
| 36951.7 | 270.6 | 0.13132126 | 48.6% HOMO → LUMO+1 |
| 39761.3 | 251.5 | 0.0605582 | 55.4% HOMO-10 → LUMO+2 |
| 34886.8 | 286.6 | 0.04175871 | 90.0% HOMO-10 → LUMO |

Triplets

| Energy (cm ⁻¹) | Wavelength (nm) | Primary Contribution |
|----------------------------|-----------------|----------------------|
| 32750.6 | 305.3 | 86.0% HOMO-10 → LUMO |

| Orbital | Energy (eV) | Visualization |
|---------|-------------|---------------|
| HOMO-10 | -8.306 | |
| HOMO-1 | -7.493 | |



[Au(CNDipp^{CC}Ph^{OMe})₂](BF₄) (2a)

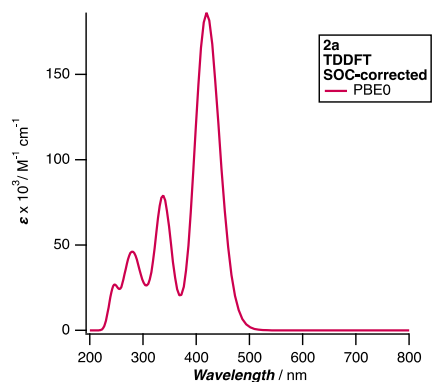


Figure 4.16. Calculated TDDFT spectra for optimized [Au(CNDipp^{CC}Ph^{OMe})₂](BF₄) (2a) structure.

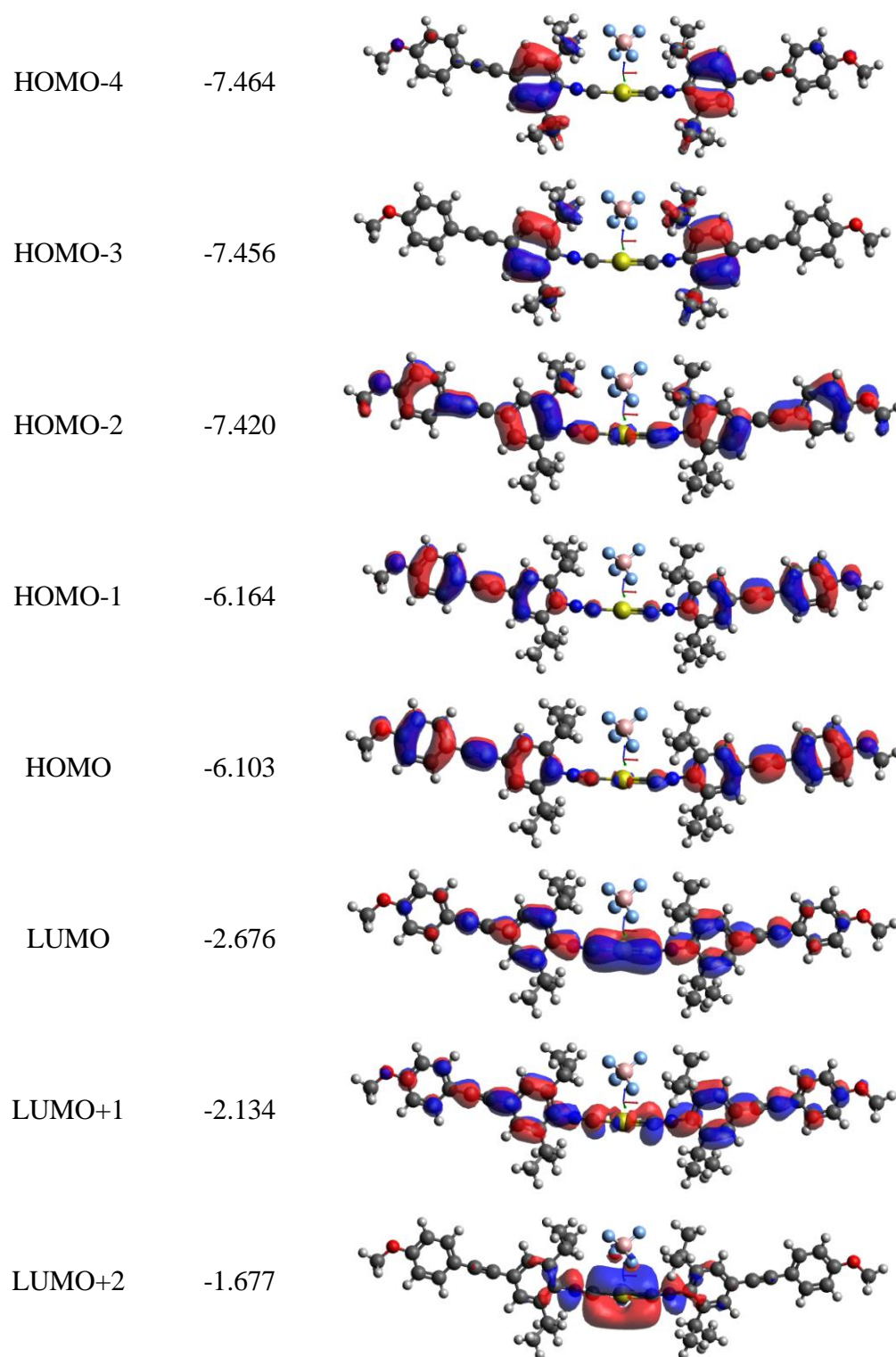
Singlets

| Energy (cm ⁻¹) | Wavelength (nm) | Osc. Strength | Primary Contribution |
|----------------------------|-----------------|---------------|-----------------------|
| 24176.4 | 413.6 | 2.69176758 | 95.0% HOMO → LUMO |
| 29648.0 | 337.3 | 0.90843697 | 92.6% HOMO-1 → LUMO+1 |
| 34568.6 | 289.3 | 0.36498570 | 64.2% HOMO-2 → LUMO |
| 37162.3 | 269.1 | 0.36400342 | 87.8% HOMO → LUMO+3 |
| 32165.3 | 310.9 | 0.14455468 | 91.5% HOMO-1 → LUMO+2 |
| 33244.3 | 300.8 | 0.08796056 | 74.2% HOMO-3 → LUMO |
| 41509.5 | 240.9 | 0.07811476 | 44.4% HOMO-4 → LUMO+2 |
| 34760.8 | 287.7 | 0.07688019 | 83.0% HOMO-8 → LUMO |

Triplets

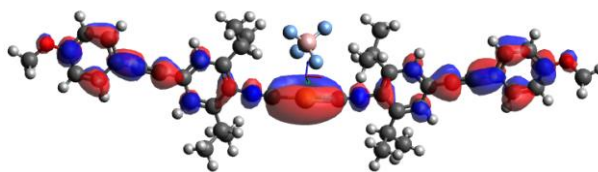
| Energy (cm ⁻¹) | Wavelength (nm) | Primary Contribution |
|----------------------------|-----------------|----------------------|
| 32680.2 | 306.0 | 88.3% HOMO-8 → LUMO |

| Orbital | Energy (eV) | Visualization |
|---------|-------------|---------------|
| HOMO-8 | -8.008 | |



LUMO+3

-1.121



[Au(CNDipp^{CC}Ph^{CN})₂](BF₄) (2b)

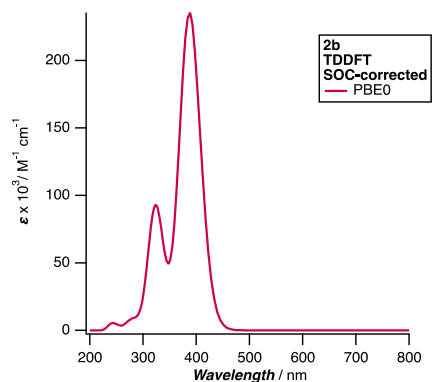


Figure 4.17. Calculated TDDFT spectra for optimized [Au(CNDipp^{CC}Ph^{CN})₂](BF₄) (2b). structure.

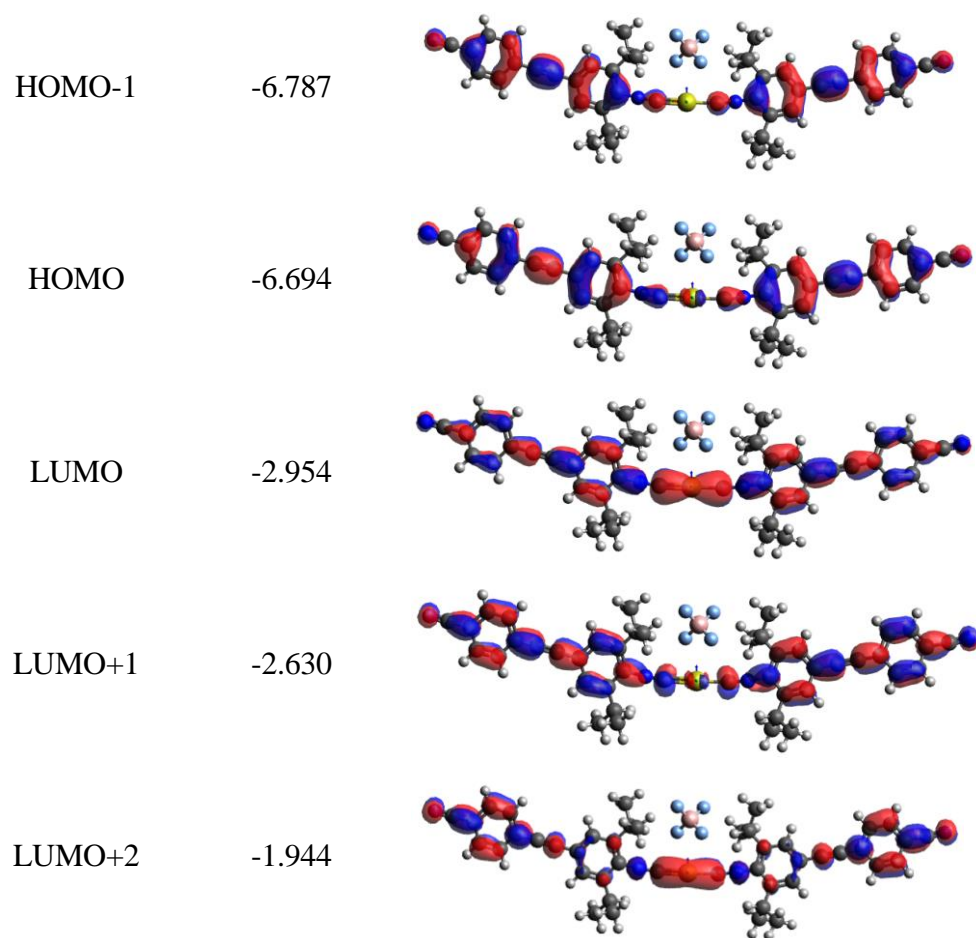
Singlets

| Energy (cm ⁻¹) | Wavelength (nm) | Osc. Strength | Primary Contribution |
|----------------------------|-----------------|---------------|-----------------------|
| 26223.0 | 381.3 | 3.52744516 | 91.3% HOMO → LUMO |
| 30827.8 | 324.4 | 0.8873105 | 90.1% HOMO-1 → LUMO+1 |
| 28036.5 | 356.7 | 0.13065436 | 92.7% HOMO-1 → LUMO |
| 32379.0 | 308.8 | 0.09997385 | 41.7% HOMO-2 → LUMO+1 |
| 35080.9 | 285.1 | 0.06440251 | 84.1% HOMO → LUMO+2 |
| 30098.8 | 332.2 | 0.06422342 | 91.1% HOMO → LUMO+1 |
| 34527.2 | 289.6 | 0.03418133 | 88.1% HOMO-8 → LUMO |

Triplets

| Energy (cm ⁻¹) | Wavelength (nm) | Primary Contribution |
|----------------------------|-----------------|----------------------|
| 32563.2 | 307.1 | 81.9% HOMO-8 → LUMO |

| Orbital | Energy (eV) | Visualization |
|---------|-------------|---------------|
| HOMO-8 | -8.168 | |
| HOMO-2 | -7.566 | |



[Au(CNDipp^{CC}-1-naph)₂](BF₄) (2c)

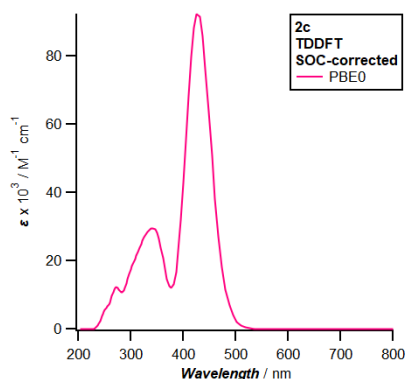


Figure 4.18. Calculated TDDFT spectra for optimized [Au(CNDipp^{CC}-1-naph)₂](BF₄) (2c) structure.

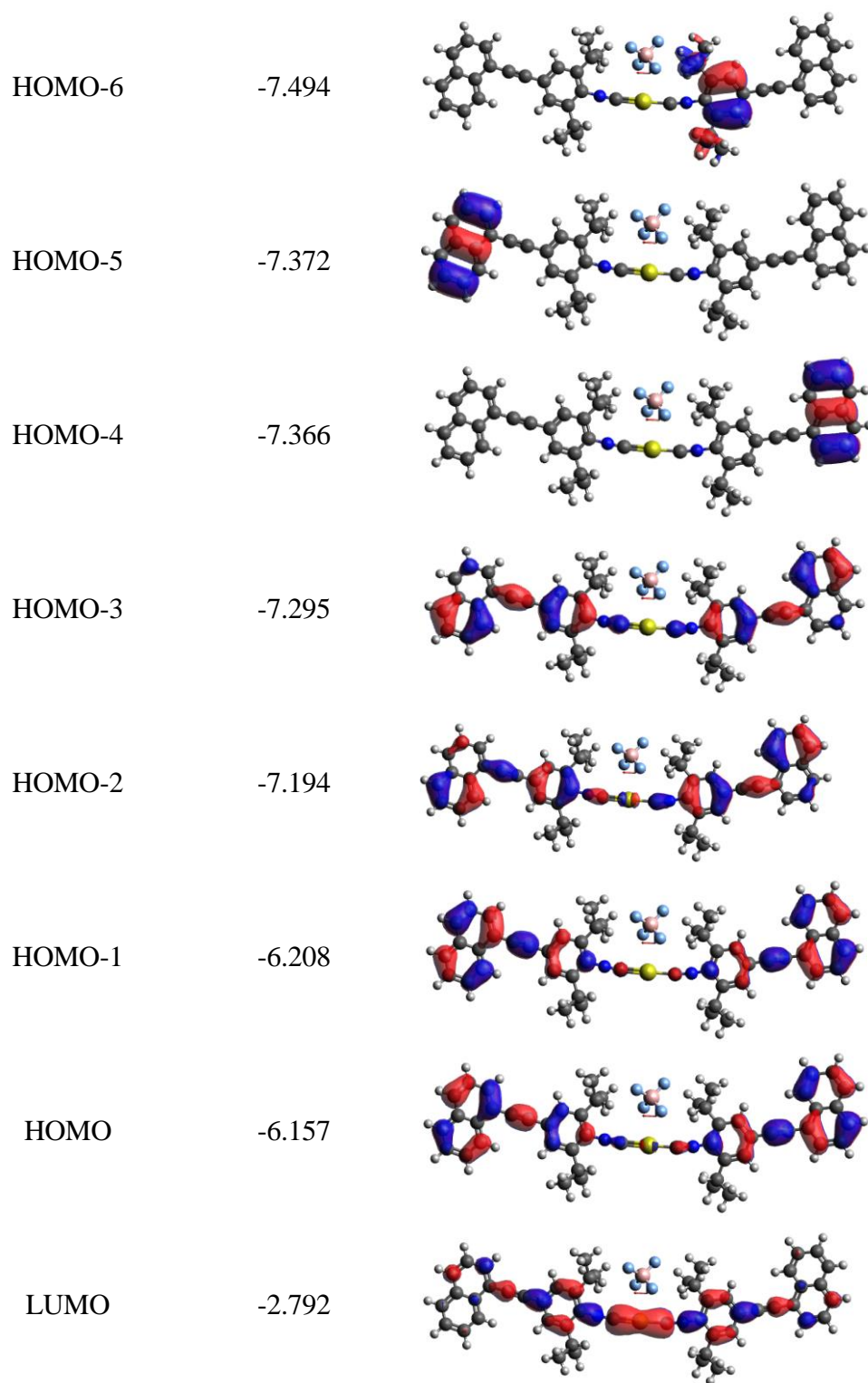
Singlets

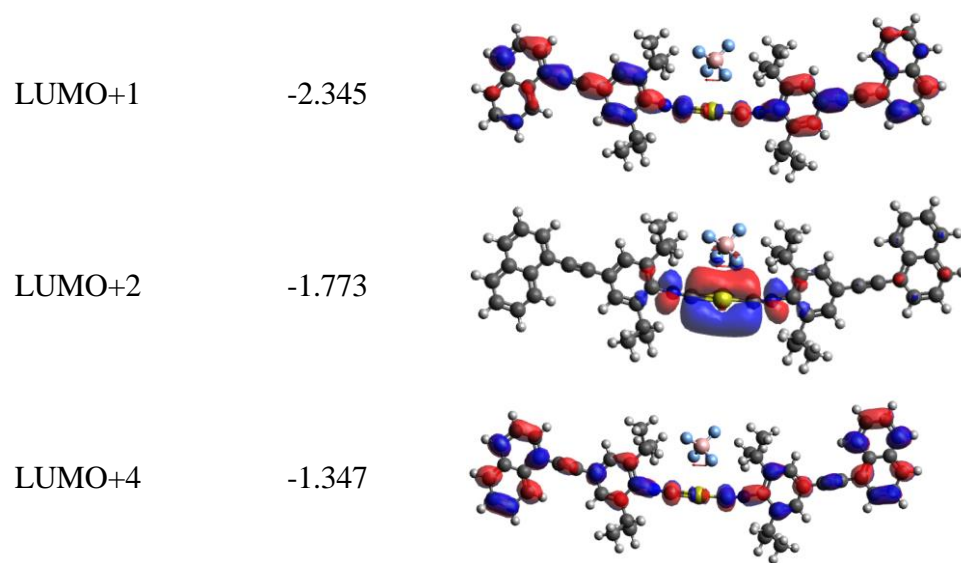
| Energy (cm ⁻¹) | Wavelength (nm) | Osc. Strength | Primary Contribution |
|----------------------------|-----------------|---------------|-----------------------|
| 23642.2 | 423.0 | 2.42420083 | 92.6% HOMO → LUMO |
| 31527.8 | 317.2 | 0.70172923 | 79.4% HOMO-2 → LUMO |
| 28568.2 | 350.0 | 0.63272413 | 91.5% HOMO-1 → LUMO+1 |
| 32856.0 | 304.4 | 0.11034389 | 28.6% HOMO-6 → LUMO |
| 36830.0 | 271.5 | 0.10588998 | 43.7% HOMO-1 → LUMO+4 |
| 39342.0 | 254.2 | 0.07628692 | 57.7% HOMO-4 → LUMO+1 |
| 24788.6 | 403.4 | 0.06907417 | 94.4% HOMO-1 → LUMO |
| 39397.5 | 253.8 | 0.0476607 | 57.5% HOMO-5 → LUMO+1 |
| 28144.9 | 355.3 | 0.04742929 | 93.0% HOMO → LUMO+1 |
| 39529.3 | 253.0 | 0.04676849 | 37.5% HOMO-3 → LUMO+2 |
| 32511.7 | 307.6 | 0.04018999 | 46.0% HOMO-3 → LUMO |
| 34648.8 | 288.6 | 0.03517789 | 91.8% HOMO-8 → LUMO |

Triplets

| Energy (cm ⁻¹) | Wavelength (nm) | Primary Contribution |
|----------------------------|-----------------|----------------------|
| 32634.9 | 306.4 | 85.4% HOMO-8 → LUMO |

| Orbital | Energy (eV) | Visualization |
|---------|-------------|---------------|
| HOMO-8 | -8.071 | |





4.5. References

- (1) Glaser, F.; Wenger, O. S., Recent Progress in the Development of Transition-Metal Based Photoredox Catalysts. *Coord Chem Rev* **2020**, 405, 213129.
- (2) Prier, C. K.; Rankic, D. A.; MacMillan, D. W., Visible Light Photoredox Catalysis with Transition Metal Complexes: Applications in Organic Synthesis. *Chem Rev* **2013**, 113 (7), 5322-63.
- (3) Shaw, M. H.; Twilton, J.; MacMillan, D. W., Photoredox Catalysis in Organic Chemistry. *J Org Chem* **2016**, 81 (16), 6898-926.
- (4) Zhao, Q.; Huang, C.; Li, F., Phosphorescent Heavy-Metal Complexes for Bioimaging. *Chem Soc Rev* **2011**, 40 (5), 2508-24.
- (5) Hagfeldt, A.; Boschloo, G.; Sun, L.; Kloo, L.; Pettersson, H., Dye-Sensitized Solar Cells. *Chem Rev* **2010**, 110 (11), 6595-663.
- (6) Crespo, O., Gold-Gold Interactions. In *Modern Supramolecular Gold Chemistry: Gold-Metal Interactions and Applications*, Laguna, A., Ed. WILEY-VCH Verlag GmbH & Co. KGaA: Weinheim, **2008**; pp 65-129.
- (7) Schmidbaur, H.; Schier, A., Auophilic Interactions as a Subject of Current Research: An update. *Chem Soc Rev* **2012**, 41 (1), 370-412.
- (8) Chow, A. L.; So, M. H.; Lu, W.; Zhu, N.; Che, C. M., Synthesis, Photophysical Properties, and Molecular Aggregation of Gold(I) Complexes Containing Carbon-Donor Ligands. *Chem Asian J* **2011**, 6 (2), 544-53.
- (9) Wu, Z.; Du, Y.; Liu, J.; Yao, Q.; Chen, T.; Cao, Y.; Zhang, H.; Xie, J., Auophilic Interactions in the Self-Assembly of Gold Nanoclusters into

Nanoribbons with Enhanced Luminescence. *Angew Chem Int Ed Engl* **2019**, 58 (24), 8139-8144.

(10) White-Morris, R. L.; Stender, M.; Tinti, D. S.; Balch, A. L.; Rios, D.; Attar, S., New Structural Motifs in the Aggregation of Neutral Gold(I) Complexes: Structures and Luminescence from (Alkyl Isocyanide)AuCN. *Inorg Chem* **2003**, 42 (10), 3237-3244.

(11) Schneider, W.; Sladek, A.; Bauer, A.; Angermaier, K.; Schmidbaur, H., Structural Investigation of Bis(Isonitrile)Gold(I) Complexes. *Z Naturforschung B* **1997**, 52 (1), 53-56.

(12) Echeverría, J., The Interplay of Non-Covalent Interactions Determining the Antiparallel Conformation of (Isocyanide)Gold(I) Dimers. *CrystEngComm* **2018**, 20 (28), 3987-3993.

(13) Forward, J. M.; Bohmann, D.; Fackler, J. P.; Staples, R. J., Luminescence Studies of Gold(I) Thiolate Complexes. *Inorg Chem* **1995**, 34 (25), 6330-6336.

(14) Fujisawa, K.; Yamada, S.; Yanagi, Y.; Yoshioka, Y.; Kiyohara, A.; Tsutsumi, O., Tuning the Photoluminescence of Condensed-Phase Cyclic Trinuclear Au(I) Complexes through Control of Their Aggregated Structures by External Stimuli. *Sci Rep* **2015**, 5, 7934.

(15) He, X.; Yam, V. W.-W., Luminescent Gold(I) Complexes for Chemosensing. *Coord Chem Rev* **2011**, 255 (17), 2111-2123.

(16) Kean, W. F.; Kean, I. R. L., Clinical Pharmacology of Gold. *Inflammopharmacology* **2008**, 16 (3), 112-125.

(17) Sutton, B. M., Gold Compounds for Rheumatoid Arthritis. *Gold Bulletin* **1986**, 19 (1), 15-16.

- (18) Deo, K. M.; Pages, B. J.; Ang, D. L.; Gordon, C. P.; Aldrich-Wright, J. R., Transition Metal Intercalators as Anticancer Agents—Recent Advances. *Int. J. Mol. Sci.* **2016**, 17 (11), 1818.
- (19) Kim, J. H.; Reeder, E.; Parkin, S.; Awuah, S. G., Gold(I/III)-Phosphine Complexes as Potent Antiproliferative Agents. *Sci Rep* **2019**, 9 (1), 12335.
- (20) Radisavljević, S.; Petrović, B., Gold(III) Complexes: An Overview on Their Kinetics, Interactions with DNA/Bsa, Cytotoxic Activity, and Computational Calculations. *Front Chem* **2020**, 8.
- (21) Zhang, Y.; Wu, M.; Dai, W.; Chen, M.; Guo, Z.; Wang, X.; Tan, D.; Shi, K.; Xue, L.; Liu, S.; Lei, Y., High Drug-Loading Gold Nanoclusters for Responsive Glucose Control in Type 1 Diabetes. *J. Nanobiotechnology* **2019**, 17 (1), 74.
- (22) Barth, A. T.; Morales, M.; Winkler, J. R.; Gray, H. B., Photoredox Catalysis Mediated by Tungsten(0) Arylisocyanides in 1,2-Difluorobenzene. *Inorg Chem* **2022**, 61 (19), 7251-7255.
- (23) Fajardo, J.; Barth, A. T.; Morales, M.; Takase, M. K.; Winkler, J. R.; Gray, H. B., Photoredox Catalysis Mediated by Tungsten(0) Arylisocyanides. *J Am Chem Soc* **2021**, 143 (46), 19389-19398.
- (24) Takematsu, K.; Wehlin, S. A. M.; Sattler, W.; Winkler, J. R.; Gray, H. B., Two-Photon Spectroscopy of Tungsten(0) Arylisocyanides Using Nanosecond-Pulsed Excitation. *Dalton Trans* **2017**, 46 (39), 13188-13193.
- (25) Kvapilová, H.; Sattler, W.; Sattler, A.; Sazanovich, I. V.; Clark, I. P.; Towrie, M.; Gray, H. B.; Záliš, S.; Vlček, A., Electronic Excited States of Tungsten(0) Arylisocyanides. *Inorg Chem* **2015**, 54 (17), 8518-8528.

- (26) Sattler, W.; Ener, M. E.; Blakemore, J. D.; Rachford, A. A.; LaBeaume, P. J.; Thackeray, J. W.; Cameron, J. F.; Winkler, J. R.; Gray, H. B., Generation of Powerful Tungsten Reductants by Visible Light Excitation. *J Am Chem Soc* **2013**, 135 (29), 10614-10617.
- (27) Mann, K. R.; Cimolino, M.; Geoffroy, G. L.; Hammond, G. S.; Orio, A. A.; Albertin, G.; Gray, H. B., Electronic Structures and Spectra of Hexakisphenylisocyanide Complexes of Cr(0), Mo(0), W(0), Mn(I), and Mn(II). *Inorg Chimica Acta* **1976**, 16, 97-101.
- (28) Mann, K. R.; Gray, H. B.; Hammond, G. S., Excited-State Reactivity Patterns of Hexakisarylisocyano Complexes of Chromium(0), Molybdenum(0), and Tungsten(0). *J Am Chem Soc* **1977**, 99 (1), 306-307.
- (29) Fajardo, J., Jr.; Schwan, J.; Kramer, W. W.; Takase, M. K.; Winkler, J. R.; Gray, H. B., Third-Generation W(CNAr)₆ Photoreductants (CNAr = Fused-Ring and Alkynyl-Bridged Arylisocyanides). *Inorg Chem* **2021**, 60 (6), 3481-3491.
- (30) Sattler, W.; Henling, L. M.; Winkler, J. R.; Gray, H. B., Bespoke Photoreductants: Tungsten Arylisocyanides. *J Am Chem Soc* **2015**, 137 (3), 1198-205.
- (31) Sheldrick, G. M., Phase Annealing in Shelx-90: Direct Methods for Larger Structures. *Acta Crystallogr. A: Found. Adv.* **1990**, 46 (6), 467-473.
- (32) Sheldrick, G. M., Crystal Structure Refinement with Shelxl. *Acta Crystallogr C Struct Chem* **2015**, 71 (Pt 1), 3-8.
- (33) Müller, P., Practical Suggestions for Better Crystal Structures. *Crystallography Reviews* **2009**, 15 (1), 57-83.
- (34) Sheldrick, G. M. Cell_Now, University of Göttingen, Germany, 2008.

- (35) Bruker Saint, Bruker-AXS Inc.: Madison, Wisconsin, USA, 2017.
- (36) Sheldrick, G. M. Twinabs, University of Göttingen, Germany, 2012.
- (37) Neese, F. The ORCA Program System. *WIREs Computational Molecular Science* **2012**, 2 (1), 73–78.
- (38) Neese, F. Software Update: The ORCA Program System, Version 4.0. *WIREs Computational Molecular Science* **2018**, 8 (1), e1327.
- (39) Becke, A. D. Density-Functional Exchange-Energy Approximation with Correct Asymptotic Behavior. *Phys. Rev. A* **1988**, 38 (6), 3098–3100.
- (40) Perdew, J. P. Density-Functional Approximation for the Correlation Energy of the Inhomogeneous Electron Gas. *Phys. Rev. B* **1986**, 33 (12), 8822–8824.
- (41) Becke, A. D. Density-functional Thermochemistry. III. The Role of Exact Exchange. *J Chem Phys* **1993**, 98 (7), 5648–5652.
- (42) Pantazis, D. A.; Chen, X.-Y.; Landis, C. R.; Neese, F. All-Electron Scalar Relativistic Basis Sets for Third-Row Transition Metal Atoms. *J. Chem. Theory Comput.* **2008**, 4 (6), 908–919.
- (43) Barone, V.; Cossi, M. Quantum Calculation of Molecular Energies and Energy Gradients in Solution by a Conductor Solvent Model. *J. Phys. Chem. A* **1998**, 102 (11), 1995–2001.

5 Spectroscopic and Magnetic Properties of Fe(II) and Co(II) Quaterpyridine Photo/electrocatalysts

5.1. Abstract

We have investigated the UV-visible-NIR, ^1H NMR, Mössbauer, and infrared spectra of structurally characterized iron(II) and cobalt(II) quaterpyridines, which function as photo/electrocatalysts for CO_2 reduction. Assignments of electronic transitions in absorption spectra are supported by time-dependent density functional theory (TD-DFT) calculations. The iron(II) quaterpyridine complexes are predominantly high spin ($S = 2$) at 293 K and convert to low spin ($S = 0$) at 257 K.

5.2. Introduction

Metal-qpy (qpy= 2,2':6',2'':6'',2''':6''',2''''-quaterpyridine) complexes are electrocatalysts for CO_2 reduction reactions. The Co(II) complex, $[\text{Co}(\text{qpy})]^{2+}$, also is a water oxidation electrocatalyst, with turnover numbers (TONs) in the range 335-1733.¹ Both $[\text{Fe}(\text{qpy})]^{2+}$ and $[\text{Co}(\text{qpy})]^{2+}$ catalyze CO_2 reduction with high selectivity for CO (>95%) at low formal overpotentials ($\eta_{\text{eff}} = 240$ mV for Co, 140 mV for Fe),^{2,3} with high Faradaic efficiencies (94% for Co, 48% for Fe). Upon visible irradiation ($\lambda_{\text{ex}} > 420$ nm), the Faradaic efficiency of Fe(II) catalysis increases to 70%.² As photocatalysts, the Fe(II) and Co(II) complexes are highly selective for CO evolution (98% for Co, 95% for Fe), with high TONs (2660 for Co, and >3000 for Fe).³ Candidate mechanisms for Fe(II) and Co(II) quaterpyridine catalysis of CO_2 reduction have been assessed by density functional theory calculations.⁴

Our interest in metal quaterpyridines is motivated by a desire to understand the electronic structure of these catalysts. Notably, these systems are structurally analogous to related tetraphenylporphyrin and phthalocyanine systems, which

serve as planar electron reservoirs to mediate electron-rich catalysis. These quaterpyridine ligands afford molecular systems with low-lying MLCT states which facilitate excited state relaxation pathways. When compared to related polypyridine systems, insights in these sterically tethered ligand scaffolds remain underdeveloped.

5.3. Results and Discussion

Synthesis and X-Ray Crystallography

Metal-qpy complexes were synthesized with noncoordinating counterions to facilitate structural analysis in nonaqueous solvents. Metalation of qpy was done by stirring ligand with a stoichiometric quantity of $M(\text{BF}_4)_2 \cdot x\text{H}_2\text{O}$ ($M = \text{Co}, \text{Fe}$) to generate $[\text{Co}(\text{qpy})(\text{MeCN})_2](\text{BF}_4)_2$ and $[\text{Fe}(\text{qpy})(\text{MeCN})_2](\text{BF}_4)_2$. The compounds were suspended in a minimal volume of MeCN under inert atmosphere, stirred at reflux for one hour, evacuated to dryness, recrystallized, and stored in a glovebox.

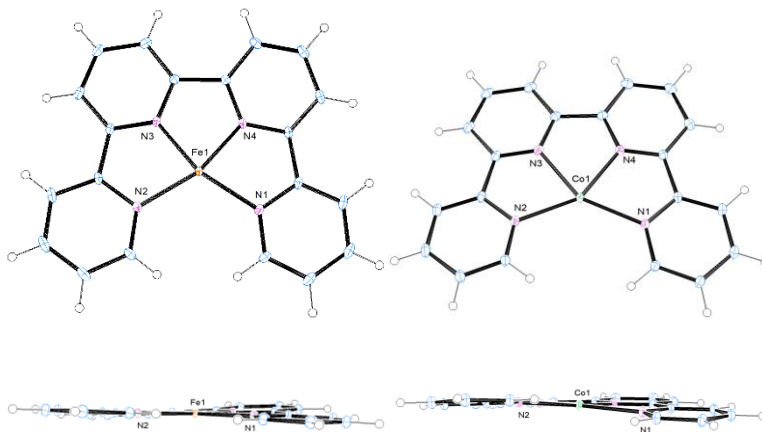


Figure 5.1. Structures of $[\text{Fe}(\text{qpy})](\text{BF}_4)_2$ (**Fe-qpy**, left) and $[\text{Co}(\text{qpy})](\text{BF}_4)_2$ (**Co-qpy**, right) showing the coordination geometry and ligand planarity. Thermal ellipsoids are shown at 30% probability, with counter ions and solvent omitted for clarity.

Vapor diffusion of Et₂O into MeCN solution affords **Fe-qpy** and **Co-qpy** crystals of sufficient size for x-ray diffraction analysis. **Figure 5.1** depicts the coordination geometry of **Fe-qpy** and **Co-qpy**. Each complex has a central metal bonded to four ligand pyridines in a planar coordination environment. Both complexes were isolated with MeCN molecules coordinated at axial positions in a pseudo-*O_h* geometry. For simplicity, we will assume *O_h* symmetry in assigning electronic structures and spectra. Structure parameters are set out in **Table 5.1**.

Table 5.1. Crystallographic structure of M-qpy (M = Fe, Co).

| Complex | $d(\text{M}-\text{N}_1)^a$ | $d(\text{M}-\text{N}_4)^a$ | $\angle(\text{N}_1-\text{M}-\text{N}_2)^b$ | $\angle(\text{N}_1-\text{M}-\text{N}_4)^b$ | $\angle(\text{N}_3-\text{M}-\text{N}_4)^b$ |
|--|----------------------------|----------------------------|--|--|--|
| Co-qpy | 2.1206(13) | 2.0810(13) | 133.95(5) | 75.80(5) | 74.67(5) |
| Fe-qpy | 2.0279(8) | 1.8789(8) | 116.52(4) | 80.83(3) | 81.84(4) |
| [Fe(qpy)(OH ₂)](ClO ₄) ₂ ^c | 2.1988(2) | 2.1384(7) | 138.59(2) | 74.14(8) | 73.11(5) |

^a In Å. ^b In °. ^c Data from ref. 5.

The metal quaterpyridine complexes have an open edge site, with a $\angle(\text{N}-\text{M}-\text{N})$ bite angle of 116.52(4)° for **Fe-qpy** and 133.95(5)° for **Co-qpy**. The metal-ligand bond lengths of **Fe-qpy** are relatively short (1.87-2.02 Å). In Fe(II) polypyridines, Fe–N bond lengths are diagnostic of the ground-state spin state, where low-spin $S = 0$ species typically have metal-ligand bond lengths that are 0.2 Å shorter than high-spin $S = 2$ states.⁶ The related complex [Fe(qpy)(OH₂)](ClO₄)₂ has longer Fe–N bond lengths (2.13-2.20 Å) along with a wider $\angle(\text{N}-\text{Fe}-\text{N})$ bite angle, 138.59(2)°. These data suggest that crystalline **Fe-qpy** has a low-spin electronic ground state. Subsequent work interrogating the **Fe-qpy** crystals at room temperature indicated the same low-spin structure (M–N bond lengths 1.89-2.03 Å). Of interest is that the bond lengths of **Co-qpy** are relatively long (2.08-2.12 Å), consistent with a high-spin $S = 3/2$ electronic ground state. The bond lengths

and angles match the parameters obtained from DFT geometry optimization (B3LYP/def2-TZVP, **Table 5.3**).

NMR Spectroscopy and Solution Magnetic Susceptibility

Paramagnetic ^1H nuclear magnetic resonance spectroscopy can shed light on the ground-state coordination environments and electronic structures of solvated quaterpyridines. Both qpy complexes exhibit sharp paramagnetic ^1H NMR features in solution (D_2O for **Fe-qpy**, CD_3CN for **Co-qpy**, **Figures 5.7** and **5.9**), where integration accords with the expected shifts for four-coordinate complexes (bis-ligated $[\text{Fe}(\text{qpy})_2]^{2+}$ was not detected).⁷ The NMR features of **Fe-qpy** are broadened in CD_3CN solution at room temperature, indicating partial population of a paramagnetic state. From Evans method analyses, both **Fe-qpy** and **Co-qpy** are high-spin in MeCN at room temperature ($4.78 \mu_{\text{B}}$ for $S = 2$ **Fe-qpy**, $3.95 \mu_{\text{B}}$ for $S = 3/2$ **Co-qpy**).

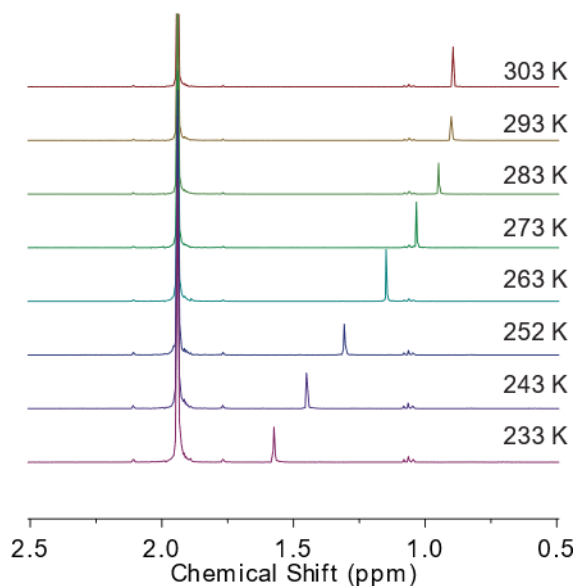


Figure 5.2. Variable temperature ^1H NMR (Evans method) of **Fe-qpy** in CD_3CN solution.

Variations in **Fe-qpy** crystal geometry indicate a sensitivity to slight environmental changes. Variable magnetic susceptibility data of solvated species were collected using the Evans method (**Figure 5.2**). When the temperature was reduced, the ^1H NMR chemical shifts decreased, consistent with spin crossover to a diamagnetic state. Analysis of chemical shifts placed the $T_{1/2}$ spin crossover at 257 K (-16°C) in solution.

Mössbauer Spectroscopy

Mössbauer isomer shifts (δ) can be used to assign **Fe-qpy** electronic structures in solids and frozen solutions (**Figure 5.3**). Data were recorded at 80 K and fit to symmetric quadrupole doublets. The isomer shift of crystalline **Fe-qpy** in a boron nitride matrix ($\delta = 1.187\text{ mm s}^{-1}$) can be assigned to high-spin $S = 2$ iron(II). The shift matches those of high-spin pseudo- O_h iron(II) complexes $[\text{Fe}(\text{py})_4\text{X}_2]$ ($\text{X} = \text{Cl, Br, I}$), which have $\delta = 1.11\text{--}1.18\text{ mm s}^{-1}$.⁸ The isomer shift of a second **Fe-qpy** sample in frozen MeCN solution ($\delta = 0.379\text{ mm s}^{-1}$) indicates population of a low-spin $S = 0$ state. This isomer shift matches those of six-coordinate $\text{Fe}^{\text{II}}(\text{Pc})(\text{py})_2$ ($\delta = 0.32\text{ mm s}^{-1}$) and $\text{Fe}^{\text{II}}(\text{TPP})(\text{py})_2$ ($\delta = 0.40\text{ mm s}^{-1}$) complexes that have planar FeN_4 ligand environments with weakly bound solvent molecules in axial positions.⁹ Of interest is that a mixture of high- and low-spin species was present in a partially ground crystalline **Fe-qpy** sample suspended in an inert boron nitride matrix.

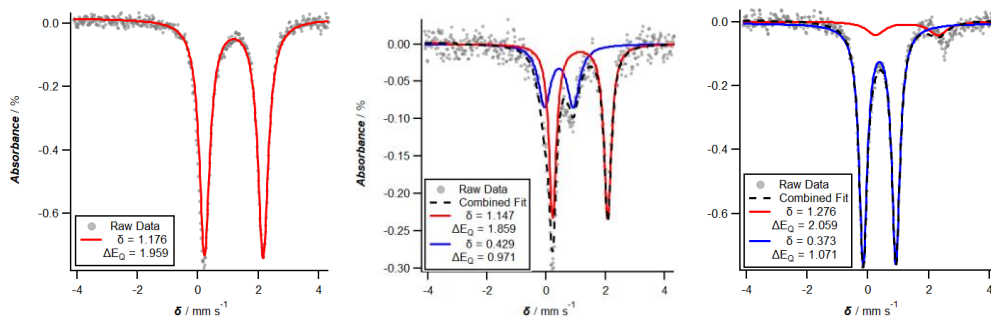


Figure 5.3. Zero-field ^{57}Fe Mössbauer spectra of **Fe-qpy** recorded at 80 K. Data are represented as grey points and fits as lines: (a) Solid ground in boron nitride, $S = 2$ (>95%); (b) Partially ground crystal in boron nitride (60% $S = 2$: 40% $S = 0$); (c) Frozen 75 mM MeCN solution, $S = 0$ (>90%).

The quadrupole splitting (ΔE_Q) is sensitive to deviations from cubic symmetry, owing to an asymmetric charge distribution about the metal center. In high-spin species, $\Delta E_Q = 1.938 \text{ mm s}^{-1}$, indicating a highly asymmetric ligand field. The low-spin complex is more centrosymmetric (reduced quadrupole splitting $\Delta E_Q = 1.071 \text{ mm s}^{-1}$); and a low-spin structure was found in the x-ray diffraction analysis. Installation of an axial acetonitrile ligand affords a complex with pseudo- O_h geometry, which stabilizes the low-spin state in a crystalline solid or frozen solution. Upon pulverization, a high-spin pseudo- O_h state with elongated metal-ligand bonds becomes populated, and the \angle (N1–Fe–N2) bite angle increases from $116.52(4)^\circ$ to $138.59(2)^\circ$ (Table 1).

Solid-State Infrared Spectroscopy

Infrared spectra of crystalline samples of **Fe-qpy** and **Co-qpy** were recorded (ATR-IR, **Figure 5.4**). Vibrational features at 934 and 1084 cm^{-1} (**Fe-qpy**) and 971 and 1076 cm^{-1} (**Co-qpy**) are assigned to in-plane ring bending modes. The data indicate that **Fe-qpy** has a high-spin ground state.

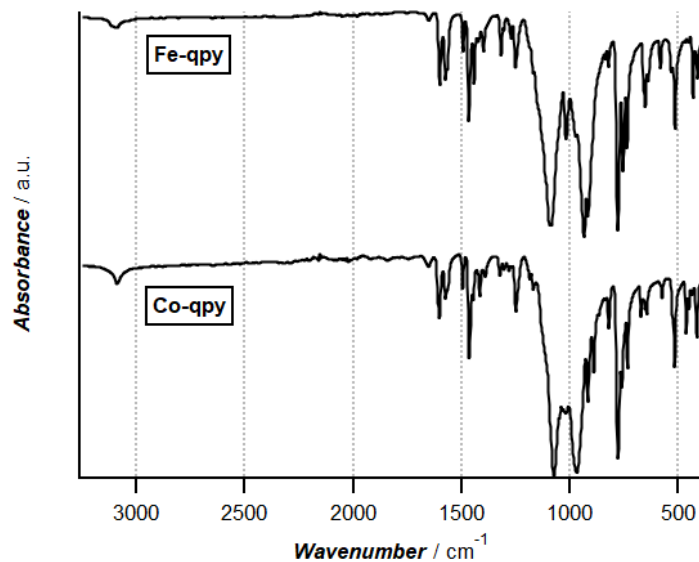


Figure 5.4. Solid-state **Co-qpy** and **Fe-qpy** infrared transmission spectra at 295 K.

UV-visible-NIR Spectroscopy

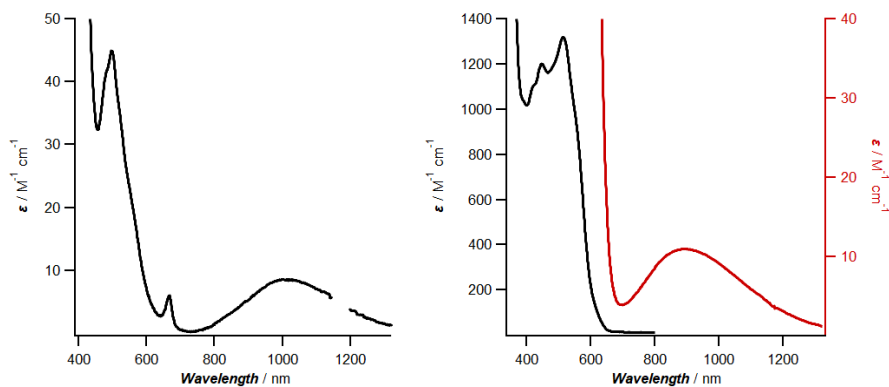


Figure 5.5. Vis-NIR absorption spectra of **Co-qpy** (left) and **Fe-qpy** (right) in MeCN solution at 295 K.

Vis-NIR absorption spectra were obtained for both complexes in MeCN solution at room temperature (**Figure 5.5**). Data and transition assignments are in Table 2. The NIR band in the **Co-qpy** spectrum is attributable to the spin-allowed ${}^4T_{1g} \rightarrow$

$^4T_{2g}$ d-d transition. The same transition assignment in the NIR spectrum of $[\text{Co}(\text{OH}_2)_6]^{2+}$ has been supported by MCD spectroscopic analysis.^{10,11} In addition, the sharp feature at $14,992\text{ cm}^{-1}$ is assigned as a spin-forbidden transition that gains intensity through spin-orbit coupling. The energies and intensities of these absorption systems are consistent with electronic structure calculations (**Table 5.6** and **5.7**).

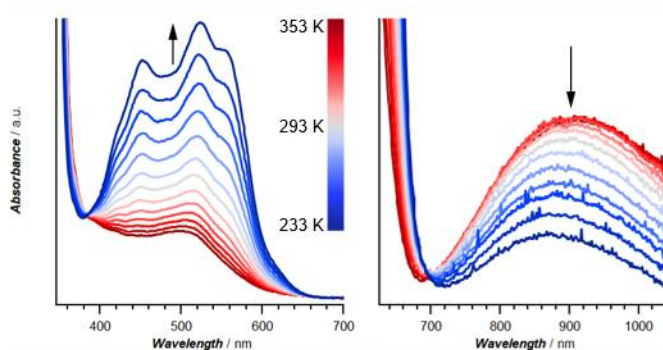


Figure 5.6. Variable temperature UV-vis absorption spectra of **Fe-qpy** in MeCN solution. Arrows indicate the direction change upon lowering the temperature.

There is a dramatic color change in MeCN solutions of **Fe-qpy** from deep red-purple (low-spin) at low temperature to pale yellow (high-spin) at higher temperatures. Measurements in MeCN over the 233 to 353 K (−40 to 80 °C) temperature range informed our interpretation of the **Fe-qpy** absorption spectrum. Heating the sample above room temperature increases the intensity of a broad band at ~900 nm and reduces the intensity in the visible region between ~400 and 650 nm (**Figure 5.6**). The near infrared feature is assigned to the $^5T_{2g} \rightarrow ^5E_g$ transition in high spin $\text{Fe}^{2+}(\text{d}^6)$. In the visible region, a broad sloping feature is observed at ~500 nm and assigned as a $^5T_{2g} \rightarrow ^5\text{MLCT}$ transition, matching transition assignments observed with time-dependent density functional theory (TD-DFT, **Table 5.4**).

When **Fe-qpy** is cooled from room temperature, an increase in absorption intensity is observed in the visible region from ~400 to 650 nm. Multiple absorption maxima appear as the absorption intensity in the infrared region decreases. The visible region features are assigned to spin-allowed metal-to-ligand charge-transfer (MLCT) transitions from a low-spin ($^1A_{1g}$) ground state, in agreement with predictions from TD-DFT calculations (**Table 5.5**). The low-temperature spectra and assignments are in general agreement those of analogous Fe(II) polypyridyl species.^{13,14}

Table 5.2. Electronic spectra and transition assignments for **M-qpy** (M = Fe, Co) complexes at 295 K

| Species | Wavelength ^a | Energy ^b | ϵ^c | Assignment |
|---------------|-------------------------|---------------------|--------------|---------------------------------------|
| Fe-qpy | 898 | 11 130 | 11 | $^5T_{2g} \rightarrow ^5E_g$ |
| | 515 | 19 418 | 1 319 | $^1A_{1g} \rightarrow ^1MLCT$ |
| | 500 | 20 000 | ^d | $^5T_{2g} \rightarrow ^5MLCT$ |
| | 448 | 22 321 | 1 193 | $^1A_{1g} \rightarrow ^1MLCT$ |
| | 425 | 23 529 | 1 092 | $^1A_{1g} \rightarrow ^1MLCT$ |
| Co-qpy | 1013 | 9 871 | 9 | $^4T_{1g}(F) \rightarrow ^4T_{2g}(F)$ |
| | 667 | 14 992 | 7 | $^4T_{1g}(F) \rightarrow ^2T_{2g}$ |
| | 497 | 20 120 | 45 | $^4T_{1g}(F) \rightarrow ^4T_{1g}(P)$ |

^a In nm. ^b In cm^{-1} . ^c In $M^{-1} cm^{-1}$. ^d Feature obscured at 295 K.

5.4. Conclusions

The absorption spectrum of **Co-qpy** is consistent with high-spin Co^{2+} - qpy in a pseudo-octahedral ligand field of moderate strength ($\Delta_o = 12\,400\,cm^{-1}$; $B = 850\,cm^{-1}$; $\Delta_o/B = 1.46$). The UV-vis-NIR absorption, 1H NMR; and Mössbauer spectra of **Fe-qpy** provide clear evidence for a complex with a ligand field strength near the spin crossover zone. Solvation in coordinating solvent reflects the ligand environment under catalytic conditions, and is thus necessary towards understanding the electronic structure of the catalyst.

5.5. Experimental Methods

General Considerations

All manipulations were conducted with Schlenk or glovebox techniques under inert nitrogen atmosphere. Solvents were sparged with Ar gas and passed through an alumina solvent purification system by SG Water SA, LLC. Non-halogenated solvents were tested with sodium benzophenone ketyl in tetrahydrofuran (THF) to confirm absence of oxygen and water. Deuterated solvents were purchased from Cambridge Isotope Laboratories, Inc. and dried over activated 3 Å molecular sieves. Ligand 2,2':6',2":6",2'''-quaterpyridine (qpy) was prepared using literature methods¹⁵ and recrystallized from acetone (diluted while heating to solubilize the material, filtered, and crystallized at -5 °C to generate colorless crystals). Boron nitride for Mössbauer spectroscopy measurements was used as received (Aldrich, 98%).

NMR Spectroscopy

NMR measurements were performed at room temperature, obtained using a Varian 400 MHz spectrometer. ^1H chemical shifts were reported in ppm relative to solvent residual signals. Magnetic susceptibility experiments were performed using Evans method, referenced using a solution of $\text{CH}_3\text{CN}:\text{CD}_3\text{CN}$ (1:10 volume). Variable temperature ^1H NMR spectroscopy (Evans method) was performed using a Bruker 400 MHz Spectrometer. As above, solutions were referenced using $\text{CH}_3\text{CN}:\text{CD}_3\text{CN}$ (1:5 volume).

UV-visible-NIR Spectroscopy

UV-visible absorption measurements were performed in acetonitrile solutions at 23 °C on a Cary 400 UV-visible spectrophotometer using 1 cm path length fused quartz cuvettes (Starna Cell).

Variable Temperature (VT) UV-visible-NIR Spectroscopy

Variable temperature UV-visible-NIR absorption measurements were performed on samples in acetonitrile solutions on a Cary 50 UV-visible spectrophotometer using 1 cm path length fused quartz cuvettes (Starna Cell). A Unisoku CoolSpeK UV cryostat and liquid nitrogen coolant were used for the experiments.

IR Spectroscopy

IR spectra were obtained in a nitrogen glovebox under anhydrous conditions. Solid samples were measured by attenuated total reflectance (ATR) infrared spectroscopy using a Bruker APLHA ATR-IR spectrometer probe. Measurements were made on a platinum sampling module and recorded in the OPUS software package.

Mössbauer Spectroscopy

Mössbauer spectra were recorded using a SEE Co. spectrometer (Edina, MN) operating in the constant acceleration mode in transmission geometry. The sample was maintained at 80 K in a SVT-400 cryostat from Janis (Wilmington, MA). The reported isomer shifts are relative to the centroid of a spectrum of α -Fe metallic foil at room temperature. Solid samples were prepared by grinding the solid material into a fine powder, diluting with boron nitride (roughly 1 Fe complex:3 boron nitride by mass) and mounting into a Delrin cup fitted with a screw cap to generate a pellet. Solution-state samples were prepared by dissolving complexes in 0.7 mL acetonitrile and freezing in a Delrin cup using the glovebox cold well (77 K). Data analyses were performed using version 4 of WMOSS program (www.wmoss.org). Quadrupole doublets were fit to Lorentzian lineshapes.

Mass Spectrometry

Electrospray ionization time-of-flight (ESI-TOF) mass spectra were obtained using a Waters LCT Premier XE Time-of-Flight mass spectrometer in the positive mode.

X-Ray Crystallography

Low-temperature (100 K) diffraction measurements were made at the Caltech Beckman Institute X-ray Crystallography Facility on a Bruker AXS D8 VENTURE KAPPA diffractometer coupled to a PHOTON II CPAD detector with Mo K_{α} radiation ($\lambda = 0.71073 \text{ \AA}$) from an $I\mu\text{S}$ micro-source. The structure was solved by direct methods using SHELXS¹⁶ and refined against F^2 on all data by full-matrix least squares with SHELXL-2017¹⁷ using established refinement techniques.¹⁸ All non-hydrogen atoms were refined anisotropically. All hydrogen atoms were included in the model at geometrically calculated positions and refined using a riding model. The isotropic displacement parameters of all hydrogen atoms were fixed to 1.2 times the U value of the atoms they are linked to (1.5 times for methyl groups). **[Co(qpy)(MeCN)₂](BF₄)₂** crystallized in the monoclinic space group $C2/c$ with half a molecule in the asymmetric unit along with one molecule of acetonitrile. **[Fe(qpy)(MeCN)₂](BF₄)₂** crystallized in the monoclinic space group $P2_1/c$ with two molecules in the asymmetric unit along with four molecules of acetonitrile.

Electronic Structure Calculations

Calculations were performed with the ORCA program package on the Caltech Resnick High Performance Computing cluster. Geometry optimizations are performed starting from the crystallographic geometry, using the B3LYP functional and def2-TZVP basis set on all atoms. The resolution of identity (RI) approximation was used to accelerate calculations. Time-dependent density functional theory (TD-DFT) calculations were performed using the CAM-B3LYP functional and def2-TZVP basis set.

[Fe(qpy)](BF₄)₂ Solid qpy (100.0 mg, 0.322 mmol) and Fe(BF₄)₂ · $x\text{H}_2\text{O}$ (108.8 mg, 0.322 mmol) were charged in a 100 mL Schlenk vessel. After evacuation, dry acetonitrile (10 mL) was added. The mixture was heated to reflux (70 °C) for one hour to ensure solubilization of qpy, generating a deep red-pink solution. The

product was evacuated to dryness with heating (70 °C) overnight to remove trace water. The Schlenk vessel was put in the glovebox, where the product was isolated via recrystallization in a cooled (−30 °C), concentrated acetonitrile solution (4 mL), generating red needles (81.3 mg, 46.0% yield). **¹H NMR** (CD₃CN, 400 MHz) : δ 132.80 (br s, 1H), 77.94 (s, 1H), 70.03 (s, 1H), 58.90 (s, 1H), 34.36 (s, 1H), 18.37 (d, 2H). **¹H NMR** (D₂O, 400 MHz) : δ 133.06 (br s, 1H), 78.24 (s, 1H), 70.33 (s, 1H), 59.11 (s, 1H), 34.64 (s, 1H), 18.33 (d, 2H), 14.70 (s, 1H). **UV–vis** (MeCN, λ (nm){ ε (cm^{−1} M^{−1}) }): 205{57566}, 230{42934}, 252{26806}, 295{30512}, 307{16956}, 330{117208}, 343{19295}, 425{1092}, 448{1193}, 515{1319}, 895{11}. **μ_{eff}** (CD₃CN, 400 MHz, Evans method): 4.78 μ_B. **IR** (ATR, 1700cm^{−1} – 400cm^{−1}): 412w, 431m, 515m, 531w, 583w, 640m, 653w, 737m, 756m, 780m, 821w, 837w, 918s, 934s, 1018m, 1084s, 1094s, 1252w, 1273w, 1318w, 1400w, 1443m, 1466m, 1492s, 1566m, 1575m, 1601m. **ESI-TOF**: m/z = 411.05 (100) [FeL(HCOO)]⁺, 412.06 (29) [FeL(H₂COO)]⁺, 409.06 (12) [FeL(COO)]⁺. **Anal. Calcd** for C₂₀H₁₄FeN₄B₂F₈: C, 44.25; H, 2.60; N, 10.32. Found C, 44.05; H, 2.80; N, 10.40.

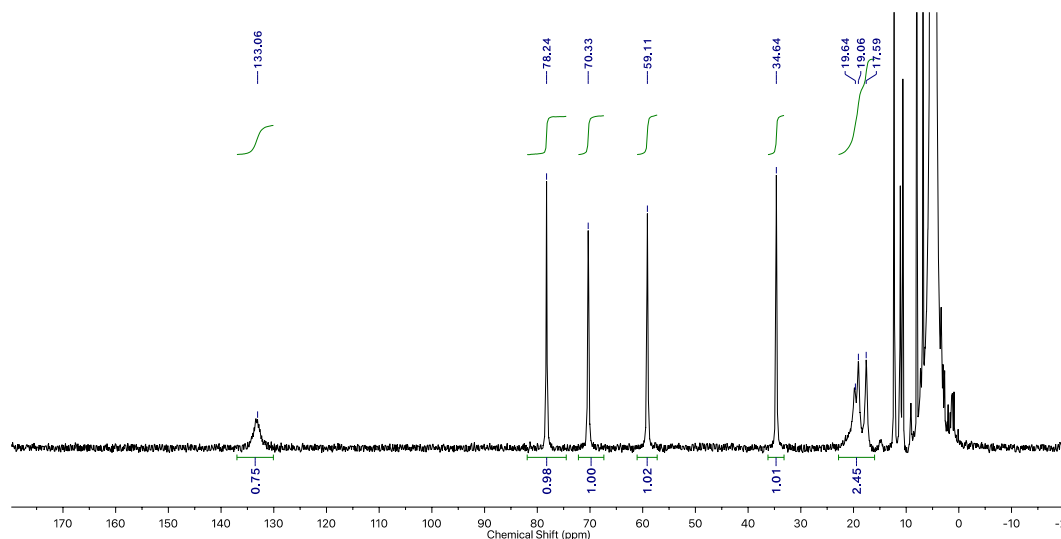


Figure 5.7. ¹H NMR (D₂O, 400 MHz) spectrum of **Fe-qpy**.

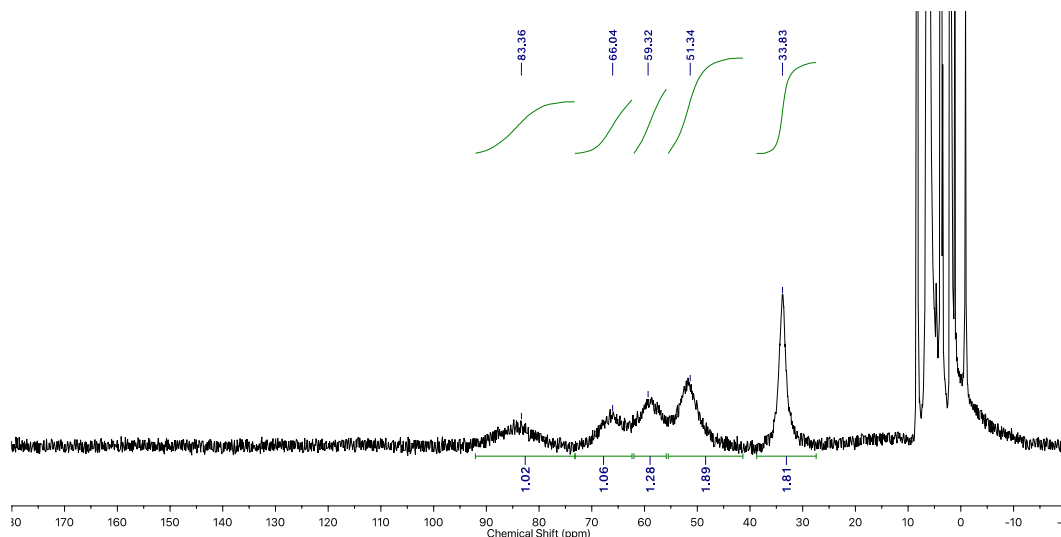


Figure 5.8. ^1H NMR (CD_3CN , 400 MHz) spectrum of **Fe-qpy**.

[Co(qpy)](BF₄)₂ Solid qpy (100.0 mg, 0.322 mmol) and $\text{Co}(\text{BF}_4)_2 \cdot x\text{H}_2\text{O}$ (109.74 mg, 0.322 mmol) were charged in a 100 mL Schlenk vessel. After evacuation, dry acetonitrile (10 mL) was added. The mixture was heated to reflux (70 °C) for one hour to ensure solubilization of qpy, generating a pink-orange solution. The product was evacuated to dryness with heating (70 °C) overnight to remove trace water. The Schlenk vessel was put in the glovebox, where the product was isolated via recrystallization in a cooled (−30 °C), concentrated acetonitrile solution (4 mL), generating large orange needles (125.4 mg, 71.0% yield). **^1H NMR** (CD_3CN , 400 MHz): δ 177.94 (br s, 1H), 138.20 and 135.46 (s, 2H), 76.31 (s, 1H), 69.69 (s, 1H), 54.26 (s, 1H), 25.75 (s, 1H). **UV-vis** (MeCN, λ (nm) { ϵ ($\text{cm}^{-1} \text{M}^{-1}$) }): 232{36449}, 248{31491}, 259{23051}, 295{36371}, 328{15793}, 335{18886}, 479{41}, 497{45}, 667{7}, 1013{9}. **IR** (ATR, 1700cm^{-1} – 400cm^{-1}): 414w, 451w, 464w, 517m, 527w, 577w, 645w, 653w, 673w, 735m, 762m, 780s, 821w, 891m, 918m, 971s, 1023m, 1076s, 1148w, 1172w, 1184w, 1250w. 1326w, 1392w, 1416w, 1447w, 1465m, 1496w, 1574w, 1603w. **μ_{eff}** (CD_3CN , 400 MHz, Evans method): $3.95 \mu_{\text{B}}$. **ESI-TOF**: m/z = 456.06 (100) $[\text{CoL}(\text{BF}_4)]^+$, 457.07 (27) $[\text{CoHL}(\text{BF}_4)]^+$,

455.07 (26) $[\text{CoL}^-(\text{BF}_4)]^+$. **Anal. Calcd** for $\text{C}_{20}\text{H}_{14}\text{CoN}_4\text{B}_2\text{F}_8$: C, 44.50; H, 2.60; N, 10.38. Found C, 41.24; H, 2.57; N, 10.14.

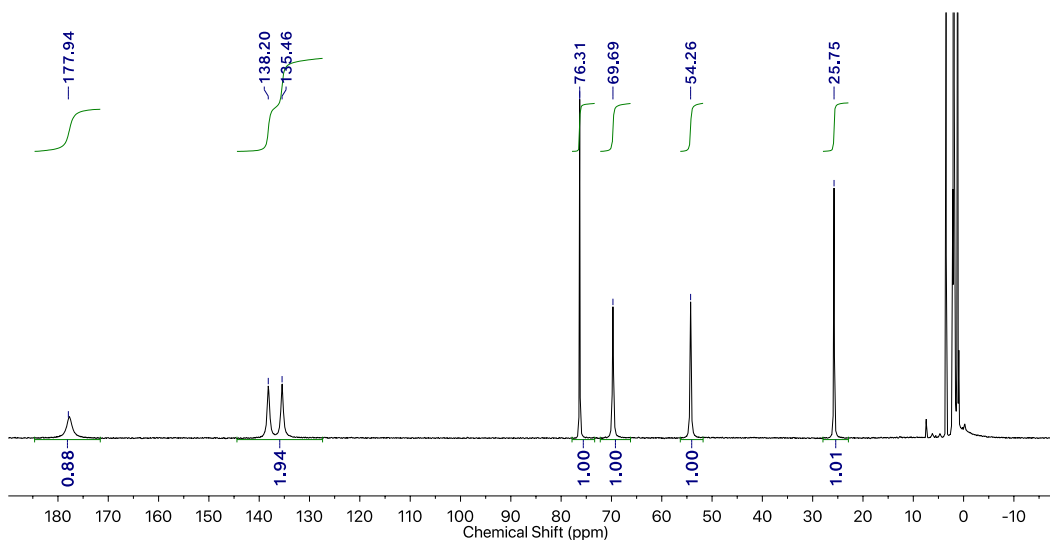


Figure 5.9. ^1H NMR (CD_3CN , 400 MHz) spectrum of **Co-qpy**.

Electronic Structure Calculations

Input Parameters

Geometry Optimization

```
! UKS UNO B3LYP RIJCOSX Def2-TZVP Zora Grid4 NoFinalGrid TightSCF
TightOpt
%method
Z_solver DIIS
Z_MaxIter 300
End
```

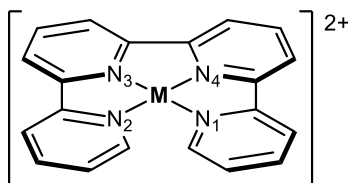
TD-DFT Calculations

```
! UKS UNO CAM-B3LYP def2-TZVP RIJCOSX TightSCF Grid5 ZORA
LargePrint
%tddft
nroots 50
maxdim 5
triplets true
end
```

Optimized Geometry Coordinates

| [Fe(qpy)(MeCN) ₂](BF ₄) ₂ <i>S</i> = 0 | | | [Fe(qpy)(MeCN) ₂](BF ₄) ₂ <i>S</i> = 2 | | | | |
|---|-------------------|-------------------|---|----|-------------------|-------------------|-------------------|
| Fe | 7.40174926170928 | 4.09094660719931 | 12.86944201273551 | Fe | 7.40096592701187 | 4.39588289113880 | 12.86816510672836 |
| N | 8.17423856079354 | 5.16505082438795 | 11.27363227951032 | N | 8.33268233868927 | 5.18700135282868 | 11.01701603185898 |
| C | 8.27599189463354 | 6.48520283358123 | 11.10790111623917 | C | 8.48781485262896 | 6.48156334469466 | 10.72452806106127 |
| H | 7.84464838674262 | 7.10304250092299 | 11.88301790106435 | H | 8.03911835012016 | 7.19076831356388 | 11.40976006780576 |
| C | 8.90078153338387 | 7.06821997826418 | 10.01216419280161 | C | 9.18264609438285 | 6.92547167875143 | 9.60792572376052 |
| H | 8.96092910662974 | 8.14494424380225 | 9.93273462290284 | H | 9.28296448073515 | 7.98422159221697 | 9.41211085953449 |
| C | 9.43924239587694 | 6.24207076195286 | 9.03862868712762 | C | 9.74038026075743 | 5.97872179714159 | 8.76181167449062 |
| H | 9.9417065977780 | 6.65864900555990 | 8.17574414278029 | H | 10.29840640456675 | 6.28207118064770 | 7.88584022612982 |
| C | 9.32490322506435 | 4.86592688125963 | 9.18897245919212 | C | 9.57352685884988 | 4.63178262678814 | 9.05283619045930 |
| H | 9.73563373422830 | 4.20223627096791 | 8.44162225028561 | H | 10.00286482236722 | 3.88419463076929 | 8.4026332794592 |
| C | 8.68731434400946 | 4.35089964125551 | 10.31059424630180 | C | 8.85852040176563 | 4.25930265980972 | 10.18605635299571 |
| C | 8.52594928980194 | 2.90328438505513 | 10.57078427767345 | C | 8.62857988782600 | 2.84076362948014 | 10.56429670513752 |
| C | 8.90917351431886 | 1.84251091576725 | 9.75160370418365 | C | 9.00699816113147 | 1.74214771136599 | 9.79457223338659 |
| H | 9.37973785615823 | 2.0165511050581 | 8.79484387909682 | H | 9.50673486269728 | 1.86618403136301 | 8.84552381519545 |
| C | 8.6711206390038 | 0.54394487385973 | 10.18666740273540 | C | 8.71658560531827 | 0.46725634877883 | 10.26268754973040 |
| H | 8.95909100697727 | -0.29226309196956 | 9.56359735492381 | H | 8.99316358102229 | -0.39956389252786 | 9.67713196542368 |
| C | 8.07321224515716 | 0.30975787381506 | 11.42265370108834 | C | 8.07487656710936 | 0.30500874560086 | 11.48309895352731 |
| H | 7.88992656747769 | -0.70016859502995 | 11.76157186705237 | H | 7.84287773569208 | -0.68409149901418 | 11.85042683640727 |
| C | 7.17157353980466 | 1.40351588944448 | 12.20097051280280 | C | 7.73695436481430 | 1.44371441191796 | 12.20971023381228 |
| N | 7.94372234062846 | 2.65191833095537 | 11.74652343764228 | N | 8.00634555573346 | 2.66591225918939 | 11.73331529215659 |
| N | 9.18290941937876 | 4.10552644489012 | 13.65908895080603 | N | 9.44913816854515 | 4.49006981691760 | 13.72841420631862 |
| C | 10.27015584132165 | 4.00408180875380 | 14.01221237316097 | C | 10.55750574460432 | 4.33287686921038 | 13.98476732436329 |
| C | 11.65496115452337 | 3.84989016529502 | 14.42037431692814 | C | 11.96021563207768 | 4.11384412356681 | 14.28579007828459 |
| H | 12.11534707929009 | 3.04044901804868 | 13.85243295406952 | H | 12.33937117843494 | 3.28407106377352 | 13.68829695769968 |
| H | 12.20449419179397 | 4.77252546826432 | 14.22797881204178 | H | 12.53532937333884 | 5.01087500730939 | 14.05228922774993 |
| H | 11.7134190393272 | 3.61068868914572 | 15.48368670180519 | H | 12.08401606234974 | 3.87208469546074 | 15.34287044658664 |
| N | 6.62924969038662 | 5.16569826642780 | 14.46522314024863 | N | 6.47093629797799 | 5.1898997289396 | 14.71880592200696 |
| C | 6.52753197430132 | 6.48588928412734 | 14.63069608135487 | C | 6.31555270648146 | 6.48486758464261 | 15.00931286658470 |
| H | 6.95841503077173 | 7.10355304853477 | 13.85518031014241 | H | 6.76423965195837 | 7.19311164729671 | 14.32307701679800 |
| C | 5.90330001769552 | 7.06918845017510 | 15.72659749210297 | C | 6.52058843121573 | 6.93033781168612 | 16.12521550147751 |
| H | 5.84320738519874 | 8.14593400595245 | 15.80578923682971 | H | 5.52011582134937 | 7.98935997863906 | 16.31946727538845 |
| C | 5.36534001360732 | 6.24331241588305 | 16.70062965282913 | C | 5.06290476900534 | 5.98476131930724 | 16.97268004005447 |
| H | 4.86335224426239 | 6.66010837091169 | 17.56368804838461 | H | 4.50471450002314 | 6.28934193782830 | 17.84812007533183 |
| C | 5.47957375357607 | 4.86713147116570 | 16.55054193879027 | C | 5.23001033173608 | 4.63740983834231 | 16.68370356477001 |
| H | 5.069223585096329 | 4.20363589045343 | 17.29827858135470 | H | 4.80065090026549 | 3.89072107923308 | 17.33493035553890 |
| C | 6.11661746955888 | 4.35182231191045 | 15.42873698969704 | C | 5.94526459681027 | 4.26334462121865 | 15.55115615784395 |
| C | 6.27788767402458 | 2.90413002145266 | 15.16895704249553 | C | 6.17572531075034 | 2.84426905841965 | 15.17522503471466 |
| C | 5.89461372947952 | 1.84364006459410 | 15.98850096309292 | C | 5.79934535083014 | 1.74687599395865 | 15.94766229665031 |
| H | 5.42413379508914 | 2.01802140239017 | 16.94524062242917 | H | 5.3009376906837 | 1.872374258883978 | 16.89721646013283 |
| C | 6.13241654502328 | 0.54492077917924 | 15.55380237473122 | C | 6.09023683078713 | 0.47130827458610 | 15.48167801279008 |
| H | 5.84436335439942 | -0.29106071443653 | 16.17714165658162 | H | 5.81517930637398 | -0.39459739262077 | 16.06929680539052 |
| C | 6.73018795471784 | 0.31029218910539 | 14.31782015077619 | C | 6.73067120355618 | 0.307204595885919 | 14.26085099839653 |
| H | 6.91331350255874 | -0.69975834473216 | 13.97918315632499 | H | 6.96322632319426 | -0.68242040667309 | 13.89529585945205 |
| C | 7.08597172933217 | 1.40378215617120 | 13.53920660824415 | C | 7.06690812101811 | 1.44474380923351 | 13.53163873163551 |
| N | 6.85998720741262 | 2.65237350666903 | 13.99324484510734 | N | 6.79664587719939 | 2.66765335622183 | 14.00576165665828 |
| N | 5.62104179064899 | 4.10456310418650 | 12.07910423290140 | N | 5.35406874372408 | 4.49349882635803 | 12.00765431287125 |
| C | 4.53430661942237 | 4.00231800778939 | 11.72461086655822 | C | 4.24566621184755 | 4.33451827947488 | 11.75254091489835 |
| C | 3.15019558005708 | 3.84718797875590 | 11.31428216905699 | C | 2.84273972928749 | 4.11398681300303 | 11.45378213988534 |
| H | 2.69044348281512 | 3.03526405393772 | 11.87917456335072 | H | 2.46524430937552 | 3.28450094458971 | 12.05273449683464 |
| H | 2.59893027524628 | 4.76830205655124 | 11.50885678359462 | H | 2.26722009736176 | 5.01075215295985 | 11.68727015354060 |
| H | 3.09335074103526 | 3.61119638688918 | 10.25020333606697 | H | 2.71751370481087 | 3.87089325368738 | 10.39718299180091 |

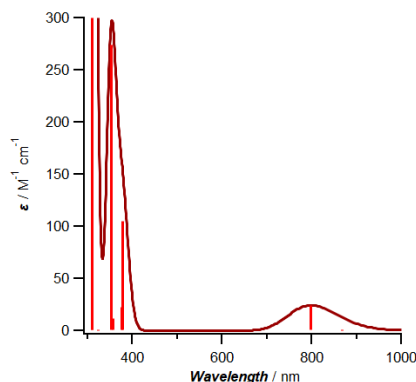
| [Co(qpy)(MeCN)₂](BF₄)₂ S = 1/2 | | | | [Co(qpy)(MeCN)₂](BF₄)₂ S = 3/2 | | | |
|--|-------------------|-------------------|-------------------|--|-------------------|--------------------|-------------------|
| Co | 11.65145244672597 | 12.37268780857638 | 10.22572056267860 | Co | 11.67499120224274 | 12.18193467231094 | 10.21989168918562 |
| N | 11.21377659091013 | 11.27894463034328 | 8.57162108403834 | N | 11.08028744750965 | 11.30029548945719 | 8.34646013252124 |
| C | 11.12104079174453 | 9.95650369496913 | 8.42488351074675 | C | 10.87896797611399 | 10.00020024875538 | 8.12078119278819 |
| H | 11.28560958535811 | 9.35804036336144 | 9.30857171277373 | H | 10.95740080233514 | 9.34132782649094 | 8.97693680432246 |
| C | 10.82465488806855 | 9.34463087107213 | 7.21355671351230 | C | 10.57550265728241 | 9.49055039941131 | 6.86623830159171 |
| H | 10.75684981369437 | 8.26709672912954 | 7.15771520037548 | H | 10.41537338161681 | 8.42912842559500 | 6.73647030608739 |
| C | 10.61742184553286 | 10.14169594705174 | 6.10013784235732 | C | 10.47627200239809 | 10.37447126304884 | 5.80230809322103 |
| H | 10.38639789575894 | 9.70142973599213 | 5.13912013663249 | H | 10.23928616433076 | 10.01744715479777 | 4.80861284925510 |
| C | 10.70117868513347 | 11.52160844330731 | 6.23876269067331 | C | 10.67239888747723 | 11.72963694775635 | 6.03164937154348 |
| H | 10.53208032552642 | 12.16491192439085 | 5.38712855532706 | H | 10.58469052363250 | 12.43196985091787 | 5.21543205046517 |
| C | 10.99202042404587 | 12.06525107172923 | 7.48084673901357 | C | 10.96980584270093 | 12.17056416324837 | 7.31610918387769 |
| N | 11.07351768848955 | 13.51513591495914 | 7.74250384981871 | C | 11.14014619684717 | 13.60435782856925 | 7.66395443549853 |
| N | 11.34538882252638 | 13.78705983394046 | 9.02049231893976 | N | 11.40318820815745 | 13.83019077824840 | 8.95138645130673 |
| C | 10.90482785077602 | 14.56113057514080 | 6.83618417781986 | C | 10.11057545044942 | 14.67463363242272 | 6.77776896795676 |
| H | 10.68463324423652 | 14.37090395577858 | 5.79582933688371 | H | 10.80751465055974 | 14.51668521861252 | 5.72974419053015 |
| C | 11.02119375294397 | 15.86623830110675 | 7.29823603503589 | C | 11.14717050341556 | 15.96580466912148 | 7.27202322014092 |
| H | 10.89232946758570 | 16.69217209078246 | 6.61122289846883 | H | 11.05203496633466 | 16.81121971872404 | 6.60334640837123 |
| C | 11.30140458695594 | 16.12228543978838 | 8.63869644998920 | C | 11.38467140450578 | 16.17671622184130 | 8.62551341352478 |
| H | 11.39320937581357 | 17.13820762101519 | 8.99641043374763 | H | 11.47103095823360 | 17.18087054380701 | 9.01523913177571 |
| C | 11.46329772147875 | 15.04276724872436 | 9.49477325367783 | C | 11.50814343340641 | 15.06604756001454 | 9.45336973254892 |
| C | 11.78469693117168 | 15.05049530952564 | 10.93791941694967 | C | 11.76434464169887 | 15.08798976136701 | 10.91734416038604 |
| N | 11.93873681015495 | 13.80103469408190 | 11.41800647080233 | N | 11.89669906269813 | 13.86872285496970 | 11.45237759017435 |
| C | 11.93154015758209 | 16.13861676690572 | 11.78638814388755 | C | 11.87413889243540 | 16.22322041363065 | 11.71403866323225 |
| H | 11.80907947578987 | 17.14978547940467 | 11.42443455494339 | H | 11.76479242409117 | 17.21433730782228 | 11.29771684923125 |
| C | 12.23922938468060 | 15.89676259135412 | 13.12338507413082 | C | 12.12932610131455 | 16.05385198248836 | 13.06999890372722 |
| H | 12.35697073875295 | 16.72926939425382 | 13.80439920427863 | H | 12.21534152235721 | 16.91874059584781 | 13.71455847953946 |
| C | 12.40128741106541 | 14.59719828143415 | 13.58909761714150 | C | 12.29354097898925 | 14.77886411152882 | 13.59732192233702 |
| H | 12.64732653758159 | 14.41827443571965 | 14.62573029597576 | H | 12.51876446986152 | 14.65404179256458 | 14.64628583374020 |
| C | 12.24493126607437 | 13.54248737332379 | 12.69111966447524 | C | 12.17992729779033 | 13.68258918648863 | 12.74221804775148 |
| C | 12.38386020557441 | 12.09679466830841 | 12.95477118005742 | C | 12.38993607811905 | 12.26183044870591 | 13.12543375814920 |
| C | 12.75415051427260 | 11.56835267276547 | 14.18194252571640 | C | 12.70292253438183 | 11.85989850834278 | 14.41925747861071 |
| H | 12.94326366531685 | 12.22071311521131 | 15.02243030026797 | H | 12.77584710231815 | 12.58401749186110 | 15.21777119529125 |
| C | 12.89588069418129 | 10.19297252799307 | 14.31899168434777 | C | 12.93223354460037 | 10.51577053378957 | 14.68175605774682 |
| H | 13.19255083976549 | 9.76539779315607 | 15.26759095239278 | H | 13.18061536904485 | 10.18923261685838 | 15.68309667124332 |
| C | 12.66068772164176 | 9.38354294931667 | 13.22021104155616 | C | 12.85036617238244 | 9.60292918277446 | 13.64076072532568 |
| H | 12.76910984458195 | 8.30924454502177 | 13.27529936274520 | H | 13.0344236930252 | 8.54886479633892 | 13.79645625874238 |
| C | 12.28548593482066 | 9.98004995843935 | 12.02339166099686 | C | 12.53117308397101 | 10.07425702570553 | 12.37519748208864 |
| H | 12.09889134359361 | 9.37334555644700 | 11.14962564494800 | H | 12.46486501781570 | 9.39286563949186 | 11.53559502838652 |
| N | 12.14347107849535 | 11.29776735959200 | 11.87780287408982 | N | 12.29937604542413 | 11.36304937534450 | 12.11840127747710 |
| N | 9.39617934523773 | 12.36389416738386 | 10.93773178761029 | N | 9.59772365103183 | 12.025777781108022 | 10.94519636380974 |
| C | 8.35013799834457 | 12.53230949273920 | 11.38327250305990 | C | 8.55029186137202 | 12.11141215169309 | 11.40739523792777 |
| C | 7.02840085057423 | 12.74637231645257 | 11.95040164536498 | C | 7.23022946222671 | 12.23033231072978 | 12.00074332957988 |
| H | 7.08584843875051 | 13.45854640882056 | 12.77446738039796 | H | 7.26130115936999 | 12.92720863177972 | 12.83926427769989 |
| H | 6.62813991362093 | 11.80450703937024 | 12.32813857043810 | H | 6.89471555622837 | 11.25738232762269 | 12.36309945334737 |
| H | 6.35523301235655 | 13.14188109351090 | 11.18918896600088 | H | 6.52112991699640 | 12.60026732314242 | 11.25924284936603 |
| N | 13.96775523736500 | 12.42602689040014 | 9.64936322402390 | N | 13.80564729553297 | 12.15075019393981 | 9.63293482629769 |
| C | 15.07809922116349 | 12.69523510635178 | 9.52405310471559 | C | 14.92995781733531 | 12.34155369259660 | 9.50075698999950 |
| C | 16.4800973392076 | 13.04997733830285 | 9.37849890465111 | C | 16.34973128319363 | 12.60196110853929 | 9.34987357887034 |
| H | 16.68151740809153 | 13.37109623110941 | 8.35521419645508 | H | 16.56587218593457 | 12.91860376605448 | 8.32815189049192 |
| H | 17.10937130137920 | 12.19101084744641 | 9.61379932636854 | H | 16.92002723240536 | 11.69994308826769 | 9.57540692249149 |
| H | 16.72848618079011 | 13.86550939469584 | 10.05825821869824 | H | 16.65338221022455 | 13.39285535548013 | 10.03645096979304 |

Table 5.3. Optimized Geometry of M-qpy (M = Fe, Co)

| Species | <i>S</i> | $d(\text{M}-\text{N}_1) / \text{\AA}$ | $d(\text{M}-\text{N}_4) / \text{\AA}$ | $\angle (\text{N}_1-\text{M}-\text{N}_2) / ^\circ$ | $\angle (\text{N}_1-\text{M}-\text{N}_4) / ^\circ$ | $\angle (\text{N}_3-\text{M}-\text{N}_4) / ^\circ$ |
|---------------|----------|---------------------------------------|---------------------------------------|--|--|--|
| Co-qpy | 1/2 | 2.02963 | 1.88025 | 115.395 | 81.330 | 82.042 |
| | 3/2 | 2.15500 | 2.09688 | 133.533 | 76.126 | 74.816 |
| Fe-qpy | 0 | 2.07293 | 1.90407 | 117.567 | 80.301 | 81.841 |
| | 2 | 2.22367 | 2.15804 | 138.346 | 74.099 | 73.277 |

Table 5.4. Calculated Electronic Transitions in $S = 2$ Fe-qp_y

| State | f_{osc} | Energy / nm | Energy / cm ⁻¹ | Transition Weight | Assignment |
|-------|-------------|-------------|---------------------------|-------------------|-----------------------------|
| 3 | 0.000045570 | 867.6 | 11526.5 | 0.671110 | ⁵ E _g |
| 4 | 0.001478292 | 797.7 | 12535.9 | 0.423588 | ⁵ E _g |
| 5 | 0.001452786 | 378.3 | 26436.9 | 0.536134 | ⁵ MLCT |
| 8 | 0.001593486 | 352.7 | 28349.5 | 0.218964 | ⁵ MLCT |

**Figure 5.10.** Calculated Fe-qp_y $S = 2$ absorption spectrum. Transitions denoted as sticks.**Table 5.5.** Calculated Electronic Transitions in $S = 0$ Fe-qp_y

| State | f_{osc} | Energy / nm | Energy / cm ⁻¹ | Transition Weight | Assignment |
|-------|-----------|-------------|---------------------------|-------------------|-------------------|
| 4 | 0.023682 | 537.0 | 18621.1 | 0.586177 | ¹ MLCT |
| 5 | 0.003392 | 458.4 | 21814.3 | 0.944909 | ¹ MLCT |
| 7 | 0.024724 | 435.3 | 22973.8 | 0.820141 | ¹ MLCT |

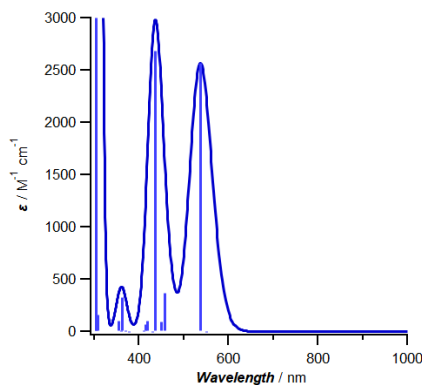
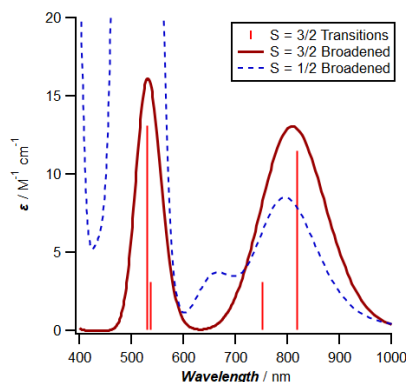
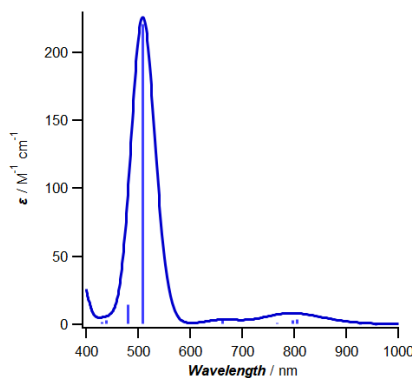
**Figure 5.11.** Calculated Fe-qp_y $S = 0$ absorption spectrum. Transitions denoted as sticks.

Table 5.6. Calculated Electronic Transitions in $S = 3/2$ Co-qpy.

| State | f_{osc} | Energy / nm | Energy / cm^{-1} | Transition Weight | Assignment |
|-------|-------------|-------------|--------------------|-------------------|-----------------|
| 3 | 0.00010613 | 818.4 | 12219.6 | 0.516844 | ${}^4T_{2g}(F)$ |
| 4 | 0.000028821 | 752.5 | 13289.7 | 0.243641 | ${}^4T_{2g}(F)$ |
| 5 | 0.000028704 | 536.6 | 18636.0 | 0.232276 | ${}^4T_{1g}(P)$ |
| 6 | 0.000120852 | 530.0 | 18869.0 | 0.253832 | ${}^4T_{1g}(P)$ |

**Figure 5.12.** Calculated Co-qpy $S = 3/2$ absorption spectrum. Transitions denoted as sticks. The $S = 1/2$ calculated spectrum is overlaid (dashed) towards assignment of ${}^4T_{1g} \rightarrow {}^2T_{2g}$ at 661 nm.**Table 5.7.** Calculated Electronic Transitions in $S = 1/2$ Co-qpy.

| State | f_{osc} | Energy / nm | Energy / cm^{-1} | Transition Weight | Assignment |
|-------|-------------|-------------|--------------------|-------------------|--------------|
| 3 | 0.000033689 | 804.7 | 12427.5 | 0.564109 | ${}^2T_{1g}$ |
| 4 | 0.000032197 | 796.6 | 12554.0 | 0.452375 | ${}^2T_{1g}$ |
| 5 | 0.00001441 | 767.3 | 13032.3 | 0.437715 | ${}^2T_{1g}$ |
| 6 | 0.000033034 | 661.1 | 15126.7 | 0.522997 | ${}^2T_{2g}$ |
| 7 | 0.002036554 | 508.9 | 19650.2 | 0.412681 | ${}^2T_{2g}$ |
| 8 | 0.000134775 | 479.5 | 20854.3 | 0.398923 | ${}^2T_{2g}$ |

**Figure 5.13.** Calculated Co-qpy $S = 1/2$ absorption spectrum. Transitions denoted as sticks.

5.6. References

- (1) Leung, C.-F.; Ng, S.-M.; Ko, C.-C.; Man, W.-L.; Wu, J.; Chen, L.; Lau, T.-C. A Cobalt(II) Quaterpyridine Complex as a Visible Light-Driven Catalyst for Both Water Oxidation and Reduction. *Energy Environ. Sci.* **2012**, 5 (7), 7903.
- (2) Guo, Z.; Cheng, S.; Cometto, C.; Anxolabéhère-Mallart, E.; Ng, S.-M.; Ko, C.-C.; Liu, G.; Chen, L.; Robert, M.; Lau, T.-C. Highly Efficient and Selective Photocatalytic CO₂ Reduction by Iron and Cobalt Quaterpyridine Complexes. *J. Am. Chem. Soc.* **2016**, 138 (30), 9413–9416.
- (3) Cometto, C.; Chen, L.; Lo, P.-K.; Guo, Z.; Lau, K.-C.; Anxolabéhère-Mallart, E.; Fave, C.; Lau, T.-C.; Robert, M. Highly Selective Molecular Catalysts for the CO₂-to-CO Electrochemical Conversion at Very Low Overpotential. Contrasting Fe vs Co Quaterpyridine Complexes upon Mechanistic Studies. *ACS Catal.* **2018**, 8 (4), 3411–3417.
- (4) Loipersberger, M.; Cabral, D. G. A.; Chu, D. B. K.; Head-Gordon, M. Mechanistic Insights into Co and Fe Quaterpyridine-Based CO₂ Reduction Catalysts: Metal–Ligand Orbital Interaction as the Key Driving Force for Distinct Pathways. *J. Am. Chem. Soc.* **2021**, 143 (2), 744–763.
- (5) Che, C.-M.; Chan, C.-W.; Yang, S.-M.; Guo, C.-X.; Lee, C.-Y.; Peng, S.-M. Synthesis, Properties and Crystal Structures of Iron-(II) and -(III) Complexes of 2,2':6',2'':6'',2'''-Quaterpyridine. *J. Chem. Soc., Dalton Trans.* **1995**, No. 18, 2961–2966.
- (6) Guionneau, P.; Marchivie, M.; Bravic, G.; Létard, J.-F.; Chasseau, D. Structural Aspects of Spin Crossover. Example of the [Fe^{II}L_n(NCS)₂] Complexes. In *Spin Crossover in Transition Metal Compounds II*; Gülich, P., Goodwin, H. A., Eds.; Springer Berlin Heidelberg: Berlin, Heidelberg, 2004; pp 97–128.

- (7) Dell'Amico, D. B.; Calderazzo, F.; Englert, U.; Labella, L.; Marchetti, F. The First Crystallographically Established Bis-Qtpy (Qtpy = 2,2':6',2'':6'',2'''-Quaterpyridine) Metal Complex. *J. Chem. Soc., Dalton Trans.* **2001**, No. 4, 357–358.
- (8) Little, B. F.; Long, G. J. Moessbauer, Electronic, and Structural Properties of Several Bis- and Tetrakis(Pyridine)Iron(II) Complexes. *Inorg. Chem.* **1978**, *17* (12), 3401–3413.
- (9) Dolphin, D.; Sams, J. R.; Tsin, T. B.; Wong, K. L. Synthesis and Moessbauer Spectra of Octaethylporphyrin Ferrous Complexes. *J. Am. Chem. Soc.* **1976**, *98* (22), 6970–6975.
- (10) Harding, M. J.; Billardon, M.; Kramer, A. The Magnetic Circular Dichroism Spectrum of the Hexaquocobalt(II) Ion in the Infra-Red Region. *Molecular Physics* **1974**, *27* (2), 457–466.
- (11) Harding, M. J.; Briat, B. The Electronic Absorption and Magnetic Circular Dichroism Spectra of Cobalt(II) Bromate Hexahydrate. *Molecular Physics* **1973**, *25* (4), 745–776.
- (12) Moll, J.; Förster, C.; König, A.; Carrella, L. M.; Wagner, M.; Panthöfer, M.; Möller, A.; Rentschler, E.; Heinze, K. Panchromatic Absorption and Oxidation of an Iron(II) Spin Crossover Complex. *Inorg. Chem.* **2022**, *61* (3), 1659–1671.
- (13) Khalil, M.; Marcus, M. A.; Smeigh, A. L.; McCusker, J. K.; Chong, H. H. W.; Schoenlein, R. W. Picosecond X-Ray Absorption Spectroscopy of a Photoinduced Iron(II) Spin Crossover Reaction in Solution. *J. Phys. Chem. A* **2006**, *110* (1), 38–44.
- (14) Constable, E. C.; Elder, S. M.; Healy, J.; Tocher, D. A. A Convenient Preparation of 2,2':6',2'':6'',2'''-Quaterpyridine; the Crystal and Molecular Structures

of 2,2':6',2'':6'',2'''-Quaterpyridine and Bis(Acetonitrile)-(2,2':6',2'':6'',2'''-Quaterpyridine)Nickel(II) Hexafluorophosphate–Acetonitrile(1/1). *J. Chem. Soc., Dalton Trans.* **1990**, No. 5, 1669–1674.

(15) Sheldrick, G. Phase Annealing in SHELX-90: Direct Methods for Larger Structures. *Acta Crystallographica Section A*, **1990**, *46*, 467–473.

(16) Sheldrick, G. SHELXT - Integrated Space-Group and Crystal-Structure Determination. *Acta Crystallographica Section A*, **2015**, *71*, 3–8.

(17) Müller, P. Practical Suggestions for Better Crystal Structures. **2009**, *15* (1), 57–83.

And God said, “Let there be light,” and there was light.

Genesis 1:3